Technische Universität München
TUM School of Engineering and Design

Structural reliability analysis accounting for spatial variability and measurements

Sebastian Karl Geyer

Vollständiger Abdruck der von der TUM School of Engineering and Design der Technischen Universität München zur Erlangung eines

Doktors der Ingenieurwissenschaften (Dr.-Ing.)

genehmigten Dissertation.

Vorsitz: Prof. Dr.-Ing. Oliver Fischer

Prüfer*innen der Dissertation:

1. Prof. Dr. sc. techn. Daniel Straub
2. Prof. Lori Graham-Brady, Ph.D.
3. Prof. Dr.-Ing. habil. Emilio Bastidas-Arteaga

Die Dissertation wurde am 13.04.2023 bei der Technischen Universität München eingereicht und durch die TUM School of Engineering and Design am 12.09.2023 angenommen.

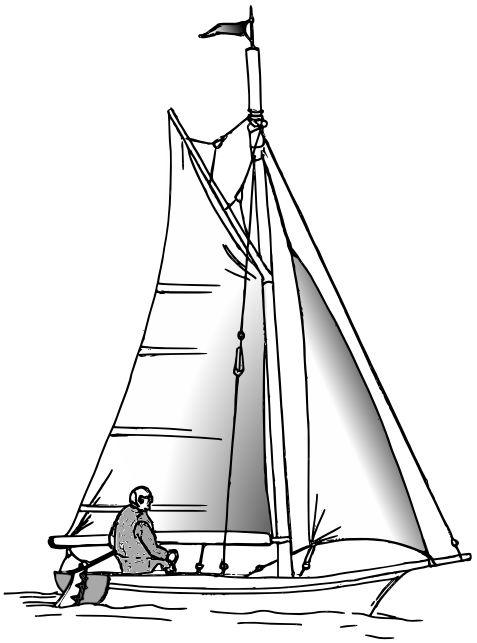

To the memory of my father
Thomas Karl Geyer

Abstract

Calculating the probability of failure is an essential step in structural reliability analysis. This task involves the selection of a mechanical model of the structural performance and the stochastic modeling of the uncertain input parameters. In the presence of spatial variability, random variables may not suffice to accurately represent the uncertainty in the input parameters. The spatially variable parameters need to be modeled as random fields, which are defined as an infinite collection of random variables indexed by a spatial coordinate. Numerical treatment of random fields requires a discretization method, which approximates a random field through a finite number of random variables. Site-specific data from measurements can be used to improve the stochastic model and to reduce the uncertainty of the input parameters. In addition to the stochastic and mechanical model, structural reliability analysis requires the choice of a reliability method to estimate the probability of failure. The computational effort and numerical accuracy of the analysis are determined by these choices.

This thesis presents methods to efficiently estimate the structural reliability in presence of spatial variation and measurement data, with focus on the stochastic modeling of spatially variable material properties. To this end, a hierarchical Bayesian model for spatially variable Gaussian quantities is developed, which allows the combination of prior information with spatial data. The conjugacy of the selected prior distribution and likelihood function enable derivation of closed-form expressions for the predictive point-in-space distribution of the random field. The model is extended for the application to the class of non-Gaussian translation random fields. In addition, an approach for learning the spatial correlation function from data is presented and further refined for the specific application to the spatial modeling of concrete strength. The performance is evaluated with case studies of ship lock chamber walls made of tamped concrete, for which strength measurements are available from core samples.

The spatial averaging method is suggested as random field discretization method. This method approximates a random field through a set of random variables representing the average behavior of the random field over a corresponding set of elemental spatial domains. Coupling the discretized random field model with a finite element model for structural analysis is then straightforward and in compliance with the underlying theory of finite element modeling. The required expressions for the application to non-homogeneous Gaussian random fields are derived and the extension to non-Gaussian translation random fields is described. This extension allows using the spatial averaging method for the random fields originating from the hierarchical Bayesian update.

The choice of an adequate reliability method depends on the problem at hand. Approximation methods and several Monte Carlo-based simulation methods are briefly described, highlighting the respective advantages and disadvantages. Using a set of typical problem characteristics, the presented reliability methods are compared with one another. In addition, the effects of spatial variability on structural reliability are discussed regarding the random field discretization and increased complexity of the problem to be solved.

Titel in deutscher Sprache

Zuverlässigkeitsanalyse von Bauwerken unter Berücksichtigung von räumlicher Variabilität und Messdaten

Zusammenfasung

Zuverlässigkeitsberechnungen für Bauwerke sind im Bereich der Quantifizierung von Unsicherheiten zu verorten und beinhalten neben der stochastischen Modellierung der unsicheren Eingangsparameter die Auswertung eines mechanischen Modells, welches das Bauwerksverhalten beschreibt. In Fällen mit räumlicher Variabilität kann es sein, dass Zufallsvariablen nicht ausreichen, um die Unsicherheiten ausreichend zu repräsentieren, weshalb räumlich variable Parameter gegebenenfalls mit Zufallsfeldern modelliert werden müssen. Zufallsfelder sind definiert als Ansammlung einer unendlichen Zahl von Zufallsvariablen, die mit einer räumlichen Koordinate versehen sind. Für die numerische Behandlung von Zufallsfeldern bedarf es deswegen einer Diskretisierungsmethode, die ein Zufallsfeld über eine begrenzte Anzahl von Zufallsvariablen approximiert. Das stochastische Modell kann mithilfe standortspezifischer Daten verbessert werden, wodurch die Unsicherheiten in den Eingangsparametern reduziert werden. Zusätzlich zum mechanischen und stochastischen Modell ist die Wahl einer Zuverlässigkeitsmethode erforderlich, mit welcher die Bauwerkszuverlässigkeit abgeschätzt werden kann. Der Rechenaufwand und die numerische Genauigkeit der Zuverlässigkeitsanalyse werden von diesen vorab getroffenen Entscheidungen bestimmt.

Diese Arbeit präsentiert Methoden für die effiziente Abschätzung der Bauwerkszuverlässigkeit unter Berücksichtigung von räumlicher Variabilität und Messdaten, wobei der Fokus auf der stochastischen Modellierung räumlich variabler Materialeigenschaften liegt. Zu diesem Zweck wird ein hierarchisches Bayes'sches Modell für räumlich variable und normalverteilte Größen entwickelt, welches die Kombination von Vorwissen und räumlichen Daten erlaubt. Durch die Konjugation der ausgewählten A-priori-Verteilung mit der Likelihood-Funktion können die Ausdrücke für die räumlichen Funktionen der Momente des prädiktiven Studentschen t-Zufallsfelds in geschlossener Form hergeleitet werden. Das Modell wird um die Anwendbarkeit auf die Klasse der *Translation Random Fields* erweitert. Zusätzlich wird eine Vorgehensweise für das Erlernen der räumlichen Korrelationsfunktion aus den Daten präsentiert und die Vorgehensweise für die spezifische Anwendung auf die Betonfestigkeit weiter verfeinert. Mithilfe von Fallstudien an Schleusenkammerwänden, für welche Daten der Betonfestigkeit aus Bohrkernen vorliegen, wird die Leistungsfähigkeit der Methodik beurteilt.

Für die Zufallsfelddiskretisierung wird die *Spatial-Averaging*-Methode vorgeschlagen. Diese Methode approximiert ein Zufallsfeld über ein Set von Zufallsvariablen, welche das gemittelte Verhalten des Zufallsfelds über ein zugehöriges Set von räumlichen Bereichen darstellen. Dadurch ist die Kopplung des diskretisierten Zufallsfelds mit einem Finite-Elemente-Modell unkompliziert und in Übereinstimmung mit der Theorie der Finite-Elemente-Methode möglich. Die erforderlichen Ausdrücke zur Anwendung auf nichthomogene Gauß'sche Zufallsfelder werden hergeleitet und die Erweiterung auf *Translation Random Fields* ist beschrieben. Diese Erweiterung erlaubt es, die *Spatial-Averaging*-Methode auf Zufallsfelder, die aus dem hierarchischen Bayes'schen Update resultieren, anzuwenden.

Die Wahl einer angemessenen Zuverlässigkeitsmethode ist abhängig von der spezifischen Problemstellung. Approximationsmethoden sowie einige Monte-Carlo-basierte Simulationsmethoden werden in dieser Arbeit kurz vorgestellt, wobei die jeweiligen Vor- und Nachteile herausgestellt werden. Mithilfe typischer Charakteristika von Problemen der Zuverlässigkeitsanalyse werden

die vorgestellten Zuverlässigkeitsmethoden untereinander verglichen. Zusätzlich werden die Auswirkungen räumlicher Variabilität auf die Bauwerkszuverlässigkeit diskutiert, wobei sowohl auf die Zufallsfelddiskretisierung als auch auf die erhöhte Komplexität des zu lösenden Problems eingegangen wird.

Acknowledgements

First and foremost, I want to thank my supervisors Daniel and Iason for all the help and guidance they provided me with during five years at the ERA group. While Daniel was my first contact person for issues regarding the broader context and the whole research project, Iason was the catalyst to all mathematical derivations and never hesitated to spend time with me on details. Although their mutual propensity for perfection surely delayed the completion or submission of some of my abstracts, papers or reports, they were the perfect one-two-punch for supervising me. Besides their professional expertise, I have to give them credit for their tremendous personal support in difficult times of my doctoral studies.

I want to express my gratitude to Lori Graham-Brady for hosting me at her group at Johns Hopkins University during my three months research stay. Besides many fruitful and inspiring scientific discussions and the familiarity she leads her group with, I especially appreciate her motivation to discuss the local sports teams and general life in Baltimore.

Although the interactions with my colleagues at ERA group were significantly reduced since March 2020, I am grateful for the wonderful time and many new friendships. Special shout-out at this point to Elizabeth, Felipe and Max, who I shared my office with. Countless times, no matter if asked or not, they gave me professional and non-professional advice. In addition, they filled the gaps in office life with stupid games, extensive coffee sessions, feminist or political discussions, and much more.

My doctoral research was funded by the *Bundesansalt für Wasserbau* (BAW) in Karlsruhe and the *Deutsche Forschungsgemeinschaft* (DFG) in the framework of the priority programme SPP 1886 by grant STR 1140/6-1. I thank these institutions for their financial support. I also thank Claus Kunz from BAW for many motivating discussions and helpful criticism, and the hospitality I was received with in Karlsruhe.

None of the research items in this thesis would have been realized without the support from my wife, Ela. The contribution of others may be placed more prominent and directly visible, but she has been my relief valve, the charger for my battery, and my safe haven. Thank you for spending your life with me.

Last but not least, I want to express my gratitude for all the love and support I have received from my family: my sisters Claudia, Raphaela, Bettina, and Cornelia, my mother Gertraud and my late father Thomas, who, besides countless other things, taught me to always look on the bright side of life.

Nuremberg, Germany

April, 2023

Table of contents

Part I

Compendium

Chapter 1

Introduction

We are surrounded by engineering structures. No matter where we go or what we do, it is almost impossible to spend a day without utilizing an engineering structure of some kind. Such engineering structure may be the house we live in, a bridge that we cross in a car or by train or simply an interesting building we pass by. Although all of these structures are assigned different tasks for our everyday life, most of them have one thing in common: they are considered reliable structures and their safe use is taken for granted. It is the main task of the field of structural reliability to ensure this by quantifying the probability of failure of structures and designing them in a way that this probability lies below an acceptable threshold. Structural failure can never be avoided completely, which raises the question of an acceptable failure probability. Choosing a pragmatic approach by counting the total number of structures in service and the number of failures per year, a seemingly accepted value for the failure probability of a structure can be estimated and lies in the order of 10^{-4} for a 50-year service life [4, 110]. Obviously, this approach neglects many factors in the calculation (besides, the quoted number is exclusively based on structures in Canada) but, nevertheless, it can serve as indicator for the risk that is accepted in a society. In fact, that value from Canada and the target levels for structural reliability of standard buildings in the European design codes for buildings and structures lie not too far apart [47].

Structural reliability analysis is a task of uncertainty quantification, i.e., the quantity of interest (in this case the probability of failure of a structure or a structural member) depends on parameters that are subject to uncertainty [69]. In engineering practice, these uncertainties are rarely explicitly accounted for, one mostly relies on application-specific rules to implicitly include uncertainty in the analysis, which saves time and effort, and allows for generalization. These rules form the framework of structural verification, in Europe nowadays standardized through the Eurocode series, e.g., for load effects [48], concrete structures [49], steel structures [50], timber structures [51] or geotechnical design [52], each of which in combination with the respective parts for specific applications. In addition to defining a way to include uncertainties, they also provide guidelines for determining the stress in structural members through simple mechanical models. For more complex problems though, the mechanical model typically involves a numerical model to determine the forces and stresses, such as a finite element model [e.g., 122, 123]. One of the key components of this standardized procedure is the independence of stochastic model and mechanical model, as illustrated in panel a of Figure 1.1. This allows the mechanical part of the verification to stay completely deterministic and thus, understanding the underlying theory of random variables and their effect on structural reliability is not required, which simplifies the application significantly.

However, there are cases where the standard procedures are not sufficient for ensuring the reliability of a structure, which is caused by various reasons, such as non-standardized material

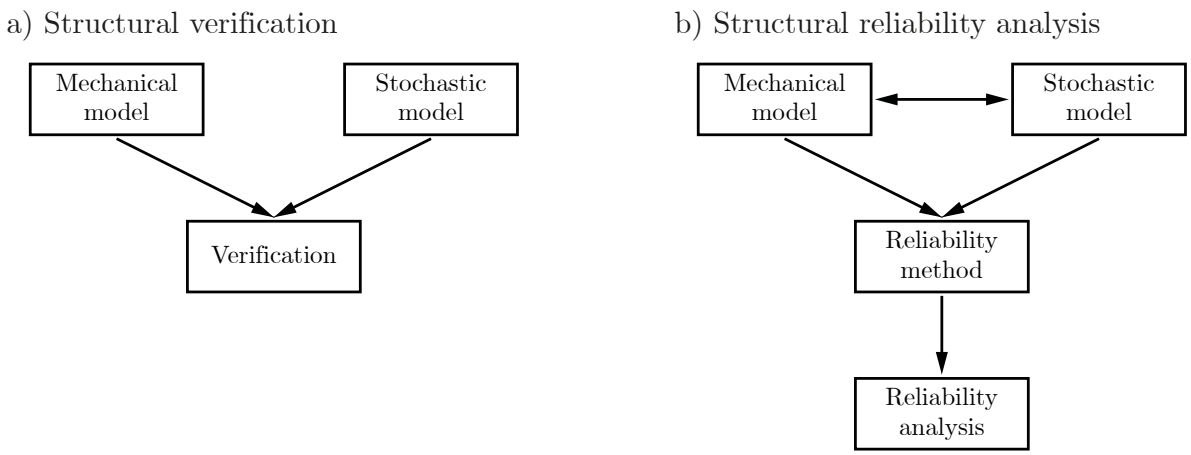

Figure 1.1: Components of structural verification (panel a) and reliability analysis (panel b). The arrows indicate dependence between the respective components.

due to the age of an existing structure, unprecedented loads on a structure, or simply the desire for an economic design, among others. In these cases, a reliability analysis of the structure needs to be conducted, where the uncertainties are explicitly accounted for by modeling them as random variables or, in the presence of spatial (temporal) variability, as random fields (random processes) [161]. The choice of an appropriate method to evaluate the reliability is an important part of reliability analysis and depends on both the stochastic and the mechanical model [e.g., 110]. In addition, modeling uncertainties in the input parameters as random quantities can lead to interactions between the mechanical and stochastic model, thus increasing the complexity of the problem. Panel b of Figure 1.1 illustrates the key components of structural reliability analysis and their potential interactions. This thesis focuses on stochastic modeling and, to some extent, reliability methods, while mechanical modeling is not investigated in detail.

1.1 Outline

This thesis is split into two parts. Part I provides a summary over the developed methods and integrates them into the framework of reliability analysis in Chapter 2. To this end, Section 2.1 gives a short introduction into the basics of probability theory, Bayesian analysis and random fields. Subsequently, Section 2.2 formulates the problem of structural reliability and presents an overview of selected reliability methods including an assessment for different problem types, before concluding with a short insight into the effects of spatial variability on structural reliability. Afterwards, approaches for learning the stochastic model for material parameters are presented in Section 2.3, where two established methods for non-spatial learning are presented first, followed by a hierarchical approach for learning a random field model. A brief summary of the results and an outlook to potential future research are given in Chapter 3. Part II consists of four journal articles, where the conducted research is described in detail. Chapter 4 uses the available literature on spatial modeling of concrete properties with data and conducts the reliability analysis of a ship lock wall. Chapter 5 derives a framework for spatial modeling of material properties with data, which is further specified for application to concrete strength in Chapter 6, including two case studies of concrete ship lock walls. Thereafter, a random field discretization method is presented in chapter 7, which is particular useful to couple the resulting random field models from the previous chapters with a numerical model for reliability analysis.

1.2 Contribution

This thesis is mainly based on four journal articles, where each article forms one chapter of Part II. Sebastian Geyer is main author of these published or submitted journal articles, as listed in the following:

- Chapter 4 (original publication [64]): S. Geyer, I. Papaioannou, C. Kunz, and D. Straub. "Reliability assessment of large hydraulic structures with spatially distributed measurements". In: *Structure and Infrastructure Engineering* 16 (4 2020), pp. 599 – 612. DOI: 10.1080/15732479.2019.1652331.

- Chapter 5 (original publication [65]): S. Geyer, I. Papaioannou, and D. Straub. "Bayesian analysis of hierarchical random fields for material modeling". In: *Probabilistic Engineering Mechanics* 66 (2021), p. 103167. DOI: 10.1016/j.probengmech.2021.103167.

- Chapter 6 (original publication [68]): S. Geyer, I. Papaioannou, and D. Straub. "Spatial modeling of concrete strength based on data". In: *Structural Safety* 103 (2023), p. 102345. DOI: 10.1016/j.strusafe.2023.102345.

- Chapter 7 (original publication [63]): S. Geyer, I. Papaioannou, L. Graham-Brady, and D. Straub. "The spatial averaging method for non-homogeneous random fields with application to reliability analysis". In: *Engineering Structures* 235 (2022), p. 113761. DOI: 10.1016/j.engstruct.2021.113761.

In addition, developing efficient structural reliability methods and advertising their use in engineering practice have been part of the doctoral research, reflected in the (co-)authorship of three additional journal articles:

- Original publication [66]: S. Geyer, I. Papaioannou, and D. Straub. "Cross entropy-based importance sampling using Gaussian densities revisited". In: *Structural Safety* 76 (2019), pp. 15–27. DOI: 10.1016/j.strusafe.2018.07.001.

- Original publication [126]: I. Papaioannou, S. Geyer, and D. Straub. "Improved cross entropy-based importance sampling with a flexible mixture model". In: *Reliability Engineering & System Safety* 191 (2019), p. 106564. DOI: 10.1016/j.ress.2019.106564.

- Original publication [67]: S. Geyer, I. Papaioannou, and D. Straub. "Problemorientierte Auswahl und Durchführung von Zuverlässigkeitsanalysen [Problem-oriented reliability analysis]". In preparation (2023).

Although the above articles do not form the main part of this thesis, excerpts thereof are included in Section 2.2.

Chapter 2

Reliability analysis with spatially distributed measurements

2.1 Stochastic framework

The methods in the subsequent chapters are embedded into a stochastic framework, which requires basic concepts of probability theory, Bayesian statistics and random field theory. In addition, some important probability distributions are provided as a reference for the reader.

2.1.1 Basics of probability theory

This section introduces some important concepts of probability theory, which are required for understanding the subsequent chapters. However, it is not a general introduction to probability theory, for which the reader is referred to standard textbooks, such as [e.g., 93, 5].

2.1.1.1 Sample space and events

Consider the sample space $\mathcal{S}$, which is defined as collection of all possible outcomes of a random experiment. Any subset $A \subseteq \mathcal{S}$ is defined as an event corresponding to a set of points in the sample space $\mathcal{S}$. Given two events A_1 and A_2, the set of points belonging to at least one of the two sets is called the union of A_1 and A_2, denoted $A_1 \cup A_2$, and the set of points belonging to both sets is termed the intersection of A_1 and A_2, denoted $A_1 \cap A_2$. A_1 and A_2 are called mutually exclusive or disjoint, if $A_1 \cup A_2 = \emptyset$, where $\emptyset$ is the empty set. Further, A_1 and A_2 are termed collectively exhaustive, if $A_1 \cup A_2 = \mathcal{S}$. These basic operations and properties can be extended to the general case of n events $A_1, \ldots, A_n$.

The probability $P(A) \in [0, 1]$ defines the likelihood of occurrence of an event A that belongs to $\mathcal{S}$ and follows the Kolmogorov axioms [93]. Particularly, the conditional probability of A_1 given A_2 is given as

$$P(A_1|A_2) = \frac{P(A_1 \cap A_2)}{P(A_2)}. \tag{2.1}$$

A_1 and A_2 are said to be statistically independent if

$$P(A_1|A_2) = P(A_1), \tag{2.2}$$

in which case $P(A_1 \cap A_2) = P(A_1)P(A_2)$.

2.1.1.2 Random variables

A random variable (RV) is defined as a function that maps from $\mathcal{S}$ to the real numbers $\mathbb{R}$. For the remainder of this thesis, the standard notation for an RV is X and a random realization of X is denoted x. Depending on the definition, an RV can be either discrete, i.e., the set of possible outcomes is finite or countably infinite, or continuous. The focus of this thesis lies on continuous RVs and hence, the following definitions aim at continuous RVs without explicitly reflecting the discrete case.

RVs are characterized by their cumulative distribution function (CDF), which is defined for X as

$$F_X(x) = P(X \leq x), \tag{2.3}$$

which suffices to completely define X. $F_X(x)$ is a non-decreasing function such that

$$\lim_{x \to -\infty} F_X(x) = 0, \tag{2.4a}$$

$$\lim_{x \to \infty} F_X(x) = 1. \tag{2.4b}$$

If $F_X(x)$ is continuous, the probability density function (PDF) can be derived as

$$f_X(x) = \frac{\mathrm{d}F_X(x)}{\mathrm{d}x}. \tag{2.5}$$

Similarly to the CDF, the PDF is sufficient to completely specify an RV. Consequently, the CDF is obtained through integrating the PDF:

$$F_X(x) = \int_{-\infty}^{x} f_X(x)\mathrm{d}x. \tag{2.6}$$

An important operation is the mathematical expectation of any function $g(X)$ of the RV X, given as

$$\mathbb{E}[g(X)] = \int_{-\infty}^{\infty} g(X) f_X(x)\mathrm{d}x. \tag{2.7}$$

Using Equation (2.7), the mean value of X, μ_X, and its variance, $\mathbb{V}[X]$, are defined as follows:

$$\mu_X = \mathbb{E}[X] = \int_{-\infty}^{\infty} x f_X(x)\mathrm{d}x, \tag{2.8a}$$

$$\mathbb{V}[X] = \mathbb{E}\left[(X - \mu_X)^2\right] = \int_{-\infty}^{\infty} (X - \mu_X)^2 f_X(x)\mathrm{d}x. \tag{2.8b}$$

In addition, $\sigma_X = \sqrt{\mathbb{V}[X]}$ denotes the standard deviation of X. $\delta_X = \frac{\sigma_X}{|\mu_X|}$ is called the coefficient of variation (CoV) of X. μ_X is the first moment of X and $\mathbb{V}[X]$ is its second central moment. Higher-order moments can be calculated accordingly [e.g., 108].

2.1.2 Random vectors

A d-dimensional random vector $\boldsymbol{X} = [X_1, \ldots, X_d]$ is defined as function that maps from the sample space $\mathcal{S}$ to $\mathbb{R}^d$. The d components of $\boldsymbol{X}$ are single RVs.

2.1.2.1 The joint distribution

In analogy to the univariate case of a single RV, a random vector $\boldsymbol{X}$ is defined by its joint CDF:

$$F_{\boldsymbol{X}}(\boldsymbol{x}) = P(X_1 \leq x_1 \cap \cdots \cap X_d \leq x_d), \tag{2.9}$$

for which the following properties hold:

$$\lim_{x_i \to -\infty} F_{\boldsymbol{X}}(\boldsymbol{x}) = 0, \; i = 1, \ldots, d, \tag{2.10a}$$

$$\lim_{x_1 \to \infty, \ldots, x_d \to \infty} F_{\boldsymbol{X}}(\boldsymbol{x}) = 1. \tag{2.10b}$$

The corresponding joint PDF is obtained through differentiation of $F_{\boldsymbol{X}}(\boldsymbol{x})$:

$$f_{\boldsymbol{X}}(\boldsymbol{x}) = \frac{\partial^d F_{\boldsymbol{X}}(\boldsymbol{x})}{\partial x_1 \ldots \partial x_d}. \tag{2.11}$$

From the joint PDF, the marginal PDF of a single component of $\boldsymbol{X}$ is obtained through marginalization:

$$f_{X_i}(x_i) = \int_{-\infty}^{\infty} \ldots \int_{-\infty}^{\infty} f_{\boldsymbol{X}}(\boldsymbol{x}) \mathrm{d}x_1 \ldots \mathrm{d}x_{i-1} \mathrm{d}x_{i+1} \ldots \mathrm{d}x_d. \tag{2.12}$$

The joint PDF of any subset of the components in $\boldsymbol{X}$ can be calculated accordingly.

2.1.2.2 Dependent and independent random variables

The conditional PDF of X_1 given $X_2 = x_2$ is defined as

$$f_{X_1|X_2}(x_1|x_2) = \frac{f_{X_1,X_2}(x_1, x_2)}{f_{X_2}(x_2)}. \tag{2.13}$$

Two RVs X_1 and X_2 are said to be statistically independent, if

$$f_{X_1|X_2}(x_1|x_2) = f_{X_1}(x_1), \tag{2.14}$$

in which case the joint PDF is given as the product of the marginal PDFs:

$$f_{X_1,X_2}(x_1, x_2) = f_{X_1}(x_1) f_{X_2}(x_2). \tag{2.15}$$

Analogously, the joint PDF of d statistically independent RVs can be expressed as the product of the marginal PDFs.

By extending Equation (2.7) to the 2-dimensional case, the covariance of X_1 and X_2 can be calculated as the mathematical expectation of the function $g(X_1, X_2) = (X_1 - \mu_{X_1})(X_2 - \mu_{X_2})$:

$$\mathbb{C}\mathrm{ov}\,[X_1, X_2] = \mathbb{E}[(X_1 - \mu_{X_1})(X_2 - \mu_{X_2})] = \int_{-\infty}^{\infty} \int_{-\infty}^{\infty} (X_1 - \mu_{X_1})(X_2 - \mu_{X_2}) f_{X_1,X_2}(x_1, x_2) \mathrm{d}x_1 \mathrm{d}x_2. \tag{2.16}$$

Normalizing the covariance with the individual standard deviations yields the correlation coefficient:

$$\rho_{X_1,X_2} = \frac{\mathbb{C}\mathrm{ov}\left[X_1, X_2\right]}{\sigma_{X_1}\sigma_{X_2}},\ \rho_{X_1,X_2} \in [-1, 1]. \tag{2.17}$$

ρ_{X_1,X_2} is a measure for the linear dependency between two RVs. If $\rho_{X_1,X_2} = 0$, X_1 and X_2 are uncorrelated RVs. Note that uncorrelated RVs are not necessarily independent, but correlated RVs are never independent. For $X_1 = X_2$, Equation (2.16) reduces to Equation (2.8b) and, as a direct consequence, $\rho_{X_1,X_1} = 1$.

2.1.2.3 Transformation of random vectors

Consider a random vector $\boldsymbol{X}$ and an injective set of functions $g_1, \ldots, g_d$, such that

$$Y_i = g(\boldsymbol{X}),\ i = 1, \ldots, d. \tag{2.18}$$

Then, the joint PDF of the vector of transformed RVs $\boldsymbol{Y} = [Y_1, \ldots, Y_d]$ is given by [e.g., 58, 113]

$$f_{\boldsymbol{Y}}(\boldsymbol{y}) = f_{\boldsymbol{X}}(\boldsymbol{x})\left|\det(\mathbf{J})_{\boldsymbol{x},\boldsymbol{y}}\right|, \tag{2.19}$$

where $\mathbf{J}$ is the $d \times d$ Jacobian matrix of the transformation with entry $J(i, j)$ defined as follows:

$$J(i, j) = \frac{\partial x_i}{\partial y_i}. \tag{2.20}$$

If at least one of the d functions is not injective, one has to account for all possible combinations of roots of Equation (2.18), which will not be further discussed.

2.1.3 Important probability distributions

Some important probability distributions that are used in this thesis are briefly described in this section. A detailed overview of a large number of continuous probability distributions can be found in [86] and [87].

2.1.3.1 Normal distribution

The normal or Gaussian distribution is one of the most important, if not the most important, probability distributions in statistics and engineering. A Gaussian RV X is completely defined by two parameters, the mean $\mu = \mathbb{E}[X]$ and the standard deviation $\sigma = \sqrt{\mathbb{V}[X]}$, and is denoted $X \sim \mathcal{N}(\mu, \sigma)$. The corresponding PDF of X is as follows [e.g., 5]:

$$f_X(x) = \frac{1}{\sigma\sqrt{2\pi}}\exp\left(-\frac{(x-\mu)^2}{2\sigma^2}\right),\ x \in (-\infty, \infty). \tag{2.21}$$

The special case of $\mu = 0$ and $\sigma = 1$ results in the standard normal distribution. The PDF of a standard normal distributed RV U is

$$f_U(u) = \varphi(u) = \frac{1}{\sqrt{2\pi}}\exp\left(-\frac{u^2}{2}\right),\ u \in (-\infty, \infty). \tag{2.22}$$

Through the linear transformation $U = \frac{X-\mu}{\sigma}$, the PDF of any Gaussian RV can be expressed in terms of $\varphi(u)$.

The CDF of X is given by

$$F_X(x) = \Phi\left(\frac{X-\mu}{\sigma}\right), \tag{2.23}$$

where $\Phi(\cdot)$ is the CDF of the standard normal distribution:

$$\Phi(u) = \int_{-\infty}^{u} \varphi(z)\mathrm{d}z. \tag{2.24}$$

The function $\Phi(\cdot)$ cannot be found analytically and needs to be evaluated numerically; standardized tables thereof can be found in almost every statistical textbook [e.g., 5, 15, 113]. The PDF and CDF of the standard normal distribution are illustrated in Figure 2.1.

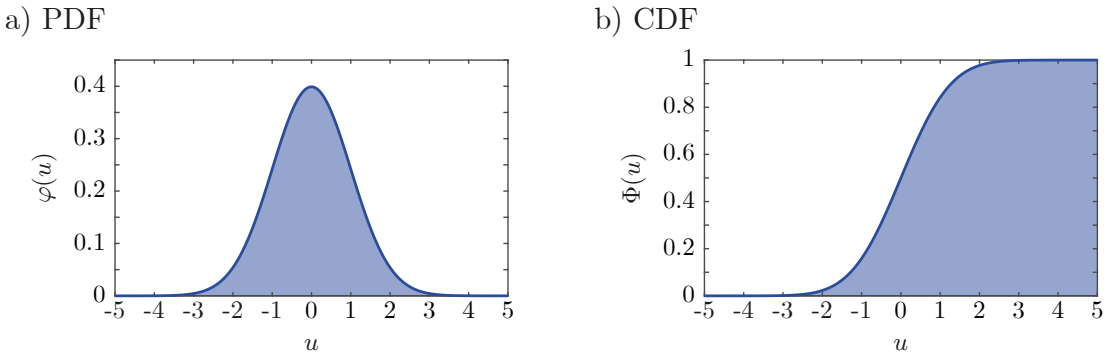

Figure 2.1: PDF $\varphi(u)$ (panel a) and CDF $\Phi(u)$ (panel b) of the standard normal distribution.

The normal distribution is often used to model uncertain quantities. One of the reasons why it is a good fit for many quantities is the central limit theorem, which states that an RV X that is defined as the sum of a large number of RVs is approximately normal distributed under certain conditions on the joint distribution of the RVs entering the sum (the conditions are fulfilled if the RVs are independent and identically distributed) [108].

2.1.3.2 Multivariate normal distribution

The joint distribution of d Gaussian RVs is the multivariate Gaussian distribution. A d-dimensional Gaussian random vector $\boldsymbol{X} = [X_1, \ldots, X_d]$, denoted $\boldsymbol{X} \sim \mathcal{N}(\boldsymbol{\mu}, \boldsymbol{\Sigma})$, has the following joint PDF [e.g., 153]:

$$f_{\boldsymbol{X}}(\boldsymbol{x}) = \frac{1}{(2\pi)^{\frac{d}{2}}\det(\boldsymbol{\Sigma})^{\frac{1}{2}}}\exp\left(-\frac{1}{2}(\boldsymbol{x}-\boldsymbol{\mu})\boldsymbol{\Sigma}^{-1}(\boldsymbol{x}-\boldsymbol{\mu})^{\mathsf{T}}\right), \tag{2.25}$$

where $\boldsymbol{\mu} = [\mu_1, \ldots, \mu_d]$ is the mean vector and $\boldsymbol{\Sigma}$ is the $d \times d$ covariance matrix with entry $\Sigma(i,j)$ defined as $\sigma_{X_i}\sigma_{X_j}\rho_{X_i,X_j}$. There, σ_{X_i} and σ_{X_j} are the standard deviations of the ith and jth Gaussian RV, respectively, and ρ_{X_i,X_j} is their correlation coefficient. The entries on the main diagonal of $\boldsymbol{\Sigma}$ are the individual variances of the RVs. If $\rho_{X_i,X_j} = 0$, X_i and X_j are not only uncorrelated but also independent, since the multivariate normal distribution can only capture linear dependency. The joint distribution of any subset of $\boldsymbol{X}$ is a multivariate Gaussian distribution [e.g., 18]. The multivariate normal distribution remains closed under linear transformations, i.e., any linear mapping of a Gaussian random vector results in a Gaussian random vector [102].

If the random vector $\boldsymbol{U} = [U_1, \ldots, U_d]$ is jointly Gaussian with $\boldsymbol{\mu} = \boldsymbol{0}_d$, i.e., a d-dimensional vector of zeros and $\boldsymbol{\Sigma} = \mathbf{I}$, i.e., the $d \times d$ identity matrix, the random variables in $\boldsymbol{U}$ are

independent standard normal random variables with joint PDF $\varphi_d(\boldsymbol{u})$:

$$\varphi_d(\boldsymbol{u}) = \frac{1}{(2\pi)^{\frac{d}{2}}} \exp\left(-\frac{1}{2}\boldsymbol{u}\boldsymbol{u}^{\mathsf{T}}\right). \tag{2.26}$$

The corresponding d-dimensional probability space is denoted $\boldsymbol{U}$-space. Figure 2.2 shows $\varphi_2(\boldsymbol{u})$ from a diagonal view (panel a) and from a top view (panel b) to show the rotational symmetry with respect to its mean, which in this case is the origin.

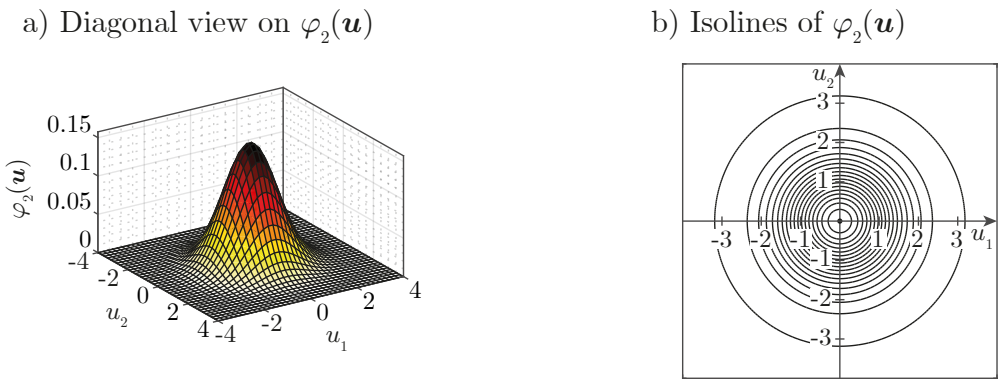

Figure 2.2: PDF of the bivariate independent standard Gaussian distribution $\varphi_2(\boldsymbol{u})$ from a diagonal view (panel a) and a top view (panel b).

2.1.3.3 Lognormal distribution

Consider an RV X, where $X \sim \mathcal{N}(\mu_X, \sigma_X)$. Then, $Y = \exp(X)$ follows the lognormal distribution with parameters $\mu_{\ln Y} = \mu_X$ and $\sigma_{\ln Y} = \sigma_X$, i.e., Y is parameterized in terms of the mean and standard deviation of the underlying normal distribution. The PDF of Y is

$$f_Y(y) = \frac{1}{y\sigma_{\ln Y}\sqrt{2\pi}} \exp\left(-\frac{(\ln(y) - \mu_{\ln Y})^2}{2\sigma_{\ln Y}^2}\right), \; y \in (0, \infty). \tag{2.27}$$

The CDF of Y is given in terms of the standard normal CDF:

$$F_Y(y) = \Phi\left(\frac{\ln(y) - \mu_{\ln Y}}{\sigma_{\ln Y}}\right). \tag{2.28}$$

The mean and variance of Y are given as [e.g., 15]

$$\mathbb{E}[Y] = \exp\left(\mu_{\ln Y} + \frac{\sigma_{\ln Y}^2}{2}\right), \tag{2.29a}$$

$$\mathbb{V}[Y] = \exp\left(2\mu_{\ln Y} + \sigma_{\ln Y}^2\right)\left(\exp\left(\sigma_{\ln Y}^2\right) - 1\right). \tag{2.29b}$$

The PDF and CDF of the lognormal distribution with parameters $\mu_{\ln Y} = 0$ and $\sigma_{\ln Y} = 1$ are illustrated in Figure 2.3.

The lognormal distribution is often used for modeling non-negative quantities, such as physical parameters (e.g., material properties).

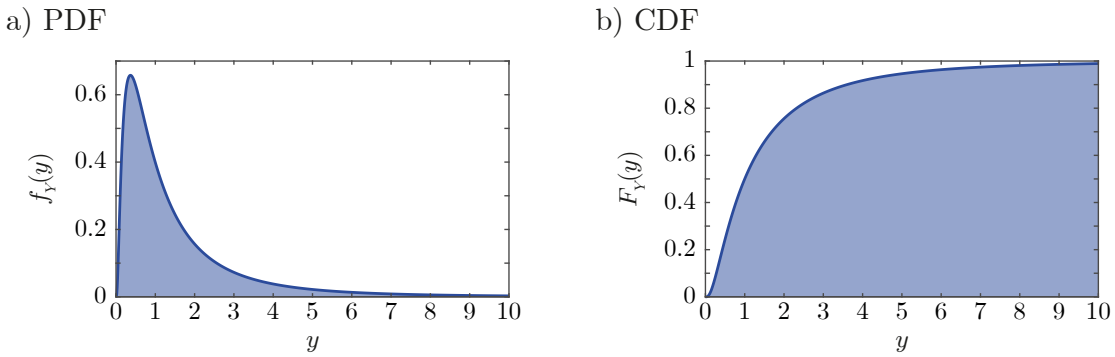

Figure 2.3: PDF $f_Y(y)$ (panel a) and CDF $F_Y(y)$ (panel b) of the lognormal distribution with parameters $\mu_{\ln Y} = 0$ and $\sigma_{\ln Y} = 1$.

2.1.3.4 Student's t-distribution

The Student's t-distribution was developed by William Sealy Gosset, an English statistician and chemist who worked for the Guinness brewery in Dublin, Ireland, where he was confronted with the problem of estimating the mean of a population from a small sample size [156]. The distribution's name stems from the fact that Gosset had to publish under a pseudonym to hide his identity and he chose the name "Student" [166].

If X follows the Student's t-distribution with parameters μ_t, λ_t and ν_t (denoted $X \sim \mathcal{T}(\mu_t, \lambda_t, \nu_t)$), its PDF is defined as [e.g., 18]

$$f_t(x) = \frac{\Gamma\left(\frac{\nu_t}{2} + \frac{1}{2}\right)}{\Gamma\left(\frac{\nu_t}{2}\right)} \left(\frac{\lambda_t}{\pi\nu_t}\right)^{\frac{1}{2}} \left(1 + \frac{\lambda_t(x-\mu_t)^2}{\nu_t}\right)^{-\frac{\nu_t}{2}-\frac{1}{2}}, \tag{2.30}$$

where $\Gamma(\cdot)$ denotes the gamma function, μ_t and λ_t are the location and scale parameter, respectively, and ν_t are the degrees of freedom. The corresponding CDF is

$$F_t(x) = F_{U_t}\left((x-\mu_t)\lambda_t^{\frac{1}{2}}\right), \tag{2.31}$$

where $F_{U_t}(\cdot)$ is the CDF of the standard Student's t-distribution, i.e., the Student's t-distribution with $\mu_t = 0$, $\lambda_t = 1$ and ν_t degrees of freedom, given by [87]

$$F_{U_t}(u_t) = 1 - \frac{1}{2}\mathcal{I}_{\frac{\nu_t}{u_t^2+\nu_t}}\left(\frac{\nu_t}{2}, \frac{1}{2}\right), \; u \in (0, \infty). \tag{2.32}$$

$\mathcal{I}_{\frac{\nu_t}{u_t^2+\nu_t}}\left(\frac{\nu_t}{2}, \frac{1}{2}\right)$ denotes the CDF of the beta distribution with parameters $\frac{\nu_t}{2}$ and $\frac{1}{2}$ evaluated at $\frac{\nu_t}{u_t^2+\nu_t}$, also known as the regularized incomplete beta function [87, 135].

The mean and variance of X following the Student's t-distribution are given as [e.g., 18]

$$\mathbb{E}[X] = \mu_t, \text{ for } \nu_t > 1, \tag{2.33a}$$

$$\mathbb{V}[X] = \frac{1}{\lambda_t}\frac{\nu_t}{\nu_t - 2}, \text{ for } \nu_t > 2. \tag{2.33b}$$

Note that the kth moment (and all higher-order moments) of the Student's t-distribution is infinite, if $k \geq \nu_t$ [87]. The special case of $\nu_t = 1$ is known as the Cauchy distribution [86], and for $\nu_t \to \infty$, the Student's t-distribution converges to the normal distribution with mean μ_t and variance λ_t^{-1} [87].

Figure 2.4 shows the PDF and CDF of the standard Student's t-distribution with varying degrees of freedom ν_t, illustrating the convergence to the standard normal distribution with increasing ν_t.

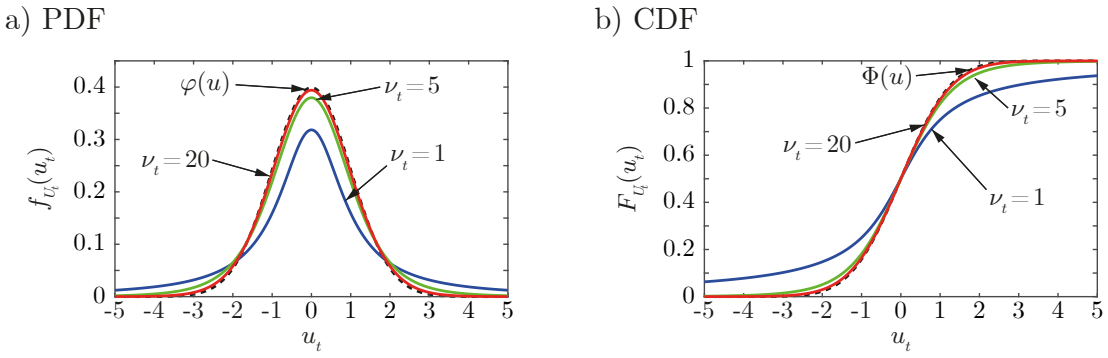

Figure 2.4: PDF $f_{U_t}(u_t)$ (panel a) and CDF $F_{U_t}(u_t)$ (panel b) of the standard Student's t-distribution with $\nu_t = 1$ (blue lines), $\nu_t = 5$ (green lines) and $\nu_t = 20$ (red lines) degrees of freedom compared to the PDF and CDF, respectively of the standard normal distribution (dashed black lines).

The Student's t-distribution can be used, for example, to estimate confidence intervals for the mean of a Gaussian distribution [87], or in Bayesian statistics, where it arises as predictive distribution for Gaussian RVs with unknown parameters [61].

2.1.3.5 Log-Student's t-distribution

The relation between the log-Student's t-distribution and the Student's t-distribution is similar to the relation between the lognormal and the Gaussian distribution, i.e., if $X \sim \mathcal{T}(\mu_t, \lambda_t, \nu_t)$, $Y = \exp(X)$ follows a log-Student's t-distribution with parameters $\mu_{\ln t} = \mu_t$, $\lambda_{\ln t} = \lambda_t$ and $\nu_{\ln t} = \nu_t$, i.e., the parameterization is done in terms of the underlying Student's t-distribution. The corresponding PDF of Y is [65]

$$f_{\ln t}(y) = \frac{1}{y} \frac{\Gamma\left(\frac{\nu_{\ln t}}{2} + \frac{1}{2}\right)}{\Gamma\left(\frac{\nu_{\ln t}}{2}\right)} \left(\frac{\lambda_{\ln t}}{\pi \nu_{\ln t}}\right)^{\frac{1}{2}} \left(1 + \frac{\lambda_{\ln t}(\ln(y) - \mu_{\ln t})^2}{\nu_{\ln t}}\right)^{-\frac{\nu_{\ln t}}{2} - \frac{1}{2}}, \quad y \in (0, \infty), \tag{2.34}$$

where $\Gamma(\cdot)$ is the gamma function. The CDF of Y is given in terms of the CDF of the underlying Student's t-distribution [160, 65]:

$$F_{\ln t}(y) = F_t(\ln(y)). \tag{2.35}$$

For a finite value of $\nu_{\ln t}$, the log-Student's t-distribution does not have mean and variance, as it does not possess finite moments of any order [65]. For $\nu_{\ln t} \to \infty$, the log-Student's t-distribution converges to the lognormal distribution with finite mean and variance.

Figure 2.5 shows the PDF and CDF of the log-Student's t-distribution with parameters $\mu_{\ln t} = 0$, $\lambda_{\ln t} = 1$ and varying degrees of freedom ν_t, and compares it to the lognormal distribution ($\nu_t \to \infty$) with parameters $\mu_{\ln Y} = 0$ and $\sigma_{\ln Y} = 1$.

Applications of the log-Student's t-distribution can be found in the field of finance for the pricing of options [28, 27], or in Bayesian statistics as predictive distribution for lognormal random fields with unknown parameters [65].

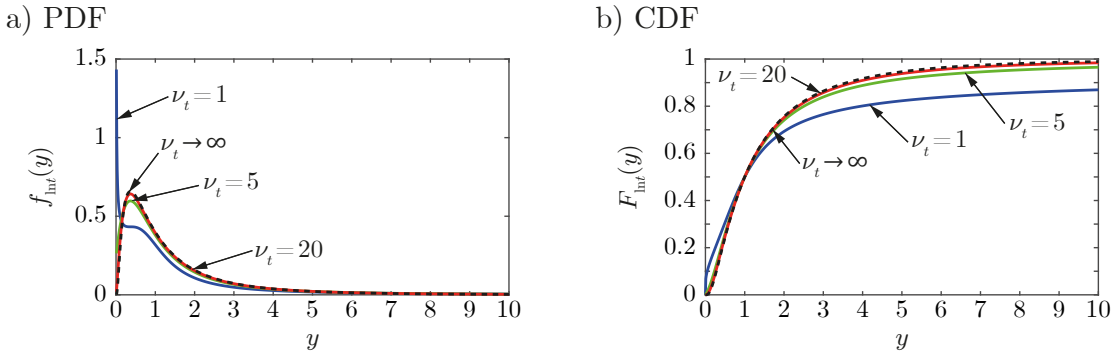

Figure 2.5: PDF $f_{\ln t}(y)$ (panel a) and CDF $F_{\ln t}(y)$ (panel b) of the log-Student's t-distribution with parameters $\mu_{\ln t} = 0$, $\lambda_{\ln t} = 1$ and $\nu_t = 1$ (blue lines), $\nu_t = 5$ (green lines), $\nu_t = 20$ (red lines) degrees of freedom compared to the PDF and CDF, respectively of the lognormal distribution with parameters $\mu_{\ln Y} = 0$ and $\sigma_{\ln Y} = 1$ (dashed black lines).

2.1.3.6 Normal-gamma distribution

The normal-gamma ($\mathcal{NG}$) distribution is a bivariate distribution used to model uncertainty on the parameters of a Gaussian RV X in the context of a Bayesian analysis [61]. More specifically, it is assumed that the mean μ_X is a Gaussian RV itself and the precision $\lambda_X = \sigma_X^{-2}$ follows the gamma distribution. The joint PDF of μ_X and λ_X is given as [e.g., 140]

$$f(\mu_X, \lambda_X) = \mathcal{C}\lambda_X^{\alpha-\frac{1}{2}} \exp\left(-\lambda_X\left(\frac{\kappa}{2}(\mu_X - \mu)^2 + \beta\right)\right), \ \mu_X \in (-\infty, \infty), \ \lambda_X \in (0, \infty). \tag{2.36}$$

α and β are the shape and rate parameter of the Gamma distribution, respectively. μ and $\kappa\lambda_X$ are the mean and precision of the normal distribution, respectively, where the coefficient κ is a concentration parameter. $\Gamma(\cdot)$ is the gamma function and $\mathcal{C}$ is a normalizing constant:

$$\mathcal{C} = \frac{\beta^\alpha \kappa^{\frac{1}{2}}}{\Gamma(\alpha)(2\pi)^{\frac{1}{2}}}. \tag{2.37}$$

The joint PDF in Equation (2.36) implies a dependency between μ_X and λ_X, since μ_X is defined conditional on λ_X ($\mu_X \sim \mathcal{N}(\mu, (\kappa\lambda_X)^{-\frac{1}{2}})$).

2.1.3.7 χ^2-distribution

A random variable X that follows the χ^2-distribution has the following PDF [86]:

$$f_{\chi^2}(x) = \frac{1}{2^{\frac{\nu_\chi}{2}}\Gamma\left(\frac{\nu_\chi}{2}\right)} x^{\frac{\nu_\chi}{2}-1} \exp\left(-\frac{x}{2}\right), x \in (0, \infty) \tag{2.38}$$

where ν_χ are the degrees of freedom of the χ^2-distribution. The corresponding CDF is defined as

$$F_{\chi^2}(x) = \frac{1}{\Gamma\left(\frac{\nu_\chi}{2}\right)} \gamma\left(\frac{\nu_\chi}{2}, \frac{x}{2}\right), \tag{2.39}$$

where $\gamma(\cdot, \cdot)$ denotes the incomplete gamma function [135]. The mean and variance of the χ^2-distribution are given as follows [86]:

$$\mathbb{E}[X] = \nu_\chi, \tag{2.40a}$$

$$\mathbb{V}[X] = 2\nu_\chi. \tag{2.40b}$$

2.1.3.8 Uniform distribution

The uniform distribution is characterized by a constant PDF over an interval of certain length [5]:

$$f_X(x) = \begin{cases} \frac{1}{b-a}, & \text{for } x \in [a,b], \\ 0, & \text{else}, \end{cases} \tag{2.41}$$

where a and b denote the lower and upper bound of the interval of definition of X. The CDF of the uniform distribution is

$$F_X(x) = \begin{cases} 0, & \text{for } x < a, \\ \frac{x-a}{b-a}, & \text{for } x \in [a,b), \\ 1, & \text{for } x \geq b, \end{cases} \tag{2.42}$$

The corresponding mean and variance are

$$\mathbb{E}[X] = \frac{a+b}{2}, \tag{2.43a}$$

$$\mathbb{V}[X] = \frac{(b-a)^2}{12}. \tag{2.43b}$$

2.1.4 Transformation to U-space

Any RV X with strictly monotonous increasing CDF $F_X(x)$ can be transformed to a standard normal random variable U by means of the following isoprobabilistic transformation [e.g., 79]:

$$U = \Phi^{-1}(F_X(x)), \tag{2.44}$$

where $\Phi^{-1}(\cdot)$ is the inverse standard normal CDF. Equation (2.44) is invertible, i.e., $X = F_X^{-1}(\Phi(u))$.

When using random vectors, it is often beneficial to transform the random vector $\boldsymbol{X}$ to a vector of uncorrelated standard normal random variables $\boldsymbol{U}$. Such procedure is called transformation from the original space to $\boldsymbol{U}$-space or simply from $\boldsymbol{X}$ to $\boldsymbol{U}$ in the following. It can be defined by means of the Nataf joint distribution model, which requires the marginal distributions $F_{X_i}(x_i),\ i = 1, \ldots, d$ and the $d \times d$ correlation matrix $\mathbf{R}_{\boldsymbol{X}}$ with entry $R_{i,j}$ given as ρ_{X_i,X_j} [119]. It has been shown that the Nataf model is equivalent to the choice of a Gaussian copula for modeling the joint distribution of $\boldsymbol{X}$ [100]. The procedure is described in the following.

Consider the random vector $\boldsymbol{Z} = [Z_1, \ldots, Z_d]$, obtained from $\boldsymbol{X}$ through the following set of marginal isoprobabilistic transformations:

$$Z_i = \Phi^{-1}(F_{X_i}(x_i)),\ i = 1, \ldots, d. \tag{2.45}$$

The Nataf model assumes that $\boldsymbol{Z}$ is jointly normal with mean vector $\boldsymbol{\mu_Z} = \mathbf{0}$ and covariance matrix $\boldsymbol{\Sigma_Z} = \mathbf{R_Z}$, where $\mathbf{R_Z}$ is the correlation matrix, i.e., $\boldsymbol{Z}$ is a vector of dependent standard normal RVs [104]. Using Equations (2.19) and (2.44), the Nataf joint PDF of $\boldsymbol{X}$ can be calculated from the joint PDF of $\boldsymbol{Z}$. The elements in $\mathbf{R_Z}$, ρ_{Z_i,Z_j}, are related to the corresponding element

in $\mathbf{R}_{\boldsymbol{X}}$ through the following integral equation [104]:

$$\rho_{X_i,X_j} = \int_{-\infty}^{\infty}\int_{-\infty}^{\infty}\left(\frac{x_i-\mu_{X_i}}{\sigma_{X_i}}\right)\left(\frac{x_j-\mu_{X_j}}{\sigma_{X_j}}\right)\varphi_{2,\rho_{Z_i,Z_j}}(z_i,z_j), \tag{2.46}$$

where $\varphi_{2,\rho_{Z_i,Z_j}}(\cdot,\cdot)$ denotes the bivariate standard normal PDF with correlation coefficient ρ_{Z_i,Z_j}. The relation in Equation (2.46) is implicit in ρ_{Z_i,Z_j} and can thus be solved iteratively to find ρ_{Z_i,Z_j}.

The random vector $\boldsymbol{Z}$ is transformed to a vector $\boldsymbol{U}$ of independent standard normal random variables through

$$\boldsymbol{U} = \mathbf{A}^{-1}\boldsymbol{Z}, \tag{2.47}$$

where $\mathbf{A}$ is the lower triangular matrix obtained from the Cholesky decomposition of $\mathbf{R}_{\boldsymbol{Z}}$, i.e., $\mathbf{R}_{\boldsymbol{Z}} = \mathbf{A}\mathbf{A}^{\mathsf{T}}$. The transformation is invertible and thus, once $\mathbf{R}_{\boldsymbol{Z}}$ is determined, the transformation from $\boldsymbol{X}$ to $\boldsymbol{U}$ and vice versa is straightforward to apply.

The Nataf model is only applicable if $\mathbf{R}_{\boldsymbol{Z}}$ is a positive definite matrix, which is not always the case, even if $\mathbf{R}_{\boldsymbol{X}}$ fulfills this criterion [104].

An alternative approach for the transformation to $\boldsymbol{U}$-space is given by the Rosenblatt transformation, in which the joint PDF of $\boldsymbol{X}$ is constructed using the conditional PDFs of the entries in $\boldsymbol{X}$ [143, 79].

2.1.5 Bayesian analysis

Bayesian analysis summarizes a methodological framework to combine data of some sort (e.g., observations, measurements) with a probabilistic model in a way that the output is again a probabilistic model. The basic principle of all methods in Bayesian analysis is the application of Bayes' rule [e.g., 61]:

$$f(\boldsymbol{\theta}|\mathbf{M}) = \frac{f(\boldsymbol{\theta})\mathrm{L}(\boldsymbol{\theta}|\mathbf{M})}{f(\mathbf{M})}, \tag{2.48}$$

where $\boldsymbol{\theta}$ is a realization of the parameter vector $\boldsymbol{\Theta}$ of uncertain parameters and $\mathbf{M}$ accounts for the data. In the context of Bayesian analysis, $f(\boldsymbol{\theta})$ is called the prior PDF of $\boldsymbol{\Theta}$, i.e., the PDF corresponding to the probability distribution of $\boldsymbol{\Theta}$ before $\mathbf{M}$ is included in the model. $\mathrm{L}(\boldsymbol{\theta}|\mathbf{M})$ is the likelihood function, which summarizes the information from the data $\mathbf{M}$. It is defined as the joint PDF of $\mathbf{M}$ conditional on $\boldsymbol{\theta}$, i.e., $\mathrm{L}(\boldsymbol{\theta}|\mathbf{M}) = f(\mathbf{M}|\boldsymbol{\theta})$. Moreover, $f(\boldsymbol{\theta}|\mathbf{M})$ is called the posterior PDF of $\boldsymbol{\Theta}$, i.e., the PDF of $\boldsymbol{\Theta}$ conditional on the information from $\mathbf{M}$. $f(\mathbf{M})$ is called evidence and forms the normalization constant of $f(\boldsymbol{\theta}|\mathbf{M})$. It is defined as $f(\mathbf{M}) = \int_{\boldsymbol{\Theta}} f(\boldsymbol{\theta})\mathrm{L}(\boldsymbol{\theta}|\mathbf{M})\mathrm{d}\boldsymbol{\theta}$. Since the denominator in Equation (2.48) is independent of $\boldsymbol{\Theta}$, the following yields the unnormalized posterior density [61]:

$$f(\boldsymbol{\theta}|\mathbf{M}) \propto f(\boldsymbol{\theta})\mathrm{L}(\boldsymbol{\theta}|\mathbf{M}). \tag{2.49}$$

At this point, only some basic Bayesian concepts are introduced, the reader is referred to [142] or [61] for a more detailed introduction.

2.1.5.1 Predictive distribution

Consider an uncertain but observable quantity X with PDF $f(x)$, where $\boldsymbol{\Theta}$ are the unknown parameters of $f(x)$ with prior distribution $f(\boldsymbol{\theta})$. In addition, information on X is available in the data set $\mathbf{M}$, e.g., in form of n direct measurements of X, i.e., $\mathbf{M} = [x_1, \ldots, x_n]$. Then, $f(\boldsymbol{\theta}|\mathbf{M})$ can be determined by means of Equation (2.48) and, consequently, the posterior predictive

distribution of X can be calculated as [61]

$$f(x|\mathbf{M}) = \int_{\boldsymbol{\Theta}} f(x|\boldsymbol{\theta}) f(\boldsymbol{\theta}|\mathbf{M}) \mathrm{d}\boldsymbol{\theta}. \tag{2.50}$$

Hence, $f(x|\mathbf{M})$ can be used for predicting X accounting for the uncertainty in the parameters of $f(x)$ and using the information from $\mathbf{M}$. Equation (2.50) can be interpreted as marginalization of the joint PDF of X and $\boldsymbol{\Theta}$ conditional on $\mathbf{M}$. Following the same logic, X can be predicted without accounting for $\mathbf{M}$, by defining the prior predictive distribution:

$$f(x) = \int_{\boldsymbol{\Theta}} f(x|\boldsymbol{\theta}) f(\boldsymbol{\theta}) \mathrm{d}\boldsymbol{\theta}. \tag{2.51}$$

2.1.5.2 Conjugate priors

In the general case, Equation (2.48) needs to be solved numerically, e.g., by means of Markov chain Monte Carlo (MCMC) methods [e.g., 23]. However, analytical expressions are available for the class of conjugate priors [140]. If the posterior distribution has the same parametric form as the prior distribution, the prior distribution is called conjugate prior for the given likelihood function and the solution of Equation (2.48) reduces to an update of the parameter vector $\boldsymbol{\Theta}$. Conjugate priors can be found for distributions that belong to the exponential family of distributions [11]. Examples for conjugate priors are a Gamma prior distribution in conjunction with a Poisson likelihood and the self-conjugate Gaussian distribution, where both prior distribution and likelihood are Gaussian, among others [e.g., 142].

2.1.5.3 Conditional Gaussian distribution

Consider a d-dimensional Gaussian random vector $\boldsymbol{X} = [X_1, \ldots, X_d]$ with mean vector $\boldsymbol{\mu}_{\boldsymbol{X}}$ and covariance matrix $\boldsymbol{\Sigma}_{\boldsymbol{X}}$:

$$\boldsymbol{X} \sim \mathcal{N}(\boldsymbol{\mu}_{\boldsymbol{X}}, \boldsymbol{\Sigma}_{\boldsymbol{X}}). \tag{2.52}$$

$\boldsymbol{X}$ can be partitioned into two random vectors $\boldsymbol{X}_1$ and $\boldsymbol{X}_2$, such that

$$\boldsymbol{X} = [\boldsymbol{X}_1 \ \boldsymbol{X}_2], \tag{2.53}$$

where $\boldsymbol{X}_1 = [X_{1,1}, \ldots, X_{1,d_1}]$, $\boldsymbol{X}_2 = [X_{2,1}, \ldots, X_{2,d_2}]$, and $d_1 + d_2 = d$. The corresponding partitions of $\boldsymbol{\mu}_{\boldsymbol{X}}$ and $\boldsymbol{\Sigma}_{\boldsymbol{X}}$ are given by

$$\boldsymbol{\mu}_{\boldsymbol{X}} = [\boldsymbol{\mu}_{\boldsymbol{X}_1} \ \boldsymbol{\mu}_{\boldsymbol{X}_2}], \tag{2.54a}$$

$$\boldsymbol{\Sigma}_{\boldsymbol{X}} = \begin{bmatrix} \boldsymbol{\Sigma}_{\boldsymbol{X}_{11}} & \boldsymbol{\Sigma}_{\boldsymbol{X}_{12}} \\ \boldsymbol{\Sigma}_{\boldsymbol{X}_{21}} & \boldsymbol{\Sigma}_{\boldsymbol{X}_{22}} \end{bmatrix}. \tag{2.54b}$$

It holds that $\boldsymbol{X}_1 \sim \mathcal{N}(\boldsymbol{\mu}_{\boldsymbol{X}_1}, \boldsymbol{\Sigma}_{\boldsymbol{X}_{11}})$, $\boldsymbol{X}_2 \sim \mathcal{N}(\boldsymbol{\mu}_{\boldsymbol{X}_2}, \boldsymbol{\Sigma}_{\boldsymbol{X}_{22}})$ (cf. Section 2.1.3.2) and, due to the symmetry of the covariance matrix, $\boldsymbol{\Sigma}_{\boldsymbol{X}_{12}}^{\mathsf{T}} = \boldsymbol{\Sigma}_{\boldsymbol{X}_{21}}$.

Using Bayes' rule, this partitioning of $\boldsymbol{X}$ can be used to derive updating rules for the distribution of $\boldsymbol{X}_1$ conditional on $\boldsymbol{X}_2$. The resulting parameters of the conditional Gaussian distribution are given by [e.g., 18]

$$\boldsymbol{\mu}_{\boldsymbol{X}_1|\boldsymbol{X}_2} = \boldsymbol{\mu}_{\boldsymbol{X}_1} + \boldsymbol{\Sigma}_{\boldsymbol{X}_{12}} \boldsymbol{\Sigma}_{\boldsymbol{X}_{22}}^{-1} (\boldsymbol{x}_2 - \boldsymbol{\mu}_{\boldsymbol{X}_2})^{\mathsf{T}}, \tag{2.55a}$$

$$\boldsymbol{\Sigma}_{\boldsymbol{X}_1|\boldsymbol{X}_2} = \boldsymbol{\Sigma}_{\boldsymbol{X}_{11}} - \boldsymbol{\Sigma}_{\boldsymbol{X}_{12}} \boldsymbol{\Sigma}_{\boldsymbol{X}_{22}}^{-1} \boldsymbol{\Sigma}_{\boldsymbol{X}_{21}}, \tag{2.55b}$$

where $\boldsymbol{x}_2$ is a realization of $\boldsymbol{X}_2$.

These updating rules for the conditional Gaussian distribution are widely used in practice, e.g., in the field of geostatistics [154, 10], Gaussian process regression [141] or random field updating [e.g., 129, 158, 64], among others.

2.1.6 Random fields

Modeling uncertainties with RVs can be insufficient in applications where the uncertain parameters vary randomly in time or space. Such uncertainties can be accounted for by modeling them as random processes or random fields, where the first one refers to the one-dimensional case and the latter one to the general d-dimensional case. A temporally variable stochastic process is a one-dimensional random field defined on an unbounded parameter space. Hence, the definitions, concepts and methods described in the following for random fields are directly applicable for spatial and temporal variability. For a detailed introduction to spatial variability and random fields, the reader is referred to [112] or [161].

2.1.6.1 Basic definitions

A random field (RF) $X(\boldsymbol{z})$ is defined as a collection of RVs indexed by a spatial coordinate $\boldsymbol{z} \in \Omega$, where $\Omega \subset \mathbb{R}^d$ is a d-dimensional spatial domain of definition [161]. For typical engineering applications, $d = 1,\ 2$ or 3, but the concept of RFs can be extended to the general d-dimensional case. For any $\boldsymbol{z} \in \Omega$, the RF reduces to an RV, i.e., the RF represents an RV at every spatial location in the domain of definition. Panel a of Figure 2.6 illustrates three independent realizations $x_1(z),\ x_2(z)$ and $x_3(z)$ of a one-dimensional RF $X(\boldsymbol{z})$. The realizations at locations z_1 and z_2 and the marginal distributions of the RVs corresponding to these locations (in this case Gaussian distributions) are illustrated in panel b and c of Figure 2.6. Two independent realizations $x_1(\boldsymbol{z})$ and $x_2(\boldsymbol{z})$ of a two-dimensional RF $X(\boldsymbol{z})$ are illustrated as surface plots in panel a of Figure 2.7, together with the corresponding projections to the plane. Two locations $\boldsymbol{z}_1 = [z_{1,1}\ z_{2,1}]$ and $\boldsymbol{z}_2 = [z_{1,2}\ z_{2,2}]$ are chosen and the corresponding realizations (green and blue dots) are extracted and plotted with the respective marginal distributions (Gaussian distributions) in panel b and c.

If the k-variate joint PDF $f_{X(\boldsymbol{z}_1),\dots,X(\boldsymbol{z}_k)}(x_1,\dots,x_k;\boldsymbol{z}_1,\dots,\boldsymbol{z}_k)$ is a multivariate Gaussian distribution for any collection of points $\boldsymbol{z}_1,\dots,\boldsymbol{z}_k \in \Omega$, an RF $X(\boldsymbol{z})$ is said to be Gaussian. In that case, $X(\boldsymbol{z})$ is fully defined by spatial functions for the mean value $\mu_X(\boldsymbol{z})$ and standard deviation $\sigma_X(\boldsymbol{z})$, and the autocorrelation function $\rho(\boldsymbol{z},\boldsymbol{z}')$ defining the spatial correlation of any two locations $\boldsymbol{z},\ \boldsymbol{z} \in \Omega$ [1, 161]. In this manuscript, only Gaussian RFs or RFs that can be expressed as function of Gaussian RFs are considered. It is worth noting that any linear mapping of a Gaussian RF gives a Gaussian RF [102].

Strictly homogeneous RFs are those, for which the k-variate joint PDF is invariant to a shift in $\boldsymbol{z}$, i.e.,

$$f_{X(\boldsymbol{z}_1),\dots,X(\boldsymbol{z}_k)}(x_1,\dots,x_k;\boldsymbol{z}_1,\dots,\boldsymbol{z}_k) = f_{X(\boldsymbol{z}_1+\boldsymbol{\xi}_{\boldsymbol{z}}),\dots,X(\boldsymbol{z}_k+\boldsymbol{\xi}_{\boldsymbol{z}})}(x_1,\dots,x_k;\boldsymbol{z}_1+\boldsymbol{\xi}_{\boldsymbol{z}},\dots,\boldsymbol{z}_k+\boldsymbol{\xi}_{\boldsymbol{z}}), \tag{2.56}$$

for any collection of points $\boldsymbol{z}_1,\dots,\boldsymbol{z}_k \in \Omega$ and any $\boldsymbol{\xi}_{\boldsymbol{z}} \in \Omega$. Equation (2.56) implies that, in a strictly homogeneous RF, $\mu_X(\boldsymbol{z})$ and $\sigma_X(\boldsymbol{z})$ are space-invariant, i.e., $\mu_X(\boldsymbol{z}) = \mu_X\ \forall\ \boldsymbol{z} \in \Omega$ and $\sigma_X(\boldsymbol{z}) = \sigma_X\ \forall\ \boldsymbol{z} \in \Omega$, and $\rho(\boldsymbol{z},\boldsymbol{z}')$ is a function of the difference in location of $\boldsymbol{z}$ and $\boldsymbol{z}'$ only, i.e., $\rho(\boldsymbol{z},\boldsymbol{z}') = \rho(\boldsymbol{\Delta}_{\boldsymbol{z},\boldsymbol{z}'})\ \forall\ \boldsymbol{z},\boldsymbol{z}' \in \Omega$, where $\boldsymbol{\Delta}_{\boldsymbol{z},\boldsymbol{z}'} = \boldsymbol{z} - \boldsymbol{z}'$ [72]. An RF is weakly homogeneous if Equation (2.56) is only valid for $k = 1$ and 2, which suffices to ensure space-invariance of the first- and second-moment functions, as stated above. Since Gaussian RFs are completely defined

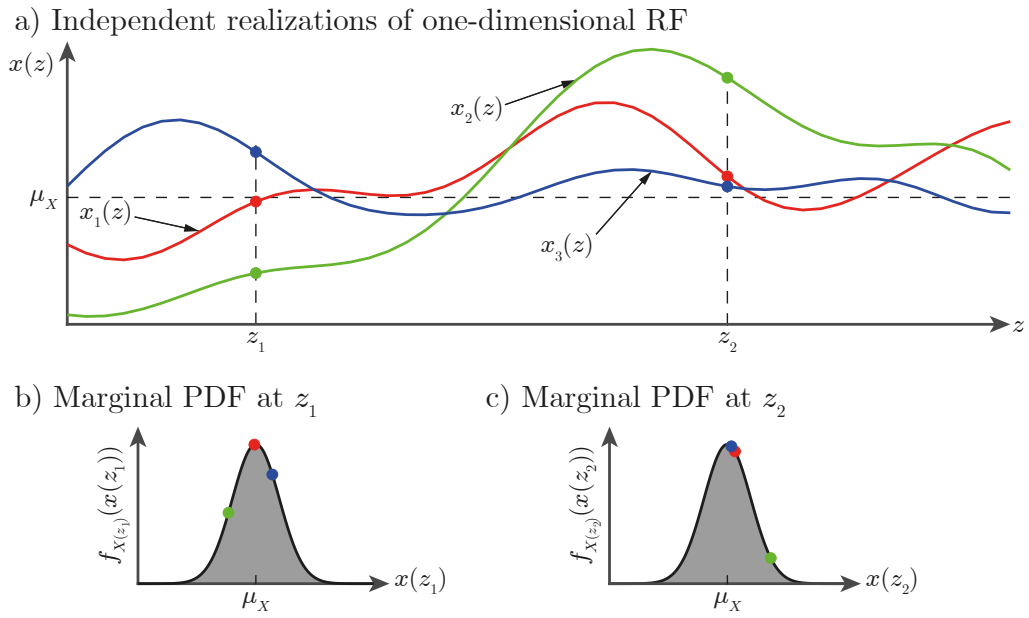

Figure 2.6: Three independent realizations of a one-dimensional RF (red, green and blue line in panel a). At locations z_1 and z_2, the values of $x(z)$ of the three realizations are extracted and assigned to the respective marginal distributions (panel b and c) in the corresponding colors.

by their first- and second moment functions, any weakly homogeneous Gaussian RF is strictly homogeneous and, thus, for the remainder of this work homogeneity implies strict homogeneity.

The spatial variability of a homogeneous RF is governed by $\rho(\boldsymbol{z}, \boldsymbol{z}')$ and can be modeled with various types of correlation functions. All correlation functions are positive definite functions for which $\rho(\boldsymbol{z}, \boldsymbol{z}) = 1$ and, as a consequence, they are bounded [1]:

$$|\rho(\boldsymbol{z}, \boldsymbol{z}')| \leq 1 \; \forall \; \boldsymbol{z}, \boldsymbol{z}' \in \Omega, \tag{2.57}$$

Classical choices for $\rho(\boldsymbol{z}, \boldsymbol{z}')$ of homogeneous RFs are the exponential correlation model $\rho_{\exp}(\boldsymbol{z}, \boldsymbol{z}')$ and the square-exponential model $\rho_{\exp^2}(\boldsymbol{z}, \boldsymbol{z}')$, which are defined as follows [e.g., 161]:

$$\rho_{\exp}(\boldsymbol{\Delta}_{\boldsymbol{z},\boldsymbol{z}'}) = \exp\left(-\frac{\|\boldsymbol{\Delta}_{\boldsymbol{z},\boldsymbol{z}'}\|}{L_c}\right), \tag{2.58a}$$

$$\rho_{\exp^2}(\boldsymbol{\Delta}_{\boldsymbol{z},\boldsymbol{z}'}) = \exp\left(-\left(\frac{\|\boldsymbol{\Delta}_{\boldsymbol{z},\boldsymbol{z}'}\|}{L_c}\right)^2\right), \tag{2.58b}$$

where L_c denotes the correlation length, which is a measure for the decay of the spatial correlation, and $\|\cdot\|$ is the Euclidean distance. Equation (2.58a) and (2.58b) represent the two extreme cases of the more flexible Matérn correlation model, defined as [112, 154]

$$\rho_\nu\left(\boldsymbol{\Delta}_{\boldsymbol{z},\boldsymbol{z}'}\right) = \frac{2^{1-\nu}}{\Gamma(\nu)}\left(\sqrt{2\nu}\,\frac{\boldsymbol{\Delta}_{\boldsymbol{z},\boldsymbol{z}'}}{L_c}\right)^\nu K_\nu\left(\sqrt{2\nu}\frac{\boldsymbol{\Delta}_{\boldsymbol{z},\boldsymbol{z}'}}{L_c}\right), \tag{2.59}$$

where $\Gamma(\cdot)$ is the gamma function and $K_\nu(\cdot)$ is the modified Bessel function of the second kind and order ν [2]. $\nu > 0$ is the smoothness parameter of the Matérn correlation model, where large values of ν imply a smooth decay of $\rho_\nu\left(\boldsymbol{\Delta}_{\boldsymbol{z},\boldsymbol{z}'}\right)$. For half-integer values of ν, $\rho_\nu\left(\boldsymbol{\Delta}_{\boldsymbol{z},\boldsymbol{z}'}\right)$ reduces to the product of an exponential term and a polynomial term [112]. $\rho_{\exp}(\boldsymbol{\Delta}_{\boldsymbol{z},\boldsymbol{z}'})$ is obtained by setting $\nu = \frac{1}{2}$, while $\nu = \infty$ results in $\rho_{\exp^2}(\boldsymbol{\Delta}_{\boldsymbol{z},\boldsymbol{z}'})$.

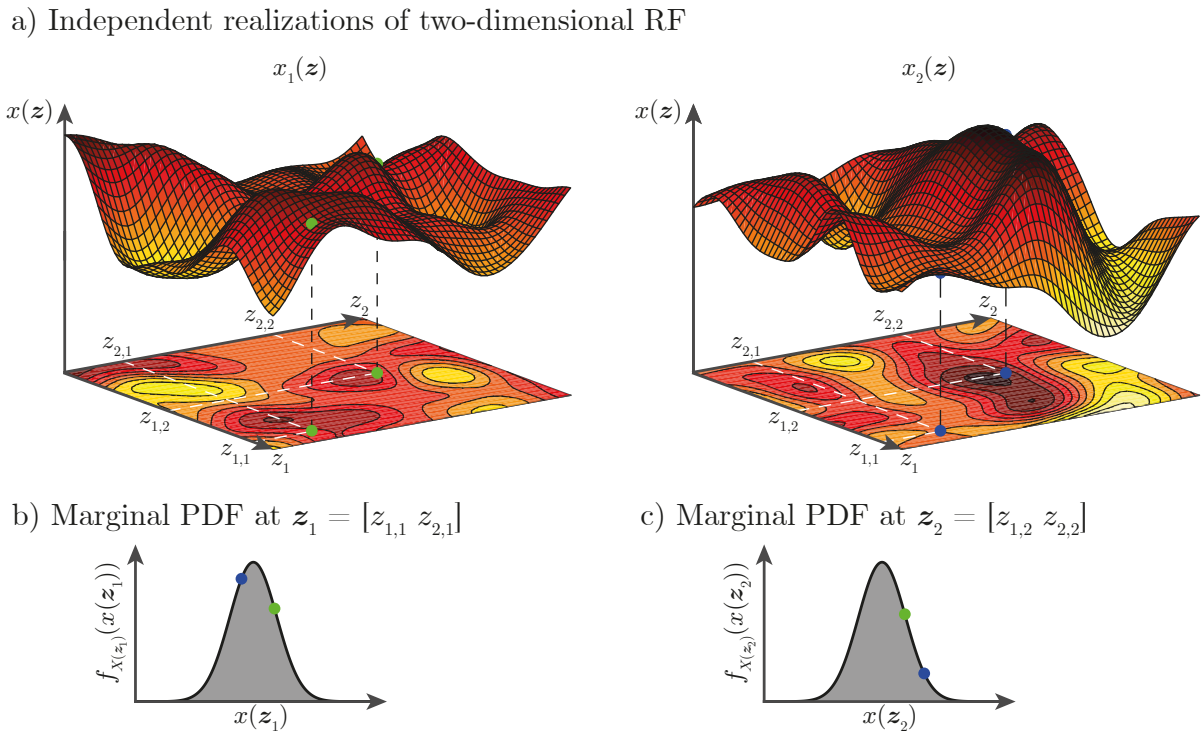

Figure 2.7: Two independent realizations of a two-dimensional RF (panel a). At locations $\boldsymbol{z}_1 = [z_{1,1}\ z_{2,1}]$ and $\boldsymbol{z}_2 = [z_{1,2}\ z_{2,2}]$, the values of $x(\boldsymbol{z})$ of the realizations are extracted and assigned to the respective marginal distributions (panel b and c) in the corresponding colors.

For strictly monotonous correlation functions (such as the Matérn correlation model), a small L_c results in fast reduction of $\rho(\boldsymbol{\Delta}_{\boldsymbol{z},\boldsymbol{z}'})$ with increasing $\boldsymbol{\Delta}_{\boldsymbol{z},\boldsymbol{z}'}$, while a large L_c means slow reduction of $\rho(\boldsymbol{\Delta}_{\boldsymbol{z},\boldsymbol{z}'})$ with increasing $\boldsymbol{\Delta}_{\boldsymbol{z},\boldsymbol{z}'}$. This implies large spatial variability for small correlation lengths and small spatial variability for large ones. In the extreme case of $L_c = 0$, $\rho(\boldsymbol{\Delta}_{\boldsymbol{z},\boldsymbol{z}'})$ reduces to

$$\rho(\boldsymbol{\Delta}_{\boldsymbol{z},\boldsymbol{z}'}) = \delta_{\boldsymbol{z},\boldsymbol{z}'}, \tag{2.60}$$

where $\delta_{\boldsymbol{z},\boldsymbol{z}'}$ denotes the Dirac delta function giving 1 if $\boldsymbol{z} = \boldsymbol{z}'$ and 0 else. The resulting RF represents a white noise field without any spatial correlation [1]. For the opposite extreme of $L_c = \infty$, $\rho(\boldsymbol{\Delta}_{\boldsymbol{z},\boldsymbol{z}'}) = 1,\ \forall\ \boldsymbol{z}, \boldsymbol{z}' \in \Omega$, i.e., the resulting RF can be expressed through a single RV and does not feature any spatial variability [1].

Figure 2.8 illustrates the effect of the correlation function on the spatial variability. Panel a shows the exponential (red), square-exponential (blue) and Matérn correlation function with $\nu = 2.5$ (green) for two different correlation lengths (L_c(dashed lines) $= 5L_c$(solid lines)). Panel b shows six RF realizations, each of which originating from a homogeneous Gaussian RF with identical point statistics but varying correlation function as indicated by the respective line color and type in panel a.

An RF is said to have an isotropic correlation structure if all spatial directions are weighed equally for the calculation of $\rho(\boldsymbol{\Delta}_{\boldsymbol{z},\boldsymbol{z}'})$. In contrast, an anisotropic correlation function can be defined, if one wants to account for different contributions of the spatial directions [e.g., 161, 168].

The effect of L_c on the decay of $\rho(\boldsymbol{\Delta}_{\boldsymbol{z},\boldsymbol{z}'})$ depends on the choice of the parametric correlation model and, hence, L_c is not an appropriate measure for comparing different correlation models. To this end, the scale of fluctuation ϑ can be calculated, which is independent of the chosen

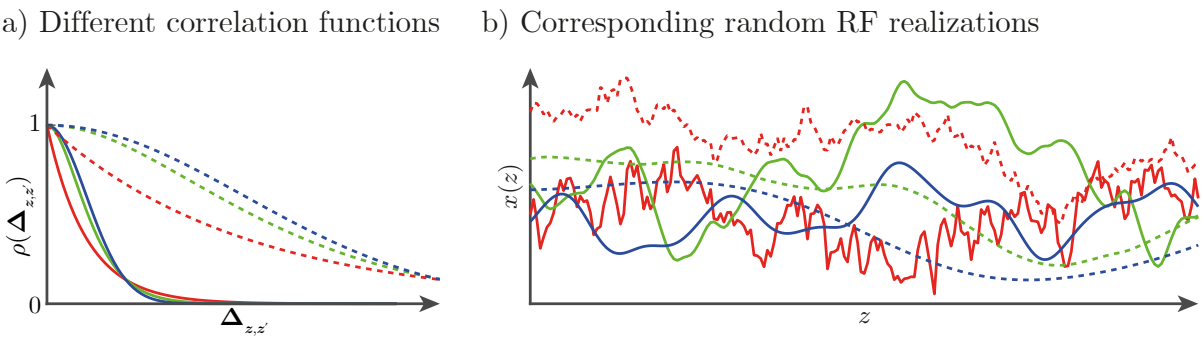

Figure 2.8: Effect of the correlation function on the spatial variability. Panel a shows six different correlation functions, where L_c is five times larger for the dashed lines than for the solid lines. The red lines denote the exponential correlation model, the green lines show the Matérn correlation model with $\nu = 2.5$ and the blue lines show the square-exponential correlation model. Panel b illustrates random realizations of homogeneous Gaussian RFs with identical point statistics and correlation function as indicated by the respective color and line type (solid/dashed) in Panel a.

correlation model and is defined as d-fold spatial integral of the correlation function [161]:

$$\vartheta = \int_{-\infty}^{\infty} \dots \int_{-\infty}^{\infty} \rho(\boldsymbol{\Delta}_{\boldsymbol{z},\boldsymbol{z}'}) \mathrm{d}z_1 \dots \mathrm{d}z_d. \tag{2.61}$$

2.1.6.2 Translation random fields

The class of translation RFs defines RFs that can be expressed as function of Gaussian RFs through a transformation of the following form [71, 102]:

$$Y(\boldsymbol{z}) = T(U(\boldsymbol{z})), \tag{2.62}$$

where $U(\boldsymbol{z})$ is a zero-mean and unit-variance Gaussian RF. If the marginal CDF of $Y(\boldsymbol{z})$ is known and strictly increasing, Eq. (2.62) can be used to find the following marginal transformation [104] (cf. Section 2.1.1.2):

$$Y(\boldsymbol{z}) = T(U(\boldsymbol{z})) = F_{Y;\boldsymbol{z}}^{-1}(\Phi(U(\boldsymbol{z}))), \tag{2.63}$$

where $F_{Y;\boldsymbol{z}}^{-1}(\cdot)$ is the inverse marginal CDF of $Y(\boldsymbol{z})$. By modeling the k-variate joint PDF of the RF by the Nataf joint distribution model (cf. Section 2.1.4), the transformation can be extended for any collection of random variables corresponding to the points $\boldsymbol{z}_1, \dots, \boldsymbol{z}_k \in \Omega$. The resulting transformation of the autocorrelation model can be approximated by empirical relations [41, 104]. Alternatively, the spatial correlation of $Y(\boldsymbol{z})$ can be defined in terms of the underlying Gaussian RF $U(\boldsymbol{z})$, in which case only the marginal transformation of Equation (2.63) is required. Some special cases of translation RFs, for which $T(\cdot)$ reduces to a simple algebraic operation, are given in the following:

- **Lognormal RF**: A lognormal RF $Y(\boldsymbol{z})$, i.e., an RF where the marginal distribution at any $\boldsymbol{z} \in \Omega$ is the lognormal distribution, can be obtained by applying the following marginal transformation:

$$Y(\boldsymbol{z}) = \exp(\mu_X(\boldsymbol{z}) + \sigma_X(\boldsymbol{z}) U(\boldsymbol{z})) = \exp(X(\boldsymbol{z})), \tag{2.64}$$

  where $X(\boldsymbol{z})$ is a Gaussian RF with mean function $\mu_X(\boldsymbol{z})$, standard deviation function $\sigma_X(\boldsymbol{z})$ and autocorrelation function $\rho(\boldsymbol{\Delta}_{\boldsymbol{z},\boldsymbol{z}'})$. Lognormal RFs are especially useful when modeling

mechanical properties, since the lognormal distribution is restricted to non-negative values.

- **Student's *t*-RF**: In a Student's t-RF $Y(\boldsymbol{z})$, the marginal distribution at any $\boldsymbol{z} \in \Omega$ is the Student's t-distribution [18]. It is related to a Gaussian RF as follows [94, 65]:

$$Y(\boldsymbol{z}) = \sqrt{\frac{\nu_Y}{\chi}} \left(\sigma_X(\boldsymbol{z}) U(\boldsymbol{z})\right) + \mu_Y(\boldsymbol{z}) = \sqrt{\frac{\nu_Y}{\chi}} X(\boldsymbol{z}) + \mu_Y(\boldsymbol{z}), \tag{2.65}$$

  where ν_Y are the degrees of freedom of the Student's t-RF $Y(\boldsymbol{z})$ and χ is an RV that follows the χ^2-distribution with ν_Y degrees of freedom (cf. Section 2.1.3.7). $X(\boldsymbol{z})$ is a zero-mean Gaussian RF with standard deviation function $\sigma_X(\boldsymbol{z})$ and autocorrelation function $\rho(\boldsymbol{\Delta}_{\boldsymbol{z},\boldsymbol{z}'})$ and $\mu_Y(\boldsymbol{z})$ is the mean function of $Y(\boldsymbol{z})$. Student's t-RFs arise, e.g., when modeling spatially variable Gaussian properties with unknown marginal RF parameters. A Bayesian approach to account for this uncertainty is described in Section 2.3.2.2 and in detail in Chapter 5 (original publication [65]).

- **Log-Student's *t*-RF**: A log-Student's t-RF $V(\boldsymbol{z})$ combines the Student's t-RF and the exponential transformation of Equation (2.64) for the lognormal RF. The marginal distribution at any $\boldsymbol{z} \in \Omega$ is the log-Student's t-distribution (cf. Section 2.1.3.5). The following marginal transformation can be defined:

$$V(\boldsymbol{z}) = \exp\left(\sqrt{\frac{\nu_V}{\chi}} \left(\sigma_X(\boldsymbol{z}) U(\boldsymbol{z})\right) + \mu_{\ln V}(\boldsymbol{z})\right) = \exp\left(\sqrt{\frac{\nu_V}{\chi}} X(\boldsymbol{z}) + \mu_{\ln V}(\boldsymbol{z})\right). \tag{2.66}$$

  $X(\boldsymbol{z})$ is a zero-mean Gaussian RF with standard deviation function $\sigma_X(\boldsymbol{z})$ and autocorrelation function $\rho(\boldsymbol{\Delta}_{\boldsymbol{z},\boldsymbol{z}'})$, and χ is an RV that follows the χ^2 distribution with ν_Y degrees of freedom (cf. Section 2.1.3.7). $\mu_{\ln V}(\boldsymbol{z})$ is the mean function of the underlying Student's t-RF. A log-Student's t-RF has the same advantages as a lognormal RF and arises when spatially variable lognormally distributed properties with unknown marginal RF parameters are modeled. The Bayesian approach in Section 2.3.2.2 and in Chapter 5 (original publication [65]) also covers log-Student's t-RFs.

2.1.6.3 Random field discretization

By definition, an RF consists of an infinite number of RVs and, thus, direct simulation of RFs is numerically infeasible. To this end, discretization methods have been developed to approximate an RF $X(\boldsymbol{z})$ as follows:

$$X(\boldsymbol{z}) \approx \hat{X}(\boldsymbol{z}), \tag{2.67}$$

where $\hat{X}(\boldsymbol{z})$ includes a finite number of RVs $[X_1, \ldots, X_n]$. Since $\hat{X}(\boldsymbol{z})$ is an approximation of $X(\boldsymbol{z})$, it yields an approximation error $\varepsilon(\boldsymbol{z}) = X(\boldsymbol{z}) - \hat{X}(\boldsymbol{z})$. This error can be quantified by introducing error measures assessing the accuracy of $\hat{X}(\boldsymbol{z})$. As Gaussian RFs are fully defined by their first- and second-moment functions, we restrict to the bias and the error variance which evaluate the error in the mean and variance, respectively, of the RF discretization [e.g., 102, 157]. Here, local error measures are defined as the relative point-wise bias and error variance:

$$\varepsilon_\mu(\boldsymbol{z}) = \frac{\mathbb{E}\left[X(\boldsymbol{z}) - \hat{X}(\boldsymbol{z})\right]}{\mathbb{E}[X(\boldsymbol{z})]}, \tag{2.68a}$$

$$\varepsilon_{\mathrm{V}}(\boldsymbol{z}) = \frac{\mathbb{V}\left[X(\boldsymbol{z}) - \hat{X}(\boldsymbol{z})\right]}{\mathbb{V}[X(\boldsymbol{z})]}. \tag{2.68b}$$

The corresponding global error measures are given by the weighted integral of the absolute value of the point-wise error [157, 16]:

$$\bar{\varepsilon}_\mu = \frac{1}{\mathrm{V}_\Omega} \int_\Omega |\varepsilon_\mu(\boldsymbol{z})| \, \mathrm{d}\boldsymbol{z}, \tag{2.69a}$$

$$\bar{\varepsilon}_\mathrm{V} = \frac{1}{\mathrm{V}_\Omega} \int_\Omega |\varepsilon_\mathrm{V}(\boldsymbol{z})| \, \mathrm{d}\boldsymbol{z}, \tag{2.69b}$$

where V_Ω is the volume of the spatial domain Ω. Alternative global error measures can be obtained by using the supremum norm of Equations (2.68a) and (2.68b) [e.g., 102].

Above error measures may be misleading if $\mathbb{E}[X(\boldsymbol{z})] \to 0$ or $\mathbb{V}[X(\boldsymbol{z})] \to 0$. In such case the point-wise bias and error variance defined by the numerator of Equation (2.68a) and Equation (2.68b), respectively, and corresponding global error measures can be employed.

Discretization methods can be divided into point discretization methods, average discretization methods and series expansion methods. An overview of existing approaches can be found in [157] or, more recently, in [106]. In the following, one selected method of each of the three classes is shortly described followed by a comparison of the methods in terms of the approximation error.

- **Point discretization methods**: In point discretization methods, the RVs $[X_1, \ldots, X_n]$ represent the values of $X(\boldsymbol{z})$ at specific points $[\boldsymbol{z}_1, \ldots, \boldsymbol{z}_n]$ within the domain of definition, which are selected based on a discretization of Ω into n sub-domains $\Omega_1, \ldots, \Omega_n$, the elements of the so-called stochastic finite element mesh. The marginal distributions of the n RVs are then given as the marginal distribution of the RF at the corresponding locations, and, as an immediate consequence, the marginal moments of $[X_1, \ldots, X_n]$ are given as the respective marginal moments of the RF. The correlation of the n RVs is calculated by means of the correlation function of $X(\boldsymbol{z})$:

  $$\rho_{X_i, X_j} = \rho(\boldsymbol{z}_i, \boldsymbol{z}_j). \tag{2.70}$$

  The midpoint (MP) method uses the midpoints (center of gravity if $d > 1$) of the stochastic finite elements as discretization points [40]. The value of $\hat{X}(\boldsymbol{z})$ is then constant within the respective element, i.e., $\hat{X}(\boldsymbol{z}) = X_i \; \forall \; \boldsymbol{z} \in \Omega_1, \; i = 1, \ldots, n$. This element-wise uniformity results in discontinuities of the RF realizations at the boundaries of the sub-domains. The point-wise error variance and a RF realization with the MP method are illustrated in Figure 2.9 (red lines). Other point discretization methods are, e.g., the shape function method [105] or the optimal linear estimation method [102].

- **Average discretization methods**: Average discretization methods approximate $X(\boldsymbol{z})$ by a set of RVs $[X_1, \ldots, X_n]$ representing weighted integrals of $X(\boldsymbol{z})$ over the corresponding elements $\Omega_1, \ldots, \Omega_n$ of the stochastic finite element mesh. The spatial averaging (SA) method is shortly described in the following and in detail in Chapter 7 (original publication [63]).

  The SA method discretizes $X(\boldsymbol{z})$ through a set of averaging RVs, where each RV is defined as the local average of $X(\boldsymbol{z})$ over the corresponding stochastic finite element [162, 161]:

  $$\hat{X}_i = \frac{1}{\mathrm{V}_{\Omega_i}} \int_{\Omega_i} X(\boldsymbol{z}) \mathrm{d}\boldsymbol{z}, \; i = 1, \ldots, n, \tag{2.71}$$

  where V_{Ω_i} is the volume of the spatial domain Ω_i. If $X(\boldsymbol{z})$ is a Gaussian RF, the n resulting averaging RVs are multivariate Gaussian through the linearity of the integral

operator in Equation (2.71) [102]. Since the joint distribution of the averaging RVs is almost impossible to obtain for non-Gaussian RFs, applicability of the SA method is restricted to Gaussian and translation RFs [40]. The marginal first- and second-order moments of the n resulting averaging RVs are obtained by integrating the spatial functions for the mean and covariance [161, 62, 63]. If $X(\boldsymbol{z})$ is homogeneous, the mean is not affected by the spatial averaging, i.e., $\mu_{\hat{X}_i} = \mu_X,\ i = 1, \ldots, n$, and the variance is simply scaled by the variance function, which accounts for the reduction of the variance through the averaging and is calculated by spatial integration of the autocorrelation function [161]. The covariance $\mathbb{C}\mathrm{ov}\left[\hat{X}_i, \hat{X}_j\right],\ i = 1, \ldots, n,\ j = 1, \ldots, n$ is evaluated by calculating the variances of several auxiliary spatial domains accounting for the size and relative position of Ω_i and Ω_j [161, 63]. Figure 2.9 shows the point-wise error variance and a RF realization with the SA method (green lines). Other average discretization methods are the weighted integral method [37, 38] and the local average subdivison [55].

- **Series discretization methods**: Series discretization methods represent $X(\boldsymbol{z})$ by a truncated sum of products of RVs and deterministic spatial functions. Unlike point and average discretization methods, these RVs are not assigned a certain spatial location or domain but a term in the series. Thus, by combination with the corresponding spatial function, each RV contributes globally to the spatial variability of $\hat{X}(\boldsymbol{z})$.

  The Karhunen–Loève (KL) expansion uses a spectral decomposition of the spatial covariance function $\mathbb{C}\mathrm{ov}\left[X(\boldsymbol{z}), X(\boldsymbol{z}')\right],\ \boldsymbol{z}, \boldsymbol{z}' \in \Omega$ to represent $X(\boldsymbol{z})$ by the following series expansion [e.g., 107, 90, 70]:

$$X(\boldsymbol{z}) = \mu_X(\boldsymbol{z}) + \sum_{i=1}^{\infty} \sqrt{\lambda_i}\phi_i(\boldsymbol{z})X_i, \tag{2.72}$$

  where the $X_i,\ i = 1, \ldots, \infty$ are zero-mean and uncorrelated RVs and the eigenvalues λ_i and corresponding eigenfunctions $\phi_i(\boldsymbol{z})$ form the so-called eigenpairs of the spatial covariance function. The eigenfunctions are orthogonal and form a complete set due to the symmetry and the positive definiteness of the covariance function [108]. The eigenpairs can be found through solving the following Fredholm integral equation [70]:

$$\int_{\Omega} \mathbb{C}\mathrm{ov}\left[X(\boldsymbol{z}), X(\boldsymbol{z}')\right] \phi_i(\boldsymbol{z}')\mathrm{d}\boldsymbol{z}' = \lambda_i\phi_i(\boldsymbol{z}),\ i = 1, \ldots, \infty. \tag{2.73}$$

  In most cases, Equation (2.73) needs to be solved numerically, e.g., by means of the Nyström method [121, 6]. By truncating the series expansion of Equation (2.72) after a finite number of terms, the KL expansion approximates $X(\boldsymbol{z})$ as [70]

$$\hat{X}(\boldsymbol{z}) = \mu_X(\boldsymbol{z}) + \sum_{i=1}^{m} \sqrt{\lambda_i}\phi_i(\boldsymbol{z})X_i, \tag{2.74}$$

  where $\lambda_i,\ i = 1, \ldots, m$ are the m largest eigenvalues of the spatial covariance function, in descending order. If $X(\boldsymbol{z})$ is a Gaussian RF, the $X_i,\ i = 1, \ldots, m$ are a set of independent standard Gaussian RVs. Note that Equation (2.74) minimizes the mean-square error in the series representation of $X(\boldsymbol{z})$ with orthogonal functions [70]. The point-wise error variance and a RF realization with the KL expansion are illustrated by blue lines in Figure 2.9. Other series discretization methods are, e.g., the expansion optimal linear estimation method [102] or the spectral representation method [152].

Figure 2.9 illustrates the discretization of a one-dimensional, homogeneous, zero-mean and unit-variance Gaussian RF with the Matérn correlation model ($\nu = 2.5$, $L_c = 0.5$) with the

three presented discretization methods (MP method, SA method, KL expansion). Panels a and b illustrate the point-wise error variance $\varepsilon_{\mathrm{V}}(\boldsymbol{z})$, calculated by means of Equation (2.68b) for $d = 4$ RVs (panel a) and $d = 10$ RVs (panel b). Panels c and d show a RF realization with the respective number of RVs and compare it to the reference realization of the RF (dashed black line). The values at the midpoints of the elements are additionally highlighted by red dots for the realization with MP, as those values are the ones valid for the whole corresponding element. Obviously, increasing the number of elements leads to a reduction of the error and, thus, to a more accurate representation of the spatial variability. Note that the bias $\varepsilon_{\mu}(\boldsymbol{z})$ is 0 for all three illustrated methods for the chosen RF parameters.

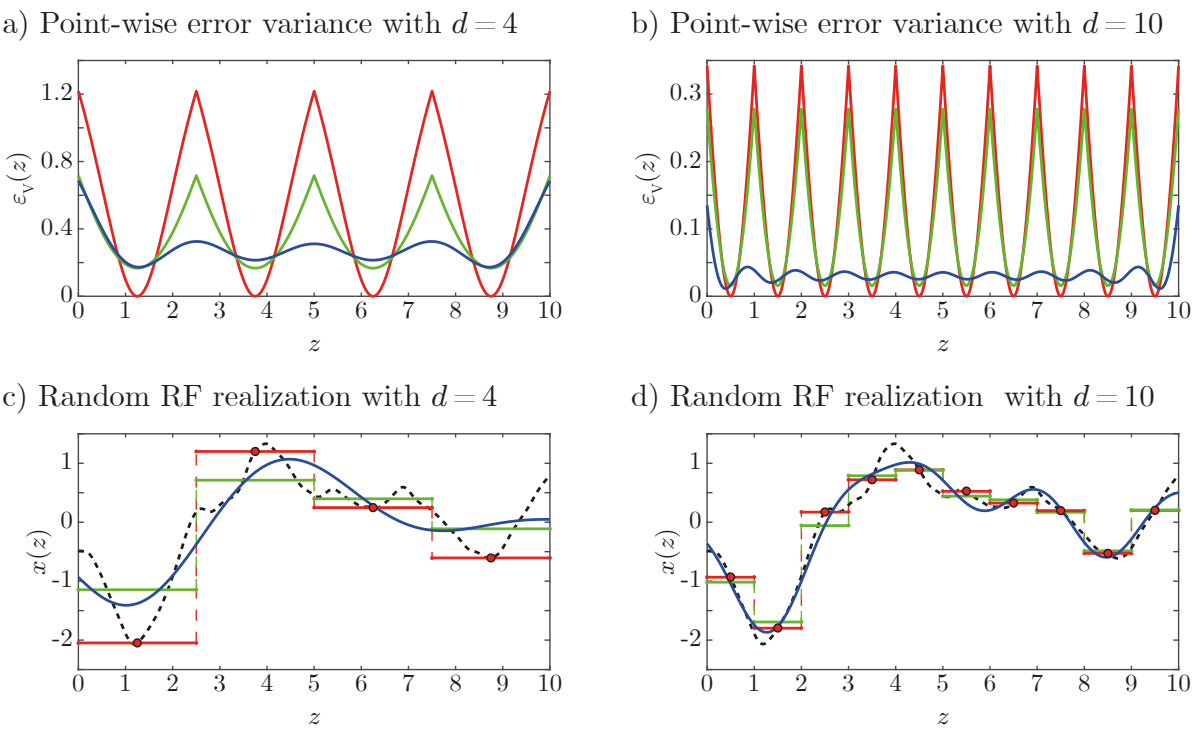

Figure 2.9: Point-wise error variance and random realization for the discretization of a one-dimensional, homogeneous, zero-mean and unit-variance Gaussian RF with the Matérn correlation model ($\nu = 2.5$, $L_c = 0.5$) with MP method, SA method and KL expansion in the domain $z \in \Omega = [0, 10]$. Panels a and b show the point-wise error variance with $d = 4$ (panel a) and $d = 10$ (panel b) RVs using MP method (red), SA method (green) and KL expansion (blue). Panels c and d illustrate the realization of the RF discretized with MP method (red), SA method (green) and KL expansion (blue) with $d = 4$ (panel c) and $d = 10$ (panel d) RVs. The dashed black lines in panel c and d illustrate the corresponding reference realization of the RF.

2.2 Structural reliability analysis

Structural design is always a trade-off between structural safety and economic efficiency, as one needs to find a solution which combines an economic design with an acceptable level of reliability. The reliability of a structure is the result of an interaction of the structural resistance R and the demand acting on the structure S. Both are typically subject to uncertainty and, thus, reliability analysis is a task of uncertainty quantification.

Uncertainty in the input parameters of a structural system can have various sources. Material parameters, for example, are inherently uncertain and, thus, the resistance of a structural member is an uncertain quantity. The same holds for the structural demand, which is uncertain due to the unpredictability of future events leading to load on the structure. Further sources of

uncertainty in structural systems include environmental conditions, human workmanship, limited amount of data, or modeling errors, among others [113, 92]. Spatial variability forms a special type of uncertainty that can be accounted for through random field modeling (cf. Section 2.1.6).

When performing reliability analysis for a system, the quantity of interest is the system's probability of failure $P_{\mathcal{F}}$, i.e., the probability of occurrence of the failure event $\mathcal{F}$ given uncertainty in the input parameters. This section gives an introduction into the problem setting of structural reliability and presents different solution strategies to solve the problem.

2.2.1 The reliability problem

The failure event $\mathcal{F}$ generally describes an unsatisfactory performance of the system for the given input. Its specific definition depends on the application at hand and is not discussed in detail at this point. For now, it is assumed that the system's performance depends on the two uncertain and statistically independent parameters R and S, modeled by RVs with prescribed marginal PDFs. In the setting of the basic structural reliability problem, failure occurs if the demand equals or exceeds the structural resistance [113]:

$$\mathcal{F} = \{S \geq R\}\,. \tag{2.75}$$

The so-called limit state function $g(\cdot)$ can be used to classify the system response. It is common practice to define $g(\cdot)$ such that non-positive values correspond to failure. That is, the limit state function and the corresponding failure event for the basic structural reliability problem read [e.g., 110, 113]

$$g\,(r, s) = r - s, \tag{2.76a}$$

$$\mathcal{F} = \{g\,(r, s) \leq 0\}\,. \tag{2.76b}$$

If the demand equals or exceeds the structural resistance, $g\,(r, s)$ gives a non-positive value, indicating system failure. Following Equation (2.76a), $P_{\mathcal{F}}$ is defined as follows:

$$P_{\mathcal{F}} = P\,(R - S \leq 0)\,. \tag{2.77}$$

2.2.1.1 Implicit reliability analysis

For most applications, it is not required to explicitly calculate $P_{\mathcal{F}}$, as structural design codes provide an efficient means to ensure an acceptable level of reliability by following a standardized verification concept. The aim of such concepts is to validate a given design with respect to a prescribed measure of the structural safety or safety factor.

The simplest way to define such a safety factor is achieved by the following equation [113]:

$$S_{\text{nom}} \leq \frac{R_{\text{nom}}}{\gamma_{\text{glob}}}, \tag{2.78}$$

where $\gamma_{\text{glob}} \geq 1$ denotes a global safety factor which can be found empirically, e.g., based on experimental observations or practical experience. S_{nom} and R_{nom} are the nominal values of the demand and resistance, respectively. Although the uncertainty in R and S plays a role for the choice of γ_{glob}, it is not explicitly taken into account. Given γ_{glob}, the design criterion of Equation (2.78) is fully deterministic. The principle of the global safety concept is illustrated in Figure 2.10, where the case of an acceptable design is shown.

Nowadays, a common approach in structural design is the partial safety concept, which forms the basis of the European design codes for buildings and structures [47]. It was originally

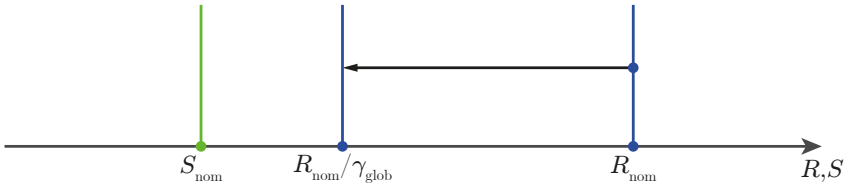

Figure 2.10: Structural design with the global safety approach, where the nominal value for the resistance R is divided by a global safety factor γ_{glob}. This figure shows an acceptable design, since $S < \frac{R}{\gamma_{\text{glob}}}$.

developed for reinforced concrete structures in the 1970s, as the design codes valid at that time did not account for various levels of uncertainty in different load types and not all potential failure modes were covered [109]. For the simple case of an $R - S$ reliability problem given in Equation (2.76a), the partial safety concept requires the following design equation to be fulfilled [109, 47, 113]:

$$S_{\text{k}} \cdot \gamma_S \leq \frac{R_{\text{k}}}{\gamma_R}, \tag{2.79}$$

where $\gamma_R \geq 1$ and $\gamma_S \geq 1$ denote partial safety factors for the structural resistance and load, respectively, and R_{k} and S_{k} are so-called characteristic values for R and S. $R_{\text{d}} = \frac{R_{\text{k}}}{\gamma_R}$ and $S_{\text{d}} = S_{\text{k}} \cdot \gamma_S$ are the design values for R and S.

Characteristic values are defined as representative values for the respective parameter of interest (in this case resistance and load). Typically, they are given as p-quantile values of the underlying probability distribution of the uncertain parameter, i.e., the characteristic value for random variable X is given by

$$X_{\text{k}} = F_X^{-1}(p), \tag{2.80}$$

where $F_X^{-1}(\cdot)$ is the inverse CDF of X. For most applications, R_{k} is given by a value from the left side of the distribution ($p \leq 0.5$), while S_{k} is chosen from the right side of the distribution ($p \geq 0.5$) to ensure a conservative estimate of the reliability.

The characteristic values and the partial safety factors depend on the specific application, i.e., the investigated limit state function. One can generally distinguish between two different types of limit states: (i) ultimate limit states (ULS) and (ii) serviceability limit states (SLS) [47]. ULS define situations that are concerned with the safety of people or the structure itself, e.g., failure of a steel canopy construction due to an exceedance of the yield stress at the fixed end [50]. By contrast, SLS are concerned with the functioning of the structure and the structural appearance, e.g., the maximum allowable deformation of a concrete ceiling or crack width control in concrete basement walls [49]. For more complex verification cases including various types of loads, the partial safety concept offers the use of combination values which account for the probability of several extreme loads occurring at the same time and the frequency of different load types [47].

Hence, in contrast to the global safety concept, the partial safety concept accounts for the uncertainty in the input variables and potential interaction between them. The resulting framework for the verification is calibrated to fulfill a predefined reliability level, i.e., to not exceed an acceptable $P_{\mathcal{F}}$. In practice, it is often assumed that the safety level of existing design codes is acceptable and, thus, newly developed approaches should not fall below [113].

Figure 2.11 illustrates the partial safety concept by means of an acceptable design case. Although the uncertainty in R and S is accounted for using a stochastic model (illustrated by the PDFs of the underlying probability distributions), it is only used to determine the respective characteristic values and to calibrate the partial safety factors. All further calculations (e.g.,

determination of the resulting stress at a specific location) remain deterministic, the partial safety concept is therefore called a semi-probabilistic concept.

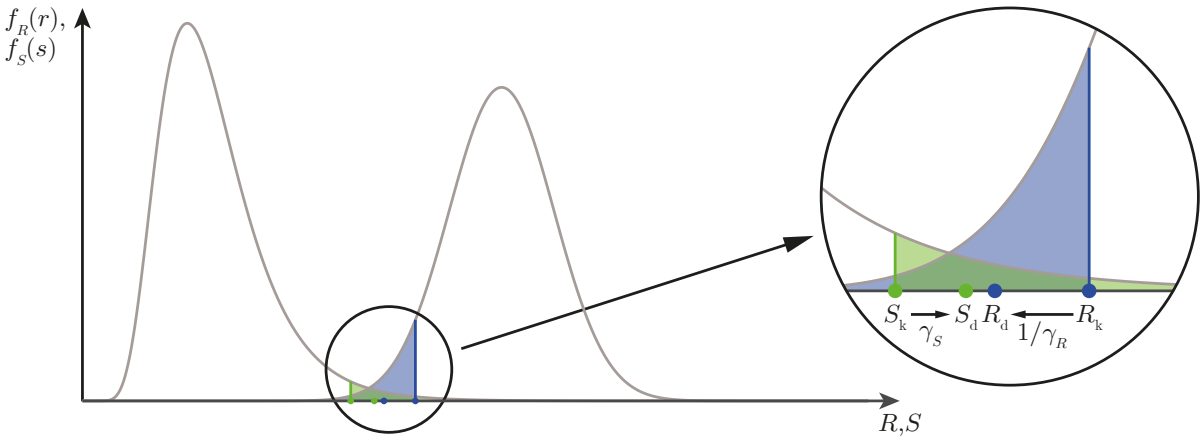

Figure 2.11: Structural design with the partial safety concept. Partial safety factors (γ_R, γ_S) are applied to the characteristic values of the resistance (R_k) and the load (S_k) to determine the design values (R_d, S_d). Here, S_d is smaller than R_d, resulting in an acceptable design. The gray lines indicate the PDFs of the underlying probability distributions.

2.2.1.2 Explicit reliability analysis

Explicit reliability analysis means calculating or (in most practical cases) estimating $P_\mathcal{F}$. The result can then be compared to the required level of reliability, i.e., a maximum acceptable failure probability $P_{\mathcal{F},\text{acc}}$. Accordingly, the design criterion to be fulfilled is

$$P_\mathcal{F} \leq P_{\mathcal{F},\text{acc}}. \tag{2.81}$$

There is no need for safety factors, as R and S are explicitly modeled as uncertain input parameters instead of reducing them to a single representative value, which is illustrated in Figure 2.12.

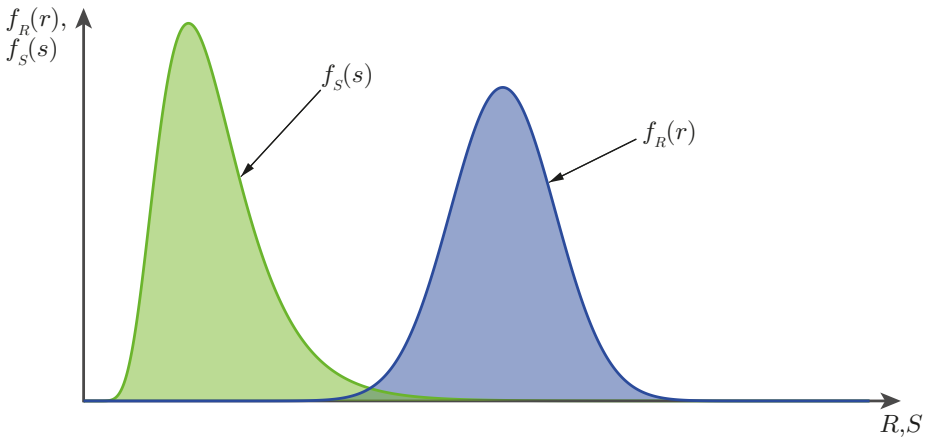

Figure 2.12: Explicit reliability analysis to determine $P_\mathcal{F}$. The uncertain parameters R and S are modeled as random variables with their respective PDFs. $P_\mathcal{F}$ is then calculated as $P_\mathcal{F} = P(R - S \leq 0)$.

For the simple $R - S$ limit state function of Equation (2.76a), $P_\mathcal{F}$ calculates by the following

convolution integral (under the assumption of independence of R and S) [113]:

$$P_{\mathcal{F}} = \int_S F_R(s) \cdot f_S(s) \mathrm{d}s. \tag{2.82}$$

However, Equation (2.82) is not applicable in the general case, i.e., when R and S are not independent, when the limit state function is not of the $R-S$ type or simply when more than two uncertain input parameters enter the limit state function. The remainder of this thesis focuses on the calculation of $P_{\mathcal{F}}$ for general reliability problems with d-dimensional input random vector $\boldsymbol{x}$ and corresponding limit state function $g(\boldsymbol{x})$, mapping from the d-dimensional stochastic input space of $\boldsymbol{X}$ to the real numbers. While in some cases, $g(\boldsymbol{x})$ may be given by a simple algebraic expression, it can also include solution of a complex numerical model (e.g., a finite element model). As before, $\mathcal{F}$ is indicated by non-positive values of $g(\boldsymbol{x})$, i.e., $\mathcal{F} = \{\boldsymbol{X} \in \mathbb{R}^d : g(\boldsymbol{x}) \leq 0\}$. For convenience, the following binary indicator function is defined:

$$\mathbb{1}\left(g\left(\boldsymbol{x}\right)\right) = \begin{cases} 0, & g\left(\boldsymbol{x}\right) > 0, \\ 1, & g\left(\boldsymbol{x}\right) \leq 0. \end{cases} \tag{2.83}$$

$P_{\mathcal{F}}$ is defined as the probability that $\mathbb{1}\left(g\left(\boldsymbol{x}\right)\right)$ takes the value 1, mathematically given in general form by the following d-dimensional integral:

$$P_{\mathcal{F}} = \int_{\Omega} \mathbb{1}(g(\boldsymbol{x})) f_{\boldsymbol{X}}\left(\boldsymbol{x}\right) \mathrm{d}\boldsymbol{x} = \mathbb{E}[\mathbb{1}(g(\boldsymbol{x}))], \tag{2.84}$$

where $f_{\boldsymbol{X}}(\cdot)$ denotes the joint PDF of $\boldsymbol{X}$ and $\Omega \in \mathbb{R}^d$ denotes the corresponding d-dimensional outcome space. Figure 2.13 illustrates a simple reliability problem of two dependent input RVs X_1 and X_2. The linear limit state function $g(x_1, x_2)$ divides the outcome space into the failure domain ($g(x_1, x_2) < 0$, red area) and the safe domain ($g(x_1, x_2) > 0$, green area) by the limit state surface ($g(x_1, x_2) = 0$, red line).

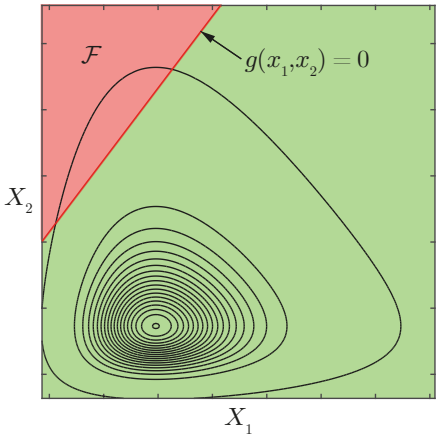

Figure 2.13: Reliability problem of two dependent RVs X_1 and X_2 and a linear limit state function $g(x_1, x_2)$. The red area denotes the failure domain and the green area indicates the safe domain, which are separated by the limit state surface, indicated by the red line. The black lines are the isolines of $f_{X_1,X_2}(x_1, x_2)$.

Typically, Equation (2.84) cannot be solved in closed form and, therefore, needs to be approximated numerically. A large variety of methods used for approximating $P_{\mathcal{F}}$ have been developed over the past decades, collected under the term structural reliability methods. The choice of an appropriate method depends on the problem type and the objective of the analysis,

and cannot be generalized. However, most reliability problems can be classified in advance according to some general characteristics, which may reduce the number of suitable methods for the approximation of $P_{\mathcal{F}}$. An overview of a number of such characteristics is given in Section 2.2.1.5.

2.2.1.3 The reliability index

Reliability indices are an alternative measure for reliability. They are a geometric interpretation of the minimum distance from the mean to the failure domain in the outcome space of the RVs, where a large distance corresponds to a large reliability index suggesting a high level of reliability. Initially defined in the 1940s as a characteristic for safety [147], various alternative formulations were proposed in the course of the subsequent decades [e.g., 60, 33, 144], before Hasofer and Lind came up with a formulation of the reliability index independent of the limit state formulation [76]. The Hasofer-Lind reliability index is discussed in detail in Section 2.2.2.1. All reliability indices have in common that an estimate of $P_{\mathcal{F}}$ can be directly obtained once the reliability index has been calculated.

Ditlevsen suggested a generalized reliability index as a direct function of $P_{\mathcal{F}}$, given by the following expression [44]:

$$\beta = -\Phi^{-1}\left(P_{\mathcal{F}}\right), \tag{2.85}$$

where $\Phi^{-1}(\cdot)$ denotes the inverse CDF of the standard normal distribution. Note that the direct geometric interpretation of β as a measure for the distance to the failure domain gets lost when using the expression of Equation (2.85) and that its direct calculation is not possible for complex reliability problems. Thus, β serves more as a tangible measure for the reliability than as a tool for estimating $P_{\mathcal{F}}$. For example, the European design codes for buildings and structures define the required reliability level in terms of a target reliability index [47]. Figure 2.14 illustrates $P_{\mathcal{F}}$ as function of the generalized reliability index β.

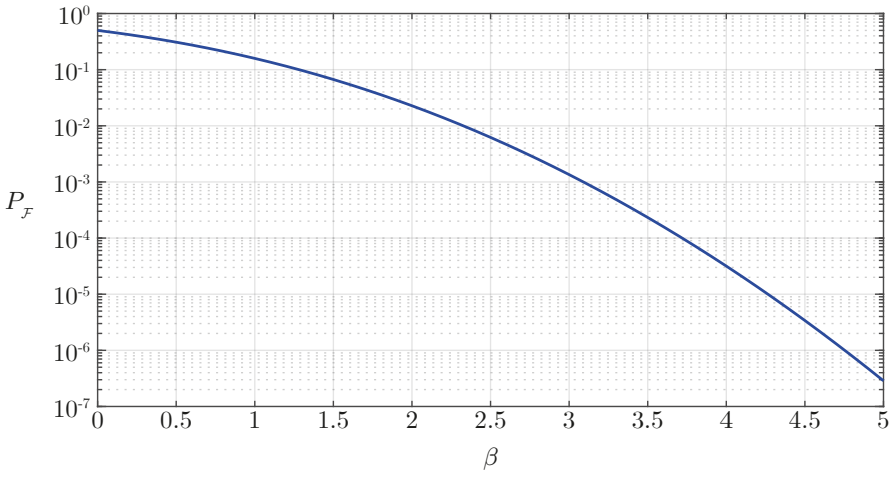

Figure 2.14: Failure probability $P_{\mathcal{F}}$ as function of the reliability index β.

2.2.1.4 Component reliability vs. system reliability

Reliability problems are not restricted to a single failure mechanism, as they can consist of several elements (e.g., structural members) with different potential failure mechanisms (e.g., exceeding a material's yield strength or its compressive strength) that need to be accounted for in order to assess the overall condition of the system. Each of these m potential failure modes corresponds to a component in the system for which an individual limit state function

$g_i(\boldsymbol{x}),\ i = 1, \ldots, m$ needs to be defined. Component reliability describes the case of a single failure mechanism, i.e., the reliability problem is stated in terms of a single limit state function ($m = 1$). By contrast, system reliability deals with the reliability analysis of multi-component systems, where several limit state functions have to be defined ($m > 1$). Note that this does not necessarily require several elements in the system, since a single element can have multiple failure modes and, thus, represent multiple components of the reliability problem.

Despite the large variety of possible component failure mechanisms, most effects on the system reliability can be captured by introducing two main categories of systems [e.g., 113, 45]:

- **Series system**: All m components of the system need to be in working condition in order for the system to be functioning. The system fails if any of the system's components fails. Accordingly, system failure of a series system $\mathcal{F}_{\text{ser}}$ is given as follows [59]:

$$\mathcal{F}_{\text{ser}} = \mathcal{F}_1 \cup \mathcal{F}_2 \cup \cdots \cup \mathcal{F}_m = \bigcup_{i=1}^{m} \mathcal{F}_i \tag{2.86}$$

  Since any component failure leads to system failure, the minimum value of the component limit state function values is decisive for identifying $\mathcal{F}_{\text{ser}}$. That is, the indicator function of Equation (2.83) can be adjusted for series system problems as follows:

$$\mathbb{1}_{\text{ser}}(g(\boldsymbol{x})) = \begin{cases} 0, & \min\{g_i(\boldsymbol{x}),\ i = 1, \ldots, m\} > 0, \\ 1, & \min\{g_i(\boldsymbol{x}),\ i = 1, \ldots, m\} \leq 0. \end{cases} \tag{2.87}$$

  An example for a series system in structural reliability is a statically determinate truss structure, which fails as soon as a single strut or tie fails. Series systems are non-redundant systems. A two-component series system problem of two RVs is illustrated in panel a of Figure 2.15. The red area denotes $\mathcal{F}_{\text{sys}}$, which is defined as the union of the two component failure events $\mathcal{F}_1 = \{g_1(x_1, x_2) \leq 0\}$ and $\mathcal{F}_2 = \{g_2(x_1, x_2) \leq 0\}$. The dashed ($g_1(x_1, x_2) = 0$) and dotted ($g_2(x_1, x_2) = 0$) black lines indicate the limit state surfaces of the components and the solid red line shows the series system's limit state surface.

- **Parallel system**: Only one component of the system needs to be working in order for the system to be functioning. The system fails only if all m components fail. For a parallel system, the failure event $\mathcal{F}_{\text{par}}$ is given as follows:

$$\mathcal{F}_{\text{par}} = \mathcal{F}_1 \cap \mathcal{F}_2 \cap \cdots \cap \mathcal{F}_m = \bigcap_{i=1}^{m} \mathcal{F}_i \tag{2.88}$$

  Since any working component suffices to avoid system failure, the maximum value of the component limit state function values is decisive for identifying $\mathcal{F}_{\text{par}}$, leading to the following indicator function for parallel systems:

$$\mathbb{1}_{\text{par}}(g(\boldsymbol{x})) = \begin{cases} 0, & \max\{g_i(\boldsymbol{x}),\ i = 1, \ldots, m\} > 0, \\ 1, & \max\{g_i(\boldsymbol{x}),\ i = 1, \ldots, m\} \leq 0. \end{cases} \tag{2.89}$$

  An example for a parallel system from the field of structural engineering is a concrete column with compression reinforcement, which only fails due to compression if both the concrete's and the reinforcement's resistance are exceeded (neglecting other failure modes, e.g., stability failure). Hence, parallel systems are redundant systems. Panel b of Figure 2.15 shows a two-component parallel system problem of two RVs. $\mathcal{F}_{\text{sys}}$ is defined by the intersection of the two component failure events $\mathcal{F}_1 = \{g_1(x_1, x_2) \leq 0\}$ and

$\mathcal{F}_2 = \{g_2(x_1, x_2) \leq 0 =\}$. The limit state surface of the parallel system is indicated by the solid red line, the dashed $(g_1(x_1, x_2) = 0)$ and dotted $(g_2(x_1, x_2) = 0)$ black lines denote the limit state surfaces of the components.

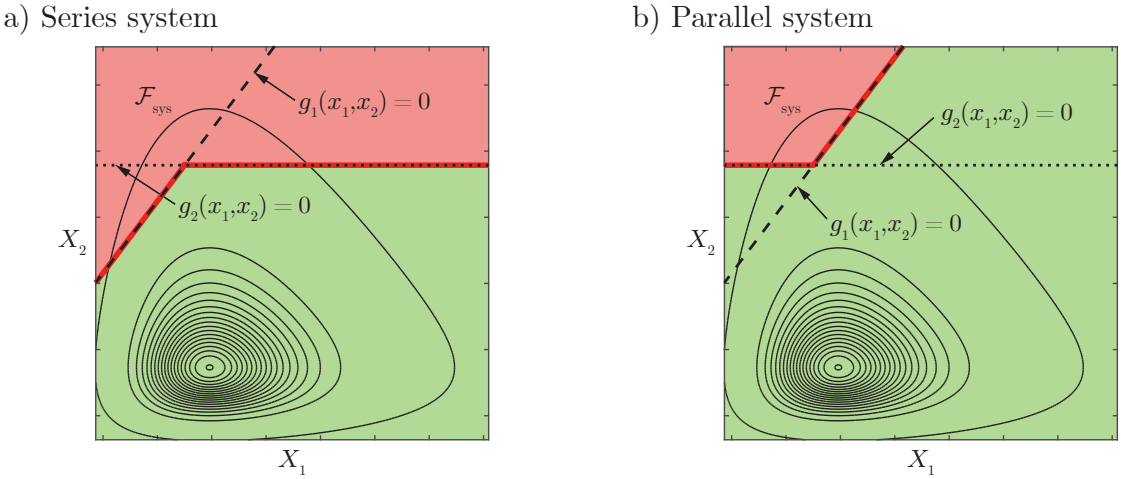

Figure 2.15: Failure domain of a series system (panel a) and a parallel system (panel b) with two components and two input RVs X_1 and X_2. For the series system, the system failure domain is given by the union of the two component failure domains, for the parallel system it is given by their intersection. The solid red line marks the limit state surface of the system, the dotted and dashed black lines mark the limit state surface of the components.

Obviously, the structure of systems does not restrict to the two elementary cases, it can be any combination of components, parallel and/or series (sub-)systems. More detailed investigation of general system reliability includes further special cases, such as the k-out-of-n system [e.g., 110] and active/passive redundancy [e.g., 101], among others.

2.2.1.5 Characteristics of reliability problems

In addition to the number of components in a system and the way the components interact regarding system failure, there are several characteristics of reliability problems that can help to identify an appropriate method for estimating $P_\mathcal{F}$. Although some of the characteristics require information that is typically available after solving the reliability problem, it is often possible to provide some information by taking a careful look at the specific problem setting or by performing a preliminary analysis. Without claiming to be exhaustive, the following list collects some important characteristics of reliability problems:

- **Number of failure regions**: A structural system can fail for different reasons. The resulting failure regions can cover different regions of Ω (multimodal failure) including intersections, subsets and disjunctions of multiple failure domains. On the contrary, unimodal failure describes the case where $g(\boldsymbol{x})$ features a single failure domain. The number of failure regions is not necessarily related to the number of components in a structural system, since a component can have several causes of failure and several components can fail for the same reason.

- **Dimensionality of $\boldsymbol{X}$**: Equation (2.84) is a problem in the d-dimensional probability space, where d is the number of RVs in $\boldsymbol{X}$. Unfortunately, the complexity of finding a good approximation for $P_\mathcal{F}$ increases rapidly with an increase in the input dimensions, a phenomenon known as the curse of dimensionality [14].

- **(Expected) range of $P_\mathcal{F}$**: Typically, $\mathcal{F}$ is a rare event and the corresponding probability $P_\mathcal{F}$ is a small probability (in structural reliability $P_\mathcal{F} \leq \mathcal{O}(10^{-3})$ [113]). Although $P_\mathcal{F}$ is not known prior to performing the reliability analysis, the type of problem may allow to specify (expected) upper and/or lower bounds on $P_\mathcal{F}$. For example, the European design codes for buildings and structures defines consequence classes for different types of buildings and recommends minimum values for the reliability index [47].
- **Computational cost for evaluating $g(\boldsymbol{x})$**: Solving the reliability problem typically requires repeatedly evaluating the limit state function. While this does not pose a significant problem in simple cases, it can dominate the computational cost of a reliability analysis if $g(\boldsymbol{x})$ includes a costly numerical model, e.g., a finite element model.
- **Numerical instability**: This characteristic is especially relevant when a complex numerical model needs to be evaluated. Such models often require a numerical solver which can lead to numerical noise, i.e., the model in $g(\boldsymbol{x})$ cannot be solved exactly but needs to be approximated.
- **Nonlinearity of $g(\boldsymbol{x})$**: Nonlinear limit state functions can have discontinuities or local extrema, which may lead to premature convergence of an optimization algorithm. In addition, the nonlinearity of $g(\boldsymbol{x})$ can result in several failure domains, which need to be accounted for when estimating $P_\mathcal{F}$.
- **Required additional information**: Although calculating $P_\mathcal{F}$ is the main goal of a reliability analysis, there are other types of information one can be interested in, e.g., the sensitivity of $P_\mathcal{F}$ with respect to the input parameters. Furthermore, not only the estimated value of $P_\mathcal{F}$ but also an estimate of the confidence in that value can be of interest.

With the above characteristics in mind, a reliability problem can be assessed before actually performing the reliability analysis. Some of the mentioned characteristics directly exclude certain types of reliability methods and can help to identify critical factors of the analysis. Such a pre-analysis is especially helpful when the computational budget is limited, i.e., in cases where one cannot afford repeated runs with different reliability methods.

2.2.2 Reliability methods

Reliability methods are developed for an efficient approximation of Equation (2.84). Most of these methods are designed to work efficiently (or even exclusively) in the independent standard normal space ($\boldsymbol{U}$-space). To achieve this, Equation (2.84) is written in the following way:

$$P_\mathcal{F} = \int_{\mathbb{R}^d} \mathbb{1}\left(G(\boldsymbol{u})\right) \varphi_d\left(\boldsymbol{u}\right) \mathrm{d}\boldsymbol{u} = \mathbb{E}[\mathbb{1}\left(G(\boldsymbol{u})\right)], \tag{2.90}$$

where $G(\boldsymbol{u}) = g\left(T^{-1}(\boldsymbol{u})\right)$ is the transformed limit state function in the equivalent $\boldsymbol{U}$-space, i.e., it is a function of the vector $\boldsymbol{U}$ of independent standard normal random variables. $T^{-1}(\cdot)$ is the inverse of an isoprobabilistic transformation $T(\cdot)$, mapping from Ω to the d-dimensional $\boldsymbol{U}$-space, e.g., by application of the Nataf joint distribution model (cf. Section 2.1.4). $\varphi_d\left(\cdot\right)$ is the PDF of the d-dimensional independent standard normal distribution.

Reliability methods can be generally divided into approximation methods and simulation methods. These two classes represent different approaches to estimate $P_\mathcal{F}$, which are described as part of the following presentation of selected reliability methods. The selection is by no means exhaustive but rather tries to give an insight into different working principles of reliability methods and the corresponding advantages/disadvantages.

2.2.2.1 First order reliability method

The first order reliability method (FORM) is an approximation method, in which the limit state surface is approximated by a first-order Taylor series expansion around the most likely failure point. Early versions of linear approximations of the limit state surface have shown to be ambiguous with respect to the limit state formulation, which made their standardized application impossible [43]. To obtain a result that is independent of the limit state formulation, the problem needs to be solved in $\boldsymbol{U}$-space [76, 79]. The most likely failure point in $\boldsymbol{U}$-space is the so-called design point $\boldsymbol{u}^*$ and, due to the properties of the $\boldsymbol{U}$-space, it is the point on the limit state surface that is closest to the origin. Integration of the probability mass contained in the d-dimensional half-hyperplane defined by the $d-1$-dimensional hyperplane perpendicular to the line segment $\overline{\mathbf{0}\boldsymbol{u}^*}$ results in the FORM estimate for the failure probability. The transformation to $\boldsymbol{U}$-space allows reducing the problem to a simple one-dimensional expression by introducing the Hasofer-Lind reliability index as the Euclidean distance from the origin to the design point, i.e., the Euclidean norm of the vector $\boldsymbol{u}^*$ [76]:

$$\beta_{\mathrm{HL}} = \|\boldsymbol{u}^*\| \,. \tag{2.91}$$

The FORM estimate for $P_{\mathcal{F}}$ can then directly be calculated as

$$P_{\mathcal{F},\mathrm{FORM}} = \Phi\left(-\beta_{\mathrm{HL}}\right). \tag{2.92}$$

Figure 2.16 illustrates the FORM approximation of a two-dimensional reliability problem. One can see the difference between the approximated failure domain through the linearization of $G(\boldsymbol{u})$ around $\boldsymbol{u}^*$ (red hatched area) and the actual failure domain of $G(\boldsymbol{u})$ (red area). In this case, $P_{\mathcal{F},\mathrm{FORM}}$ overestimates the true probability of failure, which is a typical behavior for convex failure domains. On the contrary, FORM underestimates $P_{\mathcal{F}}$ for concave failure domains. $P_{\mathcal{F},\mathrm{FORM}} = P_{\mathcal{F}}$ and, accordingly, $\beta_{\mathrm{HL}} = \beta$, only if the limit state function is a linear function in $\boldsymbol{U}$-space. Note that, in the general case, a linear limit state function in the original space does not correspond to a linear function in $\boldsymbol{U}$-space.

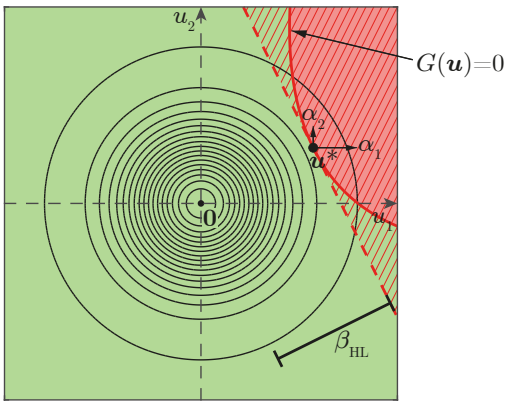

Figure 2.16: FORM approximation of a reliability problem in two-dimensional $\boldsymbol{U}$-space. β_{HL} marks the Euclidean distance from the origin to the design point $\boldsymbol{u}^*$. The red hatched area indicates the approximated failure domain obtained by the linear approximation of the limit state surface (dashed red line) while the red area shows the actual failure domain separated from the safe domain by the limit state surface (solid red line). The black concentric circles illustrate the isolines of $\varphi_2(\boldsymbol{u})$. α_1 and α_2 are the FORM sensitivity factors for $G(\boldsymbol{u})$ at $\boldsymbol{u}^*$ to a change in U_1 and U_2, respectively.

Since $P_{\mathcal{F},\mathrm{FORM}}$ is easily calculable by means of Equations (2.91) and (2.92), the challenge when using FORM lies in finding $\boldsymbol{u}^*$, for which efficient algorithms have been developed. The most

prominent ones are the Hasofer-Lind-Rackwitz-Fiessler (HL-RF) algorithm and the improved HL-RF algorithm, which are based on numerical evaluation of the limit state function gradient [76, 139, 103, 167]. The computational effort of the gradient evaluation increases with the number of RVs d entering the problem. Many modern optimization algorithms are also able to solve the problem in an efficient way.

In addition to the shape of the failure region, the accuracy of the FORM estimate depends on the problem's dimensionality and decreases with increasing d [138, 159]. This is due to the geometric properties of the probability space. In low dimensions the design point is typically located in a region where most of the probability mass is concentrated. However, this does not hold for high-dimensional problems, where the probability mass in the d-dimensional $\boldsymbol{U}$-space is concentrated around a so-called important ring with distance $\sqrt{d-\frac{1}{2}}$ from the origin [91]. In that case, not only the vicinity of $\boldsymbol{u}^*$ but also regions far away can have significant contributions to the failure domain, leading to an inaccurate estimate for $P_{\mathcal{F}}$ [159]. Hence, the application of FORM is not recommended for high-dimensional reliability problems.

A by-product of FORM are the sensitivity factors collected in the vector $\boldsymbol{\alpha}$ of unit length [78, 19]:

$$\boldsymbol{\alpha} = \frac{\boldsymbol{u}^*}{\beta_{\mathrm{HL}}}, \tag{2.93}$$

where $\alpha_i,\ i = 1, \dots d$ represents the sensitivity of $G(\boldsymbol{u})$ at $\boldsymbol{u}^*$ to a change in U_i. Small absolute values of the components in $\boldsymbol{\alpha}$ indicate minor sensitivity with respect to the corresponding RVs. If the sign of α_i is positive (negative), an increase of U_i decreases (increases) the reliability. Figure 2.16 shows the sensitivity factors α_1 and α_2 for the two-dimensional reliability problem solved with FORM.

The European design codes for buildings and structures suggest to use FORM for calculating the structural reliability, since its estimate is sufficiently accurate for most structural applications and its application is easier/less costly than that of many other reliability methods [47]. Furthermore, FORM is used for the calibration of partial safety factors in the partial safety concept (cf. Section 2.2.1.1).

The accuracy of FORM can be improved by including higher-order terms in the approximation of the limit state surface. The second order reliability method (SORM), as the name suggests, approximates it by a quadratic function, i.e., it employs a Taylor series expansion of the second order around $\boldsymbol{u}^*$ [56, 22]. This method not only requires numerical evaluation of the limit state function gradient but also of its Hessian, which significantly increases the computational effort for increasing d. Albeit to a smaller extent, SORM suffers from the same problems as FORM in high dimensions i.e., the approximation of the failure region around the design point becomes inaccurate [138]. SORM and other approximation methods are not discussed in detail in this thesis.

2.2.2.2 Monte Carlo simulation

Monte Carlo simulation (MCS) forms the foundation for all simulation reliability methods. It can be used for various types of problems involving uncertainty and is not restricted to the field of reliability analysis. The general aim is to approximate the solution of a problem numerically by repeatedly drawing samples from the joint distribution of the uncertain input parameters and evaluating the numerical model for these samples to obtain samples from the output quantity/quantities of interest, whose probability distribution can be estimated using statistical methods [115, 146]. The term Monte Carlo was coined in the 1940s, when it was used as a code word for secret work related to the atomic bomb [114]. In applications for reliability

analysis, MCS approximates $P_{\mathcal{F}}$ by the following estimate:

$$P_{\mathcal{F},\mathrm{MCS}} = \frac{1}{n_{\mathrm{MCS}}} \sum_{i=1}^{n_{\mathrm{MCS}}} \mathbb{1}\left(g\left(\boldsymbol{x}_i\right)\right), \tag{2.94}$$

where $\boldsymbol{x}_i,\ i = 1, \ldots, n_{\mathrm{MCS}}$ are a set of independent samples from $f_{\boldsymbol{X}}(\boldsymbol{x})$. $P_{\mathcal{F},\mathrm{MCS}}$ is an unbiased estimator for $P_{\mathcal{F}}$, i.e., $\mathbb{E}[P_{\mathcal{F},\mathrm{MCS}}] = P_{\mathcal{F}}$, and converges to $P_{\mathcal{F}}$ with probability 1 for $n_{\mathrm{MCS}} \to \infty$ by the law of large numbers [146]. The variance of $P_{\mathcal{F},\mathrm{MCS}}$ is

$$\mathbb{V}[P_{\mathcal{F},\mathrm{MCS}}] = \frac{1}{n_{\mathrm{MCS}}} P_{\mathcal{F}}\left(1 - P_{\mathcal{F}}\right), \tag{2.95}$$

and the corresponding CoV is given by

$$\delta_{P_{\mathcal{F},\mathrm{MCS}}} = \frac{\sqrt{\mathbb{V}[P_{\mathcal{F},\mathrm{MCS}}]}}{\mathbb{E}[P_{\mathcal{F},\mathrm{MCS}}]} = \sqrt{\frac{1 - P_{\mathcal{F}}}{n_{\mathrm{MCS}} P_{\mathcal{F}}}}. \tag{2.96}$$

Hence, the accuracy of MCS is a function of the target quantity $P_{\mathcal{F}}$ and the number of samples used to build the MCS estimator. As mentioned earlier, $P_{\mathcal{F}}$ is typically a rare event ($P_{\mathcal{F}} \ll 1$), which allows approximating $\delta_{P_{\mathcal{F},\mathrm{MCS}}}$ as [146]

$$\delta_{P_{\mathcal{F},\mathrm{MCS}}} \approx \sqrt{\frac{1}{n_{\mathrm{MCS}} P_{\mathcal{F}}}}. \tag{2.97}$$

From this, the required sample size to achieve a certain level of accuracy δ_{t} can be calculated:

$$n_{\mathrm{req}} = \frac{1}{\delta_{\mathrm{t}}^2 P_{\mathcal{F}}}. \tag{2.98}$$

Obviously, MCS is not efficient for estimating rare event probabilities, as this would require a very large number of samples, for which a potentially costly numerical model needs to be evaluated. Figure 2.17 shows two independent runs of MCS to solve a two-dimensional reliability problem. The number of samples is chosen as $n_{\mathrm{MCS}} = 10^3$, resulting in estimates of $P_{\mathcal{F},\mathrm{MCS}} = 1 \times 10^{-3}$ (panel a) and 6×10^{-3} (panel b), which underlines the large uncertainty of $P_{\mathcal{F},\mathrm{MCS}}$. In both runs, the vast majority of samples falls into the safe domain (white circles in green area) and, thus, are completely neglected in the calculation of the MCS estimate by means of Equation (2.94). The reference failure probability of the shown problem is $P_{\mathcal{F}} = 4.0 \times 10^{-3}$, i.e., $\delta_{P_{\mathcal{F},\mathrm{MCS}}} = 0.5$ with the chosen sample size. For comparison, a target CoV of the estimate of $\delta_{\mathrm{t}} = 0.1$ would require a sample size of $n_{\mathrm{req}} = 25000$.

A large variety of simulation methods have been developed to overcome the inefficiency of MCS by reducing the variance of the MCS estimator, some of which are discussed in the following.

2.2.2.3 Importance sampling

Importance sampling (IS) tries to reduce the variance of the MCS estimate by increasing the portion of samples located in the failure domain. This is achieved by drawing samples not from the nominal distribution of the input RVs but from an alternative distribution, the so-called IS density $h(\boldsymbol{u})$ [88]. For IS, Equation (2.90) is rewritten as follows [e.g., 97, 146, 113]:

$$P_{\mathcal{F}} = \int_{\mathbb{R}^d} \mathbb{1}\left(G(\boldsymbol{u})\right) \frac{\varphi_d\left(\boldsymbol{u}\right)}{h(\boldsymbol{u})} h(\boldsymbol{u}) \mathrm{d}\boldsymbol{u}. \tag{2.99}$$

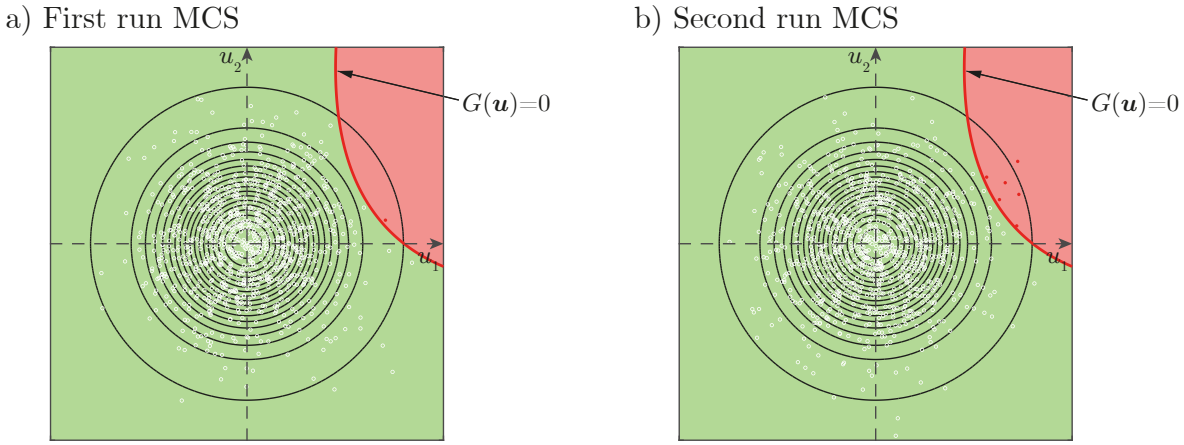

Figure 2.17: Two independent MCS runs to estimate $P_{\mathcal{F}}$ for a reliability problem in two-dimensional $\boldsymbol{U}$-space with $n_{\text{MCS}} = 10^3$ in each run. In the first run (panel a), only a single failure sample (red dots) can be observed, while six samples fall into the failure domain in the second run (panel b). The white circles indicate the samples that fall into the safe domain.

Under the condition that the failure domain is included in the support of $h(\boldsymbol{u})$, this modification does not alter the value of the integral. The IS estimate of $P_{\mathcal{F}}$ is given as

$$P_{\mathcal{F},\text{IS}} = \frac{1}{n_{\text{IS}}} \sum_{i=1}^{n_{\text{IS}}} \mathbb{1}\left(G\left(\boldsymbol{u}_i\right)\right) \frac{\varphi_d\left(\boldsymbol{u}_i\right)}{h(\boldsymbol{u}_i)} = \frac{1}{n_{\text{IS}}} \sum_{i=1}^{n_{\text{IS}}} \mathbb{1}\left(G\left(\boldsymbol{u}_i\right)\right) w(\boldsymbol{u}_i), \tag{2.100}$$

where the set of samples $\boldsymbol{u}_i,\ i = 1, \ldots, n_{\text{IS}}$ are distributed according to $h(\boldsymbol{u})$. Their corresponding IS weights $w(\boldsymbol{u}_i) = \frac{\varphi_d(\boldsymbol{u}_i)}{h(\boldsymbol{u}_i)},\ i = 1, \ldots, n_{\text{IS}}$ account for the fact that the samples are drawn from an alternative density. Equation (2.100) yields an unbiased estimate of $P_{\mathcal{F}}$ with variance given as

$$\mathbb{V}[P_{\mathcal{F},\text{IS}}] = \frac{1}{n_{\text{IS}}} \mathbb{V}_h[\mathbb{1}(G(\boldsymbol{u}))w(\boldsymbol{u})], \tag{2.101}$$

where $\mathbb{V}_h[\cdot]$ denotes the variance with respect to $h(\boldsymbol{u})$. An estimator for the CoV of the IS estimate can be constructed using a set of n_{IS} samples from $h(\boldsymbol{u})$:

$$\hat{\delta}_{P_{\mathcal{F},\text{IS}}} = \frac{1}{P_{\mathcal{F},\text{IS}}} \sqrt{\frac{1}{n_{\text{IS}}(n_{\text{IS}}-1)} \sum_{i=1}^{n_{\text{IS}}} \left(\mathbb{1}(G(\boldsymbol{u}_i))w(\boldsymbol{u}_i) - P_{\mathcal{F},\text{IS}}\right)^2}. \tag{2.102}$$

Obviously, the choice of $h(\boldsymbol{u})$ is crucial for the quality of the IS estimate. There is a theoretically optimal IS density $h^*(\boldsymbol{u})$, for which the variance of the IS estimate is zero. For solving the problem of Equation (2.100), it is defined as [17, 146]

$$h^*(\boldsymbol{u}) = \frac{\mathbb{1}(G(\boldsymbol{u}))\varphi_d\left(\boldsymbol{u}\right)}{\int_{\mathbb{R}^d} \mathbb{1}(G(\boldsymbol{u}))\varphi_d\left(\boldsymbol{u}\right) \mathrm{d}\boldsymbol{u}}. \tag{2.103}$$

The expression in the denominator of Equation (2.103) equals $P_{\mathcal{F}}$. In fact, $h^*(\boldsymbol{u})$ is the nominal density censored at the failure domain and the denominator is merely a normalization constant ensuring $\int_{\mathbb{R}^d} h^*(\boldsymbol{u})\mathrm{d}\boldsymbol{u} = 1$. Hence, application of $h^*(\boldsymbol{u})$ would require knowledge of $P_{\mathcal{F}}$, i.e., the very quantity one is interested in estimating, which makes its direct application impossible. In practice, the goal is to find a density which sufficiently reduces $\mathbb{V}[P_{\mathcal{F},\text{IS}}]$. Early versions of IS simply shifted the mean value of $\varphi_d\left(\boldsymbol{u}\right)$ towards the failure domain and/or modified the variance [e.g., 75, 150, 81, 54, 113]. Figure 2.18 illustrates an IS run with $h(\boldsymbol{u})$ chosen as $\varphi(\boldsymbol{u} - \boldsymbol{\mu}_{\text{IS}})$, where $\boldsymbol{\mu}_{\text{IS}} = \boldsymbol{u}^*$, i.e., the most likely failure point/design point. The sample size is $n_{\text{IS}} = 1000$

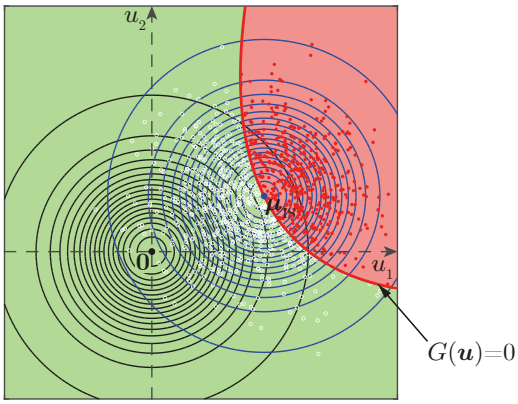

Figure 2.18: Solution of a reliability problem in two-dimensional $\boldsymbol{U}$-space with IS based on $n_{\mathrm{IS}} = 10^3$ samples. $h(\boldsymbol{u})$ is chosen as $\varphi(\boldsymbol{u}-\boldsymbol{\mu}_{\mathrm{IS}})$, i.e., a shifted independent standard normal distribution. The blue lines show the isolines of $h(\boldsymbol{u})$ and the black lines show the isolines of the nominal density $\varphi(\boldsymbol{u})$. The samples that fall into the failure domain are indicated by red dots, while the samples in the safe domain are illustrated by white circles.

and the estimated failure probability is $P_{\mathcal{F},\mathrm{IS}} = 3.7 \times 10^{-3}$, i.e., close to the reference failure probability of $P_{\mathcal{F}} = 4.0 \times 10^{-3}$, with corresponding CoV estimate of $\hat{\delta}_{P_{\mathcal{F},\mathrm{IS}}} = 0.06$.

Sequential IS techniques have become more popular in the recent years, as they are more flexible and generally applicable. These methods employ the knowledge about the existence of $h^*(\boldsymbol{u})$ to find a near-optimal density by repeatedly generating samples $\boldsymbol{u}$ and evaluating $G(\boldsymbol{u})$. In each step of the sequence, the resulting outcomes of the limit state function are used to select an elite set of samples or to weight the samples, such that samples closer to the failure domain are selected/assigned a larger weight. The samples for the next step are then generated based on these elite samples/weights, either by fitting a parametric density with the selected/weighted samples, or by use of a conditional sampling algorithm accounting for the selection/weights. This procedure attempts to approach the failure domain in a step-wise manner until a sufficiently large portion of the samples fall into the failure domain, which are then used to estimate $P_{\mathcal{F}}$ by means of Equation (2.100). Although various sequential approaches exist [e.g., 25, 117, 13, 127], we restrict the presentation to cross entropy-based methods that aim at minimizing the Kullback-Leibler divergence between a chosen parametric density and $h^*(\boldsymbol{u})$ [145, 96].

The Kullback-Leibler divergence or relative cross entropy (CE) is a measure for the difference between two PDFs [96]. Assuming a parametric density $h(\boldsymbol{u},\boldsymbol{\theta})$, where $\boldsymbol{\theta} \in \boldsymbol{\Theta}$ denotes the vector of distribution parameters, a near-optimal IS density can be found by minimizing the Kullback-Leibler divergence between $h^*(\boldsymbol{u})$ and $h(\boldsymbol{u},\boldsymbol{\theta})$ with respect to $\boldsymbol{\theta}$. Making use of Equation (2.103), this is equivalent to solving the following optimization problem [96]:

$$\underset{\boldsymbol{\theta}\in\boldsymbol{\Theta}}{\arg\min}\ D_{\mathrm{KL}}\left(h^*(\boldsymbol{u}), h(\boldsymbol{u},\boldsymbol{\theta})\right) = \underset{\boldsymbol{\theta}\in\boldsymbol{\Theta}}{\arg\max} \int_{\mathbb{R}^d} \mathbb{1}\left(G(\boldsymbol{u})\right)\varphi_d(\boldsymbol{u})\ln\left(h(\boldsymbol{u},\boldsymbol{\theta})\right)\mathrm{d}\boldsymbol{u}. \tag{2.104}$$

Starting from an initial sampling density $h(\boldsymbol{u},\boldsymbol{\theta}_0)$, CE-based importance sampling approximates a near-optimal IS density by repeatedly estimating a set of parameters $\boldsymbol{\theta}$ that minimize $D_{\mathrm{KL}}\left(h^*(\boldsymbol{u}), h(\boldsymbol{u},\boldsymbol{\theta})\right)$ based on a set of samples. These parameters are then used to generate the samples for the next iteration. To guide the algorithm towards the failure domain, a set of intermediate domains is introduced. In the standard CE method, the intermediate domain of the current step is defined in a way that a certain percentage of the samples are located in that domain (the samples with the lowest limit state function values, typically 5% to 20% of the samples), in which case only these elite samples are used for updating the parameters [96, 66, 98, 165]. Recently, we proposed the improved cross entropy (iCE) method, which accounts for

all samples in the parameter update [126]. It does so by introducing a smooth approximation of the indicator function $\mathbb{1}(G(\boldsymbol{u}))$ that has been used for sequential importance sampling [13, 127, 125].

The parametric form of $h(\boldsymbol{u}, \boldsymbol{\theta})$ is an important factor in CE-based (and other sequential) IS approaches. Critical factors are the number of input random variables d and the number of failure domains. The standard choice for problems in $\boldsymbol{U}$-space is the multivariate Gaussian distribution, which shows good performance in low dimensions for both unimodal and multimodal failure [66]. A Gaussian mixture distribution, i.e., a weighted sum of multivariate Gaussian distributions has been proposed to efficiently cover multimodal failure domains, but the superiority over the single Gaussian distribution largely depends on prior knowledge about the number and location of the failure domains [98, 66]. With an increase in d, the quality of performance of Gaussian distributions decreases rapidly, which can be attributed to the increasing number of parameters to be estimated ($\mathcal{O}(d^2)$) and the degeneracy of the IS weights $w(\boldsymbol{u})$ [e.g., 8, 146, 126]. If d is sufficiently large, the probability mass of the standard normal distribution concentrates around a so-called important ring with distance $\sqrt{d - \frac{1}{2}}$ from the origin [91, 87]. Then, the von Mises-Fisher (vMF) distribution or a mixture of several vMF distributions can be used as IS density, since it allows to sample from the surface of a d-dimensional hypersphere [111, 165]. That model can be extended by introducing a Nakagami distribution to sample the radius from. The resulting von Mises-Fisher-Nakagami (vMFN) distribution or a mixture of vMFN distributions can be used as a flexible parametric IS density for problems in low to moderately high dimensions ($d \leq \mathcal{O}(10^2)$) with unimodal and multimodal failure domains [126].

If $h(\boldsymbol{u}, \boldsymbol{\theta})$ is a member of the exponential family of distributions, the parameter update in each step of CE-based IS is available in closed form [146]. However, this does not hold for the general case or when using mixture distributions, in which case the parameters can only be found approximately or via an iterative procedure. An elegant solution to this updating problem for mixture distributions is provided by the expectation-maximization (EM) algorithm, where the assignment of the samples to the mixture components is treated as missing data and the problem is solved by alternatively calculating the expected log-likelihood and finding the parameters that maximize the expected log-likelihood [36, 29]. By extending the procedure for the use of weighted samples, the EM algorithm can be directly applied for the parameter update in the CE and iCE method if $h(\boldsymbol{u}, \boldsymbol{\theta})$ is a mixture distribution, e.g., a Gaussian mixture [66] or a vMFN mixture [126].

Figure 2.19 illustrates the principle of the CE method. Panel a shows the first level of the CE method, where $n_{\mathrm{IS}} = 500$ samples are drawn from $h(\boldsymbol{u}, \boldsymbol{\theta}_0)$, in this case from $\varphi_2(\boldsymbol{u})$. Based on the resulting limit state function values, the intermediate domain (red area) is defined such that 10% of the samples are located in that domain (red dots). The mean vector and covariance matrix of the multivariate Gaussian distribution are then updated based on these elite samples only. Panel b shows the final (here fourth) level of the CE method, where most of the samples are located in the failure domain. The dashed red lines show the boundaries of the intermediate domains of the previous levels. The resulting failure probability estimate is $P_{\mathcal{F},\mathrm{IS}} = 3.6 \times 10^{-3}$ and the CoV of the estimate is $\hat{\delta}_{P_{\mathcal{F},\mathrm{IS}}} = 0.07$, achieved with $4 \cdot n_{\mathrm{IS}} = 2000$ samples in total.

2.2.2.4 Subset simulation

Subset simulation (SuS) has been developed for efficiently estimating $P_{\mathcal{F}}$ in problems with many input RVs [7, 9]. In SuS, $\mathcal{F}$ is expressed by an intersection of l nested events F_j, $j = 1, \ldots, l$, such that the following holds:

$$\mathcal{F}_0 \supset \mathcal{F}_1 \supset \cdots \supset \mathcal{F}_l = \mathcal{F}, \tag{2.105}$$

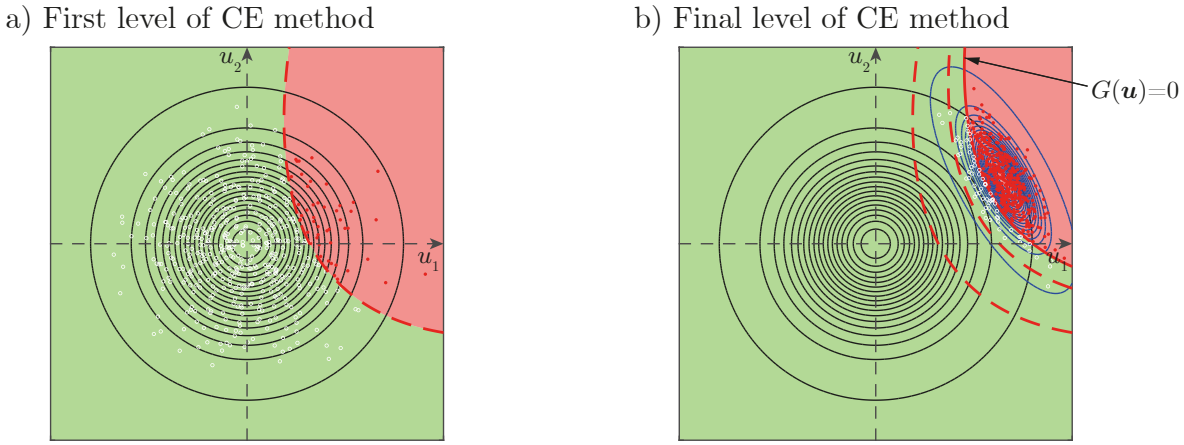

Figure 2.19: Solution of a reliability problem in two-dimensional $\boldsymbol{U}$-space with the CE method and the multivariate Gaussian distribution as parametric IS density. Panel a shows the first level, where samples are generated from the nominal density $\varphi(\boldsymbol{u})$. 10% of the samples are selected as elite samples (those that fall into the intermediate domain indicated by the red area) and used for the parameter update. The final level of the CE method is illustrated in panel b, where a large portion of the samples falls into the failure domain (red dots). The dashed red lines illustrate the limits of the intermediate domains, the black lines show the isolines of $\varphi_2(\boldsymbol{u})$ and the blue lines show the isolines of $h(\boldsymbol{u}, \boldsymbol{\theta})$ in the final step.

where each $\mathcal{F}_j$ is defined as

$$\mathcal{F}_j = \{\boldsymbol{U} \in \mathbb{R}^d : G(\boldsymbol{u}) \leq \xi_j\}, \text{ with } \infty = \xi_0 > \xi_1 > \cdots > \xi_l = 0. \tag{2.106}$$

Hence, starting from the certain event $\mathcal{F}_0$, SuS defines a series of conditional events with decreasing probability, which sequentially approach $\mathcal{F}$. The SuS estimator for $P_\mathcal{F}$ is then constructed as the product of the conditional probabilities of the series of nested events [7]:

$$P_{\mathcal{F},\text{SuS}} = \prod_{j=1}^{l} P_{\mathcal{F}_j|\mathcal{F}_{j-1},\text{SuS}}. \tag{2.107}$$

In each step j, $P_{\mathcal{F}_j|\mathcal{F}_{j-1},\text{SuS}}$ is estimated through an MCS estimate:

$$P_{\mathcal{F}_j|\mathcal{F}_{j-1},\text{SuS}} = \frac{1}{n_\text{SuS}} \sum_{i=1}^{n_\text{SuS}} \mathbb{1}_j(G(\boldsymbol{u}_i)), \tag{2.108}$$

where the indicator function $\mathbb{1}_j(G(\boldsymbol{u}_i))$ gives 1 if $g(\boldsymbol{u}_i) \leq \xi_j$ and 0 else. The $\boldsymbol{u}_i$, $i = 1, \ldots n_\text{SuS}$ are samples distributed according to $\varphi_d(\boldsymbol{u}|\mathcal{F}_{j-1})$, i.e., samples from the nominal density censored at the intermediate domain of the previous step. The ξ_j are chosen such that a certain percentage p_0 of the samples are located in the respective intermediate domain. Effective values of p_0 are typically in the order of $p_0 \in [0.1,\ 0.3]$ [170]. These elite samples are then used as basis for the generation of a new set of n_SuS independent samples for the next step, all of which need to be located inside the intermediate domain of the current step. This can be done efficiently by means of MCMC algorithms [e.g., 23, 124, 169, 170]. When the failure domain is reached, i.e., a minimum of $p_0 n_\text{SuS}$ samples are located in the failure domain, $P_\mathcal{F}$ is estimated by means of Equation (2.107). For finite n_SuS, $P_{\mathcal{F},\text{SuS}}$ is a biased estimate, since the samples to estimate the sequence of nested events are not completely independent and the intermediate thresholds are chosen adaptively [7, 20]. Assuming independence of the estimates for the conditional probabilities, the CoV of $P_{\mathcal{F},\text{SuS}}$ can be approximated by a first-order Taylor series expansion

through the CoVs of the probability estimates for the nested sequence of events [7].

Figure 2.20 shows the final level of a SuS run resulting in an estimated failure probability of $P_{\mathcal{F},\mathrm{SuS}} = 3.9 \times 10^{-3}$, slightly below the reference value of $P_{\mathcal{F}} = 4.0 \times 10^{-3}$. The red dashed lines show the thresholds $\xi_j,\ j = 1, 2$ defining the intermediate events $\mathcal{F}_j,\ j = 1, 2$ on the way to reaching the failure domain $\mathcal{F}$ bounded by the limit state surface indicated by the solid red line.

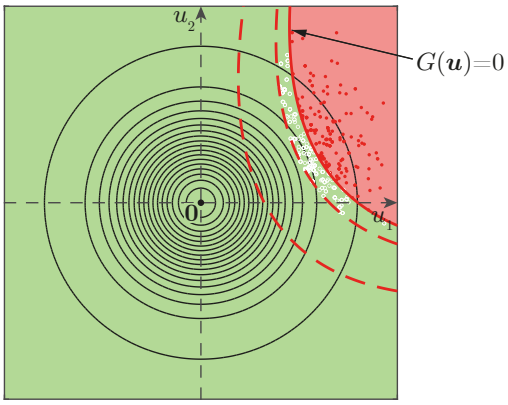

Figure 2.20: Solution of a reliability problem in two-dimensional $\boldsymbol{U}$-space with SuS using a sample size of $n_{\mathrm{SuS}} = 500$ per level and $p_0 = 0.1$ (cf. panel a of Figure 2.19 for the initial MCS level and the corresponding selection of the $p_0 n_{\mathrm{SuS}}$ elite samples). A large portion of the samples falls into the failure domain (red dots) in the final level of SuS. The dashed red lines illustrate the limits of the intermediate domains and the black lines show the isolines of $\varphi_2(\boldsymbol{u})$.

2.2.2.5 Line sampling

Line sampling (LS) approximates $P_{\mathcal{F}}$ by identifying an important direction $\boldsymbol{\alpha}_{\mathrm{LS}}$ in $\boldsymbol{U}$-space that points towards the failure domain and reducing the reliability problem to a set of one-dimensional root finding problems along the important direction. The initial formulation of LS aims at improving the accuracy of FORM estimates by choosing $\frac{\boldsymbol{u}^*}{\beta_{\mathrm{HL}}}$ as important direction and, thus, requires running a FORM analysis before applying LS [80]. The generalization of LS to a stand-alone simulation method allows to drop this requirement and use any reasonably chosen direction as important direction $\boldsymbol{\alpha}_{\mathrm{LS}}$ [95].

The LS algorithm is based on solving Equation (2.90) in a rotated coordinate space. Although the following approach provides an elegant solution to this problem, it is not the only way to solve the problem. Assume a $d-1$-dimensional hyperplane through the origin and perpendicular to $\boldsymbol{\alpha}_{\mathrm{LS}}$, onto which a d-dimensional standard normal random vector $\boldsymbol{U}$ is projected, e.g., by applying the following projection:

$$\boldsymbol{U}^{\perp}_{\boldsymbol{\alpha}_{\mathrm{LS}}} = \boldsymbol{U} - (\boldsymbol{U} \bullet \boldsymbol{\alpha}_{\mathrm{LS}})\, \boldsymbol{\alpha}^{\mathsf{T}}_{\mathrm{LS}}, \tag{2.109}$$

where $\bullet$ denotes the dot product. n_{LS} samples are generated from $\varphi_d(\boldsymbol{u})$ and projected onto the hyperplane by application of Equation (2.109). Starting from the projected samples $\boldsymbol{u}^{\perp}_{\boldsymbol{\alpha}_{\mathrm{LS}},i},\ i = 1, \ldots, n_{\mathrm{LS}}$, a line search in direction $\boldsymbol{\alpha}_{\mathrm{LS}}$ is conducted for each sample to find the limit state surface $G\left(\boldsymbol{u}^{\perp}_{\boldsymbol{\alpha}_{\mathrm{LS}},i} + d_i \boldsymbol{\alpha}_{\mathrm{LS}}\right) = 0$. The unbiased LS estimator for $P_{\mathcal{F}}$ reads as follows [80, 95]:

$$P_{\mathcal{F},\mathrm{LS}} = \frac{1}{n_{\mathrm{LS}}} \sum_{i=1}^{n_{\mathrm{LS}}} \Phi\left(-d_i\right), \tag{2.110}$$

where $d_i,\ i = 1, \ldots n_{\mathrm{LS}}$ denotes the distance from the respective projected sample $\boldsymbol{u}^{\perp}_{\boldsymbol{\alpha}_{\mathrm{LS}},i}$ to the

limit state surface in direction $\boldsymbol{\alpha}_{\mathrm{LS}}$. It can be shown that the variance of $P_{\mathcal{F},\mathrm{LS}}$ is bounded by the variance of the MCS estimator, i.e., $\mathbb{V}[P_{\mathcal{F},\mathrm{LS}}] \leq \mathbb{V}[P_{\mathcal{F},\mathrm{MCS}}]$ for $n_{\mathrm{LS}} = n_{\mathrm{MCS}}$ [95]. However, this inequality does not account for the fact that the line search algorithm to determine d_i typically requires more than a single limit state function evaluation leading to a larger computational cost. Figure 2.21 shows an LS run with $\boldsymbol{\alpha}_{\mathrm{LS}}$ obtained from a FORM analysis (cf. Section 2.2.2.1 and Fig 2.16) resulting in $P_{\mathcal{F},\mathrm{LS}} = 4.2 \times 10^{-3}$, i.e., slightly larger than the true probability of failure of $P_{\mathcal{F}} = 4.0 \times 10^{-3}$. In panel a, the gray circles show the projected samples on the hyperplane, from which the line search algorithm is initiated in direction $\boldsymbol{\alpha}_{\mathrm{LS}}$ to find the corresponding point on the limit state surface (black dots). Panel b shows the individual contributions to $P_{\mathcal{F},\mathrm{LS}}$ exemplarily for two of the ten samples.

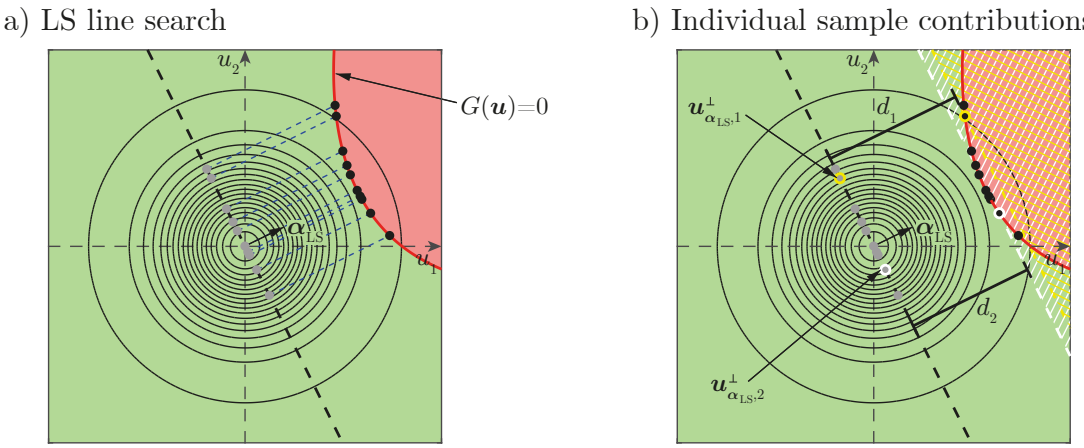

Figure 2.21: Solution of a reliability problem in two-dimensional $\boldsymbol{U}$-space with LS using a sample size of $n_{\mathrm{LS}} = 10$. Panel a shows the projected samples (gray dots) located on the hyperplane perpendicular to $\boldsymbol{\alpha}_{\mathrm{LS}}$ (black dashed line). The blue dashed lines show the line search in direction $\boldsymbol{\alpha}_{\mathrm{LS}}$ from the projected samples to the corresponding points on the limit state surface (black dots). The individual contributions to $P_{\mathcal{F},\mathrm{LS}}$ are exemplarily shown for two samples ($\boldsymbol{u}^{\perp}_{\boldsymbol{\alpha}_{\mathrm{LS}},1}$ (yellow circle) and $\boldsymbol{u}^{\perp}_{\boldsymbol{\alpha}_{\mathrm{LS}},2}$ (white circle)) in panel b. Therein, d_1 and d_2 indicate the distances to the limit state surface, the white and yellow hatched areas represent the corresponding contributions to $P_{\mathcal{F},\mathrm{LS}}$.

The efficiency of LS largely depends on the choice of $\boldsymbol{\alpha}_{\mathrm{LS}}$. This choice can be based on, e.g., information on a design point [80, 95], sampling in the failure domain [95], exchange of potential and kinetic energy in systems describing conservative inelastic structures [134], or evaluation of the gradient of $G(\boldsymbol{u})$ [133].

Advanced line sampling (ALS) further extends the LS approach by introducing an adaptive choice of the important direction, thus, allowing for a poor initial choice of $\boldsymbol{\alpha}_{\mathrm{LS}}$ [34]. In addition, ALS reduces the computational cost of the line search by making use of information on the distance to the failure domain of the sample closest to the current sample on the hyperplane [34]. The efficiency can be further improved by combination line sampling (CLS), which introduces weights for the adaptively chosen important directions [128]. The weights represent the relative importance of the direction in the contribution to the estimate for $P_{\mathcal{F}}$ and can be calculated in a heuristic manner. The resulting estimators for $P_{\mathcal{F}}$ in ALS and CLS remain unbiased and, similar to LS, their variance is bounded by the variance of the MCS estimator [128]. LS and its adaptive variants are especially useful for problems with unimodal failure domains, but can be extended to multimodal failure domains by accounting for several important directions separately [149].

2.2.2.6 Comparison of methods

Several classes of reliability methods have been presented in the previous sections, each of which is more suitable for specific problem types. In this section, the characteristics presented in Section 2.2.1.5 are employed for a short comparison of the presented methods in tabulated form in Table 2.1. The rating of the methods is based on a three-stage scale, where "+" refers to good suitability for problems of the respective category, "O" to limited suitability and "−" indicates that the method should not be used for problems of that category. In addition to the presented characteristics, two further criteria are considered in the comparison, namely the computational budget $\mathcal{B}$ and the required accuracy $\mathcal{G}$. The methods are split into the two categories "approximation methods" and "simulation methods".

The computational budget is an important criterion when $G(\boldsymbol{u})$ includes a complex numerical model. The presented methods have been categorized into three classes according to the available computational budget as follows:

- $\mathcal{B}_1$: Only a small number of samples can be evaluated ($N = \mathcal{O}(10^2)$).
- $\mathcal{B}_2$: An intermediate to moderately large number of samples can be evaluated ($N = \mathcal{O}(10^2) - \mathcal{O}(10^5)$).
- $\mathcal{B}_3$: A very large number of samples can be evaluated.

Depending on the type of analysis, the required degree of accuracy can vary, which is accounted for by a two-stage categorization:

- $\mathcal{G}_1$: Information on the magnitude or an upper bound of $P_\mathcal{F}$ is sufficient (e.g., $P_\mathcal{F} \leq 10^{-4}$).
- $\mathcal{G}_2$: $P_\mathcal{F}$ needs to be evaluated to the highest possible degree of accuracy.

Table 2.1: Comparison of the presented reliability methods for different problem types. The symbols represent the following suitability: "+" good suitability, "O" limited suitability, "−" No/severely limited suitability. The superscripts indicate additional information provided in the text.

Characteristic of problem setting	Approximation		Simulation			
	FORM	SORM	MCS	IS	SuS	LS
Computational budget	$\mathcal{B}_1$ (1)	$\mathcal{B}_1$ (1)	$\mathcal{B}_3$ (2)	$\mathcal{B}_2$	$\mathcal{B}_2$	$\mathcal{B}_1$
Required accuracy	$\mathcal{G}_1$ (3)	$\mathcal{G}_2$	$\mathcal{G}_2$	$\mathcal{G}_2$	$\mathcal{G}_2$	$\mathcal{G}_2$
Multimodal failure	− (4)	− (4)	+	O (5)	+	O (6)
High-dimensional input random vector	−	−	+	O (7)	+ (8)	O (9)
Very small failure probability	+	+	−	+	+	+
Black box analysis	O	O	+	+	+	+
Numerical instability	−	−	+	+	+	+
Nonlinearity of limit state function	O	+	+	+	+	+
Availability of gradient information	+	+	−	−	−	O
Information on accuracy of the estimate	−	−	+	+	O	O

As this simplification cannot account for all possible variants of the compared methods, some additional information is provided in the following list, referring to the superscript in the respective cell of Table 2.1.

(1) The computational cost of FORM and SORM strongly depends on the number of input random variables d and increases with increasing d. However, as they are not recommended for solving high-dimensional problems in general (cf. line "High-dimensional input random vector" in Table 2.1), they are categorized as $\mathcal{B}_1$ for low-dimensional problems.

(2) Apart from the complexity of $G(\boldsymbol{u})$, the computational cost of MCS only depends on $P_{\mathcal{F}}$. Since we are interested in evaluating the probability of a rare event, MCS requires a large number of samples and, thus, is categorized as $\mathcal{B}_3$.

(3) The accuracy of FORM depends on the nonlinearity of $G(\boldsymbol{u})$ with decreasing accuracy for increasing nonlinearity. If $G(\boldsymbol{u})$ is a linear function of $\boldsymbol{U}$, FORM results in the exact solution.

(4) Approximation methods can be used for multimodal failure domains by additional runs to find all design points [39]. In system reliability problems, the failure event can be approximated through the minimal cut set of the component failure events [77]. However, some of the presented simulation methods are more suitable for this type of problems.

(5) The suitability of IS for multimodal failure domains depends on the choice of the IS density $h(\boldsymbol{u})$. Using mixture distributions and/or prior information on the number of failure domains can be helpful in that case.

(6) LS can be used for multimodal failure domains by accounting for several important directions.

(7) For efficiently solving high-dimensional problems, $h(\boldsymbol{u})$ needs to be chosen accordingly.

(8) SuS is the classic choice for reliability analysis in high dimensions. However, the performance depends on the choice of the algorithm for the generation of the conditional samples in the series of nested events. If the MCMC algorithm performs well in high dimensions, SuS can solve high-dimensional problems.

(9) Finding an important direction becomes difficult in high dimensions. If an adequate choice of the important direction can be made, LS is able to perform well in high dimensions.

2.2.3 Structural reliability with random fields

The focus in Section 2.2.2 is put on the description and illustration of reliability methods, where the origin of the d RVs entering the input vector $\boldsymbol{U}$ is not part of the discussion. In the following, we consider the special case in which a subset of $\boldsymbol{U}$ are RVs used to discretize one or several RFs, i.e., $\boldsymbol{U} = [\boldsymbol{U}_{\mathrm{RF}}, \boldsymbol{U}_{\mathrm{RV}}]$, where $\boldsymbol{U}_{\mathrm{RF}} = [U_{\mathrm{RF},1}, \ldots, U_{\mathrm{RF},d_1}]$ are the d_1 RVs used to discretize the RF(s), $\boldsymbol{U}_{\mathrm{RV}} = [U_{\mathrm{RV},1}, \ldots, U_{\mathrm{RV},d_2}]$ are the d_2 remaining uncertain input variables, and $d = d_1 + d_2$. $\boldsymbol{U}_{\mathrm{RV}}$ can include RVs that are directly connected to the spatial variability (e.g., when using a Student's t-RF that is expressed as function of a Gaussian RF and one additional RV, cf. Section 2.1.6.2), but does not depend on the chosen RF discretization. In contrast, the dimensionality of $\boldsymbol{U}_{\mathrm{RF}}$ is determined by the RF discretization method and the chosen number of elements/terms (cf. Section 2.1.6.3).

2.2.3.1 Effects of spatial variability on structural reliability

Modeling an uncertain quantity X as spatially variable RF $X(\boldsymbol{z})$ instead of an RV requires a change of perspective on the mechanical model in the reliability analysis. Typically, X represents

a load on a structure or a material property of a structural member. If X is modeled space-invariant, the mechanical model can often be evaluated for some carefully selected realizations of X to determine critical regions or potential failure modes; this does no longer hold for spatially variable inputs [42]. In that case, the location of potential failure strongly depends on the RF parameters, the RF discretization and the specific RF realization. The number of potential failure surfaces can further increase if several parameters are modeled as RFs. In some cases, modeling spatial variability may even lead to completely new failure modes. However, modeling spatial variability also enables accounting for effects that decrease the variability of the system response, e.g., averaging processes or redistribution of loads/stresses within the mechanical model.

Hence, the effects of spatial variability on structural reliability can only be correctly accounted for by a spatial view on the mechanical model and the stochastic model throughout the analysis. To avoid this additional effort, simplified approaches have been developed, e.g., replacing a spatially variable load by an equivalent uniformly distributed load [110, 113, 83]. Another approach aims at replacing the input RF(s) by an RV for the system response, however, suffering from the limited applicability to complex structures [151, 24, 89]. Alternatively, one can model the spatially variable property with a single RV by accounting for the spatial variability through the spatial averaging approach (cf. Section 2.1.6.3), which has proven to be especially useful for geotechnical applications [e.g., 136, 31, 129].

2.2.3.2 One-dimensional beam example

A simple one-dimensional beam example is chosen to illustrate the effect of spatially variable load and/or resistance variables, and the type and degree of accuracy of the RF discretization. The system response is evaluated using Euler-Bernoulli beam theory [e.g., 12]. A statically indeterminate two-span steel beam is investigated, with a length of $L = 6\,\mathrm{m}$ per span and subject to uniform vertical load q, as illustrated in Figure 2.22. The cross section has a height of $H = 140\,\mathrm{mm}$ and a moment of inertia of $I_y = 1050\,\mathrm{cm}^4$ with a load from self-weight of $g = 0.25\,\mathrm{kNm}^{-1}$. Initially, the steel yield strength f_y is modeled as lognormal RV with mean $\mu_{f_y} = 280\,\mathrm{MPa}$ and CoV $\delta_{f_y} = 0.07$ [84], the vertical load is modeled as normal RV with mean $\mu_q = 5\,\mathrm{kNm}^{-1}$ and CoV $\delta_q = 0.4$, and the beam flexibility F is constant throughout the beam. f_y and q are assumed to be independent. Through the constant beam flexibility, the internal forces are independent of F and can directly be calculated. The location of the maximum absolute bending moment is at the support in the center and its value is $M_{y,\max} = \frac{|q+g|L^2}{8}$ [3]. The resulting yield stress is calculated as $\sigma_{y,\max} = \frac{M_{y,\max}}{I_y}\frac{H}{2}$.

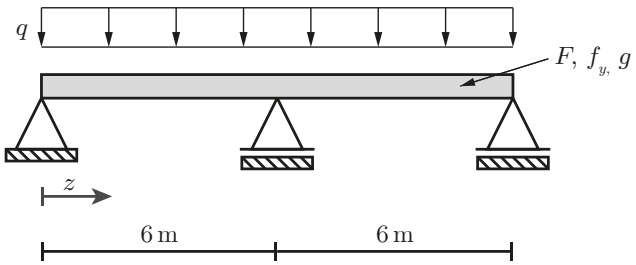

Figure 2.22: Statically indeterminate two-span steel beam under uniform vertical load q. The beam flexibility F and yield strength f_y are constant throughout the beam. q, F and f_y are independent RVs, the self-weight g is deterministic.

The limit state function is defined as exceedance of the yield strength, i.e.,

$$g(f_y, q) = f_y - \frac{M_{y,\max}(q)}{I_y}\frac{H}{2} = f_y - \frac{|g+q|L^2 H}{16 I_y}. \tag{2.111}$$

The transformed limit state function in $\boldsymbol{U}$-space reads

$$G(\boldsymbol{u}) = \exp\left(\mu_{\ln,f_y} + \sigma_{\ln,f_y} u_1\right) - \frac{|g+\mu_q+\sigma_q u_2|L^2 H}{16 I_y}, \tag{2.112}$$

where $\mu_{\ln,f_y} = 5.632$ and $\sigma_{\ln,f_y} = 0.070$ are the parameters of the lognormal distribution of f_y (cf. Section 2.1.3.3), and $\sigma_q = 2\,\mathrm{kNm}^{-1}$ is the standard deviation of q. Since Equation (2.111) represents an $R-S$ reliability problem, the failure probability can be obtained through numerical integration by application of Equation (2.82), resulting in $P_{\mathcal{F},RV} = 2.60 \times 10^{-2}$. Using FORM to estimate the failure probability, the design point is found at $\boldsymbol{u}^* = [-0.5771, 1.8462]$ and the corresponding estimate for the failure probability is calculated as $P_{\mathcal{F},\mathrm{FORM}} = 2.65 \times 10^{-2}$, i.e., FORM slightly overestimates $P_{\mathcal{F},RV}$. Hence, the limit state surface is mildly convex in $\boldsymbol{U}$-space.

Next, the load and the beam flexibility are modeled as one-dimensional RFs, instead of RVs. $q(z)$ is a Gaussian RF with parameters μ_q and δ_q as before, and the exponential correlation model with $L_c = 2\,\mathrm{m}$. The beam flexibility $F(z)$ is a Gaussian RF with mean $\mu_F = 0.5\,\mathrm{MN}^{-1}\mathrm{m}^{-2}$, CoV $\delta_F = 0.05$ and the exponential correlation model with $L_c = 4\,\mathrm{m}$. f_y, $q(z)$ and $F(z)$ are assumed to be independent [84]. The situation is illustrated in Figure 2.23.

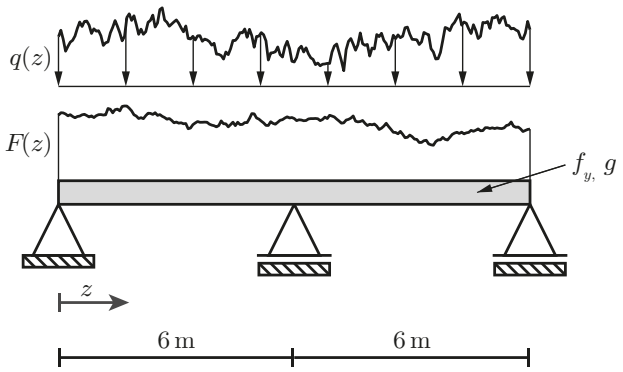

Figure 2.23: Statically indeterminate two-span steel beam under spatially variable vertical load $q(z)$ and with spatially variable beam flexibility $F(z)$ (each illustrated by a random realization of the RF). The random yield strength f_y is constant throughout the beam. $q(z)$, $F(z)$ and f_y are independent, the self-weight g is deterministic.

The MP method and SA method are used for the RF discretization and the results are compared. The RFs are discretized with $\frac{d_1}{2}$ RVs per RF, i.e., the total number of RVs entering the problem is $d_1 + 1$. The system response is evaluated with the linear finite element method based on the Euler-Bernoulli beam theory with 100 equisized finite elements [122, 123], and the failure probability is estimated with MCS using $N_{\mathrm{MCS}} = 1 \times 10^6$ samples. The reference failure probability is calculated as $P_{\mathcal{F},RF} = 4.27 \times 10^{-4}$. It is obtained using the MP method with $\frac{d_1}{2} = 100$ RVs per RF, which equals the number of finite elements used to evaluate the system response. $P_{\mathcal{F},RF}$ is approximately 60 times smaller than $P_{\mathcal{F},RV}$, because for each random realization of the spatially variable input variables ($q(z)$ and $F(z)$) large parts of the variability average out over the beam length. Thus, the effective variability of the random fields entering the mechanical model is smaller than the variability of their marginal distributions. Consequently, the variability of the system response (maximum bending moment) is significantly lower compared to the case without accounting for spatial variability, where the full variability

of the marginal distributions directly transfers to the mechanical model and propagates to the system response.

For $\frac{d_1}{2} = 1$, the MP method neglects the spatial variability and the problem reduces to the space-invariant problem, as illustrated in Figure 2.22 with the corresponding failure probability estimate of $P_{\mathcal{F},MP,d_1} = P_{\mathcal{F},MP,2} = P_{\mathcal{F},RV} = 2.60 \times 10^{-2}$. This behavior is typical for point discretization methods, where the marginal distribution of the discretization is defined through the marginal distribution of the RF (cf. Section 2.1.6.3). Conversely, the SA method with $\frac{d_1}{2} = 1$ underestimates the failure probability, as it results in an estimate of $P_{\mathcal{F},SA,d_1} = P_{\mathcal{F},SA,2} = 2.56 \times 10^{-4}$. This is caused by the averaging of $q(z)$ and $F(z)$ over the whole beam length, which leads to an underestimation of the spatial variability entering the problem. By increasing the number of RVs in the RF discretization, both the MP method and the SA method converge to the reference solution with increasing number of RVs. The convergence of the estimates to the reference failure probability as a function of the number of RVs to discretize the RFs d_1 is illustrated in Figure 2.24.

Accounting for the spatial variability introduces uncertainty in the location of failure, as two additional potential failure locations within the two beam spans (close to $z = 2.45\,\text{m}$ and close to $z = 9.55\,\text{m}$) can be identified. However, $P_{\mathcal{F},RF}$ is dominated by failure at the support in the center of the beam, the other two failure modes only play a minor role. They require either a strongly asymmetric realization of $q(z)$, for which the bending moment becomes significantly larger in one field than in the other or, alternatively, a realization of $F(z)$ which gives the beam a significantly higher flexibility at the support than within the beam spans.

Additionally, the exact location of failure becomes uncertain due to the non-constant beam flexibility, meaning that failure does not have to occur, e.g., exactly at the support in the center, but can also occur a little to the right/left side of the support, depending on the realization of the RFs. Hence, with the RF approach, the beam shows three potential failure regions compared to one distinct failure location with the RV approach.

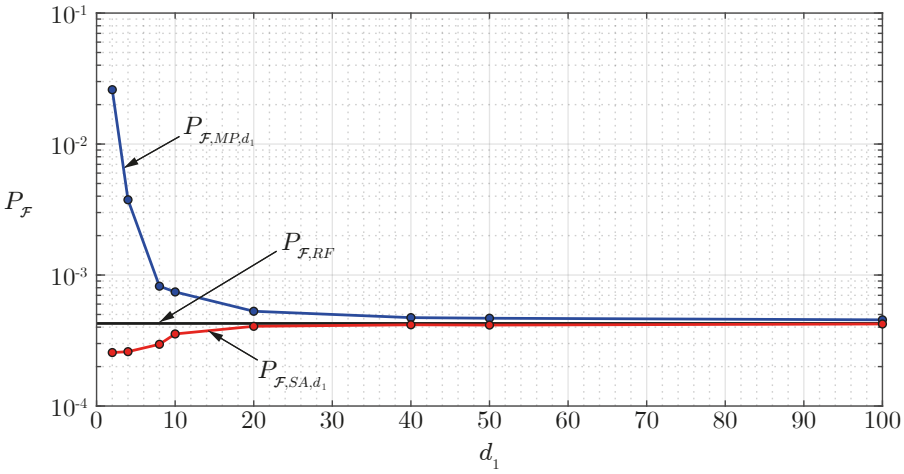

Figure 2.24: Convergence of the failure probability estimate evaluated with the MP method ($P_{\mathcal{F},MP,d_1}$, blue line) and SA method ($P_{\mathcal{F},SA,d_1}$, red line) to the reference solution $P_{\mathcal{F},RF}$ (black line) with increasing number of RVs to discretize the two RFs. The number of RVs d_1 for evaluating $P_{\mathcal{F},MP,d_1}$ (blue dots), $P_{\mathcal{F},SA,d_1}$ (red dots), respectively, are chosen such that $\frac{d_1}{2}$ equals an integer.

Although the results of this simple beam example are not surprising (the locations of the maximum span moment of a two-span beam with constant flexibility lie within the two additional failure regions), they illustrate the potential effect of accounting for spatial variability on structural reliability. Neglecting the spatial variability or approximating it with a coarse

RF discretization can lead to wrong estimates for $P_{\mathcal{F}}$. Conservative estimates can lead to an uneconomic design of structures or unnecessary repair/replacement measures, but non-conservative estimates may pose a safety risk. In addition, potential failure domains can remain undetected if spatial variability is not accounted for, which, even if those failure regions may not be dominating $P_{\mathcal{F}}$, is undesirable with respect to structural safety. This can be avoided by modeling spatially variable properties with RFs using a sufficiently fine discretization. In that case, however, the model complexity increases and estimating $P_{\mathcal{F}}$ becomes more difficult. In the present beam example, the computational cost of evaluating the model increases drastically when using RFs because the standardized solutions for beam structures are only applicable for (piece-wise) constant beam flexibility and simple geometric load cases [3] and, thus, the limit state function involves evaluating a finite element model instead of the simple algebraic expression of Equation (2.112). Furthermore, the dimensionality of $\boldsymbol{U}$ increases from $d = 3$ without spatial variability to $d \geq 21$ ($d_1 = 20$) with the MP method and $d \geq 11$ ($d_1 = 10$) with the SA method for achieving an acceptable level of accuracy in this case, which limits application of some of the reliability methods described in Section 2.2.2.

It is also important to be aware of the accuracy of the numerical model, e.g., for this example, a finer discretization with the MP method than for the reference solution would not lead to more accurate results, since the stochastic discretization would then exceed the mechanical discretization, leading to nothing but a waste of computational resources. In order to achieve a more accurate solution, both the stochastic and the mechanical model need to be refined.

The observed effects are magnified by extending the problem setting from a simple linear beam to more complex structures, where potential failure modes may be less obvious than in this case and the effects of neglecting spatial variability can be both uneconomic or unsafe. The interaction of various structural elements and different uncertain input parameters further complicate an assessment of the adequacy of the chosen stochastic model.

2.3 Learning the stochastic material model from data

Performing reliability analysis requires a stochastic model of the uncertain input quantities. If data is available, e.g., from measurements or data bases, this information can be used to learn a tailor-made stochastic model for the problem at hand. Since the focus of this thesis lies on the spatial variability of material properties, the following sections aim at concepts that are used for learning stochastic models of material properties. Nevertheless, the underlying theory can be adjusted for general use in structural reliability or other engineering applications.

2.3.1 Random variable approach

Modeling the uncertain quantity of interest as RV means neglecting potential spatial variability and spatial correlation of the data. Since most approaches in engineering practice are restricted to modeling RVs, they are briefly introduced in this section.

2.3.1.1 Frequentist vs. Bayesian perspective

Two main approaches can be distinguished in statistical inference, corresponding to two different ways to interpret probabilities: (i) frequentist approaches and (ii) Bayesian approaches. The frequentist perspective treats probability as long-run averages of occurrence of events, i.e., the probability of an event is defined as the relative frequency of an event given a large number of repeated trials [e.g., 82]. The Bayesian perspective on the other hand views probability as a degree of belief, depending on the available information and, thus, is far more subjective than

the frequentist perspective [e.g., 142]. Further interpretations of probability exist, but are not discussed this this point, an overview can be found in [73]. Answering the question whether Bayesian or frequentist statistics are preferable in statistical inference would go far beyond the scope of this thesis. Depending on the application, the one or the other may yield certain (dis)advantages over the other one. However, it is worth noting that many frequentist results can be derived in a Bayesian way or form special cases of Bayesian results. For example, maximum likelihood estimation, a popular approach to estimate parameters in a frequentist way, yields the same results as the Bayesian maximum a-posteriori estimation with uniform prior distribution (although their interpretation differs) [118]. Various applications of learning a stochastic model from data in a frequentist or Bayesian way can be found in the literature and are not listed here, the interested reader is referred to [15] for applications related to civil engineering or to [61] for Bayesian approaches to statistical inference.

2.3.1.2 Established methods to include measurements

The partial safety concept is built upon the use of quantile values as characteristic values of material properties (cf. Section 2.2.1.1). Two different approaches to estimate quantile values of an uncertain material property X from measurement data $\boldsymbol{x}_m = [x_{m,1}, \dots, x_{m,n}]$ are described in the following. The first one uses Bayesian statistics and is included in EN 1990 in Annex D.7 as well as in EN 13791 [47, 46]. It is described in detail in Chapter 4 (original publication [64]) and Chapter 5 (original publication [65]). The second one is based on a frequentist approach and is included in a guideline of the *Bundesanstalt für Wasserbau* (BAW, Federal Waterways Engineering and Research Institute, Germany), where it is used for estimating characteristic values of concrete compressive strength in existing hydraulic structures [26]. Both require only the number of measurements n, the sample mean $\bar{\mu}_X$ and the sample CoV $\bar{\delta}_X = \frac{\bar{\sigma}_X}{\bar{\mu}_X}$, where $\bar{\sigma}_X^2$ is the sample variance, and assumptions on the distribution of X. $\bar{\mu}_X$ and $\bar{\sigma}_X^2$ are given as

$$\bar{\mu}_X = \frac{1}{n} \sum_{i=1}^{n} x_{m,i}, \tag{2.113a}$$

$$\bar{\sigma}_X^2 = \frac{1}{n-1} \sum_{i=1}^{n} \left(x_{m,i} - \bar{\mu}_X\right)^2, \tag{2.113b}$$

where $x_{m,i},\ i = 1, \dots n$ are the measurement values.

- **Bayesian approach**: It is assumed that X follows a normal distribution with unknown parameters μ_X and λ_X, which are the mean value and precision, respectively. The uncertainty on μ_X and λ_X is accounted for by a normal-gamma ($\mathcal{NG}$) distribution, i.e., μ_X follows a normal distribution conditional on λ_X, and λ_X follows a gamma distribution (cf. Section 2.1.3.6). The prior parameters of the $\mathcal{NG}$ distribution are chosen as $[\mu_0, \kappa_0, \alpha_0, \beta_0] = [/, 0, -\frac{1}{2}, 0]$, resulting in a non-informative prior distribution [35]. The posterior predictive distribution of X is available in closed form; it is the Student's t-distribution with location parameter $\mu_t = \bar{\mu}_X$, scale parameter $\lambda_t = \frac{n(n-1)}{(n+1)} \cdot \left(\sum_{i=1}^{n} \left(x_{m,i} - \bar{\mu}_X\right)^2\right)^{-1}$, and $\nu_t = n - 1$ degrees of freedom (cf. Section 2.3.2.3).

  The procedure is standardized by normalizing the posterior predictive distribution. Consequently, the quantile values of the posterior predictive distribution are determined via standardized coefficients $k_{n,\mathrm{B}}$:

$$k_{n,\mathrm{B}} = -F_t^{-1}(p)\sqrt{\frac{n+1}{n}}, \tag{2.114}$$

where $F_t^{-1}(\cdot)$ is the inverse CDF of the standard Student's t-distribution with $n-1$ degrees of freedom ($\mu_t = 0$, $\lambda_t = 1$) and $p = 0.05$, since the characteristic value in this approach is defined as the 5% quantile value. Through the standardization, $k_{n,\mathrm{B}}$ only depends on n and can easily be tabulated. The characteristic value $x_{\mathrm{k,B}}$ can then be determined as follows:

$$x_{\mathrm{k,B}} = \bar{\mu}_X(1 - k_{n,\mathrm{B}} \cdot \bar{\delta}_X). \tag{2.115}$$

The method is also applicable in the case when the property Y is assumed to follow a lognormal distribution and measurement data $\boldsymbol{y}_m = [y_{m,1}, \ldots, y_{m,n}]$ is available. The characteristic value of Y can then be calculated as

$$y_{\mathrm{k,B}} = \exp\left(\bar{\mu}_X(1 - k_{n,\mathrm{B}} \cdot \bar{\delta}_X)\right), \tag{2.116}$$

where $\bar{\mu}_X$ and $\bar{\delta}_X$ are the sample mean and sample CoV calculated by means of Equations (2.113a) and (2.113b) with the logarithmic samples $x_{m,i} = \ln(y_{m,i})$, $i = 1, \ldots, n$.

- **Frequentist approach**: It is assumed that X follows a normal distribution with unknown parameters. The aim of the procedure is the estimation of the 5% quantile value with 95% confidence. To this end, the normal distribution is replaced by a Student's t-distribution with $\nu_t = n - 1$ degrees of freedom to account for the finite sample size [132]. The 5% quantile value $x_{0.05}$ itself follows a Student's t-distribution with $\nu_t = n - 1$ degrees of freedom, location parameter $\mu_{t,0.05} = x_{0.05}$ and unknown scale parameter [132]. The scale parameter is approximated through a second-order Taylor series expansion around $\mu_{t,0.05}$ [132, 57].

  For application purpose, the method is brought to the same format as the Bayesian approach presented above:

$$x_{\mathrm{k,F}} = \bar{\mu}_X(1 - k_{n,\mathrm{F}} \cdot \bar{\delta}_X). \tag{2.117}$$

  The extension to a lognormal property Y with available measurement data $\boldsymbol{y}_m = [y_{m,1}, \ldots, y_{m,n}]$ is performed in a similar manner as for the Bayesian approach, i.e.,

$$y_{\mathrm{k,F}} = \exp\left(\bar{\mu}_X(1 - k_{n,\mathrm{F}} \cdot \bar{\delta}_X)\right), \tag{2.118}$$

  with the sample mean $\bar{\mu}_X$ and sample CoV $\bar{\delta}_X$ respectively, of the logarithmic samples $x_{m,i} = \ln(y_{m,i})$, $i = 1, \ldots, n$.

In practice, the only difference between the two approaches lies in the coefficients $k_{n,\mathrm{B}}$, $k_{n,\mathrm{F}}$ respectively. Thus, they are listed in Table 2.2 for different sample sizes n. While the Bayesian approach directly aims at estimating the 5% quantile, the frequentist approach tries to estimate the 5% quantile value with 95% confidence. This additional conservatism is reflected by larger values of $k_{n,\mathrm{F}}$ compared to $k_{n,\mathrm{B}}$ for finite sample size n. Both approaches converge to a coefficient of 1.64 for $n \to \infty$ because the parameters of the normal distribution can (theoretically) be determined exactly in that case and no uncertainty remains ($1.64 = -\Phi^{-1}(0.05)$). Figure 2.25 illustrates the behavior of the mean estimated characteristic value for the two approaches and the corresponding two-sided 90% intervals. While for the Bayesian approach (panel a), the mean value $\mu_{x_{\mathrm{k,B}}}$ converges to the true 5% quantile value with increasing sample size n, for the more conservative frequentist approach (panel b), the 95% quantile value of the estimated characteristic value almost equals the true 5% quantile value for sample size $n \geq 5$.

It is important to note that both presented approaches are only applicable if a number of requirements are fulfilled: the samples need to be statistically independent, they have to be taken randomly in space and the sample size needs to be representative for the quantity of

Table 2.2: Coefficients $k_{n,\mathrm{B}}$ and $k_{n,\mathrm{F}}$ for selected values of the sample size n.

n	3	4	5	6	8	10	20	30	50	100	∞
$k_{n,\mathrm{B}}$	3.37	2.63	2.34	2.18	2.01	1.92	1.77	1.73	1.69	1.67	1.64
$k_{n,\mathrm{F}}$	6.36	4.65	3.94	3.54	3.10	2.86	2.38	2.21	2.06	1.92	1.64

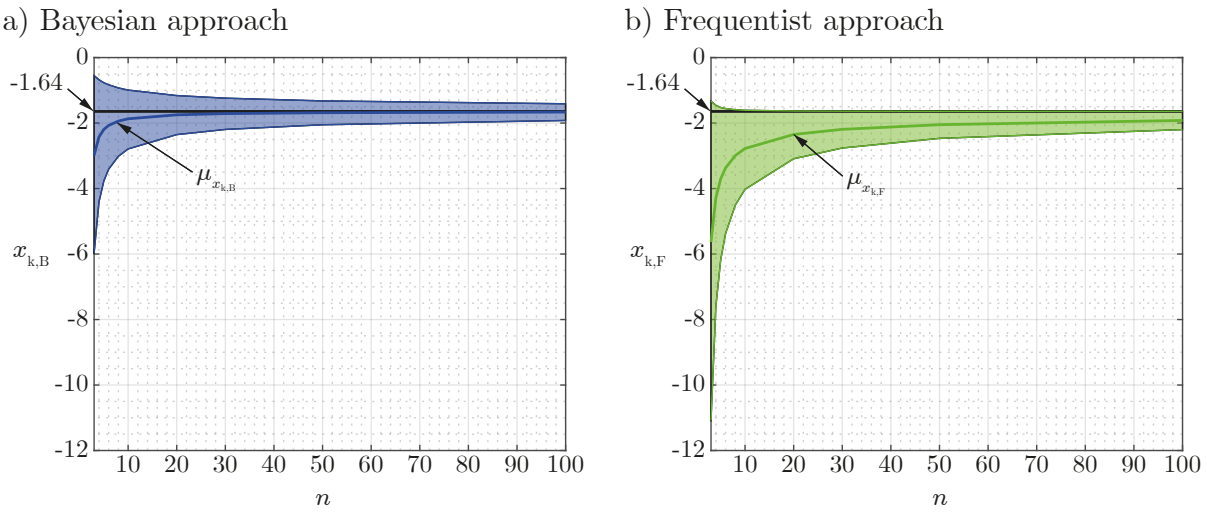

Figure 2.25: Behavior of the mean of the estimated characteristic value for the Bayesian (panel a, $\mu_{x_{\mathrm{k,B}}}$) and the frequentist (panel b, $\mu_{x_{\mathrm{k,F}}}$) approach and the corresponding two-sided 90% intervals (shaded areas) for increasing sample size n. The black horizontal line indicates the reference solution for the 5% quantile value of a standard normal distribution ($-1.64 = \Phi^{-1}(0.05)$).

interest [137, 57]. The last condition is typically assumed to be fulfilled by requiring a minimum sample size for the investigated structure [46], but only little attention is paid to the other two conditions and they are often violated in practice.

2.3.2 Random field updating

Modeling spatially variable material properties requires an RF model, as introduced in Section 2.1.6. The RF parameters can be learned from data, if available. Bayesian approaches are well-suited for such applications, as they allow to combine prior information and site-specific information to build a stochastic model and, thus, this study is limited to Bayesian methods to learn RF models from data.

The spatial variability introduces an additional level of complexity to the stochastic model and various approaches have been developed to tackle the problem of statistical inference in the presence of spatial variability. In the civil engineering community, the potential of modeling spatial variability has been especially recognized in the field of geotechnical engineering [131, 164]. Consequently, many of the available approaches have been developed and/or applied for geotechnical purposes [e.g., 130, 32, 129, 85, 30, 163, 116]. Furthermore, Bayesian learning has been used for solving inverse problems with spatial variability, using response measurements, for example in mechanical engineering [e.g., 155, 158] or hydrological problem settings [99]. It has also been applied for identifying the spatial variability of material properties in the microstructure [148].

Bayesian learning of RF parameters has been applied for many years in the field of geostatistics to interpolate spatial data through kriging [154, 74, 10]. Other closely related applications can be found in the field of machine learning, in the context of Gaussian process regression [e.g.,

141].

2.3.2.1 Bayesian updating of Gaussian random fields

If the spatial variability is modeled with a Gaussian RF and the likelihood function of the data is Gaussian, the RF can be updated in closed form. The reason for this is the self-conjugacy of the Gaussian distribution (cf. Section 2.1.5.2), i.e., if the prior RF and the likelihood function are both Gaussian, the posterior RF is also Gaussian.

Assume a Gaussian RF $X(\boldsymbol{z})$ with prior parameters mean value μ'_X, standard deviation σ'_X and correlation function $\rho'(\boldsymbol{z}_i, \boldsymbol{z}_j)$. In addition, assume that n measurements of X and the corresponding measurement locations are available, collected in $\boldsymbol{x}_m = [x_{m,1}, \dots, x_{m,n}]$ and $\boldsymbol{z}_m = [\boldsymbol{z}_{m,1}, \dots, \boldsymbol{z}_{m,n}]$, respectively. In that case, the following updating rules for the mean function and covariance function of the RF $X(\boldsymbol{z})$ can be derived [e.g., 154]:

$$\mu''_X(\boldsymbol{z}) = \mu'_X + \boldsymbol{R}_{\boldsymbol{z}_m}(\boldsymbol{z}) \cdot \mathbf{R}^{-1}_{\boldsymbol{z}_m,\boldsymbol{z}_m} \cdot (\boldsymbol{x}_m - \mu'_X)^{\mathsf{T}}, \tag{2.119a}$$

$$\mathbb{C}\mathrm{ov}''_X(\boldsymbol{z}_i, \boldsymbol{z}_j) = (\sigma'_X)^2 \cdot \left(\rho(\boldsymbol{z}_i, \boldsymbol{z}_j) - \boldsymbol{R}_{\boldsymbol{z}_m}(\boldsymbol{z}_i) \cdot \mathbf{R}^{-1}_{\boldsymbol{z}_m,\boldsymbol{z}_m} \cdot \boldsymbol{R}^{\mathsf{T}}_{\boldsymbol{z}_m}(\boldsymbol{z}_j)\right). \tag{2.119b}$$

$\boldsymbol{R}_{\boldsymbol{z}_m}(\boldsymbol{z})$ is a $1 \times n_m$ row vector function with element i equal to $\rho'(\boldsymbol{z}, \boldsymbol{z}_{m,i})$ and $\mathbf{R}_{\boldsymbol{z}_m,\boldsymbol{z}_m}$ is an $n_m \times n_m$ matrix with element (i, j) equal to $\rho'(\boldsymbol{z}_{m,i}, \boldsymbol{z}_{m,j})$. Figure 2.26 shows the Bayesian update of a one-dimensional Gaussian RF $X(z)$ by means of Equations (2.119a) and (2.119b). The red dots show the measurements $x_{m,i},\ i = 1, \dots, n$ at locations $z_{m,i},\ i = 1, \dots, n$. $x'_{0.025}$ and $x'_{0.975}$ are the lower and upper bound of the prior two-sided 95% interval, respectively. These bounds and the prior mean value μ'_X are illustrated by dashed black lines. The posterior mean $\mu''_X(\boldsymbol{z})$ connects the measurements and reflects the information on $X(z)$ in the regions around the measurements. The lower and upper bound of the posterior two-sided 95% interval ($x''_{0.025}(z)$ and $x''_{0.975}(z)$) illustrate the reduction of the uncertainty in regions that are spatially correlated with one or several of the measurement locations. No uncertainty remains at the measurement locations, the interval bounds coincide with the posterior mean at these locations.

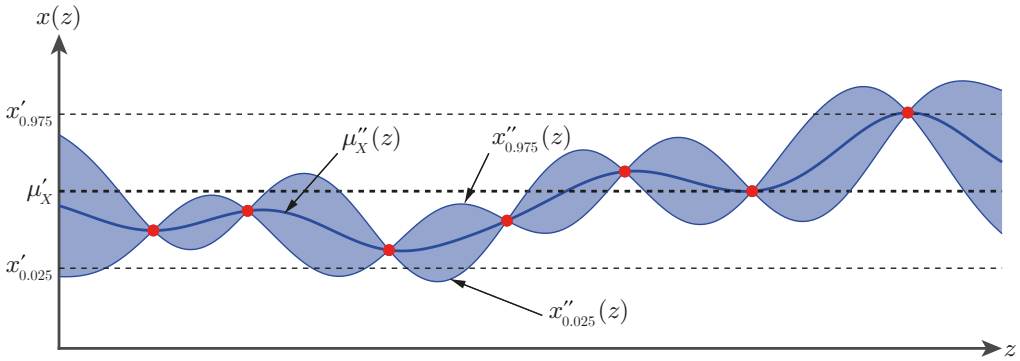

Figure 2.26: Bayesian updating of a one-dimensional Gaussian RF $X(z)$ with spatial data (red dots). μ'_X, $x'_{0.025}$ and $x'_{0.975}$ are the prior mean value and the bounds of the prior two-sided 95% interval. $\mu''_X(z)$, $x''_{0.025}(z)$ and $x''_{0.975}(z)$ are the spatial posterior mean and the spatial bounds of the posterior two-sided 95% interval (shaded area).

Equations (2.119a) and (2.119b) can be extended to the case where the measurements in $\boldsymbol{x}_m$ are associated with an additive zero-mean Gaussian measurement error ε, i.e., $x_{m,i} = x(\boldsymbol{z}_{m,i}) + \varepsilon_i,\ i = 1, \dots, n_m$. Assuming independence of the measurement error at different locations, the updating rules for the Gaussian RF are

$$\mu''_X(\boldsymbol{z}) = \mu'_X + \boldsymbol{R}_{\boldsymbol{z}_m}(\boldsymbol{z}) \cdot \mathbf{R}^{-1}_{\boldsymbol{z}_m,\varepsilon} \cdot (\boldsymbol{x}_m - \mu'_X)^{\mathsf{T}}, \tag{2.120a}$$

$$\mathbb{C}\mathrm{ov}''_X(\boldsymbol{z}_i, \boldsymbol{z}_j) = (\sigma'_X)^2 \cdot \left(\rho(\boldsymbol{z}_i, \boldsymbol{z}_j) - \boldsymbol{R}_{\boldsymbol{z}_m}(\boldsymbol{z}_i) \cdot \mathbf{R}^{-1}_{\boldsymbol{z}_m,\varepsilon} \cdot \boldsymbol{R}^{\mathsf{T}}_{\boldsymbol{z}_m}(\boldsymbol{z}_j)\right). \tag{2.120b}$$

$\mathbf{R}_{\boldsymbol{z}_m,\varepsilon} = \mathbf{R}_{\boldsymbol{z}_m,\boldsymbol{z}_m} + \mathbf{R}_\varepsilon$, where $\mathbf{R}_\varepsilon = \left(\frac{\sigma_\varepsilon}{\sigma'_X}\right)^2 \cdot \mathbf{I}$, where $\mathbf{I}$ is the $n_m \times n_m$ identity matrix and σ_ε is the standard deviation of the measurement error. $\boldsymbol{R}_{\boldsymbol{z}_m}(\boldsymbol{z})$ and $\mathbf{R}_{\boldsymbol{z}_m,\boldsymbol{z}_m}$ are defined as in Equations (2.119a) and (2.119b). The extended Gaussian RF update including measurement error is illustrated in Figure 2.27. Unlike Figure 2.26, some uncertainty remains at the measurement locations. The additional uncertainty also affects the posterior mean $\mu''_X(\boldsymbol{z})$, which does not connect the measurements anymore, but bypasses them, as can be seen in the magnified area.

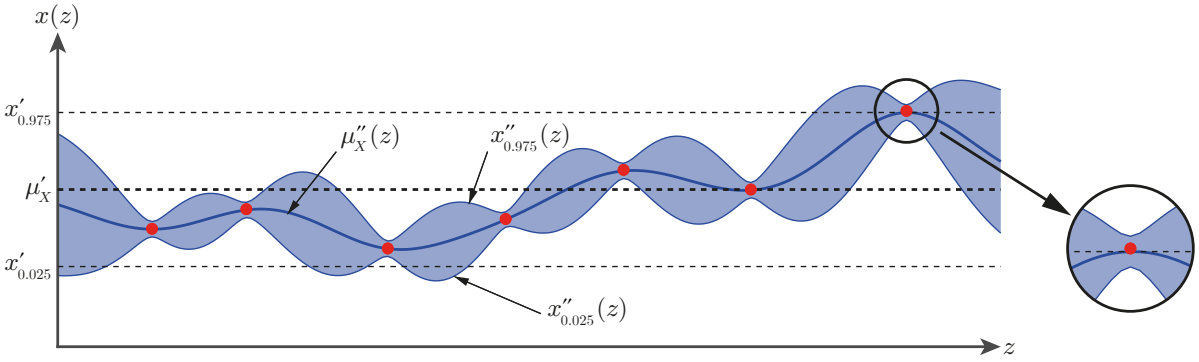

Figure 2.27: Bayesian updating of a one-dimensional Gaussian RF $X(z)$ with spatial data (red dots) and zero-mean Gaussian measurement error. μ'_X, $x'_{0.025}$ and $x'_{0.975}$ are the prior mean value and the bounds of the prior two-sided 95% interval. $\mu''_X(z)$, $x''_{0.025}(z)$ and $x''_{0.975}(z)$ are the spatial posterior mean and the spatial bounds of the posterior two-sided 95% interval (shaded area).

Equations (2.119a) and (2.119b) are directly applicable for translation RFs $Y(\boldsymbol{z})$ by transforming the data $\boldsymbol{y}_m = [y_{m,1}, \ldots, y_{m,n}]$ to the Gaussian space and performing the update for the underlying Gaussian RF (cf. Section 2.1.6.2). Since the underlying posterior RF is also Gaussian, the back-transformation to the original space can be performed analogously. If one wants to account for a measurement error, this has to be included in the transformation and the measurement error in the transformed space needs to be additive and Gaussian. Analytical expressions exist for the special case of a lognormal RF and measurements associated with a multiplicative lognormal measurement error [e.g., 65].

2.3.2.2 Hierarchical update for Gaussian random fields

The analytical update presented in Section 2.3.2.1 requires defining the prior parameters μ'_X and σ'_X of the marginal RF distribution. If these parameters are unknown, a hierarchical Bayesian approach can be used for learning the RF model. Hierarchical Bayesian approaches are used in the context of Bayesian linear regression [e.g., 61] and hierarchical spatial modeling [e.g., 21]. The methodology presented in the following employs existing results from these fields to derive a comprehensive hierarchical RF model. The theoretical framework and mathematical derivations are extensively described in Chapter 5 (original publication [65]) and, thus, are only briefly summarized in the following.

Consider a Gaussian RF $X(\boldsymbol{z})$ with unknown marginal parameters mean value μ_X and precision $\lambda_X = \sigma_X^{-2}$, and spatial correlation function $\rho(\boldsymbol{z}, \boldsymbol{z}')$. Note that only the prior point statistics need to be space-invariant, while the hierarchical approach can handle arbitrary correlation functions. A total of n spatially distributed measurements of $X(\boldsymbol{z})$ are available and collected in $\mathbf{M} = [\mathbf{M}_1, \ldots, \mathbf{M}_n]^{\mathsf{T}}$, whereby each $\mathbf{M}_i$ contains the measurement outcome $x_{m,i}$ and the corresponding measurement location $\boldsymbol{z}_{m,i}$, i.e., $\mathbf{M}_i = [x_{m,i}, \boldsymbol{z}_{m,i}]$. The uncertainty in μ_X and λ_X is modeled by an $\mathcal{NG}$ distribution $f(\mu_X, \lambda_X)$, where μ_X follows a normal distribution

conditional on λ_X and λ_X follows a gamma distribution (cf. Section 2.1.3.6). In addition to $\rho(\boldsymbol{z}, \boldsymbol{z}')$, the prior $\mathcal{NG}$ distribution parameters have to be chosen. Figure 2.28 illustrates the structure of the hierarchical model in a graph, where the circular nodes denote uncertain quantities and the rectangular node denotes a chosen correlation function. The gray boxes show examples/possible realizations of the respective model components, i.e., two possible $\mathcal{NG}$ distributions for the marginal RF parameters, a number of possible correlation models, several random realizations of RFs with different correlation functions, and two potential data sets of one-dimensional RFs.

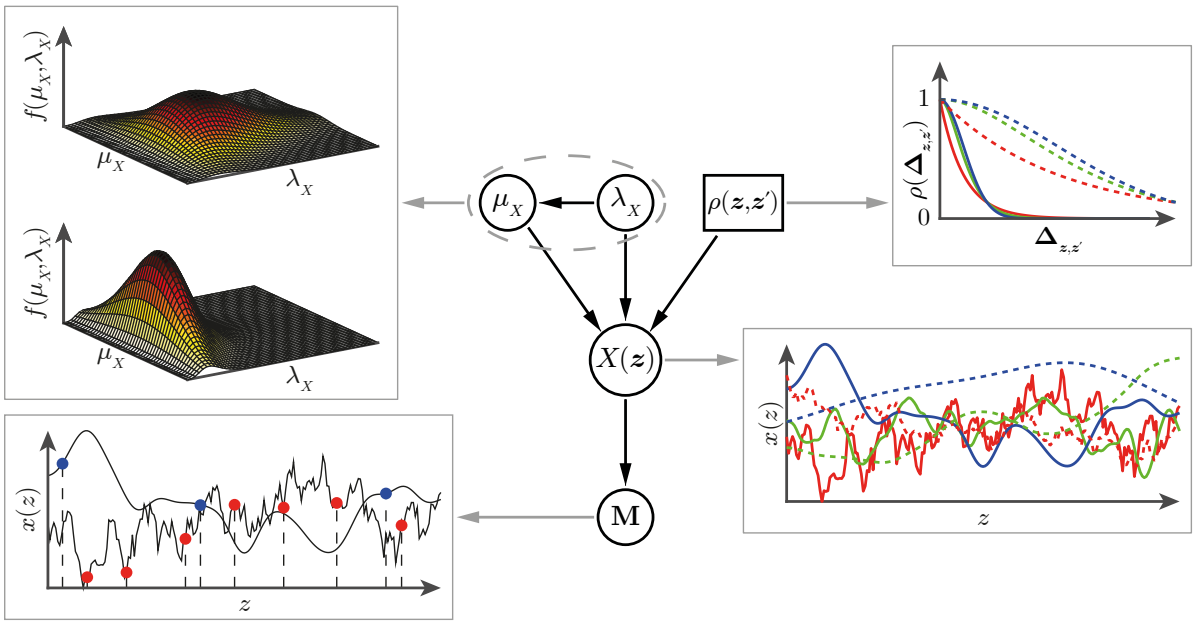

Figure 2.28: Hierarchical RF model to learn $X(\boldsymbol{z})$ from data. μ_X and λ_X are the mean and precision of the RF $X(\boldsymbol{z})$ (jointly modeled by an $\mathcal{NG}$ distribution) and $\mathbf{M}$ represents the measurement data. $\rho(\boldsymbol{z}, \boldsymbol{z}')$ denotes the chosen spatial autocorrelation function.

The Bayesian updating procedure consists of two steps. First, the posterior distribution of μ_X and λ_X, $f(\mu_X, \lambda_X|\mathbf{M})$ is obtained through combining $f(\mu_X, \lambda_X)$ and the likelihood function $\mathrm{L}(\mu_X, \lambda_X|\mathbf{M})$, which includes the information of $\mathbf{M}$. Since the $x_{m,i}$ in $\mathbf{M}$ are samples from a Gaussian RF, a multivariate Gaussian likelihood is formulated. The $\mathcal{NG}$ distribution is a conjugate prior for the Gaussian likelihood and, thus, $f(\mu_X, \lambda_X|\mathbf{M})$ is again an $\mathcal{NG}$ distribution. In a second step, the posterior predictive RF is obtained, which has Student's t-marginal distribution. The expressions for the spatial moment functions are available in closed form and given by (cf. Chapter 5)

$$\mu_t(\boldsymbol{z}) = \mu_n + \boldsymbol{R}_{\boldsymbol{z},m}\mathbf{R}_m^{-1}(\boldsymbol{x}_m - \mu_n\mathbf{1}_n)^{\mathsf{T}}, \tag{2.121a}$$

$$\lambda_t(\boldsymbol{z}_1, \boldsymbol{z}_2) = \frac{\alpha_n}{\beta_n}\left(\rho(\boldsymbol{z}_1, \boldsymbol{z}_2) - \boldsymbol{R}_{\boldsymbol{z}_1,m}\mathbf{R}_m^{-1}\boldsymbol{R}_{\boldsymbol{z}_2,m}^{\mathsf{T}} + \left(1 - \boldsymbol{R}_{\boldsymbol{z}_1,m}\mathbf{R}_m^{-1}\mathbf{1}_n^{\mathsf{T}}\right)\kappa_n^{-1}\left(1 - \boldsymbol{R}_{\boldsymbol{z}_2,m}\mathbf{R}_m^{-1}\mathbf{1}_n^{\mathsf{T}}\right)\right)^{-1}. \tag{2.121b}$$

$\boldsymbol{R}_{\boldsymbol{z},m}$ is a $1 \times n$ row vector function with element i defined as $\rho(\boldsymbol{z}, \boldsymbol{z}_{m,i})$. $\boldsymbol{R}_{\boldsymbol{z}_1,m}$ and $\boldsymbol{R}_{\boldsymbol{z}_2,m}$ are defined accordingly. $\mathbf{R}_m$ is the $n \times n$ correlation matrix of the measurement locations, where $R_m(i,j)$ is defined as $\rho(\boldsymbol{z}_{m,i}, \boldsymbol{z}_{m,j})$. $\mathbf{1}_n$ is a $1 \times n$ vector of ones. μ_n, κ_n, α_n and β_n are the

parameters of $f(\mu_X, \lambda_X|\mathbf{M})$, given by the following set of Equations (cf. Chapter 5):

$$\mu_n = \frac{\kappa_0\mu_0 + \mathbf{1}_n\mathbf{R}_m^{-1}\boldsymbol{x}_m^\mathsf{T}}{\kappa_0 + \mathbf{1}_n\mathbf{R}_m^{-1}\mathbf{1}_n^\mathsf{T}}, \tag{2.122a}$$

$$\kappa_n = \kappa_0 + \mathbf{1}_n\mathbf{R}_m^{-1}\mathbf{1}_n^\mathsf{T}, \tag{2.122b}$$

$$\alpha_n = \alpha_0 + \frac{n}{2}, \tag{2.122c}$$

$$\beta_n = \beta_0 + \frac{1}{2}\left(\boldsymbol{x}_m\mathbf{R}_m^{-1}\boldsymbol{x}_m^\mathsf{T} + \frac{\kappa_0\mu_0^2\mathbf{1}_n\mathbf{R}_m^{-1}\mathbf{1}_n^\mathsf{T} - 2\kappa_0\mu_0\mathbf{1}_n\mathbf{R}_m^{-1}\boldsymbol{x}_m^\mathsf{T} - (\mathbf{1}_n\mathbf{R}_m^{-1}\boldsymbol{x}_m^\mathsf{T})^2}{\kappa_0 + \mathbf{1}_n\mathbf{R}_m^{-1}\mathbf{1}_n^\mathsf{T}}\right), \tag{2.122d}$$

where μ_0, κ_0, α_0 and β_0 are the chosen parameters of $f(\mu_X, \lambda_X)$. In addition to $\mu_t(\boldsymbol{z})$ and $\lambda_t(\boldsymbol{z}_1, \boldsymbol{z}_2)$, the degrees of freedom ν_t have to be calculated for the posterior predictive RF. ν_t is space-invariant and given as

$$\nu_t = 2\alpha_n. \tag{2.123}$$

The posterior predictive RF is fully defined by the parameters specified by Equations (2.121a), (2.121b) and (2.123) and belongs to the class of translation RFs, i.e., it can be expressed as function of a Gaussian RF (cf. Section 2.1.6.2).

Figure 2.29 shows a one-dimensional posterior predictive Student's t-RF with parameters learned from the measurements illustrated by red dots. The spatial posterior predictive mean value $\mu_t(\boldsymbol{z})$ is represented by the solid blue line and the shaded area denotes the 95% interval. Comparing Figure 2.29 to Figure 2.26 (which is on the same scale and based on the same data $\mathbf{M}$ and the same spatial correlation function) reveals the additional uncertainty in regions away from the measurements, when the marginal RF parameters are modeled uncertain, as the 95% intervals are wider than in the case with fixed prior parameters.

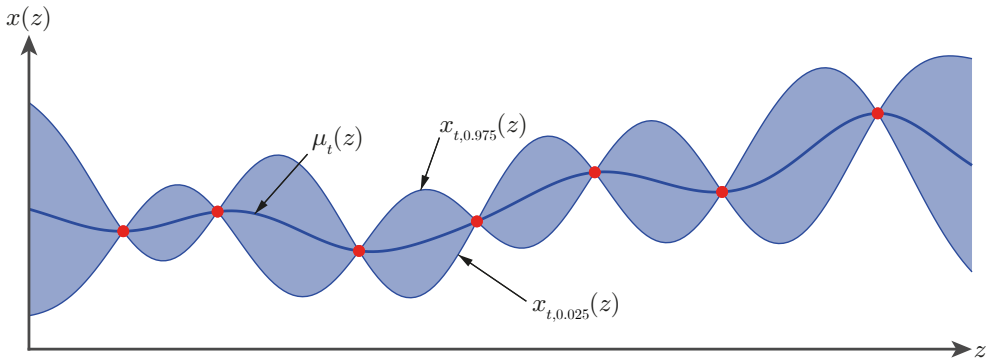

Figure 2.29: Posterior predictive Student's t-RF resulting from a hierarchical Bayesian updating of a one-dimensional Gaussian RF with spatial data (red dots). $\mu_t(z)$, $x_{t,0.025}(z)$ and $x_{t,0.975}(z)$ are the spatial posterior mean and the spatial bounds of the posterior two-sided 95% interval (shaded area).

The hierarchical model can be extended to non-Gaussian prior RFs, if the prior RF belongs to the class of translations RFs. In that case, the updating needs to be conducted for the underlying Gaussian RF, resulting in an underlying Student's t-RF. In the special case of a lognormal prior RF, the posterior predictive RF has log-Student's t-marginal distribution and, thus, also belongs to the class of translation RFs (cf. Section 2.1.6.2).

The analytical update is conditional on the choice of the prior spatial correlation function $\rho(\boldsymbol{z}, \boldsymbol{z}')$, which can be a challenging task in practical applications. In the context of Gaussian

process regression, maximum likelihood estimation and/or cross-validation is often used to determine the parameters of the correlation function [e.g., 141]. Alternatively, the parameters can be learned in a Bayesian way by modeling the parameters of the correlation function as random variables with associated prior distribution. Employing the maximum a-posteriori estimate yields a Bayesian point estimate of the correlation parameters, which can then be used for the analytical update [118, 65]. If the full posterior distribution of the correlation parameters is to be included in the Bayesian RF update, the posterior predictive RF parameters need to be approximated numerically, for example through MCMC algorithms [e.g., 23]. However, the analytical expressions for the posterior predictive RF can still be used in combination with numerical approximation algorithms, for example when evaluating spatial quantile values of the RF, as shown in Chapter 6 (original publication [68]).

Uncertainty in the measurements can be included in the hierarchical model and the analytical update by slightly modifying the definition of λ_X to the overall precision of the Gaussian RF and an additive Gaussian measurement error, i.e., $\lambda_X = \left(\lambda_{X,\mathrm{RF}}^{-1} + \sigma_\varepsilon^2\right)^{-1}$, leading to an adjustment of the spatial correlation function [65]. In that case, the posterior predictive RF parameters include a contribution from the measurement error and, consequently, predictions based on the update are inherently noisy.

2.3.2.3 Connection to Bayesian approach of EN 1990 and EN 13791

The Bayesian approach for calculating characteristic values of material properties of EN 1990 and EN 13791, as described in Section 2.3.1.2, is a special case of the presented hierarchical Bayesian model [64, 65]. It is obtained by using a non-informative prior $\mathcal{NG}$ distribution ($[\mu_0, \kappa_0, \alpha_0, \beta_0] = [/, 0, -\frac{1}{2}, 0]$, where the "/" indicates that μ_0 can be chosen arbitrarily), assuming independence of the random variables corresponding to the measurement locations ($\mathbf{R}_m = \mathbf{I}$), neglecting measurement error ($\sigma_\varepsilon = 0$) and neglecting the spatial correlation of the RF ($\rho(\boldsymbol{z}, \boldsymbol{z}') = \delta_{\boldsymbol{z},\boldsymbol{z}'}$, cf. Equation (2.60)). In this case, Equations (2.122a) to (2.122d) simplify and the parameters of the posterior $\mathcal{NG}$ distribution are given as [65]

$$\mu_n = \frac{\mathbf{1}_n \boldsymbol{x}_m^\mathsf{T}}{n} \tag{2.124a}$$

$$\kappa_n = n, \tag{2.124b}$$

$$\alpha_n = \frac{n-1}{2}, \tag{2.124c}$$

$$\beta_n = \frac{1}{2}\left(\boldsymbol{x}_m \boldsymbol{x}_m^\mathsf{T} - \frac{\left(\mathbf{1}_n \boldsymbol{x}_m^\mathsf{T}\right)^2}{n}\right). \tag{2.124d}$$

Consequently, the space-invariant posterior predictive Student's t-distribution can be derived. Its location parameter μ_t and scale parameter λ_t are obtained through simplification of Equations (2.121a) and (2.121b). This results in the following set of parameters [137, 65]:

$$\mu_t = \mu_n, \tag{2.125a}$$

$$\lambda_t = \frac{\alpha_n}{\beta_n\left(1 + \kappa_n^{-1}\right)}, \tag{2.125b}$$

$$\nu_t = 2\alpha_n, \tag{2.125c}$$

where μ_n, κ_n, α_n and β_n are calculated by means of Equations (2.124a) to (2.124d).

2.3.2.4 Spatial variability of concrete strength

Application of the hierarchical Bayesian RF update to material properties requires an understanding of the type of variability in the investigated material and the way the data is extracted. The spatial variability of concrete strength calls for particular attention since concrete is a composite material that can be divided into the two phases of cement matrix and aggregate, each with different mechanical properties [e.g., 120]. In the case of existing concrete structures, measurements are often based on samples taken from the structure. In that case, the measurement outcome is not defined as a point-in-space property but as the property of an element of finite size [53]. An approach to dealing with the combination of these two effects (composite material and finite sample size) in the context of Bayesian RF learning of concrete strength is described in Chapter 6 (original publication [68]). An important part of the approach is the division of the spatial variability of concrete strength into micro-scale and meso-scale variability, which is accounted for by modifying the spatial correlation function $\rho(\boldsymbol{z}, \boldsymbol{z}')$ as follows:

$$\rho(\boldsymbol{z}, \boldsymbol{z}') = \gamma_{\text{micro}} \cdot \rho_{\text{micro}}(\boldsymbol{z}, \boldsymbol{z}') + (1 - \gamma_{\text{micro}}) \cdot \rho_{\text{meso}}(\boldsymbol{z}, \boldsymbol{z}'), \tag{2.126}$$

where $\gamma_{\text{micro}} \in [0, 1]$ denotes the share of correlation associated with the micro-scale variability, and $\rho_{\text{micro}}(\boldsymbol{z}, \boldsymbol{z}')$ and $\rho_{\text{meso}}(\boldsymbol{z}, \boldsymbol{z}')$ are the spatial correlation functions for the micro- and meso-scale variability, respectively. If the parameters of $\rho(\boldsymbol{z}, \boldsymbol{z}')$ are part of the Bayesian updating, i.e., they are treated as uncertain, it is suggested to replace $\rho_{\text{micro}}(\boldsymbol{z}, \boldsymbol{z}')$ by the Dirac delta function $\delta_{\boldsymbol{z},\boldsymbol{z}'}$ (cf. Equation (2.60)), since the concrete sample size makes learning of the micro-scale correlation function practically impossible.

Chapter 3

Concluding remarks

Reconsider the key components of structural reliability analysis, as illustrated in Figure 1.1. The chapters in Part II mainly focus on the stochastic model of spatially variable material properties entering the analysis and, to a minor extent, their coupling with finite element models. In addition, reliability analyses are conducted making use of the developed stochastic approaches and their coupling with finite element models. Figure 3.1 summarizes the main contributions, a more detailed summary is given in the following. Although not being part of the core articles of this thesis, the choice of an appropriate reliability method has been investigated during the doctoral research and is included in Section 2.2.

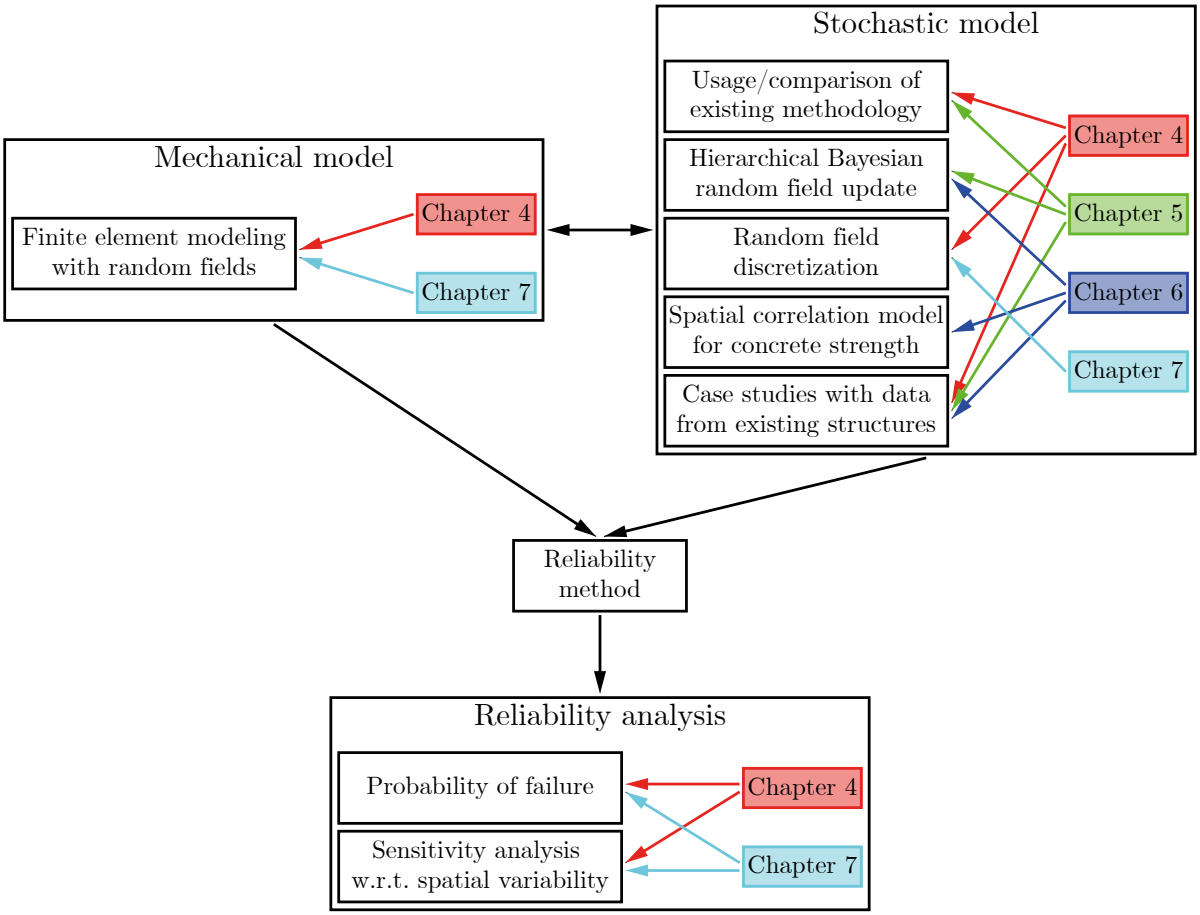

Figure 3.1: Main contributions of the journal articles forming Part II of this thesis to the components of reliability analysis.

3.1 Summary

Chapter 4 presents a coherent methodology for reliability assessment of large hydraulic structures. While the currently applied methods used for structural verification of such structures do not account for spatial variability, we suggest to model the concrete compressive strength as random field and use measurement data to obtain the random field parameters. To this end, an approach for modeling spatially variable concrete strength from the literature is coupled with an analytical Bayesian update of Gaussian random fields. The resulting non-homogeneous random fields are discretized by means of the Karhunen–Loève expansion. The studied ship lock wall is modeled with a two-dimensional nonlinear finite element model using the commercial software SOFiSTiK. Subset simulation is employed for conducting the reliability analysis with prior and posterior parameters, and for parameter studies regarding the correlation length and the measurement error. In addition, the standardized approach in Annex D.7 of EN 1990 for estimating characteristic values is described.

In Chapter 5, a comprehensive hierarchical Bayesian approach for modeling spatially variable material properties with data is derived, since the results of Chapter 4 indicate that the available literature on spatial modeling of concrete strength is not sufficient. The proposed methodology makes use of the conjugacy of Gaussian likelihood and normal-gamma prior distribution to obtain analytical expressions for the parameters of a global posterior distribution for the random field parameters. Furthermore, analytical expressions for the posterior predictive non-homogeneous random field, which has Student's t-marginal distribution, are presented. The parameter choice of the prior spatial correlation function is discussed and the maximum a-posteriori estimate is suggested as point estimate of the parameters, including the required equations for numerical treatment of the optimization problem. It is shown that the presented hierarchical Bayesian approach is a generalization of the approach underlying the standardized procedure in Annex D.7 of EN 1990. Extension to non-Gaussian prior random fields is discussed and the required equations for a lognormal prior distribution are derived. In that case, the posterior predictive random field has log-Student's t-marginal distribution. The generation of samples from the posterior predictive random field completes the theoretical part of the chapter, before the efficacy of the methodology is illustrated by means of two numerical examples.

Chapter 6 refines the hierarchical approach of Chapter 5 for specific application to concrete strength random fields for which spatial measurements are available. The composite nature of concrete is reflected in a customized correlation function accounting for variability at the micro-scale. The prior parameter choice of the random field marginal distribution is addressed by providing their maximum-likelihood-estimates using past data. Besides, Bayesian learning of the random field parameters without site-specific data is briefly described including analytical expressions for the random field parameters. Two extensive case studies of ship lock walls with spatial measurements of the concrete strength are carried out to test the ability of the framework to identify the random field parameters. The results reveal that, although certain ranges of high probability can be found, the uncertainty in the random field parameters is too high to be learned from the data alone. Additional empirical studies are required, especially to formulate informative prior distributions, which can have significant impact on the posterior estimates.

Last but not least, Chapter 7 deals with random field discretization with the spatial averaging method. The method is extended for the application to non-homogeneous Gaussian random fields and equations are provided for the one- and two-dimensional case. In addition, applicability of the spatial averaging method to non-homogeneous and non-Gaussian random fields is described and the required transformations are derived for random fields with lognormal, Student's t- and log-Student's t-marginal distribution. That is, the spatial averaging method can be applied to random fields originating from the hierarchical Bayesian update of Chapters 5 and 6. A

one-dimensional beam example with spatially variable beam flexibility shows the ability of the method to capture the effects of a random field through discretization with a feasible number of random variables and illustrates the straightforward combination with the mesh of a finite element model. In a second numerical investigation, sliding of a ship lock wall is investigated, where the friction coefficient is modeled as two-dimensional random field. The results show that the failure mechanism is an important factor in the choice of the number of random variables in the discretization, which leads to an interaction of mechanical model and stochastic model. It is also shown that an intelligent mesh choice for the random field discretization can significantly reduce the computational effort.

3.2 Outlook

The developments and investigations of this doctoral research constitute the groundwork for reliability analysis of structures with spatially variable input parameters. On this basis, future research can be conducted to increase the applicability of the methodology and to enable simplifications and calibrations for practical application in structural verification. The proposed hierarchical random field modeling approach assumes homogeneity of the prior random field and is only discussed for the univariate case, i.e., only one spatially variable property is modeled. Extension of the methodology to non-homogeneous prior random fields and multivariate random fields could promote the application to other fields, such as geotechnical engineering or meteorology, where often data of multiple parameters at the same location is available and closely related concepts for spatial updating have already been established.

One of the most critical points in random field modeling is the choice of the spatial correlation function and its parameters, as the spatial variability is dominated by that choice. When modeling concrete strength random fields, the available recommendations and the additional results from this doctoral research are not sufficient to make an educated choice of these parameters. Additional empirical studies are inevitable for reducing the uncertainty in the correlation parameters, on the basis of which one can reduce the parameter range and define informative prior distributions. When investigating historic tamped concrete, it appears that the spatial variability is dominated by the micro-scale variability of the concrete strength. If additional studies confirm this initial result, the validity of the current definition of characteristic values for structural verification needs to be re-evaluated, as they might be too conservative.

For practical application, concepts for the incorporation of spatial variability into standardized structural verification formats need to be developed. The investigated spatial averaging method in conjunction with the hierarchical Bayesian random field approach can be the entry point here, since they allow to determine a random variable representing the average behavior of a material property over a certain spatial domain taking into account the effect of spatial data. The critical parameter in this procedure is the size of the averaging domain, which depends not only on the random field, but also on the investigated failure mechanism. For example, local failure modes are more sensitive to local extreme values of the spatially variable material property than regional or even global failure modes. Once the averaging domain has been identified and the corresponding random variable has been determined, calculation of characteristic values for direct application in structural verification is straightforward. Hence, detailed studies on the relevant failure mechanisms and the effects of spatial variability in the material parameters on the system response are required, opening up a wide field of potential investigations.

Coupling random fields with commercial finite element software is not always straightforward and often requires deep understanding of both random fields and finite element modeling. To this end, using the spatial averaging method as discretization method yields two advantages: first, the resulting random variables directly represent the random field average on a specific spatial

domain, which, if the finite elements are chosen as the spatial averaging domains, simplifies coupling the stochastic model with the mechanical model and supports the understanding of the effects of spatial variability in practice. Secondly, the use of spatial averages is in accordance with the general concept of finite element modeling, where a structure is represented by an arrangement of spatial elements coupled through boundary conditions. The interactions between adjacent elements are calculated based on the integrals of forces and stresses in combination with the element stiffness within each individual element. The degree of accuracy is strongly related to the coarseness of the finite element mesh, which is directly transferable to the spatial averaging method. Making use of these advantages can help motivating the use of random fields in practical applications and developing finite element software with built-in toolboxes for spatial variability.

References

[1] P. Abrahamsen. *A review of Gaussian random fields and correlation functions*. 2nd ed. Norwegian Computing Center, 1997.

[2] M. Abramowitz and I. Stegun. *Handbook of mathematical functions with formulas, graphs and mathematical tables*. National Bureau of Standards applied mathematics series 55. New York City, NY: Dover, 1965.

[3] A. Albert, ed. *Schneider - Bautabellen für Ingenieure: mit Berechnungshinweisen und Beispielen*. 24th ed. Reguvis Fachmedien, 2020.

[4] D. E. Allen. "Criteria for design safety factors and quality assurance expenditure". In: *Proceedings of the third international conference on structrual safety and reliability*. Ed. by T. Moan and M. Shinozuka. Elsevier Scientific, 1981, pp. 667–678.

[5] R. Ash. *Basic probability theory*. Dover books on mathematics. Mineola, NY: Dover, 2012.

[6] K. E. Atkinson. *The numerical solution of integral equations of the second kind*. Cambridge monographs on applied and computational mathematics. Cambridge University Press, 1997.

[7] S.-K. Au and J. L. Beck. "Estimation of small failure probabilities in high dimensions by subset simulation". In: *Probabilistic Engineering Mechanics* 16.4 (2001), pp. 263–277.

[8] S.-K. Au and J. L. Beck. "Important sampling in high dimensions". In: *Structural Safety* 25.2 (2003), pp. 139–163.

[9] S.-K. Au and Y. Wang. *Engineering risk assessment with subset simulation*. John Wiley & Sons Singapore, 2014.

[10] S. Banerjee, B. P. Carlin, and A. E. Gelfand. *Hierarchical modeling and analysis for spatial data*. 2nd ed. Chapman & Hall/CRC monographs on statistics & applied probability. Boca Raton, FL: CRC, 2014.

[11] O. Barndorff-Nielsen. *Information and exponential families in statistical theory*. Wiley series in probability and statistics. John Wiley & Sons United Kingdom, 2014.

[12] O. Bauchau and J. Craig. *Structural analysis: with applications to aerospace structures*. Solid mechanics and its applications. Springer Netherlands, 2009.

[13] P. Beaurepaire, H. Jensen, G. Schuëller, and M. Valdebenito. "Reliability-based optimization using bridge importance sampling". In: *Probabilistic Engineering Mechanics* 34 (2013), pp. 48–57.

[14] R. E. Bellman. *Adaptive control processes: a guided tour*. Princeton, NJ: Princeton University Press, 1961.

[15] J. Benjamin and C. Cornell. *Probability, statistics, and decision for civil engineers*. New York City, NY: McGraw-Hill, 1970.

[16] W. Betz, I. Papaioannou, and D. Straub. "Numerical methods for the discretization of random fields by means of the Karhunen-Loève expansion". In: *Computer Methods in Applied Mechanics and Engineering* 271 (2014), pp. 109–129.

[17] G. Biondini. “Chapter 2 - An introduction to rare event simulation and importance sampling”. In: *Big Data Analytics 33*. Ed. by V. Govindaraju, V. V. Raghavan, and C. Rao. Elsevier, 2015, pp. 29–68.

[18] C. M. Bishop. *Pattern recognition and machine learning*. Information science and statistics. New York City, NY: Springer, 2006.

[19] P. Bjerager and S. Krenk. “Parametric sensitivity in first order reliability theory”. In: *Journal of Engineering Mechanics* 115.7 (1989), pp. 1577–1582.

[20] Z. I. Botev and D. P. Kroese. “Efficient Monte Carlo simulation via the generalized splitting method”. In: *Statistics and Computing* 22.1 (2012), pp. 1–16.

[21] G. Box and G. Tiao. *Bayesian inference in statistical analysis*. revised new. Wiley Classics Library. Hoboken, NJ: John Wiley & Sons, 2011.

[22] K. Breitung. “Asymptotic approximations for multinormal integrals”. In: *Journal of Engineering Mechanics* 110.3 (1984), pp. 357–366.

[23] S. Brooks, A. Gelman, G. Jones, and X.-L. Meng. *Handbook of Markov chain Monte Carlo*. Chapman & Hall/CRC handbooks of modern statistical methods. Boca Raton, FL: CRC, 2011.

[24] C. G. Bucher and M. Shinozuka. “Structural response variability II”. In: *Journal of Engineering Mechanics* 114.12 (1988), pp. 2035–2054.

[25] C. G. Bucher. “Adaptive sampling - an iterative fast Monte Carlo procedure”. In: *Structural Safety* 5.2 (1988), pp. 119–126.

[26] Bundesanstalt für Wasserbau. *Bewertung der Tragfähigkeit bestehender, massiver Wasserbauwerke [Assessment of the bearing capacity of existing, massive hydraulic structures]*. BAW guideline, 2016.

[27] D. T. Cassidy, M. J. Hamp, and R. Ouyed. “Log Student’s t-distribution-based option sensitivities: Greeks for the Gosset formulae”. In: *Quantitative Finance* 13.8 (2013), pp. 1289–1302.

[28] D. T. Cassidy, M. J. Hamp, and R. Ouyed. “Pricing European options with a log Student’s t-distribution: a Gosset formula”. In: *Physica A: Statistical Mechanics and its Applications* 389.24 (2010), pp. 5736–5748.

[29] Y. Chen and M. R. Gupta. *EM demystified: an expectation-maximization tutorial*. Tech. rep. UWEETR-2010-0002. University of Washington, 2010.

[30] J. Ching and K.-K. Phoon. “Characterizing uncertain site-specific trend function by sparse Bayesian learning”. In: *Journal of Engineering Mechanics* 143.7 (2017), p. 04017028.

[31] J. Ching, X.-W. Tong, and Y.-G. Hu. “Effective Young’s modulus for a spatially variable soil mass subjected to a simple stress state”. In: *Georisk: Assessment and Management of Risk for Engineered Systems and Geohazards* 10.1 (2016), pp. 11–26.

[32] J. Ching and J.-S. Wang. “Application of the transitional Markov chain Monte Carlo algorithm to probabilistic site characterization”. In: *Engineering Geology* 203 (2016), pp. 151–167.

[33] C. A. Cornell. “A probability-based structural code”. In: *Journal of the American Concrete Institute* 66 (12 1969), pp. 974–985.

[34] M. de Angelis, E. Patelli, and M. Beer. “Advanced line sampling for efficient robust reliability analysis”. In: *Structural Safety* 52 (2015), pp. 170–182.

[35] M. DeGroot. *Optimal Statistical Decisions*. McGraw-Hill series in probability and statistics. New York City, NY: McGraw-Hill, 1969.

[36] A. P. Dempster, N. M. Laird, and D. B. Rubin. "Maximum likelihood from incomplete data via the EM algorithm". In: *Journal of the Royal Statistical Society. Series B (Methodological)* 39.1 (1977), pp. 1–38.

[37] G. Deodatis. "Weighted integral method. I: stochastic stiffness matrix". In: *Journal of Engineering Mechanics* 117.8 (1991), pp. 1851–1864.

[38] G. Deodatis and M. Shinozuka. "Weighted integral method. II: response variability and reliability". In: *Journal of Engineering Mechanics* 117.8 (1991), pp. 1865–1877.

[39] A. Der Kiureghian and T. Dakessian. "Multiple design points in first and second-order reliability". In: *Structural Safety* 20.1 (1998), pp. 37–49.

[40] A. Der Kiureghian and J.-B. Ke. "The stochastic finite element method in structural reliability". In: *Probabilistic Engineering Mechanics* 3.2 (1988), pp. 83–91.

[41] A. Der Kiureghian and P.-L. Liu. "Structural reliability under incomplete probability information". In: *Journal of Engineering Mechanics* 112.1 (1986), pp. 85–104.

[42] A. Der Kiureghian and Y. Zhang. "Space-variant finite element reliability analysis". In: *Computer Methods in Applied Mechanics and Engineering* 168.1 (1999), pp. 173–183.

[43] O. Ditlevsen. *Structural reliability and the invariance problem*. Report No. 22, Solid mechanics division. University of Waterloo, 1973.

[44] O. Ditlevsen. "Generalized second moment reliability index". In: *Journal of Structural Mechanics* 7.4 (1979), pp. 435–451.

[45] O. Ditlevsen and H. O. Madsen. *Structural reliability methods*. New York City, NY: John Wiley & Sons, 1996.

[46] *EN 131791:2019. Assessment of in-situ compressive strength in structures and precast concrete components*. European Standard, 2019.

[47] *EN 1990:2002. Eurocode 0: basis of structural and geotechnical design*. European Standard, 2002.

[48] *EN 1991-1-1. Eurocode 1: actions on structures - part 1-1: general actions - densities, self-weight, imposed loads for buildings*. European Standard, 2002.

[49] *EN 1992-1-1:2004. Eurocode 2: design of concrete structures - part 1-1: general rules and rules for buildings*. European Standard, 2004.

[50] *EN 1993-1-1:2005. Eurocode 3: design of steel structures - part 1-1: general rules and rules for buildings*. European Standard, 2020.

[51] *EN 1995-1-1:2004. Eurocode 5: design of timber structures - part 1-1: general - common rules and rules for buildings*. European Standard, 2010.

[52] *EN 1997-1:2004. Eurocode 7: geotechnical design - part 1: general rules*. European Standard, 2014.

[53] *EN 206-1:2000. Concrete - Part 1: Specification, performance, production and conformity*. European Standard, 2000.

[54] S. Engelund and R. Rackwitz. "A benchmark study on importance sampling techniques in structural reliability". In: *Structural Safety* 12.4 (1993), pp. 255–276.

[55] G. A. Fenton and E. H. Vanmarcke. "Simulation of random fields via local average subdivision". In: *Journal of Engineering Mechanics* 116.8 (1990), pp. 1733–1749.

[56] B. Fiessler, H.-J. Neumann, and R. Rackwitz. “Quadratic limit States in structural reliability”. In: *Journal of the Engineering Mechanics Division* 105.4 (1979), pp. 661–676.

[57] L. Fischer. “Bestimmung der 5%-Quantile im Zuge der Bauwerksprüfung [Determination of 5% quantile values in the course of inspection of structures]”. In: *Bautechnik* 72.11 (1995), pp. 712–722.

[58] H. Freeman. *Introduction to statistical inference*. Addison-Wesley series in advanced physics. Reading, MA: Addison-Wesley, 1963.

[59] A. M. Freudenthal. “Safety, reliability and structural design”. In: *Journal of the Structural Division* 87 (3 1961), pp. 1–16.

[60] A. M. Freudenthal. “Safety and the probability of structural failure”. In: *Transactions of the American Society of Civil Engineers* 121.1 (1956), pp. 1337–1375.

[61] A. Gelman, J. Carlin, H. Stern, D. Dunson, A. Vehtari, and D. Rubin. *Bayesian data analysis*. 3rd. Chapman & Hall/CRC texts in statistical science. Boca Raton, FL: CRC, 2013.

[62] S. Geyer, I. Papaioannou, C. Kunz, and D. Straub. “Bayesian reliability assessment with spatially variable measurements: the spatial averaging approach”. In: *Proceedings of the 13th international conference on application of statistics and probability in civil engineering*. Ed. by J. Song. Seoul: Seoul National University open repository, 2019, pp. 1–8.

[63] S. Geyer, I. Papaioannou, L. Graham-Brady, and D. Straub. “The spatial averaging method for non-homogeneous random fields with application to reliability analysis”. In: *Engineering Structures* 253 (2022), p. 113761.

[64] S. Geyer, I. Papaioannou, C. Kunz, and D. Straub. “Reliability assessment of large hydraulic structures with spatially distributed measurements”. In: *Structure and Infrastructure Engineering* 16 (4 2020), pp. 599–612.

[65] S. Geyer, I. Papaioannou, and D. Straub. “Bayesian analysis of hierarchical random fields for material modeling”. In: *Probabilistic Engineering Mechanics* 66 (2021), p. 103167.

[66] S. Geyer, I. Papaioannou, and D. Straub. “Cross entropy-based importance sampling using Gaussian densities revisited”. In: *Structural Safety* 76 (2019), pp. 15–27.

[67] S. Geyer, I. Papaioannou, and D. Straub. *Problemorientierte Auswahl und Durchführung von Zuverlässigkeitsanalysen [Problem-oriented reliability analysis]*. In preparation. 2023.

[68] S. Geyer, I. Papaioannou, and D. Straub. “Spatial modeling of concrete strength based on data”. In: *Structural Safety* 103 (2023), p. 102345.

[69] R. Ghanem, D. Higdon, and H. Owhadi, eds. *Handbook of uncertainty quantification*. Springer International, 2017.

[70] R. G. Ghanem and P. D. Spanos. *Stochastic finite elements. A spectral approach*. revised. Dover civil and mechanical engineering. Mineola, NY: Dover, 2012.

[71] M. Grigoriu. “Crossings of non-Gaussian translation processes”. In: *Journal of Engineering Mechanics* 110.4 (1984), pp. 610–620.

[72] M. Grigoriu. *Stochastic systems: uncertainty quantification and propagation*. Springer series in reliability engineering. Springer London, 2012. 532 pp.

[73] A. Hájek. “Interpretations of probability”. In: *The Stanford encyclopedia of philosophy (fall 2019 edition)*. Ed. by E. N. Zalta. 2019.

[74] M. S. Handcock and M. L. Stein. "A Bayesian analysis of kriging". In: *Technometrics* 35.4 (1993), pp. 403–410.

[75] A. Harbitz. "Efficient and accurate probability of failure calculation by use of the importance sampling technique". In: *Proceedings of the 4th international conference on applications of statistics and probability in soil and structural engineering*. Ed. by G. Augusti, A. Borri, and O. Vannuchi. Pitagora Editrice, 1983, pp. 825–836.

[76] A. M. Hasofer and N. C. Lind. "Exact and invariant second moment code format". In: *Journal of the Engineerings Mechanics Division* 100 (1974), pp. 111–121.

[77] M. Hohenbichler and R. Rackwitz. "First-order concepts in system reliability". In: *Structural Safety* 1.3 (1982), pp. 177–188.

[78] M. Hohenbichler and R. Rackwitz. "Sensitivity and importance measures in structural reliability". In: *Civil Engineering Systems* 3.4 (1986), pp. 203–209.

[79] M. Hohenbichler and R. Rackwitz. "Non-normal dependent vectors in structural reliability". In: *Journal of the Engineerings Mechanics Division* 107 (1981), pp. 1227–1238.

[80] M. Hohenbichler and R. Rackwitz. "Improvement of second-order reliability estimates by importance sampling". In: *Journal of Engineering Mechanics* 114.12 (1988), pp. 2195–2199.

[81] Y. Ibrahim. "Observations on applications of importance sampling in structural reliability analysis". In: *Structural Safety* 9.4 (1991), pp. 269–281.

[82] E. T. Jaynes. *Probability theory: the logic of science*. Ed. by G. L. Bretthorst. New York City, NY: Cambridge University, 2003.

[83] *JCSS probabilistic model code. Part 2 - load models*. Joint Committee on Structural Safety, 2001.

[84] *JCSS probabilistic model code. Part 3 - resistance models*. Joint Committee on Structural Safety, 2001.

[85] S.-H. Jiang, I. Papaioannou, and D. Straub. "Bayesian updating of slope reliability in spatially variable soils with in-situ measurements". In: *Engineering Geology* 239 (2018), pp. 310–320.

[86] N. Johnson, S. Kotz, and N. Balakrishnan. *Continuous univariate distributions: volume 1*. Wiley series in probability and mathematical statistics: applied probability and statistics. New York City, NY: John Wiley & Sons, 1994.

[87] N. Johnson, S. Kotz, and N. Balakrishnan. *Continuous univariate distributions: volume 2*. Wiley series in probability and mathematical statistics: applied probability and statistics. New York City, NY: John Wiley & Sons, 1995.

[88] H. Kahn. "Use of different Monte Carlo sampling techniques". In: *Symposium on Monte Carlo methods*. Ed. by H. Meyer. New York City, NY: John Wiley & Sons, 1956, pp. 146–190.

[89] A. Kardara, C. G. Bucher, and M. Shinozuka. "Structural response variability III". In: *Journal of Engineering Mechanics* 115.8 (1989), pp. 1726–1747.

[90] K. Karhunen. *Über lineare Methoden in der Wahrscheinlichkeitsrechnung [On linear methods in probability theory]*. Annales Academiae scientiarum Fennicae. Series A. 1, Mathematica - Physica 37. Suomalainen Tiedeakatemia, 1947.

[91] L. Katafygiotis and K. Zuev. "Geometric insight into the challenges of solving high-dimensional reliability problems". In: *Probabilistic Engineering Mechanics* 23.2 (2008), pp. 20–218.

[92] A. D. Kiureghian and O. Ditlevsen. "Aleatory or epistemic? Does it matter?" In: *Structural Safety* 31.2 (2009), pp. 105–112.

[93] A. N. Kolmogorov. *Foundations of the theory of probability*. 2nd English edition. New York City, NY: Chelsea, 1956.

[94] S. Kotz and S. Nadarajah. *Multivariate t-distributions and their applications*. Cambridge University, 2004.

[95] P. Koutsourelakis, H. Pradlwarter, and G. Schuëller. "Reliability of structures in high dimensions, part I: algorithms and applications". In: *Probabilistic Engineering Mechanics* 19.4 (2004), pp. 409–417.

[96] D. P. Kroese, R. Y. Rubinstein, and P. W. Glynn. "Chapter 2 - The cross-entropy method for estimation". In: *Handbook of statistics 31*. Ed. by C. Rao and V. Govindaraju. Elsevier, 2013, pp. 19–34.

[97] D. P. Kroese, T. Taimre, and Z. I. Botev. *Handbook of Monte Carlo methods*. Wiley series in probability and statistics. Hoboken, NJ: John Wiley & Sons, 2011.

[98] N. Kurtz and J. Song. "Cross-entropy-based adaptive importance sampling using Gaussian mixture". In: *Structural Safety* 42 (2013), pp. 35–44.

[99] J. Latz, M. Eisenberger, and E. Ullmann. "Fast sampling of parameterised Gaussian random fields". In: *Computer Methods in Applied Mechanics and Engineering* 348 (2019), pp. 978–1012.

[100] R. Lebrun and A. Dutfoy. "An innovating analysis of the Nataf transformation from the copula viewpoint". In: *Probabilistic Engineering Mechanics* 24.3 (2009), pp. 312–320.

[101] M. Lemaire, A. Chateauneuf, and J.-C. Mitteau. *Structural reliability*. Hoboken, NJ: John Wiley & Sons, 2009.

[102] C.-C. Li and A. D. Kiureghian. "Optimal discretization of random fields". In: *Journal of Engineering Mechanics* 119.6 (1993), pp. 1136–1154.

[103] P.-L. Liu and A. Der Kiureghian. "Optimization algorithms for structural reliability". In: *Structural Safety* 9.3 (1991), pp. 161–177.

[104] P.-L. Liu and A. D. Kiureghian. "Multivariate distribution models with prescribed marginals and covariances". In: *Probabilistic Engineering Mechanics* 1.2 (1986), pp. 105–112.

[105] W. K. Liu, T. Belytschko, and A. Mani. "Random field finite elements". In: *International Journal for Numerical Methods in Engineering* 23 (1986), pp. 1831–1845.

[106] Y. Liu, J. Li, S. Sun, and B. Yu. "Advances in Gaussian random field generation: a review". In: *Computational Geosciences* 23.5 (2019), pp. 1011–1047.

[107] M. Loève. "Fonctions aléatoires de second ordre [Random functions of second order]". In: *Revue scientifique* 84.4 (1946), pp. 195–206.

[108] M. Loève. *Probability theory I*. 4th ed. Graduate texts in mathematics. New York City, NY: Springer, 1977.

[109] J. G. MacGregor. "Safety and limit states design for reinforced concrete". In: *Canadian Journal of Civil Engineering* 3.4 (1976), pp. 484–513.

[110] H. O. Madsen, S. Krenk, and N. C. Lind. *Method of Structural Safety*. Mineola, NY: Dover, 2006.

[111] K. V. Mardia and P. E. Jupp. *Directional Statistics*. Wiley series in probability and statistics. New York City, NY: John Wiley & Sons, 2000.

[112] B. Matérn. *Spatial Variation*. Lecture notes in statistics. Springer, 1986.

[113] R. Melchers and A. Beck. *Structural reliability analysis and prediction*. 3rd ed. Hoboken, NJ: John Wiley & Sons, 2018.

[114] N. Metropolis. "The beginning of the Monte Carlo method". In: *Los Alamos Sciene* 15 (1987), pp. 125–130.

[115] N. Metropolis and S. Ulam. "The Monte Carlo method". In: *Journal of the American Statistical Association* 44.247 (1949), pp. 335–341.

[116] S. Montoya-Noguera, T. Zhao, Y. Hu, Y. Wang, and K.-K. Phoon. "Simulation of non-stationary non-Gaussian random fields from sparse measurements using Bayesian compressive sampling and Karhunen–Loève expansion". In: *Structural Safety* 79 (2019), pp. 66–79.

[117] J. Morio. "Non-parametric adaptive importance sampling for the probability estimation of a launcher impact position". In: *Reliability Engineering & System Safety* 96.1 (2011), pp. 178–183.

[118] K. P. Murphy. *Machine learning: a probabilistic perspective*. Adaptive computation and machine learning. Cambridge, MA: MIT, 2013.

[119] A. Nataf. "Détermination des distributions de probabilités dont les marges sont données [Determination of probability distributions whose marginals are given]". In: *Comptes rendus hebdomaires des séances de l'Académie des sciences* 225 (1962), pp. 42–43.

[120] A. Neville. *Properties of Concrete*. 5th ed. Pearson, 2011.

[121] E. J. Nyström. "Über die praktische Auflösung von Integralgleichungen mit Anwendungen auf Randwertaufgaben [On the practical solution of integral equations with applications to boundary value problems]". In: *Acta Mathematica* 54 (1930), pp. 185–204.

[122] E. Oñate. *Structural analysis with the finite element method. Linear statics. Volume 1: basis and solids*. Lecture notes on numerical methods in engineering and sciences. New York City, NY: Springer Science+Business Media, 2009.

[123] E. Oñate. *Structural analysis with the finite element method. Linear statics. Volume 2: beams, plates and shells*. Lecture notes on numerical methods in engineering and sciences. New York City, NY: Springer Science+Business Media, 2013.

[124] I. Papaioannou, W. Betz, K. Zwirglmaier, and D. Straub. "MCMC algorithms for subset simulation". In: *Probabilistic Engineering Mechanics* 41 (2015), pp. 89–103.

[125] I. Papaioannou, K. Breitung, and D. Straub. "Reliability sensitivity estimation with sequential importance sampling". In: *Structural Safety* 75 (2018), pp. 24–34.

[126] I. Papaioannou, S. Geyer, and D. Straub. "Improved cross entropy-based importance sampling with a flexible mixture model". In: *Reliability Engineering & System Safety* 191 (2019), p. 106564.

[127] I. Papaioannou, C. Papadimitriou, and D. Straub. "Sequential importance sampling for structural reliability analysis". In: *Structural Safety* 62 (2016), pp. 66–75.

[128] I. Papaioannou and D. Straub. "Combination line sampling for structural reliability analysis". In: *Structural Safety* 88 (2021), p. 102025.

[129] I. Papaioannou and D. Straub. "Learning soil parameters and updating geotechnical reliability estimates under spatial variability - theory and application to shallow foundations". In: *Georisk: Assessment and Management of Risk for Engineered Systems and Geohazards* 11.1 (2017), pp. 116–128.

[130] I. Papaioannou and D. Straub. "Reliability updating in geotechnical engineering including spatial variability of soil". In: *Computers and Geotechnics* 42 (2012), pp. 44–51.

[131] K.-K. Phoon and F. H. Kulhawy. "Characterization of geotechnical variability". In: *Canadian Geotechnical Journal* 36.4 (1999), pp. 612–624.

[132] E. J. Plate. *Statistik und angewandte Wahrscheinlichkeitslehre für Bauingenieure [Statistics and applied probability theory for civil engineers]*. Ernst & Sohn, 1993.

[133] H. Pradlwarter, M. Pellissetti, C. Schenk, G. Schuëller, A. Kreis, S. Fransen, A. Calvi, and M. Klein. "Realistic and efficient reliability estimation for aerospace structures". In: *Computer Methods in Applied Mechanics and Engineering* 194.12 (2005), pp. 1597–1617.

[134] H. Pradlwarter, G. Schuëller, P. Koutsourelakis, and D. Charmpis. "Application of line sampling simulation method to reliability benchmark problems". In: *Structural Safety* 29.3 (2007), pp. 208–221.

[135] W. H. Press, S. A. Teukolsky, W. T. Vetterling, and B. P. Flannery. *Numerical recipes - the art of scientific computing*. 3rd ed. New York City, NY: Cambridge University, 2007.

[136] R. Rackwitz. "Reviewing probabilistic soils modelling". In: *Computers and Geotechnics* 26.3 (2000), pp. 199–223.

[137] R. Rackwitz. "Predictive distribution of strength under control". In: *Matériaux et Constructions* 16 (1983), pp. 259–267.

[138] R. Rackwitz. "Reliability analysis—a review and some perspectives". In: *Structural Safety* 23.4 (2001), pp. 365–395.

[139] R. Rackwitz and B. Fießler. "Structural reliability under combined random load sequences". In: *Computers & Structures* 9 (1978), pp. 489–494.

[140] H. Raiffa and R. Schlaifer. *Applied statistical decision theory*. Studies in managerial economics. Cambridge, MA: Division of research, graduate school of business administration, Harvard University, 1961.

[141] C. E. Rasmussen and C. K. I. Williams. *Gaussian processes for machine learning*. Adaptive computation and machine learning. Cambridge, MA: MIT, 2006.

[142] C. P. Robert. *The Bayesian choice: from decision-theoretic foundations to computational implementation*. 2nd ed. New York City, NY: Springer Science+Business Media, 2007.

[143] M. Rosenblatt. "Remarks on a multivariate transformation". In: *The Annals of Mathematical Statistics* 23.3 (1952), pp. 470–472.

[144] E. Rosenblueth and L. Esteva. "Reliability basis for some Mexican codes". In: *ACI Symposium Publication*. Vol. 31. 1972, pp. 1–42.

[145] R. Y. Rubinstein. "The cross-entropy method for combinatorial and continuous optimization". In: *Methodology And Computing In Applied Probability* 1.2 (1999), pp. 127–190.

[146] R. Y. Rubinstein and D. P. Kroese. *Simulation and the Monte Carlo method*. 3rd. Hoboken, NJ: John Wiley & Sons, 2017.

[147] R. A. Rzhanitzyn. "Design of structures with considerations of plastic properties of materials". In: *Stroivoenmorizdat, Moscow* (1949).

[148] D. Savvas, I. Papaioannou, and G. Stefanou. "Bayesian identification and model comparison for random property fields derived from material microstructure". In: *Computer Methods in Applied Mechanics and Engineering* 365 (2020), p. 113026.

[149] G. Schuëller, H. Pradlwarter, and P. Koutsourelakis. "A critical appraisal of reliability estimation procedures for high dimensions". In: *Probabilistic Engineering Mechanics* 19.4 (2004), pp. 463–474.

[150] G. Schuëller and R. Stix. "A critical appraisal of methods to determine failure probabilities". In: *Structural Safety* 4.4 (1987), pp. 293–309.

[151] M. Shinozuka. "Structural response variability". In: *Journal of Engineering Mechanics* 113.6 (1987), pp. 825–842.

[152] M. Shinozuka and G. Deodatis. "Simulation of multi-dimensional Gaussian stochastic fields by spectral representation". In: *Applied Mechanics Reviews* 49.1 (1996), pp. 29–53.

[153] T. T. Soong. *Fundamentals of probability and statistics for engineers*. John Wiley & Sons United Kingdom, 2004.

[154] M. Stein. *Interpolation of spatial data: some theory for kriging*. Springer series in statistics. New York City, NY: Springer, 1999.

[155] D. Straub and I. Papaioannou. "Bayesian updating with structural reliability methods". In: *Journal of Engineering Mechanics* 141.3 (2015), p. 04014134.

[156] Student (W. S. Gosset). "The probable error of a mean". In: *Biometrika* 6.1 (1908), pp. 1–25.

[157] B. Sudret and A. Der Kiureghian. *Stochastic finite element methods and reliability: a state-of-the-art report*. Report on research No. UCB/SEMM-2000/08. University of California, Berkeley, 2000.

[158] F. Uribe, I. Papaioannou, W. Betz, and D. Straub. "Bayesian inference of random fields represented with the Karhunen-Loève expansion". In: *Computer Methods in Applied Mechanics and Engineering* 358 (2020), p. 112632.

[159] M. Valdebenito, H. Pradlwarter, and G. Schuëller. "The role of the design point for calculating failure probabilities in view of dimensionality and structural nonlinearities". In: *Structural Safety* 32.2 (2010), pp. 101–111.

[160] L. H. Vanegas and G. A. Paula. "Log-symmetric distributions: statistical properties and parameter estimation". In: *Brazilian Journal of Probability and Statistics* 30.2 (2016), pp. 196–220.

[161] E. Vanmarcke. *Random fields: analysis and synthesis*. Revised and expanded new edition. World Scientific, 2010.

[162] E. Vanmarcke and M. Grigoriu. "Stochastic finite element analysis of simple beams". In: *Journal of Engineering Mechanics* 109.5 (1983), pp. 1203–1214.

[163] Y. Wang and T. Zhao. "Statistical interpretation of soil property profiles from sparse data using Bayesian compressive sampling". In: *Géotechnique* 67.6 (2017), pp. 523–536.

[164] Y. Wang, Z. Cao, and D. Li. "Bayesian perspective on geotechnical variability and site characterization". In: *Engineering Geology* 203 (2016), pp. 117–125.

[165] Z. Wang and J. Song. "Cross-entropy-based adaptive importance sampling using von Mises-Fisher mixture for high dimensional reliability analysis". In: *Structural Safety* 59 (2016), pp. 42–52.

[166] S. L. Zabell, S. M. Stigler, J. Aldrich, A. W. F. Edwards, E. Seneta, P. Diaconis, and E. Lehmann. “On Student’s 1908 article "The probable error of a mean"”. In: *Journal of the American Statistical Association* 103.481 (2008), pp. 1–20.

[167] Y. Zhang and A. Der Kiureghian. “Two improved algorithms for reliability analysis”. In: *Reliability and optimization of structural systems: proceedings of the sixth IFIP WG7.5 working conference on reliability and optimization of structural systems 1994*. Ed. by R. Rackwitz, G. Augusti, and A. Borri. Boston, MA: Springer US, 1995, pp. 297–304.

[168] H. Zhu and L. Zhang. “Characterizing geotechnical anisotropic spatial variations using random field theory”. In: *Canadian Geotechnical Journal* 50.7 (2013), pp. 723–734.

[169] K. Zuev and L. Katafygiotis. “Modified Metropolis–Hastings algorithm with delayed rejection”. In: *Probabilistic Engineering Mechanics* 26.3 (2011), pp. 405–412.

[170] K. M. Zuev, J. L. Beck, S.-K. Au, and L. S. Katafygiotis. “Bayesian post-processor and other enhancements of subset simulation for estimating failure probabilities in high dimensions”. In: *Computers & Structures* 92 - 93 (2012), pp. 283–296.

Part II

Original papers

Chapter 4

Reliability assessment of large hydraulic structures with spatially distributed measurements

Original publication

S. Geyer, I. Papaioannou, C. Kunz, and D. Straub. "Reliability assessment of large hydraulic structures with spatially distributed measurements". In: *Structure and Infrastructure Engineering* 16 (4 2020), pp. 599 – 612. DOI: 10.1080/15732479.2019.1652331.

Author's contribution

Sebastian Geyer, Iason Papaioannou, Claus Kunz, and Daniel Straub developed the concept to account for spatial data in the reliability assessment of hydraulic structures. Sebastian Geyer wrote the code underlying the numerical studies and carried out all numerical experiments. Sebastian Geyer wrote the original draft of the manuscript, which was then edited and finalized by himself, Iason Papaioannou, Claus Kunz, and Daniel Straub.

Abstract

Hydraulic structures, such as ship locks and weirs, form an essential part of waterway networks. An efficient life-cycle management is necessary to manage these large concrete structures safely and economically. Inspections and material testing form an important part of this process, as they enable an improved assessment of the condition, materials and properties of the structure. Traditionally, the limited data from tests is used to estimate probability distributions of material parameters; characteristic values for the assessment are then obtained from these distributions. Spatial correlation between measurement locations or different material layers is typically neglected. In this contribution, the spatially variable material parameters are modelled with random fields. The available data from local measurements is used to update the distribution of the random fields using Bayesian analysis. For comparison, the approach of Eurocode 0 for obtaining characteristic values is also applied. The structural reliability is then calculated applying subset simulation. It is shown that the employed random field modelling approach provides a more detailed statement about the material parameters. The results of an application to a ship lock wall demonstrate that modelling the spatial variability of concrete properties can

increase the reliability estimate of large hydraulic structures when measurement information is included.

4.1 Introduction

Waterway networks are large infrastructure systems. For example, the German waterway network measures ≈ 8000 km in length. The inland waterway is regulated through a large number of hydraulic structures, including 310 ship locks and 320 weirs [33]. Large portions of these structures have been in service for more than 70 years and about 25 % of them have an age of more than 100 years, which is the design working life of these types of structures. Because of thorough maintenance throughout the design working life, many of these aged structures are still in a good condition. However, the structural verification concept of the current European standards is intended for newly built structures and is based on conservative assumptions [9, 10, 11]. Hence, existing structures are seemingly unsafe because of changing verification concepts.

The approach proposed by [19] accounts for this by adapting the partial safety factors for the structural analysis of aged hydraulic structures. This model takes into account that the remaining lifetime of an existing structure is shorter than the intended design working life and that no failure has occurred so far. This knowledge allows reducing the partial safety factors while ensuring that the prescribed reliability throughout the design working life can be sustained.

The *Bundesanstalt für Wasserbau* (Federal Waterways Engineering and Research Institute, Germany), has published a guideline for the verification of existing hydraulic structures [4]. Therein, a verification procedure is proposed, consisting of three stages (A, B and C) with complexity and accuracy of model and input parameters increasing from stage A to stage C. If a structure cannot be verified according to stages A and B, in stage C probabilistic methods can be used to perform a structural reliability analysis considering the uncertainties in the input variables.

The massive shape and size of typical hydraulic structures leads to varying material properties within a structure. To consider this spatial variability explicitly, uncertainties need to be modelled as random fields instead of random variables in a probabilistic approach [32]. An efficient life-cycle management typically includes inspections during a hydraulic structure's design working life to assess the structural state. Such inspections involve taking samples of the built-in materials for material tests. Data from material tests can be used to reduce uncertainties and update model predictions. Detailed on-site inventory can be included in the approach proposed by [19].

If a fully probabilistic approach is used, available data can be used to estimate a probability distribution model for use in the reliability analysis. Bayesian analysis offers a consistent means of combining information from different sources to learn probabilistic models. Therein, the prior knowledge of uncertain parameters is updated with measurement information employing Bayes' rule (e.g. [2, 6, 24, 28]). This analysis is often performed without accounting for the measurement locations in the probabilistic model building. However, this is of great relevance in the context of large hydraulic structures, for which data is typically sparse. Bayesian analysis facilitates spatial modelling, and thus enables learning the spatial variability of uncertain parameters using spatially distributed measurements.

In this contribution, it is proposed to consider the spatial variability of material parameters in the reliability assessment of hydraulic structures through a detailed random field modelling. Measurement data is employed to learn the distribution of the random fields and update the structural reliability. To demonstrate the added value of the proposed method, a comparison with a standard approach for incorporating measurement data that does not account for the spatial variability of the parameters is performed. This study is an extended version of the one presented in [15].

The outline of the paper is as follows. In section 4.2, a coherent methodology for the reliability assessment of hydraulic structures is presented. First, an introduction to spatial variability and the random field model used to describe the spatial variation of concrete is presented. Next, a classical distribution fitting approach for incorporating measurement data is described. Then Bayesian updating is described for updating the random field model with spatially distributed measurements. Afterwards, the basic ideas of structural reliability are reviewed including a brief introduction to subset simulation, which is the method employed in the reliability analysis. The presented methodology is used in Section 4.3 to perform a reliability analysis for the chamber wall of a ship lock and results are compared for varying modelling choices. The obtained results are discussed in Section 4.4 before the conclusions in Section 4.5.

4.2 Methodology

Reliability analysis of hydraulic structures including spatially variable measurements requires probabilistic modelling, parameter updating, finite element modelling and the actual reliability analysis. In this section, suitable methods are presented for these different steps, which are targeted towards the application to large hydraulic structures.

4.2.1 Modelling spatial variability of concrete properties

Due to inherent variability in materials, different environmental conditions during the construction process and throughout the service life, different levels of craftsmanship and other influencing factors, material properties vary in space. Modelling these properties as random variables implies perfect correlation between material parameters at different spatial locations. This assumption may be adequate for certain materials and structures, but is inappropriate for the modelling of large hydraulic structures. Neglecting the spatial variability in these structures may result in an over-conservative estimate of the structural condition.

Spatially variable properties are probabilistically modelled as random fields. A random field can be defined as a collection of random variables indexed by a spatial coordinate $\mathbf{z} \in \Omega$, where Ω is a one-, two- or three-dimensional spatial domain. At each point in space, $X(\mathbf{z})$ is a random variable with probability density function (PDF) $f_X(x, \mathbf{z})$. This results in an infinite number of random variables that define the random field and hence discretization approaches are needed to represent random fields in practice. The spatial correlation of the random field at different points is described by the autocorrelation function $\rho(\mathbf{z}, \mathbf{z}')$ [32].

If a random field is homogeneous, the marginal PDF $f_X(x, \mathbf{z})$ is the same for any $\mathbf{z}$ and thus $f_X(x, \mathbf{z}) = f_X(x)$. Furthermore, the mean and standard deviation of a homogeneous random field are space-invariant and the correlation $\rho(\mathbf{z}, \mathbf{z}')$ of two points $\mathbf{z}$ and $\mathbf{z}'$ is a function of the difference in location $\mathbf{z} - \mathbf{z}'$ only. If the joint distribution between any collection of points in Ω is jointly Gaussian then the random field X is said to be Gaussian and is fully described by its mean value μ_X, standard deviation σ_X and the autocorrelation function $\rho(\mathbf{z}, \mathbf{z}')$ [32]. In this study, random fields that can be expressed as functions of Gaussian random fields are considered.

4.2.1.1 The Karhunen-Loève expansion

To represent a random field with a finite number of random variables, a discretization method is required. The chosen method here is the truncated Karhunen-Loève (KL) expansion, which approximates a random field X by a sum over m terms [26]:

$$X(\mathbf{z}) \approx \hat{X}(\mathbf{z}) = \mu_X(\mathbf{z}) + \sigma_X(\mathbf{z}) \cdot \sum_{i=1}^{m} \sqrt{\lambda_i} \cdot \varphi_i(\mathbf{z}) \cdot U_i, \tag{4.1}$$

where the $U_i,\ i = 1, ..., m$ are uncorrelated random variables with zero mean and unit variance. If X is a Gaussian random field, the variables $U_i,\ i = 1, \ldots, m$ are independent standard normal random variables. The λ_i and $\varphi_i(\cdot),\ i = 1, \ldots, m$ are the m largest eigenvalues and corresponding eigenfunctions (eigenpairs) found by solving the following integral eigenvalue problem [16]:

$$\int_\Omega \rho(\mathbf{z}, \mathbf{z}') \cdot \varphi_i(\mathbf{z}')\, \mathrm{d}\mathbf{z}' = \lambda_i \cdot \varphi_i(\mathbf{z}). \tag{4.2}$$

The required number of terms m in the KL expansion to obtain an accurate discrete representation of the random field depends on the domain Ω and the autocorrelation function $\rho(\mathbf{z}, \mathbf{z}')$. A measure to estimate the accuracy of the approximation is given by the relative variance error [30]:

$$\varepsilon_{\mathrm{V}}(\mathbf{z}) = \frac{\mathrm{Var}\left[X(\mathbf{z}) - \hat{X}(\mathbf{z})\right]}{\mathrm{Var}\left[X(\mathbf{z})\right]}. \tag{4.3}$$

The normalized global variance error can be determined by integration of $\varepsilon_{\mathrm{V}}(\mathbf{z})$ over the domain Ω and normalization with the volume of Ω. This global error measure is given as follows [3, 30]:

$$\bar{\varepsilon}_{\mathrm{V}} = 1 - \frac{1}{|\Omega|} \sum_{i=1}^{m} \lambda_i \int_\Omega \frac{\varphi_i^2(\mathbf{z})}{\sigma^2(\mathbf{z})} \mathrm{d}\mathbf{z}. \tag{4.4}$$

If the variance of the random field is constant over the domain (as is the case for homogeneous random fields), Equation (4.4) can be reduced to the following expression [3]:

$$\bar{\varepsilon}_{\mathrm{V}} = 1 - \frac{\sum_{i=1}^{m} \lambda_i}{|\Omega| \cdot \sigma^2}. \tag{4.5}$$

4.2.1.2 Probabilistic model of concrete properties

The Joint Committee on Structural Safety (JCSS) has published a probabilistic model code (PMC) that includes recommendations for modelling concrete with spatially variable parameters [18]. The PMC proposes to model concrete properties as functions of the basic compressive strength f_{c0}, which is defined by a random field with lognormal marginal distribution. $f_{c0}(\mathbf{z})$ is modelled by application of the KL expansion based on an underlying Gaussian random field:

$$f_{c0}(\mathbf{z}) = \exp\left(f_{c,\ln}(\mathbf{z})\right), \tag{4.6}$$

$$f_{c,\ln}(\mathbf{z}) = \mu_{c,\ln}(\mathbf{z}) + \sigma_{c,\ln}(\mathbf{z}) \cdot \sum_{i=1}^{m} \sqrt{\lambda_i} \cdot \varphi_i(\mathbf{z}) \cdot U_i, \tag{4.7}$$

where $\mu_{c,\ln}(\mathbf{z})$ and $\sigma_{c,\ln}(\mathbf{z})$ are the parameters of the lognormal random field f_{c0}, that is, the mean and standard deviation of the underlying Gaussian random field $f_{c,\ln}$. For the spatial correlation of concrete, the PMC recommends the following autocorrelation function and corresponding autocovariance function for the random field $f_{c,\ln}(\mathbf{z})$ [18]:

$$\rho_{c,\ln}(\Delta_{\mathbf{z},\mathbf{z}'}) = \rho_0 + (1 - \rho_0) \cdot \exp\left(\frac{-\Delta_{\mathbf{z},\mathbf{z}'}^2}{\ell_c^2}\right), \tag{4.8}$$

$$\Sigma_{c,\ln}(\Delta_{\mathbf{z},\mathbf{z}'}) = \sigma_{c,\ln}^2 \cdot \rho_{c,\ln}(\Delta_{\mathbf{z},\mathbf{z}'}), \tag{4.9}$$

where $\Delta_{\mathbf{z},\mathbf{z}'} = \|\mathbf{z} - \mathbf{z}'\|$ denotes the spatial distance of $\mathbf{z}$ and $\mathbf{z}'$. ρ_0 is the lower bound on the correlation within one structure and ℓ_c denotes the correlation length. ρ_0 reflects that $\sigma_{c,\ln}^2$ is

the variance associated with a concrete parameter in different structures. The variance in a single structure is smaller, which is modelled by ρ_0. Figure 4.1 illustrates this autocorrelation function as function of the spatial distance of two points (left panel) and shows the correlation in two dimensions as function of the canonical distances $\mathbf{z}_1 - \mathbf{z}_1'$ and $\mathbf{z}_2 - \mathbf{z}_2'$ (right panel). The

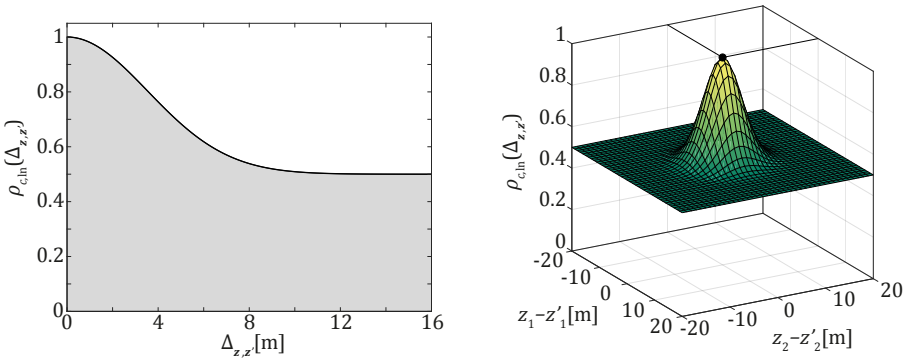

Figure 4.1: Correlation model for modelling the random field $f_{c,\ln}(\mathbf{z})$ with a correlation length of $\ell_c = 5\,\mathrm{m}$ and a lower bound on the correlation of $\rho_0 = 0.5$. The left panel illustrates the decrease of the correlation as function of the spatial distance of two points while the right panel shows the correlation in two dimensions as function of the canonical distances $\mathbf{z}_1 - \mathbf{z}_1'$ and $\mathbf{z}_2 - \mathbf{z}_2'$.

compressive strength $f_c(\mathbf{z})$, tensile strength $f_{ct}(\mathbf{z})$ and Young's modulus $E_c(\mathbf{z})$ of concrete can then be modelled based on $f_{c0}(\mathbf{z})$ as follows [18]:

$$f_c(\mathbf{z}) = \alpha \cdot (f_{c0}(\mathbf{z}))^{\vartheta} \cdot Y_1, \tag{4.10}$$

$$f_{ct}(\mathbf{z}) = 0.3 \cdot f_c(\mathbf{z})^{\frac{2}{3}} \cdot Y_2, \tag{4.11}$$

$$E_c(\mathbf{z}) = 10.5 \cdot f_c(\mathbf{z})^{\frac{1}{3}} \cdot \frac{Y_3}{1 + \beta \cdot \phi_t}. \tag{4.12}$$

The parameters α, ϑ, β and the creep coefficient ϕ_t are deterministic values that are selected based on in situ environmental conditions, concrete age and loading conditions. The parameters Y_1, Y_2 and Y_3 are lognormal distributed random variables that account for additional variations and whose recommended parameters are listed in Table 4.1.

Table 4.1: Additional random variables for concrete properties, defined by their mean value μ and coefficient of variation CV [18].

Parameter	Distribution	μ	CV
Y_1	lognormal	1.00	0.06
Y_2	lognormal	1.00	0.30
Y_3	lognormal	1.00	0.15

4.2.2 Inclusion of data in the analysis

As part of the maintenance of hydraulic structures, samples of the built-in material are often taken and tests are performed to obtain information on the material parameters. Let $\mathbf{X}$ denote

the vector of random variables representing the uncertain structural parameters. Information from material tests can be used to update the distribution of the model parameters $\mathbf{X}$. The updating procedure can be done with Bayesian analysis, through application of Bayes' rule:

$$f''_{\mathbf{X}}(\mathbf{x}) \propto L(\mathbf{x}) \cdot f'_{\mathbf{X}}(\mathbf{x}), \tag{4.13}$$

where $L(\mathbf{x})$ is the likelihood function, $f'_{\mathbf{X}}(\mathbf{x})$ is the prior distribution of $\mathbf{X}$, reflecting the knowledge on $\mathbf{X}$ before the information becomes available, and $f''_{\mathbf{X}}(\mathbf{x})$ is the posterior distribution of $\mathbf{X}$. $L(\mathbf{x})$ is proportional to the probability of the information given a parameter state $\mathbf{x}$ [13]. In the general case, solution of Equation (4.13) needs to be done numerically, for example, through sampling techniques, due to the intractability of the normalizing constant. Analytical solutions for the posterior distribution are available in some special cases, when using conjugate priors [13].

4.2.2.1 Traditional approaches to include measurement data

The limited data available from tests can be used to fit probability distributions of material parameters through application of standard distribution fitting approaches [e.g., 12, 34]. Characteristic values for the design are then obtained from the fitted distributions.

The uncertainty in the fitted distribution arising from the limited amount of data can be modelled through a Bayesian approach, as is done by the approach in Annex D.7 of Eurocode 0 [9]. This method determines the characteristic value of a normal or lognormal distribution with either known or unknown coefficient of variation. Characteristic values can be estimated based on the sample mean and the sample standard deviation of the (logarithmic) measurements and an additional factor, which depends on the amount of data and accounts for the uncertainty in the fitted distribution through the posterior predictive distribution of the parameter. A more detailed description of the method and its underlying model can be found in Appendix 4.A.

Another way to determine characteristic values is the approach proposed in [8]. It only requires the sample mean value and the minimum value of the measurements. These methods are straightforward to apply and hence are widely used in practice. However, they do not account for the locations of the measurements. Moreover, as the uncertainty in the underlying distribution is comparatively high for a small amount of data, the resulting characteristic value is often conservative.

4.2.2.2 Bayesian analysis of random fields

In this Section, an approach that accounts for the additional information available by assigning the spatial locations to the measured values is introduced. Consider the case where the information is available in the form of direct measurements of a continuous quantity Q. Usually, measurements are associated with a measurement error. For the application on random fields in hydraulic concrete structures, it is assumed that the measurement error ϵ is multiplicative and follows a lognormal distribution with parameters $\mu_{\epsilon,\ln} = 0$ (i.e. with median of 1) and $\sigma_{\epsilon,\ln}$. That is, a measurement outcome q_m is defined by

$$q_m = q \cdot \epsilon. \tag{4.14}$$

The available measurements for the application in this paper are measurements of the basic compressive strength of the concrete f_{c0}. Application of Equation (4.14) and taking the logarithm results in the following:

$$\ln(f_{c0,m}) = f_{c,\ln} + \ln(\epsilon). \tag{4.15}$$

As ϵ follows a lognormal distribution, $\ln(\epsilon)$ follows a normal distribution with mean $\mu_{\epsilon,\ln} = 0$ and standard deviation $\sigma_{\epsilon,\ln}$. Statistical independence between the measurement errors is assumed.

The prior distribution of f_{c0} is modelled with a homogeneous lognormal random field. Therefore, the prior distribution of $f_{c,\ln}$ at any selection of points in the spatial domain is the joint Gaussian distribution with moments evaluated from its mean $\mu'_{c,\ln}$ and autocovariance function $\Sigma'_{c,\ln}(\Delta_{\mathbf{z},\mathbf{z}'})$.

For this special case, an analytical solution of Equation (4.13) for the posterior distribution of the random field $f_{c,\ln}(\mathbf{z})$ exists. It is a Gaussian random field with mean function and autocovariance function given by [e.g., 22, 27]

$$\mu''_{c,\ln}(\mathbf{z}) = \mu'_{c,\ln} + \boldsymbol{\Sigma}_{c,\ln}(\mathbf{z}) \cdot \boldsymbol{\Sigma}_{m,\epsilon}^{-1} \cdot \Delta_m, \tag{4.16}$$

$$\Sigma''_{c,\ln}(\mathbf{z},\mathbf{z}') = \Sigma'_{c,\ln}(\Delta_{\mathbf{z},\mathbf{z}'}) - \boldsymbol{\Sigma}_{c,\ln}(\mathbf{z}) \cdot \boldsymbol{\Sigma}_{m,\epsilon}^{-1} \cdot \boldsymbol{\Sigma}_{c,\ln}(\mathbf{z}')^{\mathsf{T}}. \tag{4.17}$$

$\boldsymbol{\Sigma}_{c,\ln}(\mathbf{z})$ is a $1 \times n_m$ row vector function with element i equal to $\Sigma'_{c,\ln}(\Delta_{\mathbf{z},\mathbf{z}_i})$, where $\mathbf{z}_i$, $i = 1,\ldots,n_m$ denotes the measurement locations. $\boldsymbol{\Sigma}_{m,\epsilon}$ is defined as $\boldsymbol{\Sigma}_m + \boldsymbol{\Sigma}_\epsilon$, where $\boldsymbol{\Sigma}_m$ is an $n_m \times n_m$ matrix with element (i,j) equal to $\Sigma'_{c,\ln}\left(\Delta_{\mathbf{z}_i,\mathbf{z}_j}\right)$ and $\boldsymbol{\Sigma}_\epsilon$ is an $n_m \times n_m$ diagonal matrix with the log-error variance $\sigma^2_{\epsilon,ln}$ on the diagonal. The off-diagonal terms of $\boldsymbol{\Sigma}_\epsilon$ are 0 because of the assumption of statistical independence between the measurement errors. Δ_m is a $n_m \times 1$ column vector containing the measurement data with element i equal to $\left(\ln(f_{c0,m}(\mathbf{z}_i)) - \mu'_{c,\ln}\right)$.

As $f''_{c,\ln}(\mathbf{z})$ is a Gaussian random field, $f''_{c0}(\mathbf{z})$ is a lognormal random field with parameters $\mu''_{c,\ln}(\mathbf{z})$ and $\Sigma''_{c,\ln}(\mathbf{z},\mathbf{z}')$. Having evaluated the posterior distribution, the reliability conditional on the measurements can be estimated with any structural reliability method, for example, subset simulation which is presented in Section 4.2.3.

4.2.3 Reliability analysis with subset simulation

The main task of a reliability analysis is to identify the probability of a failure event F of the system of interest, defined as

$$F = \{\mathbf{x} \in \mathbb{R}^n : g(\mathbf{x}) \leq 0\}, \tag{4.18}$$

where $\mathbf{x}$ denotes the outcome of an n-dimensional random vector $\mathbf{X}$ collecting all uncertain input variables and $g(\mathbf{x})$ is the limit state function, which evaluates the performance of the system for a given realization $\mathbf{x}$. Non-positive values of $g(\mathbf{x})$ indicate failure of the system.

It is common to transform the problem to the outcome space of independent standard Normal random variables $\mathbf{U}$ by an isoprobabilistic transformation $\mathbf{U} = T(\mathbf{X})$, for example, the Rosenblatt transformation [17] or the Nataf transformation [5]. The failure probability is given by the following n-fold integral in standard Normal space:

$$P_F = \int_{\mathbb{R}^n} \mathbb{1}(G(\mathbf{u}) \leq 0) \cdot \phi(\mathbf{u})\, \mathrm{d}\mathbf{u}, \tag{4.19}$$

where $\phi(\cdot)$ is the PDF of the n-dimensional standard normal distribution, $G(\cdot) = g(T^{-1}(\cdot))$ is the transformed limit state function in standard Normal space and $\mathbb{1}(G(\mathbf{u}) \leq 0)$ is an indicator function which returns 1 if $G(\mathbf{u}) \leq 0$ and 0 otherwise. Typically, an analytical solution of Equation (4.19) to obtain P_F is not available and it needs to be solved numerically.

There exist a large number of approaches to estimate P_F, that is, to approximate the solution of Equation (4.19) [e.g., 20], amongst which the methods based on Monte Carlo simulation (MCS) are the most robust ones when the limit state function depends on outcomes of a black-box numerical model, for example, a finite element model. Because crude MCS is inefficient for

the estimation of rare event probabilities, several methods have been developed to increase its efficiency. In the context of assessing large hydraulic structures, subset simulation (SuS) is utilized, which can handle problems with a large number of random variables [1].

SuS expresses the event of interest (the failure event F) as an intersection of l nested events F_i, such that:

$$F_0 \supset F_1 \supset \cdots \supset F_l = F. \tag{4.20}$$

Each F_i is defined as

$$F_i = \{\mathbf{u} \in \mathbb{R}^n : G(\mathbf{u}) \leq \xi_i\}, \text{ with } \infty = \xi_0 > \xi_1 > \cdots > \xi_l = 0. \tag{4.21}$$

The probability of failure can then be expressed as a product of the conditional probabilities of each subset F_i given that F_{i-1} has occurred [1]. Starting with an initial Monte Carlo step by generating n_s samples from $\phi(\mathbf{u})$ and evaluating $G(\mathbf{u})$ for these samples, the SuS algorithm proceeds to the failure domain in the outcome space of $\mathbf{U}$, that is, the set for which $G(\mathbf{u}) \leq 0$, by repeatedly sampling from distributions conditional on each previous intermediate domain, that is, the domain of event F_{i-1} . This can be done by Markov chain Monte Carlo (MCMC) algorithms [21]. In each step, the conditional intermediate failure probability is estimated based on n_s available samples by a Monte Carlo estimate as follows:

$$\hat{P}_{F_i|F_{i-1}} = \frac{1}{n_s} \cdot \sum_{j=1}^{n_s} \mathbb{1}(G(\mathbf{u}_j) \leq \xi_i). \tag{4.22}$$

In the final level of the SuS algorithm, that is, when the number of samples that fall into the failure domain is sufficiently large, P_F can be estimated as

$$\hat{P}_F = \prod_{i=1}^{l} \hat{P}_{F_i|F_{i-1}}. \tag{4.23}$$

Figure 4.2 illustrates the sequential approach of SuS for a two-dimensional problem of uncorrelated standard normal random variables with $n_s = 1000$ samples per level. The failure domain is the red area of the panels in Figure 4.2. The intermediate thresholds are chosen such that $\hat{P}_{F_i|F_{i-1}} = 0.1$. In the first level (left panel of Figure 4.2), the samples are generated from the nominal density of $\mathbf{U}$, that is, the two-dimensional standard normal PDF. Evaluation of the limit state function results in the first intermediate event F_1, the samples that fall into the corresponding domain are marked red. The 1000 samples in level 2 (centre panel of Figure 4.2) are generated conditional on F_1 and are thus closer to the actual failure domain. The portion of the samples falling in the second intermediate domain are marked red in the centre panel of Figure 4.2. A new set of 1000 samples are generated conditional on F_2 in level 3 (right panel of Figure 4.2). In this case, $\hat{P}_{F_3|F_2} > 0.1$ and thus the sampling procedure is terminated and the failure probability can be estimated by application of Equation (4.23).

SuS estimates efficiently small failure probabilities through reducing the problem to the estimation of a set of larger conditional probabilities. Moreover, tailored MCMC algorithms such as the the dimension-independent conditional sampling algorithm [21] result in a performance of SuS that is independent of the input dimension. This makes SuS a popular choice for high dimensional reliability problems, for example, problems that involve discrete random field representations. An estimate of the variability of $\hat{P}_F$ can be calculated within the SuS algorithm without additional model evaluations [1].

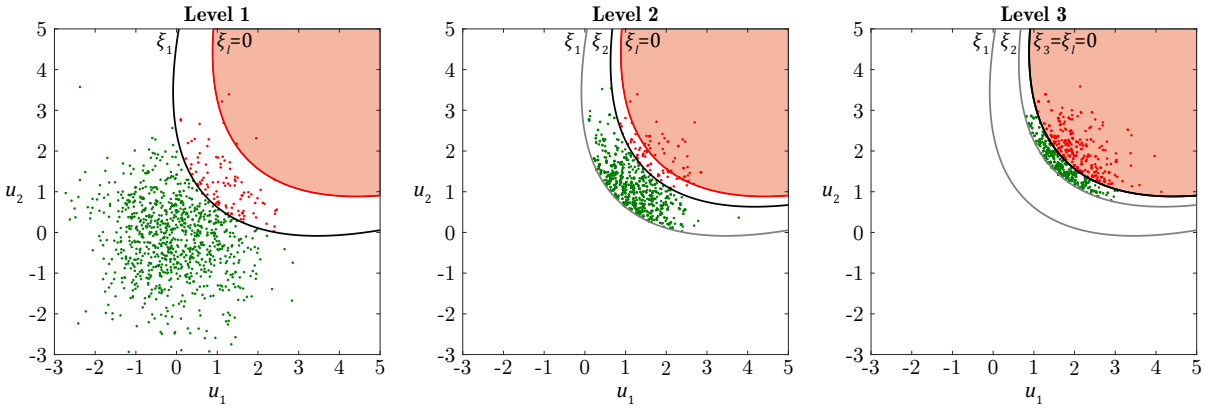

Figure 4.2: Illustration of the sequential approach of SuS. Starting from an initial MCS level (left panel), SuS advances to the failure domain (red area) by repeatedly sampling conditional on the intermediate domains of the previous levels (gray lines).

4.3 Assessment of a ship lock wall

A structural assessment and a reliability analysis are performed for the chamber wall of a ship lock. The proposed methodology is applied and results illustrate the influence of the spatial variability and measurement information on the computed reliability. The mean estimates of the failure probabilities are averaged from ten independent SuS runs for each parameter setup. The uncertainty on the mean estimate is calculated based on the estimate in [1].

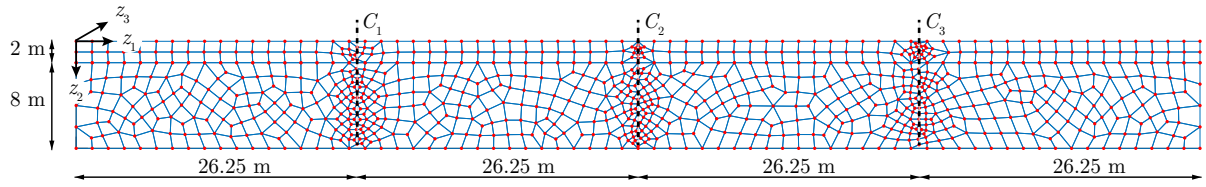

Figure 4.3: Finite element mesh of the investigated ship lock chamber wall consisting of 985 nodes and 837 quadrilateral elements. The location of the core samples C_1, C_2 and C_3 are indicated by the dashed black lines.

4.3.1 Structural model

The investigated ship lock is located at the German river *Hunte* and was built in the 1920s, that is, it has been in service for almost 100 years. The height of its chamber wall is 10 m and its length is 105 m. Several repair actions on the tamped concrete have been conducted throughout the design working life. The most substantial repair action was done in 1983, when the upper 2 m of the chamber wall were rebuilt completely with reinforced concrete.

The wall is modelled with a two-dimensional nonlinear finite element model with 985 nodes and 837 quadrilateral elements in the commercial software SOFiSTiK [25]. The material is modelled with the elastoplastic Drucker-Prager model [7]. The wall thickness is modelled constant as 2 m. The finite element mesh is illustrated in Figure 4.3. The mesh is refined in three regions; these are the locations where core samples have been taken to measure the concrete properties (core samples C_1, C_2 and C_3 indicated by dashed black lines in Figure 4.3).

As the focus in this study lies on modelling the concrete parameters, the foundation and the horizontal bedding are modelled very stiff, that is, the bottom edge and the two side edges are assumed to be clamped. Furthermore, the effect of the reinforcement in the upper 2 m is not

taken into consideration. For a qualitative comparison of different probabilistic models for the concrete properties this approximation is not substantial.

4.3.2 Concrete parameters

The structure consists of two parts of different concrete types. The basic compressive strength of each part is modelled separately by a lognormal distribution assuming statistical independence between the two parameters. The parameters $\mu'_{c,\ln,2}$ and $\sigma'_{c,\ln,2}$ for the concrete of the upper part are chosen as $\mu'_{c,\ln,2} = 3.85$ and $\sigma'_{c,\ln,2} = 0.123$, which corresponds to concrete grade C35 [18]. As the PMC does not give values for tamped concrete from the 1920s, the parameters for the bottom part are estimated conservatively with $\mu'_{c,\ln,1} = 2.80$ and $\sigma'_{c,\ln,1} = 0.411$, based on available measurement data of the structure from the 1960s and 1970s. Table 4.2 shows the corresponding mean values and CVs of the basic compressive strengths $f'_{c0,1}$ and $f'_{c0,2}$. The compressive strength, tensile strength and Young's modulus of the concrete are modelled based on the basic compressive strength by application of Equations (4.10) to (4.12). The deterministic parameters α, ϑ and β are chosen globally as follows: $\alpha = 0.8$, $\vartheta = 0.96$, $\beta = 0.8$ [18]. The creep coefficient for the concrete in the bottom part is chosen as $\phi_{t,1} = 4$ and for the one in the upper part as $\phi_{t,2} = 2$.

Table 4.2: Basic compressive strengths of the concrete types, defined by their mean value μ and coefficient of variation CV.

Parameter	Distribution	μ [N/mm^2]	CV
$f'_{c0,1}$	lognormal	47.4	0.124
$f'_{c0,2}$	lognormal	17.9	0.429

4.3.3 Loads and limit state function

A variety of loads act on this type of hydraulic structures. In addition to permanent loads from self-weight and earth pressure, structures are also subjected to variable loads like water and ground water pressure or traffic loads [10]. In order to assess the effect of different modelling approaches for the material properties, the analysis is restricted to the self-weight and the horizontal earth pressure from the backfill at normal ground water level, both modelled deterministically. The resulting load situation without self-weight (upper part: 25 kN/m^3, bottom part: 20 kN/m^3) is illustrated in Figure 4.4.

In a structural analysis, different serviceability and ultimate limit states have to be considered [9]. The verification has to be done for each of these limit states separately. As the aim is a qualitative estimate of the probability of failure, the analysis is restricted to a deformation-based global failure criterion. Hence, the following limit state function is defined:

$$G(\mathbf{u}) = w_{z_3,\mathrm{lim}} - \max(w_{z_3,j}(\mathbf{u}), j = 1, \ldots, 985), \tag{4.24}$$

where $w_{z_3,\mathrm{lim}}$ is the maximum allowable out-of-plane displacement and $w_{z_3,j}$ is the out-of-plane displacement of node j. This limit state function does not consider local failure modes, which might lead to a non-conservative estimate of the probability of failure. The failure criterion $w_{z_3,\mathrm{lim}}$ is chosen as $w_{z_3,\mathrm{lim}} = 0.35$ m.

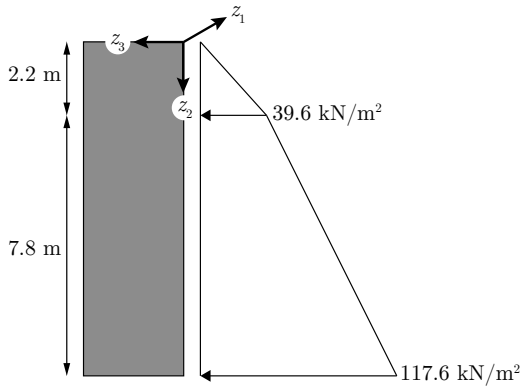

Figure 4.4: Acting load on the ship lock wall from horizontal earth pressure at normal ground water level.

4.3.4 Reliability analysis with prior parameters

The reliability is estimated with SuS. In the simulation, $n_s = 1000$ samples are evaluated per level and the intermediate failure probability is chosen as 0.1. In a first analysis, spatial variability of the material parameters is not considered and the basic concrete compressive strengths of the two layers are modelled as two independent lognormal random variables with parameters $\mu'_{c,\ln,1}$, $\sigma'_{c,\ln,1}$ and $\mu'_{c,\ln,2}$, $\sigma'_{c,\ln,2}$. For each of the two concrete layers, the calculation of the compressive strength $f_c(\mathbf{z})$, tensile strength $f_{ct}(\mathbf{z})$ and Young's modulus $E_c(\mathbf{z})$ of the concrete according to Equation (4.6) and Equations (4.10) to (4.12) requires three additional random variables Y_1, Y_2 and Y_3, as defined in Table 4.1. Thus, the total number of dimensions is $n'_{RV} = 8$. SuS results in an estimate of $\hat{P}'_{F,RV} = 4.3 \times 10^{-3}$ with coefficient of variation $\hat{CV}_{\hat{P}'_{F,RV}} = 0.06$.

For the reliability analysis with spatially variable concrete parameters, the lower bound on the correlation ρ_0 and correlation length ℓ_c are chosen as $\rho_0 = 0.5$ and $\ell_c = 5\,\mathrm{m}$, which are the default parameters proposed by [18]. The number of terms in the KL expansion is chosen such that the average relative variance error over the domain, calculated by means of Equation (4.5), is smaller than 10 %. With the chosen correlation length and autocorrelation function, the required number of terms for the prior random field $f_{c,\ln}(\mathbf{z})$ is $m'_1 = 14$ for the upper part and $m'_2 = 25$ for the bottom part. As in the previous analysis, the calculation of $f_c(\mathbf{z})$, $f_{ct}(\mathbf{z})$ and $E_c(\mathbf{z})$ requires three additional random variables Y_1, Y_2 and Y_3 per concrete layer. Hence, the resulting total number of dimensions in the prior reliability analysis with random fields is $n'_{RF} = 45$.

Two possible realizations of the random fields $f'_{c0,1}(\mathbf{z})$ and $f'_{c0,2}(\mathbf{z})$ are shown in Figure 4.5. The newer concrete in the upper part has a larger mean basic compressive strength than the concrete in the bottom part. The spatial variability of both random fields is clearly visible and it can also be seen that the locations of maximum or minimum values of the random fields vary from one realization to another.

SuS estimates the failure probability as $\hat{P}'_{F,RF} = 2.0 \times 10^{-3}$ with coefficient of variation $\hat{CV}_{\hat{P}'_{F,RF}} = 0.07$. That is, the modelling of the concrete properties as random fields reduces the estimated failure probability by approximately 50 %. Table 4.3 compares the estimates for the different approaches. It is noted that the concrete parameters at each point of the random field follow the same probability distributions as the corresponding random variables in the previous approach. The difference in the failure probability only stems from the spatial modelling with random fields.

The limit state function in Equation (4.24) is based on the maximum out-of-plane displace-

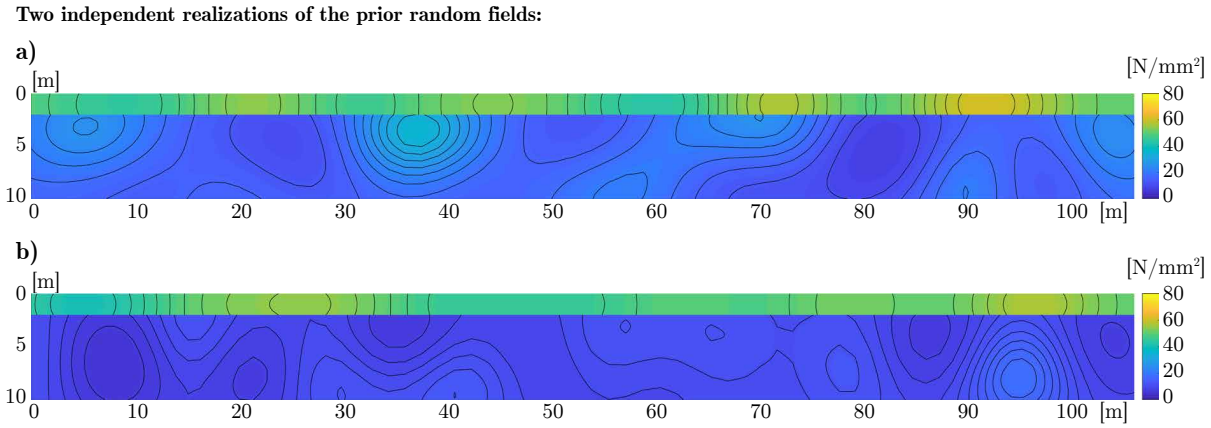

Figure 4.5: Two independent realizations of the prior random fields $f'_{c0,1}(\mathbf{z})$ and $f'_{c0,2}(\mathbf{z})$ representing the basic compressive strength of the old tamped concrete in the bottom part and the modern concrete in the upper part.

Table 4.3: Estimates of the probability of failure $\hat{P}_F$ and its coefficient of variation $\hat{CV}_{\hat{P}_F}$ for the different modelling approaches obtained with subset simulation.

Modelling approach	$\hat{P}_F$	$\hat{CV}_{\hat{P}_F}$
Prior random variables	4.3×10^{-3}	0.06
Posterior random variables	3.0×10^{-3}	0.06
Prior random fields	1.9×10^{-3}	0.07
Posterior random fields	1.9×10^{-4}	0.08

ment of the ship lock wall. Typically, displacements of structures are mainly determined by the global stiffness of the structure. In this case, the variance of the global average of the Young's modulus decreases when accounting for the spatial variability in the basic compressive strength due to the spatial averaging effect of the random fields [32]. Without accounting for spatial variability the variance of the global average is equal to the variance of the Young's modulus at each location as it is modelled by a single random variable. A decrease in the variance of the global average of the basic compressive strength results in a decrease of the variance of the displacement and thus in a decrease of the failure probability.

4.3.5 Reliability analysis including measurement information

During an extensive inspection on the ship lock in 2014, three vertical core samples were taken from the chamber wall. The locations of the core samples are indicated in Figure 4.3. A total of 33 measurements of the concrete compressive strength are available from these samples, 9 from the upper part and 24 from the bottom part. This information is used to learn the probabilistic model of the concrete strength. Table 4.4 lists the measurement information and locations.

4.3.5.1 Traditional distribution fitting approach

An approach to include available data in the structural analysis following Eurocode 0 was discussed in Section 4.2.2.1. Now the data of Table 4.4 is used to fit the underlying Student-t distribution for the basic concrete compressive strength (cf. Appendix 4.A). For the concrete in

Table 4.4: Measurements of the basic compressive strength of the concrete obtained from the three core samples C_1, C_2 and C_3. The measurement locations are also indicated in Figure 4.3.

Part of the wall	$C1$ $(z_1 = 26.25\,\text{m})$		$C2$ $(z_1 = 52.5\,\text{m})$		$C3$ $(z_1 = 78.75\,\text{m})$	
	z_2 [m]	$f_{c0,m}$ [N/mm^2]	z_2 [m]	$f_{c0,m}$ [N/mm^2]	z_2 [m]	$f_{c0,m}$ [N/mm^2]
Top	0.32	61.1	0.43	79.0	0.43	58.1
	1.00	59.4	1.15	76.2	1.13	70.4
	1.45	35.9	1.65	71.8	1.81	71.2
Bottom	2.40	29.2	2.21	21.2	2.34	18.5
	3.24	15.5	3.25	16.0	3.34	10.3
	4.25	8.7	4.05	32.0	4.17	13.2
	5.15	12.3	5.33	20.7	5.24	14.5
	6.12	16.2	6.15	13.8	6.27	25.4
	7.33	11.6	7.25	12.1	7.12	14.5
	8.15	13.4	8.40	8.6	8.23	13.2
	9.05	13.9	9.45	14.8	9.08	33.0

the top level of the ship lock wall, the following parameters of the Student-t distribution are obtained:

$$\bar{a}_{f_{c,\ln},1} = \bar{\mu}_{f_{c,\ln},1} = 4.149, \tag{4.25}$$

$$\bar{b}_{f_{c,\ln},1} = \bar{\sigma}_{f_{c,\ln},1} \cdot \sqrt{\frac{n_{m,1}+1}{n_{m,1}}} = 0.252, \tag{4.26}$$

$$\nu_{f_{c,\ln},1} = n_{m,1} - 1 = 8. \tag{4.27}$$

The resulting parameters for the concrete in the bottom level are:

$$\bar{a}_{f_{c,\ln},2} = \bar{\mu}_{f_{c,\ln},2} = 2.751, \tag{4.28}$$

$$\bar{b}_{f_{c,\ln},2} = \bar{\sigma}_{f_{c,\ln},2} \cdot \sqrt{\frac{n_{m,2}+1}{n_{m,2}}} = 0.375, \tag{4.29}$$

$$\nu_{f_{c,\ln},2} = n_{m,2} - 1 = 23. \tag{4.30}$$

In correspondence to the approach in the PMC, the basic concrete compressive strength is calculated from $f_{c,\ln,1}$ or $f_{c,\ln,2}$ by applying Equation (4.6).

It is noted that the direct fitting of a lognormal distribution, that is, without accounting for the uncertainty due to the finite number of measurements, would result in characteristic values of 42.8 N/mm^2 for the top level and 8.6 N/mm^2 for the bottom level (if the 5 %-quantile value is defined as the characteristic value). The characteristic value that is obtained by means of the Eurocode 0 approach for the case of unknown coefficient of variation of the basic compressive strength is 39.6 N/mm^2 for the top level and 8.2 N/mm^2 for the bottom level. These values coincide with the 5 %-quantile values of the described fitted Student-t distributions in combination with the transformation of Equation (4.6).

Running SuS with the fitted Student-t distributions results in an estimate for the failure probability of $\hat{P}''_{F,RV} = 3.0 \times 10^{-3}$ with coefficient of variation $\hat{CV}_{\hat{P}''_{F,RV}} = 0.06$. This probability is smaller than the failure probability estimated with the prior random variable approach. Table 4.3 compares the result to the other estimates.

4.3.5.2 Bayesian updating of random fields

The measurements are now used to update the random field model of the concrete strength through application of Bayesian analysis. A multiplicative, lognormal distributed measurement error with median 1 and standard deviation 0.1 is assumed for the Bayesian updating. The corresponding mean and standard deviation of $\ln(\epsilon)$ are $\mu_{\epsilon,\ln} = 0$ and $\sigma_{\epsilon,\ln} = 0.0993$. The updating of the random fields is done by evaluating Equations (4.16) and (4.17), resulting in non-homogeneous random fields defined by their autocovariance function and mean function. The mean and standard deviation of the updated random fields representing the basic compressive strength of the concrete $f''_{c0,1}(\mathbf{z})$ and $f''_{c0,2}(\mathbf{z})$ are illustrated in Figure 4.6.

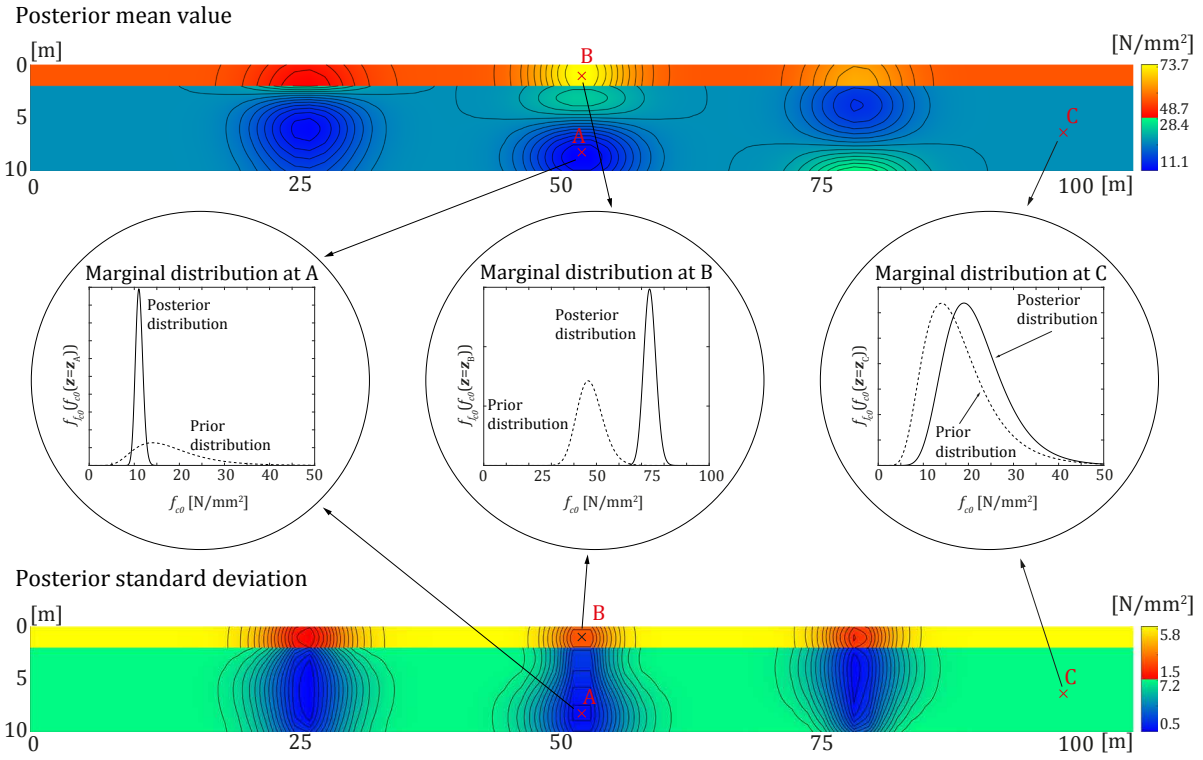

Figure 4.6: Posterior mean (top) and posterior standard deviation (bottom) of the random fields $f_{c0,1}(\mathbf{z})$ and $f_{c0,2}(\mathbf{z})$ representing the basic compressive strength of the old tamped concrete in the bottom part and the modern concrete in the upper part. The prior and posterior marginal distributions are illustrated in the middle for three selected points.

Obviously, the core samples have an impact on the parameters, especially in the direct

vicinity of the measurement locations.

The overall mean strength of the concrete of the upper part is higher than implied by the prior model, as its mean value ranges from $47.2\,\mathrm{N/mm^2}$ to $72.1\,\mathrm{N/mm^2}$, whereas the prior assumption is $47.4\,\mathrm{N/mm^2}$. In the regions far away from the measurements, the mean value is around $58.7\,\mathrm{N/mm^2}$. This effect illustrates the global effect of the updating procedure, which derives from the fact that the minimum correlation between any two points of the ship lock wall is 0.5. The mean value of the bottom part strength shows a large spatial variability, as it varies between $11.1\,\mathrm{N/mm^2}$ and $28.4\,\mathrm{N/mm^2}$. The extreme values are located at the measurement points. In the regions far away from the measurements, the mean value converges to $\approx 22.0\,\mathrm{N/mm^2}$.

The standard deviation of the concrete of the upper part changes significantly in the regions close to the core samples, where it is reduced by the Bayesian updating. With increasing distance from the measurement locations, the standard deviation converges to $5.77\,\mathrm{N/mm^2}$, which is only slightly smaller than the prior standard deviation. The standard deviation of the concrete of the bottom part near the measurements is reduced by almost 95 %. However, at any point it is reduced by a minimum of 7 %. Reasons for the larger global updating effect compared to the standard deviation of the upper part are the larger number of measurement points in the bottom part and the large variability in the prior model.

In addition to the parameters, the marginal prior and posterior distributions at three different points of the ship lock wall are extracted and shown in Figure 4.6. The points A and B show a large reduction of the variability of the marginal distribution while the change in the distribution at point C is comparatively small. The large influence of the data at points A and B is due to the small distance of the points to the measurement points. Point C is far away from any measurement point and thus only the global updating effect of the Bayesian analysis remains.

As in the prior analysis, the number of terms in the KL expansion is chosen such that the average relative variance error is smaller than 10 %. Evaluation of Equation (4.4) results in a required number of terms of $m_1'' = 18$ for the upper part and $m_2'' = 43$ for the bottom part. The increase in the required number of terms in the KL expansion is due to the fact that the autocovariance functions of the posterior random fields are not isotropic anymore, they are explicit functions of the spatial locations and thus more complex to approximate [31]. Including the three additional lognormal random variables for each random field to model all concrete parameters, the total number of dimensions in the posterior reliability analysis is $n_{RF}'' = 67$.

Two possible realizations of the posterior random fields $f_{c0,1}''(\mathbf{z})$ and $f_{c0,2}''(\mathbf{z})$ are shown in Figure 4.7. It can be seen that the variability in the regions around the measurements is decreased, the measurement values are clearly reflected by regions of high or low values in both realizations.

SuS estimates the failure probability with the updated parameters as $\hat{P}_{F,RF}'' = 1.9 \times 10^{-4}$ with coefficient of variation $\hat{CV}_{\hat{P}_{F,RF}''} = 0.08$, which is a large reduction compared to the spatial modelling without Bayesian updating and the random variable approach including measurement information (cf. Table 4.3). That is, by including the measurement information in the random field model, the calculated reliability of the ship lock wall increases significantly. The conservative assumption of the prior model is corrected, as evident from the decrease of the standard deviation of the tamped concrete. In the regions close to the core samples, the updated random fields clearly reflect the measurement results, giving an indication about regions of low or high quality concrete.

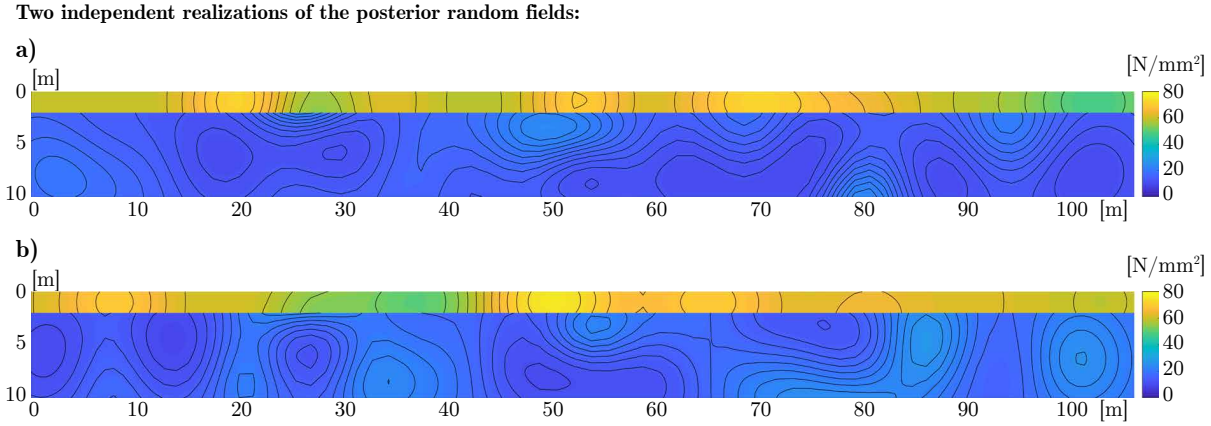

Figure 4.7: Two independent realizations of the posterior random fields $f''_{c0,1}(\mathbf{z})$ and $f''_{c0,2}(\mathbf{z})$ representing the basic compressive strength of the old tamped concrete in the bottom part and the modern concrete in the upper part including the information from the measurements.

4.3.6 Parameter study on the correlation length

The autocorrelation model of a random field controls the spatial fluctuation of the field. In addition, it determines the range of influence of the measurements in a Bayesian analysis. That is, the correct choice of the autocorrelation model and its parameters are crucial for the accuracy of the reliability analysis. In this study, the correlation model of the PMC by JCSS [18] is used, as presented in Section 4.2.1.2. The sensitivity of the structural reliability on the correlation length ℓ_c is investigated by performing a parameter study.

A change in the correlation length changes the solution of the KL eigenvalue problem of Equation (4.2) and thus the average variance error of the truncated KL expansion of Equation (4.4). The required number of terms for approximating the random fields with the initial correlation length of $\ell_c = 5\,\text{m}$ in the prior analysis is $m'_1 = 14$ for the top layer and $m'_2 = 25$ for the bottom layer. These numbers increased in the posterior analysis to $m''_1 = 18$ for the top layer and $m''_2 = 43$ for the bottom layer. This results in a total number of random variables of $n'_{RV} = 45$ and $n''_{RV} = 67$ random variables to estimate the failure probability. Table 4.5 shows the required number of KL terms and the resulting total number of random variables for varying correlation length in the prior and posterior reliability analysis. The correlation length has a strong influence on the required number of KL terms, a small correlation length results in a large number of required KL terms to achieve the same level of accuracy in terms of the average variance error. It is noted that the accuracy of the SuS estimate for the failure probability does not depend on the number of random variables [1, 21].

Figure 4.8 illustrates the effect of a varying correlation length on the failure probability for the prior and posterior analysis. It plots the estimated failure probability obtained with SuS, $\hat{P}_F$, against the prior correlation length ℓ_c of the random fields. The blue shaded area indicates $\hat{P}_F \pm \hat{\sigma}_{\hat{P}_F}$. In the prior analysis, $\hat{P}_F$ appears to increase with increasing ℓ_c, while in the posterior analysis $\hat{P}_F$ increases first before eventually decreasing again. This results from the two processes that are influenced by the correlation length.

On the one hand, the spatial fluctuation of the random fields decreases with increasing correlation length, which increases the variance of the global average of the random fields. As the spatial fluctuation decreases, the variance of the global average of the random field increases. The limiting case of an infinite correlation length corresponds to a single random variable per random field, as all points of the random field are fully correlated. As described in Section 4.3.4, the limit state function is dominated by the global stiffness of the structure and an increased

Table 4.5: Required number of terms in the truncated KL expansion to approximate the random fields with an average variance error of $\bar{\varepsilon}_V \leq 10\,\%$ as function of the correlation length ℓ_c. m_1' (m_1'') is the number of terms for the prior (posterior) top level random field, m_1' (m_1'') the number of terms for the prior (posterior) bottom level random field. n_{RV}' (n_{RV}'') is the total number of random variables in the prior (posterior) subset simulation.

Correlation length	Prior analysis			Posterior analysis		
ℓ_c [m]	m_1'	m_2'	n_{RV}'	m_1''	m_2''	n_{RV}''
3.33	21	49	76	28	77	111
5	14	25	45	18	43	67
7.5	9	13	28	12	25	43
10	7	8	21	10	19	35
15	5	5	16	7	13	26
20	4	4	14	5	11	22

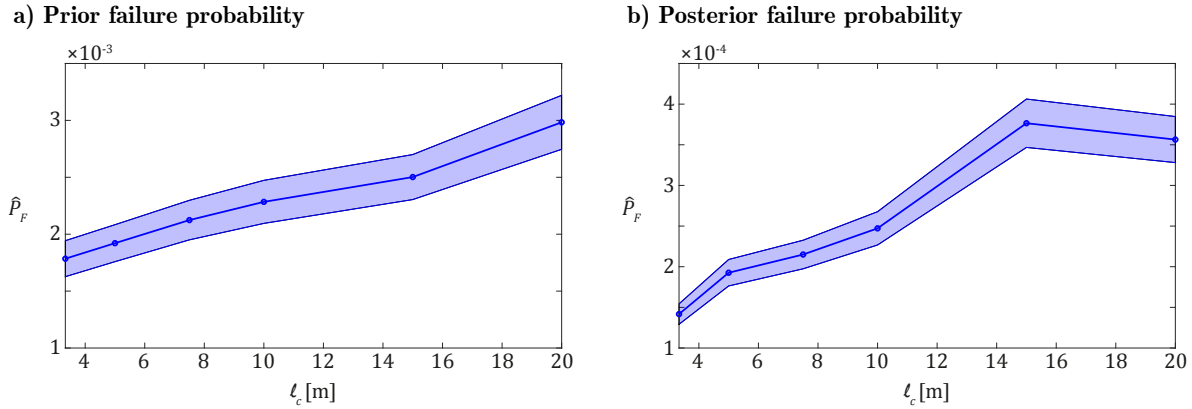

Figure 4.8: Prior (left panel) and posterior (right panel) estimate of the failure probability $\hat{P}_F \pm \hat{\sigma}_{\hat{P}_F}$ obtained with SuS as a function of the prior correlation length of the random fields to model the basic compressive strength.

variance of the global average of the random fields results in a larger failure probability. This effect can be observed in the prior and posterior analysis.

On the other hand, the influence range of the measurement values increases with an increasing correlation length because the autocorrelation function decreases slower with increasing distance. The Bayesian analysis reduces the variability of the underlying Gaussian random fields, as it reduces the uncertainty about their outcome. The higher the correlation length, the stronger the influence of the measurements on the variability of the random field, which leads to a reduction of the failure probability for increasing correlation length.

The reduction in the variability of the underlying Gaussian random field by the Bayesian analysis is independent of the measurement values, only the number of measurements and their locations are relevant. However, the measurement values determine the posterior mean function of the underlying Gaussian random field and thus the parameters of the posterior lognormal random field. Hence, the results in the right panel of Figure 4.8 are also conditional on the measurement outcome. The results of the posterior analysis suggest that for $\ell_c \leq 15\,\text{m}$, the

effect of the reduced spatial fluctuation on $\hat{P}_F$ is dominant for a change in ℓ_c, whereas the global effect of the Bayesian analysis dominates for $\ell_c > 15\,\mathrm{m}$.

4.3.7 Parameter study on the standard deviation of the measurement error

Another parameter that influences the Bayesian updating of the random field model by means of Equations (4.16) and (4.17) is the standard deviation of the measurement error. To illustrate this, the reliability analysis is performed for varying values of the standard deviation of the multiplicative, lognormal distributed measurement error.

The values are chosen as $\sigma_\epsilon = 0.05,\ 0.075,\ 0.15,\ 0.2$. The corresponding values of the standard deviation of the logarithmic measurement error are $\sigma_{\epsilon,\ln} = 0.0499,\ 0.0747,\ 0.1476,\ 0.1944$. The results of the reliability analysis are compared to the ones obtained with the initial choice of $\sigma_\epsilon = 0.1$. Figure 4.9 shows the resulting probability of failure as function of σ_ϵ. Again, the blue shaded area indicates $\hat{P}_F \pm \hat{\sigma}_{\hat{P}_F}$.

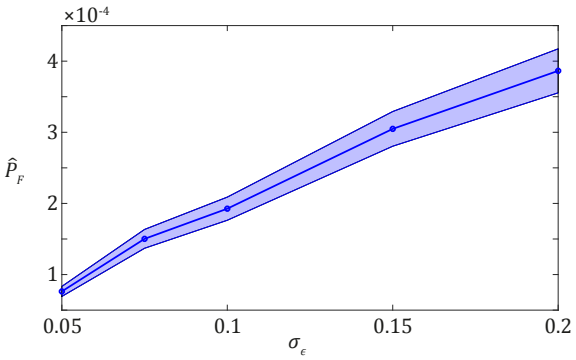

Figure 4.9: Posterior estimate of the failure probability $\hat{P}_F \pm \hat{\sigma}_{\hat{P}_F}$ obtained with SuS as a function of the standard deviation of the multiplicative, lognormal distributed measurement error.

It is shown that an increasing standard deviation of the measurement error results in a larger estimate of the probability of failure. The reason for this behavior is that a large value of σ_ϵ results in a reduced impact of the measurements and hence reduces the effect of the Bayesian updating on the random field model. The resulting posterior random field parameters are closer to the prior parameters. This is also reflected in the estimate of the posterior failure probability, which is closer to the prior estimate for a large standard deviation of the measurement error.

The standard deviation of the measurement error can also be seen as the level of confidence in the available data, where a small value expresses high confidence in the data. That is, the standard deviation of the measurement error can be employed as a tool to combine measurement data from different sources (e.g. data of different age or from various measurement techniques) with different levels of significance or accuracy.

4.4 Discussion

The proposed methodology for Bayesian analysis and reliability updating with spatial data is applied to the reliability assessment of a chamber wall of a ship lock in Germany. As several assumptions and simplifications are made, the resulting estimates listed in Table 4.3 are to be seen as qualitative assessments of the different investigated approaches. For instance, loads are modelled deterministically. For a detailed reliability analysis of the structure, furthermore, local and global failure modes based on stress (ultimate limit state) and deformation (serviceability limit state) have to be taken into account. Furthermore, the reinforcement in the concrete of the upper part and additional foundation parameters have to be modelled.

Nevertheless, the results in Table 4.3 indicate that modelling the spatial variability with random fields and Bayesian updating of the distribution parameters can increase the structural reliability estimate. The effect of Bayesian updating is higher for the random field approach than it is for the random variable approach. The reason for this is that the update of the random variables following Eurocode 0 assumes no prior information on the distribution parameters in contrast to the JCSS model which makes use of an informative prior for the concrete strength [9, 18].

Further attention needs to be paid to the modelling of the measurement error, as this significantly influences the effect of measurement data. Especially the variance of the error has to be calibrated for the applied testing method and the assumption of statistical independence of test errors needs to be verified.

The probabilistic modelling of aged tamped concrete in large hydraulic structures remains to be investigated in further studies, as the prior model used in this study does not explicitly address this concrete type. Due to the long construction periods at that time, the assumption of an isotropic autocorrelation function might not hold as the structure consists of different layers from subsequent steps in the construction process. Besides, additional studies need to be performed to validate the applied autocorrelation model, as the random field modelling largely depends on the choice of the autocorrelation function. Very little literature is available on the choice of a correlation model for concrete structures. Especially the correlation length and a potential minimum correlation ρ_0 within a structure are parameters that need to be chosen carefully. It should also be investigated if a hierarchical random field modelling is not better suited to reflect the structure-to-structure variability than the minimum correlation ρ_0.

Moreover, Bayesian updating is not always as straightforward as in this special case of the lognormal random field with direct measurements. For advanced problem settings without analytical solution, one needs to resort to numerical (e.g., sampling) techniques to derive the posterior distribution. For example, one can make use of the Bayesian updating with structural reliability methods environment, which reduces the reliability updating problem to solving one parallel system and one component problem [28, 29].

In the case where functional expressions for the posterior random fields are available, the spatial averaging method can be applied to reduce the dimensionality of the random field to a feasible set of random variables [14, 32]. The advantage of this approach is that it can be coupled easily with commercial finite element software, as the averaging domains can be chosen in order to match the finite element mesh. This is not the case for series expansion methods, such as the Karhunen-Loève expansion, where an additional interpolation on the Gauss points of the finite element mesh is required, resulting in considerable implementation effort [23].

4.5 Conclusions

Reliability assessment of existing large hydraulic structures is an important task because of the considerable age of many of these structures. Data of on-site investigations is often the basis for modelling material properties in the structural analysis. This paper investigates the effect of modelling spatial variability in large hydraulic structures. It is proposed to model concrete properties as random fields thus including the inherent spatial variability of these parameters in the reliability analysis. The probabilistic model used for the concrete is based on modelling the basic compressive strength as a random field; the actual compressive strength, tensile strength and Young's modulus are defined as functions of this random field and additional random variables.

Following Eurocode 0 it is proposed to use Bayesian analysis to include available information from measurements in the random field model. A special case is described, where an analytical

solution is available to update a lognormal random field. The updating rules are defined as functions of the prior parameters, the available data and an error term to include uncertainty in the measurement results.

The application of the methodology to the deformation analysis of a ship lock wall illustrates the effect of modelling spatial variability and including measurement information on the calculated reliability. The results show that the explicit modelling of spatial variability and the Bayesian updating have a significant impact on the reliability estimate of large hydraulic structures and can provide an improved assessment of the structural condition. In the presented case study, the spatial modelling of concrete properties reduces the estimated failure probability by $\approx 50\,\%$ compared to the failure probability estimate obtained when the concrete properties are modelled as random variables with the prior parameters. Bayesian updating of the random fields also has a strong impact on the reliability estimate, as the computed posterior failure probability decreases by an order of magnitude compared to the random field approach without Bayesian updating. Comparison of the results to the reliability obtained with the fitted Student-t distribution that is the underlying model for obtaining characteristic values following Eurocode 0 shows that modelling of spatial variability with random fields can improve the calculated reliability of a structure, as the additional information available from the measurement locations can be included in the model. In addition, the proposed method allows for including prior information, which is available from the nominal concrete strength at the time of construction.

Disclosure statement

No potential conflict of interest was reported by the authors.

4.A Characteristic values according to Eurocode 0

Underlying the method in Annex D.7 of Eurocode 0 [9] is the use of Bayesian statistics to determine characteristic values of material properties that follow a normal or lognormal distribution. It differentiates between two cases: (i) the coefficient of variation of the property is known and hence only the mean has to be estimated, and (ii) the mean and the variance are unknown. This appendix focuses on explaining the latter case, since it is employed in Section 4.3.5.1.

In general, a characteristic value is defined as a specific quantile value of the underlying probability distribution. That is, the characteristic value of a random variable X, defined as the p-quantile value, can be obtained as follows:

$$x_{k,p} = F_X^{-1}(p), \tag{4.31}$$

where $F_X^{-1}(\cdot)$ is the inverse cumulative distribution function (CDF) of X. For material properties, the characteristic value is typically defined as the $5\,\%$-quantile value. The method in Annex D.7 of Eurocode 0 defines the characteristic value as quantile value of the posterior predictive distribution of X [13]. It assumes that no prior information on the distribution of X is available, which is equivalent to assuming a diffuse (noninformative) prior distribution in the context of Bayesian analysis. If X describes a quantity that follows a normal distribution with unknown mean and variance, the predictive distribution is a Student-t distribution. The estimation of the parameters of the posterior predictive distribution is based on n_m test results $x_{m,i},\ i = 1, \ldots, n_m$.

Three parameters have to be estimated for the Student-t distribution: the number of degrees of freedom ν, location parameter a and scale parameter b. The number of degrees of freedom is directly determined by the amount of data, $\nu = n_m - 1$. The location parameter is estimated as

the sample mean of the data:

$$\bar{a} = \bar{\mu} = \frac{1}{n_m} \sum_{i=1}^{n_m} x_{m,i}. \tag{4.32}$$

The estimated scale parameter is defined by

$$\bar{b} = \sqrt{\frac{1}{n_m - 1} \sum_{i=1}^{n_m} (x_{m,i} - \bar{a})^2} \cdot \sqrt{\frac{n_m + 1}{n_m}}. \tag{4.33}$$

The characteristic value of X can be obtained by applying Equation (4.31) using the inverse CDF of the Student-t distribution with parameters $n_m - 1$, $\bar{a}$ and $\bar{b}$. To generalize the approach, the random variable X can be transformed to a standard Student-t distributed random variable U ($a = 0,\ b = 1$) as follows:

$$U = \frac{X - \bar{a}}{\bar{b}}. \tag{4.34}$$

It is noted that ν is not affected by this transformation. Therefore, the characteristic value of X corresponding to the p-quantile value is defined as

$$x_{k,p} = \bar{a} + \bar{b} \cdot u_{k,p}, \tag{4.35}$$

where $u_{k,p}$ is the p-quantile value of the standard Student-t distribution with $n_m - 1$ degrees of freedom, that is, the inverse CDF of the standard Student-t distribution with $n_m - 1$ degrees of freedom, evaluated at p. A modified but equivalent version of Equation (4.35) is used in Eurocode 0 for $p = 0.05$:

$$x_{k,p} = \bar{\mu} \cdot \left(1 - k_{n_m} \cdot \bar{\delta}_X\right), \tag{4.36}$$

where $\bar{\delta}_x = \frac{\bar{\sigma}}{\bar{\mu}}$ is the sample coefficient of variation of X. $\bar{\mu}$ is the sample mean (Equation (4.32)) and $\bar{\sigma}$ is the sample standard deviation, given by

$$\bar{\sigma} = \sqrt{\frac{1}{n_m - 1} \sum_{i=1}^{n_m} (x_{m,i} - \bar{\mu})^2}. \tag{4.37}$$

k_{n_m} is the factor that accounts for the limited amount of data:

$$k_{n_m} = -u_{k,p} \cdot \sqrt{\frac{n_m + 1}{n_m}}, \tag{4.38}$$

where $u_{k,0.05}$ is the inverse CDF of the standard Student-t distribution with $n_m - 1$ degrees of freedom, evaluated at 0.05.

The method can also be applied if X follows a lognormal distribution. In this case, the parameters of the predictive Student-t distribution are estimated for the distribution of $\ln(X)$. Accordingly, the location and scale parameters are estimated as

$$\bar{a}_{\ln} = \bar{\mu}_{\ln,m} = \frac{1}{n_m} \sum_{i=1}^{n_m} \ln\left(x_{m,i}\right), \tag{4.39}$$

$$\bar{b}_{\ln} = \sqrt{\frac{1}{n_m - 1} \sum_{i=1}^{n_m} \left(\ln\left(x_{m,i}\right) - \bar{a}_{\ln}\right)^2} \cdot \sqrt{\frac{n_m + 1}{n_m}}. \tag{4.40}$$

Equations (4.34) and (4.35) can be used to determine the characteristic value for $\ln(X)$, from

which the characteristic value for X can be calculated as follows:

$$x_{k,p} = \exp\left(\bar{a}_{\ln} - \bar{b}_{\ln} \cdot u_{k,p}\right). \tag{4.41}$$

This equation also appears in a different, yet equivalent version in Eurocode 0:

$$x_{k,p} = \exp\left(\bar{\mu}_{\ln} - k_{n_m} \cdot \bar{\sigma}_{\ln}\right), \tag{4.42}$$

where k_{n_m} follows the definition in Equation (4.38), $\bar{\mu}_{\ln}$ is the sample mean of the logarithmic measurements (Equation (4.40)) and $\bar{\sigma}_{\ln}$ is the sample standard deviation of the logarithmic measurements:

$$\bar{\sigma}_{\ln} = \sqrt{\frac{1}{n_m - 1} \sum_{i=1}^{n_m} \left(\ln\left(x_{m,i}\right) - \bar{\mu}_{\ln}\right)^2}. \tag{4.43}$$

Eurocode 0 provides a table with values of k_{n_m} for different n_m. This enables direct calculation of characteristic values based on $\bar{\mu}$ and $\bar{\sigma}$ ($\bar{\mu}_{\ln}$ and $\bar{\sigma}_{\ln}$).

By replacing the normal (lognormal) distribution with the Student-t distribution, one accounts for the uncertainty in the fitted distribution arising from the limited amount of available data. By fitting a normal or lognormal distribution directly from the data, one typically underestimates the variability of the property of interest (e.g., [2]). The Student-t distribution compensates this error as its tails are heavier than these of a normal distribution. For $n_m \to \infty$, the Student-t distribution converges to a normal distribution. It is pointed out that this approach does not include measurement uncertainty and does not account for any prior information on the material properties.

References

[1] S.-K. Au and J. L. Beck. "Estimation of small failure probabilities in high dimensions by subset simulation". In: *Probabilistic Engineering Mechanics* 16.4 (2001), pp. 263–277.

[2] J. Benjamin and C. Cornell. *Probability, statistics, and decision for civil engineers*. New York City, NY: McGraw-Hill, 1970.

[3] W. Betz, I. Papaioannou, and D. Straub. "Numerical methods for the discretization of random fields by means of the Karhunen-Loève expansion". In: *Computer Methods in Applied Mechanics and Engineering* 271 (2014), pp. 109–129.

[4] Bundesanstalt für Wasserbau. *Bewertung der Tragfähigkeit bestehender, massiver Wasserbauwerke [Assessment of the bearing capacity of existing, massive hydraulic structures]*. BAW guideline, 2016.

[5] A. Der Kiureghian and P.-L. Liu. "Structural reliability under incomplete probability information". In: *Journal of Engineering Mechanics* 112.1 (1986), pp. 85–104.

[6] D. Diamantidis. *Report 32: probabilistic assessment of existing structures - a publication for the Joint Committee on Structural Safety (JCSS)*. RILEM, 2001.

[7] D. C. Drucker and W. Prager. "Soil mechanics and plastic analysis or limit design". In: *Quarterly of Applied Mathematics* 10.2 (1952), pp. 157–165.

[8] *EN 131791:2019. Assessment of in-situ compressive strength in structures and precast concrete components*. European Standard, 2019.

[9] *EN 1990:2002. Eurocode 0: basis of structural and geotechnical design*. European Standard, 2002.

[10] *EN 1991-1-1. Eurocode 1: actions on structures - part 1-1: general actions - densities, self-weight, imposed loads for buildings*. European Standard, 2002.

[11] *EN 1992-1-1:2004. Eurocode 2: design of concrete structures - part 1-1: general rules and rules for buildings*. European Standard, 2004.

[12] M. H. Faber, J. Köhler, and J. D. Sørensen. "Probabilistic modeling of graded timber material properties". In: *Structural Safety* 26.3 (2004), pp. 295–309.

[13] A. Gelman, J. Carlin, H. Stern, D. Dunson, A. Vehtari, and D. Rubin. *Bayesian data analysis*. 3rd. Chapman & Hall/CRC texts in statistical science. Boca Raton, FL: CRC, 2013.

[14] S. Geyer, I. Papaioannou, C. Kunz, and D. Straub. "Bayesian reliability assessment with spatially variable measurements: the spatial averaging approach". In: *Proceedings of the 13th international conference on application of statistics and probability in civil engineering*. Ed. by J. Song. Seoul: Seoul National University open repository, 2019, pp. 1–8.

[15] S. Geyer, I. Papaioannou, D. Straub, and C. Kunz. "Reliability assessment of large hydraulic structures with spatially distributed measurements". In: *Proceedings of the sixth international symposium on life-cycle civil engineering*. Ed. by R. Caspeele, L. Taerwe, and D. M. Frangopol. CRC Press/Balkema, 2018, pp. 361–368.

[16] R. G. Ghanem and P. D. Spanos. *Stochastic finite elements. A spectral approach*. revised. Dover civil and mechanical engineering. Mineola, NY: Dover, 2012.

[17] M. Hohenbichler and R. Rackwitz. "Non-normal dependent vectors in structural reliability". In: *Journal of the Engineerings Mechanics Division* 107 (1981), pp. 1227–1238.

[18] *JCSS probabilistic model code. Part 3 - resistance models*. Joint Committee on Structural Safety, 2001.

[19] C. Kunz. "Ein Konzept für Teilsicherheitsbeiwerte für bestehende Wasserbauwerke [Partial safety factors for existing hydraulic structures]". In: *Bautechnik* 92.8 (2015), pp. 549–556.

[20] M. Lemaire, A. Chateauneuf, and J.-C. Mitteau. *Structural reliability*. Hoboken, NJ: John Wiley & Sons, 2009.

[21] I. Papaioannou, W. Betz, K. Zwirglmaier, and D. Straub. "MCMC algorithms for subset simulation". In: *Probabilistic Engineering Mechanics* 41 (2015), pp. 89–103.

[22] I. Papaioannou and D. Straub. "Learning soil parameters and updating geotechnical reliability estimates under spatial variability - theory and application to shallow foundations". In: *Georisk: Assessment and Management of Risk for Engineered Systems and Geohazards* 11.1 (2017), pp. 116–128.

[23] W. H. Press, S. A. Teukolsky, W. T. Vetterling, and B. P. Flannery. *Numerical recipes - the art of scientific computing*. 3rd ed. New York City, NY: Cambridge University, 2007.

[24] C. P. Robert. *The Bayesian choice: from decision-theoretic foundations to computational implementation*. 2nd ed. New York City, NY: Springer Science+Business Media, 2007.

[25] SOFiSTiK AG. *SOFiSTiK Basisfunktionalitäten [SOFiSTiK Basics]*. User manual. Oberschleißheim, Germany, 2017.

[26] P. Spanos and R. Ghanem. "Stochastic finite element expansion for random media". In: *Journal of Engineering Mechanics* 15.5 (1989), pp. 1035–1053.

[27] D. Straub. "Reliability updating with inspection and monitoring data in deteriorating reinforced concrete slabs". In: *Proceedings of the 11th international conference on applications of statistics and probability in civil engineering*. Ed. by M. H. Faber, J. Köhler, and K. Nishijima. CRC Press/Balkema, 2011, pp. 2309–2316.

[28] D. Straub and I. Papaioannou. "Bayesian updating with structural reliability methods". In: *Journal of Engineering Mechanics* 141.3 (2015), p. 04014134.

[29] D. Straub, I. Papaioannou, and W. Betz. "Bayesian analysis of rare events". In: *Journal of Computational Physics* 314 (2016), pp. 538–556.

[30] B. Sudret and A. Der Kiureghian. *Stochastic finite element methods and reliability: a state-of-the-art report*. Report on research No. UCB/SEMM-2000/08. University of California, Berkeley, 2000.

[31] F. Uribe, I. Papaioannou, W. Betz, and D. Straub. "Bayesian inference of random fields represented with the Karhunen-Loève expansion". In: *Computer Methods in Applied Mechanics and Engineering* 358 (2020), p. 112632.

[32] E. Vanmarcke. *Random fields: analysis and synthesis*. Revised and expanded new edition. World Scientific, 2010.

[33] A. Westendarp, H. Becker, J. Bödefeld, H. Fleischer, C. Kunz, M. Maisner, H. Müller, A. Rahimi, T. Reschke, and F. Spörel. "Erhaltung und Instandsetzung von massiven Verkehrswasserbauwerken [Maintenance and repair of massive hydraulic structures]". In: *Beton-Kalender 2015*. Hoboken, NJ: John Wiley & Sons, 2014, pp. 185–246.

[34] D. F. Wiśniewski, P. J. Cruz, A. A. R. Henriques, and R. A. Simões. "Probabilistic models for mechanical properties of concrete, reinforcing steel and pre-stressing steel". In: *Structure and Infrastructure Engineering* 8.2 (2012), pp. 111–123.

Chapter 5

Bayesian analysis of hierarchical random fields for material modeling

Original publication

S. Geyer, I. Papaioannou, and D. Straub. "Bayesian analysis of hierarchical random fields for material modeling". In: *Probabilistic Engineering Mechanics* 66 (2021), p. 103167. DOI: 10.1016/j.probengmech.2021.103167.

Author's contribution

Sebastian Geyer, Iason Papaioannou, and Daniel Straub developed the concept underlying the hierarchical Bayesian model. The mathematical derivations were carried out by Sebastian Geyer and Iason Papaioannou. Sebastian Geyer wrote the code underlying the numerical studies and carried out all numerical experiments. Sebastian Geyer wrote the original draft of the manuscript, which was then edited and finalized by himself, Iason Papaioannou, and Daniel Straub.

Abstract

In probabilistic assessments, spatially variable material properties are modeled with random fields. These random fields can be learned from spatial data by means of Bayesian analysis. This paper presents analytical expressions for the Bayesian analysis of hierarchical Gaussian random fields. We model the prior spatial distribution by a Gaussian random field with normal-gamma distributed mean and precision and make use of the conjugacy of prior distribution and likelihood function to find the posterior distribution of the random field parameters. We present closed-form expressions for the spatial mean and precision function of the posterior predictive Student's t-random field. Furthermore, we discuss the application of the hierarchical model to non-Gaussian random fields (translation random fields) and show the connection of the methodology to the Bayesian approach of EN 1990 for estimating characteristic values for material parameters. The method is illustrated on two spatial data sets of concrete and soil strength parameters.

5.1 Introduction

Setting up an engineering model requires definition of material properties. To correctly account for their inherent randomness, such material properties are commonly modeled probabilistically. A probabilistic representation with random variables is sufficient for modeling materials without or with negligible spatial variability. However, in many applications the effects of the spatial variability of materials should not be neglected in the modeling process. This is the case, e.g., with soil parameters in geotechnical assessments [39], and material parameters in assessments of large concrete structures [e.g., 22].

Spatially variable uncertain quantities can be modeled by random fields (RFs). An RF represents a random variable at each point of a spatial domain [51]. A complete definition of the RF requires specification of the joint distribution of the variables corresponding to any collection of points of the spatial domain. This is nontrivial in general with the exception of Gaussian and a special case of non-Gaussian RFs, termed translation RFs. Translation RFs are RFs that can be expressed as functions of Gaussian RFs [24], e.g., a lognormal RF can be expressed as the exponential of a Gaussian RF. A Gaussian RF implies that the joint distribution for any collection of points is multivariate Gaussian and can be completely defined by the first- and second-moment functions [1]. Gaussian RFs have well established statistical properties and a variety of methods are available for simulating them [e.g., 32].

RFs can be learned from data through Bayesian analysis [21]. In the general case, such an update needs to be done numerically with methods usually based on Monte Carlo sampling, including Markov chain Monte Carlo methods [8], sequential Monte Carlo methods [18, 12] and subset simulation [48, 5, 49]. However, Gaussian RFs enable the use of conjugate priors to learn the RF parameters via a closed-form update in a Bayesian analysis [38, 22].

RFs have been used for a long time in the field of geostatistics for the interpolation of spatial data by means of kriging, which includes Bayesian inference of Gaussian RF parameters [e.g., 47, 25]. A comprehensive review of hierarchical Bayesian analysis with spatial data from the viewpoint of geostatistics can be found in [3]. More recently, these approaches have gained importance in the field of machine learning. They are used for Gaussian process regression, which is a versatile surrogate model for random functions with noisy observations [43]. In the engineering community, the potential of accounting for spatial variability within Bayesian analysis has been recognized especially in the field of geotechnical engineering [e.g., 19, 15, 54, 28]. Therein, it is often essential to identify site-specific trend functions of soil properties in addition to the inherent spatial variability. Recently, attempts have been made to simultaneously learn the trend function and autocovariance function with sparse measurements in a Bayesian analysis. The approach of [14, 13, 16] applies sparse Bayesian learning to learn the trend function of the RF and subsequently draws samples from the posterior distribution of the RF parameters through Markov chain Monte Carlo methods. The authors of [53] applied Bayesian compressive sampling to represent non-homogeneous RFs. This approach does not require the explicit choice of a prior RF model. It expresses the RF as a superposition of a set of basis functions and evaluates the posterior distribution of the coefficients of these functions using sparse measurements. The method has been combined with the Karhunen-Loève expansion to obtain realizations of the RF [56, 55, 35], and has been recently extended to treat multi-dimensional and cross-correlated RFs [26, 58].

Bayesian approaches have also found their way into other engineering fields, e.g., for estimating design values of structural material properties when samples are available [4, 41], which is also included in the current European standards for constructions (EN 1990) [20].

The aim of this paper is to present a hierarchical Bayesian model for material properties modeled with Gaussian or translation RFs. Hierarchical Gaussian Bayesian models have been well

developed in the context of Bayesian linear regression [e.g., 21] and hierarchical spatial modeling [e.g., 7]. This work applies existing results from these fields to derive a comprehensive hierarchical RF model that can be used in the context of stochastic material modeling. We make use of the fact that the normal-gamma distribution is the conjugate prior for the mean and precision of a Gaussian RF to obtain the posterior distribution of the RF parameters. The posterior predictive RF is a non-homogeneous RF with Student's t-marginal distribution. Importantly, given a prior distribution for the RF parameters and a chosen autocorrelation function, all steps of the Bayesian analysis can be performed in closed form, providing marginal and multivariate solutions for the posterior predictive RF model. This property should simplify application in practice, especially in engineering domains where accounting for spatial variability is currently not common practice. Moreover, we discuss how existing approaches for simulation of Gaussian RFs can be applied to generate realizations of the derived RF model. The application to situations with non-Gaussian translation prior RFs is investigated and for the specific case of lognormal prior distribution, the equations for the required transformation are given. Furthermore, we discuss the influence of the prior correlation function and a posterior point estimate of its parameters. Finally, we show that the presented updating approach is a generalization of the Bayesian approach for evaluation of characteristic values of EN 1990.

The structure of the paper is as follows. Section 5.2 presents the structure of the hierarchical RF, followed by a short review of Bayesian analysis and a step-by-step presentation of the proposed Bayesian updating procedure. Section 5.3 applies the method to two examples from different engineering fields (geotechnical engineering and structural engineering). A summary and main conclusions are given in Section 5.4. The analytical expressions for updating the RF are derived in Appendices 5.A to 5.C and Appendix 5.D describes properties of the log-Student's t-distribution.

5.2 Methodology

In a Gaussian RF $X(\boldsymbol{z})$, the joint distribution of $\{X(\boldsymbol{z}_i), i = 1, \dots, n\}$ for any $\boldsymbol{z}_i \in \Omega \subset \mathbb{R}^d$ and $n \in \mathbb{N}$ is jointly Gaussian, with Ω denoting the domain of definition of the RF and d the spatial dimension of Ω [1]. This RF is fully described by the spatial functions for the mean value, the variance and the autocorrelation. Closed-form solutions are available for the posterior distribution of the RF given data $\mathbf{M}$ of X [21, 6]. We consider a prior RF for $X(\boldsymbol{z})$ with homogeneous point statistics, i.e., a-priori the RF has constant mean and variance. The vector of uncertain hyperparameters is $\boldsymbol{\theta} = [\mu_X, \lambda_X]^\mathsf{T}$, where μ_X is the mean value and λ_X is the precision (inverse of the variance). The assumption of prior homogeneity is a simplification and limits the application to cases without a spatial trend of the RF or cases where a homogeneous RF $X(\boldsymbol{z})$ can be obtained from the actual RF by a normalization operation [e.g., 51] or by de-trending methods [e.g., 52, 40].

Figure 5.1 summarizes the investigated problem setting, where the nodes represent uncertain quantities (the random variables and the RF) and the arrows denote the direct dependencies among them [e.g., 27]. $\boldsymbol{\tau}$ is the vector of correlation parameters, i.e., the parameters of the autocorrelation function of the RF. These are initially considered as deterministic; the estimation of $\boldsymbol{\tau}$ from the data $\mathbf{M}$ is discussed in Section 5.2.7. It is worth noting that the method can handle arbitrary autocorrelation functions, i.e., we do not require the autocorrelation function to depend on the difference in location, although in most applications this is a standard choice. The aim of the analysis is to learn $X(\boldsymbol{z})$ conditional on $\mathbf{M}$. The individual steps of the analysis are derived in the following, preceded by a short introduction to the basics of Bayesian analysis.

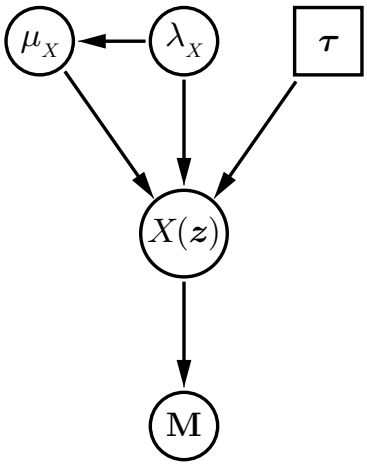

Figure 5.1: The hierarchical RF model to learn $X(\boldsymbol{z})$ from $\mathbf{M}$. μ_X and λ_X are the mean and precision of the RF $X(\boldsymbol{z})$ and $\mathbf{M}$ is the measurement data. $\boldsymbol{\tau}$ is the vector of parameters of the autocorrelation function.

5.2.1 Bayesian analysis

When performing a Bayesian analysis, the first step is setting up a prior joint probability density function (PDF) of the parameters $\boldsymbol{\theta}$. The prior PDF $f(\boldsymbol{\theta})$ is then updated to the posterior PDF $f(\boldsymbol{\theta}|\mathbf{M})$ with data $\mathbf{M}$, by application of Bayes' rule [21]:

$$f(\boldsymbol{\theta}|\mathbf{M}) \propto f(\boldsymbol{\theta}) \cdot \mathrm{L}(\boldsymbol{\theta}|\mathbf{M}), \tag{5.1}$$

where $\mathrm{L}(\boldsymbol{\theta}|\mathbf{M})$ is the likelihood function, summarizing the information from the data $\mathbf{M}$. Note that a single data point $\mathbf{M}_i$ may contain various types of information, including the measurement outcome, the measurement location or time, the used measurement device and the environmental conditions at the time of the measurement. In this paper, we focus on the case where $\mathbf{M}$ contains spatially distributed measurements of an RF $X(\boldsymbol{z})$. Hence, each $\mathbf{M}_i$ includes the measurement outcome $x_{m,i}$ and the corresponding measurement location $\boldsymbol{z}_{m,i}$, i.e., $\mathbf{M}_i = [x_{m,i}, \boldsymbol{z}_{m,i}]$. Given a set of n direct measurements of the RF $X(\boldsymbol{z})$, $\mathbf{M} = [\mathbf{M}_1,\ \mathbf{M}_2, \ldots,\ \mathbf{M}_n]^\mathsf{T}$, with measurement outcomes $\boldsymbol{x}_m = [x_{m,1},\ x_{m,2}, \ldots,\ x_{m,n}]^\mathsf{T} \subseteq \mathbb{R}^n$ and corresponding measurement locations $\mathbf{Z}_m = [\boldsymbol{z}_{m,1},\ \boldsymbol{z}_{m,2}, \ldots,\ \boldsymbol{z}_{m,n}]^\mathsf{T} \subseteq \mathbb{R}^{n \times d}$, the joint likelihood is the PDF of $X(\boldsymbol{z})$ at locations $\mathbf{Z}_m$ conditional on $\boldsymbol{\theta}$:

$$\mathrm{L}(\boldsymbol{\theta}|\mathbf{M}) = f(\boldsymbol{x}_m; \mathbf{Z}_m|\boldsymbol{\theta}). \tag{5.2}$$

5.2.2 Prior model

We consider a Gaussian RF $X(\boldsymbol{z})$ whose parameter vector $\boldsymbol{\theta}$ has a normal-gamma ($\mathcal{NG}$) prior, with PDF [e.g., 42, 41, 7]

$$\begin{aligned} f(\boldsymbol{\theta}) &= \mathcal{NG}(\mu_X, \lambda_X|\mu_0, \kappa_0, \alpha_0, \beta_0) = \mathcal{N}(\mu_X|\mu_0, \kappa_0\lambda_X) \cdot \mathcal{G}(\lambda_X|\alpha_0, \beta_0) \\ &= \mathcal{C}_0 \lambda_X^{\alpha_0 - \frac{1}{2}} \exp\left(-\lambda_X \left(\frac{\kappa_0}{2}(\mu_X - \mu_0)^2 + \beta_0\right)\right). \end{aligned} \tag{5.3}$$

$\Gamma(\cdot)$ is the gamma function and $\mathcal{C}_0$ is a normalizing constant, given by

$$\mathcal{C}_0 = \frac{\beta_0^{\alpha_0} \kappa_0^{\frac{1}{2}}}{\Gamma(\alpha_0)(2\pi)^{\frac{1}{2}}}. \tag{5.4}$$

The spatial variability of the prior RF is determined by its autocorrelation function $\rho(\boldsymbol{z}_1, \boldsymbol{z}_2)$ [1, 51]. A classical choice for the autocorrelation function is the Matérn model, which includes the exponential model and the square-exponential model [33, 1, 43].

5.2.3 Likelihood function

The likelihood function for learning the RF $X(\boldsymbol{z})$ with spatially distributed measurements $\mathbf{M}$ is given by Equation (5.2). For the Gaussian RF this translates to:

$$\mathrm{L}(\boldsymbol{\theta}|\mathbf{M}) = \frac{\lambda_X^{\frac{n}{2}}}{(2\pi)^{\frac{n}{2}} \left(\det(\mathbf{R}_m)\right)^{\frac{1}{2}}} \exp\left(-\frac{\lambda_X}{2} (\boldsymbol{x}_m - \mu_X \mathbf{1}_n) \mathbf{R}_m^{-1} (\boldsymbol{x}_m - \mu_X \mathbf{1}_n)^{\mathsf{T}}\right), \tag{5.5}$$

where $\mathbf{R}_m$ is the correlation matrix of the measurement locations with entry $R_{m,i,j}$ calculated as $\rho(\boldsymbol{z}_{m,i}, \boldsymbol{z}_{m,j})$. $\mathbf{1}_n$ denotes a $1 \times n$-vector of ones.

Uncertainty in the measurement procedure can be accounted for by including a measurement error ε_i. Assuming an additive measurement error yields the following relation between the actual value x at location $\boldsymbol{z}_{m,i}$ and the measured value $x_{m,i}$:

$$x_{m,i} = x(\boldsymbol{z}_{m,i}) + \varepsilon_i. \tag{5.6}$$

The error ε_i is often modeled by a zero-mean Gaussian random variable with standard deviation σ_ε and statistical independence between the measurement errors at different locations is assumed. In such case, the methodology presented in the following sections is applicable with a minor modification: λ_X does not describe the precision of $X(\boldsymbol{z})$ but the overall precision of $X(\boldsymbol{z}) + \varepsilon$, i.e.,

$$\lambda_X = \left(\lambda_{X,\mathrm{RF}}^{-1} + \sigma_\varepsilon^2\right)^{-1}, \tag{5.7}$$

where $\lambda_{X,\mathrm{RF}}$ is the precision of $X(\boldsymbol{z})$. Moreover, the autocorrelation function describing the overall variability reads

$$\rho(\boldsymbol{z}_i, \boldsymbol{z}_j) = \rho_{\mathrm{RF}}(\boldsymbol{z}_i, \boldsymbol{z}_j) \cdot (1 - \gamma_\varepsilon) + \delta(i,j) \cdot \gamma_\varepsilon, \tag{5.8}$$

where $\rho_{\mathrm{RF}}(\boldsymbol{z}_i, \boldsymbol{z}_j)$ denotes the spatial correlation function of $X(\boldsymbol{z})$ and $\gamma_\varepsilon = \sigma_\varepsilon^2 \lambda_X \in (0,\ 1)$ is the portion of the overall variance attributed to the measurement error. $\delta(i,j)$ is the Dirac delta function returning 1 if $i = j$ and 0 otherwise.

5.2.4 Posterior distribution of the parameters

In the general case, Equation (5.1) needs to be solved numerically, e.g. through sampling techniques, due to the intractability of the normalizing constant. However, analytical solutions for the posterior distribution are available in some special cases, when using conjugate priors [21, 42]. The chosen $\mathcal{NG}$ prior distribution and the multivariate Gaussian likelihood of Equation (5.5) are conjugate. Hence, the posterior distribution of $\boldsymbol{\theta}$ can be derived analytically and has the same parametric form as the prior, i.e., it is a $\mathcal{NG}$ distribution. The Bayesian updating simplifies to an update of the parameters of the $\mathcal{NG}$ distribution [17, 7]:

$$f(\boldsymbol{\theta}|\mathbf{M}) = \mathcal{NG}(\mu_X, \lambda_X|\mu_n, \kappa_n, \alpha_n, \beta_n) = \mathcal{C}_n \lambda_X^{\alpha_n - \frac{1}{2}} \exp\left(-\lambda_X \left(\frac{\kappa_n}{2} (\mu_X - \mu_n)^2 + \beta_n\right)\right), \tag{5.9}$$

where the normalizing constant $\mathcal{C}_n$ is given by

$$\mathcal{C}_n = \frac{\beta_n^{\alpha_n} \kappa_n^{\frac{1}{2}}}{\Gamma(\alpha_n)(2\pi)^{\frac{1}{2}}}. \tag{5.10}$$

The parameters of the posterior distribution can be obtained with the following set of equations:

$$\mu_n = \frac{\kappa_0 \mu_0 + \mathbf{1}_n \mathbf{R}_m^{-1} \boldsymbol{x}_m^\mathsf{T}}{\kappa_0 + \mathbf{1}_n \mathbf{R}_m^{-1} \mathbf{1}_n^\mathsf{T}}, \tag{5.11}$$

$$\kappa_n = \kappa_0 + \mathbf{1}_n \mathbf{R}_m^{-1} \mathbf{1}_n^\mathsf{T}, \tag{5.12}$$

$$\alpha_n = \alpha_0 + \frac{n}{2}, \tag{5.13}$$

$$\beta_n = \beta_0 + \frac{1}{2}\left(\boldsymbol{x}_m \mathbf{R}_m^{-1} \boldsymbol{x}_m^\mathsf{T} + \frac{\kappa_0 \mu_0^2 \mathbf{1}_n \mathbf{R}_m^{-1} \mathbf{1}_n^\mathsf{T} - 2\kappa_0 \mu_0 \mathbf{1}_n \mathbf{R}_m^{-1} \boldsymbol{x}_m^\mathsf{T} - \left(\mathbf{1}_n \mathbf{R}_m^{-1} \boldsymbol{x}_m^\mathsf{T}\right)^2}{\kappa_0 + \mathbf{1}_n \mathbf{R}_m^{-1} \mathbf{1}_n^\mathsf{T}} \right). \tag{5.14}$$

A derivation of the parameters in Equations (5.11) to (5.14) can be found in [21] in the context of Bayesian linear regression. For easier accessibility, we provide the derivations in Appendix 5.A.

5.2.5 Marginal posterior predictive distribution

Typically, the goal is to make predictions about the quantity of interest X. To this end, one needs the posterior predictive distribution of X, which is obtained by marginalization of the joint PDF of X conditional on $\boldsymbol{\theta}$ and the posterior distribution of $\boldsymbol{\theta}$ given $\mathbf{M}$. When X is modeled by a single random variable and the measurement points are uncorrelated, the posterior predictive distribution is given as [41, 19, 21]

$$f(x|\boldsymbol{x}_m) = \int_{\boldsymbol{\Theta}} f(x|\boldsymbol{\theta})\, f(\boldsymbol{\theta}|\boldsymbol{x}_m)\, \mathrm{d}\boldsymbol{\theta}, \tag{5.15}$$

where $\boldsymbol{\Theta}$ denotes the domain of definition of $\boldsymbol{\theta}$. The conditional independence between X given $\boldsymbol{\theta}$ and $\mathbf{M}$ does no longer hold when X is modeled as an RF. Instead, the posterior and the posterior predictive distribution of X will depend on the spatial location $\boldsymbol{z}$. In RF theory, the PDF of the RF $X(\boldsymbol{z})$ at location $\boldsymbol{z}$ is termed marginal (or first order) PDF of $X(\boldsymbol{z})$. The marginal posterior predictive PDF of $X(\boldsymbol{z})$, denoted $f(x;\boldsymbol{z}|\mathbf{M})$, is given as

$$f(x;\boldsymbol{z}|\mathbf{M}) = \int_{\boldsymbol{\Theta}} f(x;\boldsymbol{z}|\boldsymbol{\theta},\mathbf{M})\, f(\boldsymbol{\theta}|\mathbf{M})\, \mathrm{d}\boldsymbol{\theta}. \tag{5.16}$$

Here, $f(x;\boldsymbol{z}|\boldsymbol{\theta},\mathbf{M})$ is the marginal PDF of $X(\boldsymbol{z})$ given $\boldsymbol{\theta}$ and $\mathbf{M}$, which requires an additional updating step. In this step, the prior is the marginal PDF of $X(\boldsymbol{z})$ given $\boldsymbol{\theta}$, $f(x;\boldsymbol{z}|\boldsymbol{\theta})$, which is a Gaussian PDF with parameters μ_X and λ_X. The posterior PDF $f(x;\boldsymbol{z}|\boldsymbol{\theta},\mathbf{M})$ is again a Gaussian PDF with parameters $\mu_{\boldsymbol{z}}''$ and $\lambda_{\boldsymbol{z}}''$, which can be calculated by application of the following updating rules for the conditional Gaussian distribution [47, 6, 51]:

$$\mu_{\boldsymbol{z}}'' = \mu_X + \boldsymbol{R}_{\boldsymbol{z},m} \mathbf{R}_m^{-1} \left(\boldsymbol{x}_m - \mu_X \mathbf{1}_n\right)^\mathsf{T}, \tag{5.17}$$

$$\lambda_{\boldsymbol{z}}'' = \lambda_X \left(1 - \boldsymbol{R}_{\boldsymbol{z},m} \mathbf{R}_m^{-1} \boldsymbol{R}_{\boldsymbol{z},m}^\mathsf{T}\right)^{-1}, \tag{5.18}$$

where $\boldsymbol{R}_{\boldsymbol{z},m} : \mathbb{R}^d \to \mathbb{R}^{1\times n}$ is a row vector function with element i defined as $\rho(\boldsymbol{z}, \boldsymbol{z}_{m,i})$ with n being the number of measurements and $\mathbf{R}_m$ is given by Equation (5.8). The integral in Equation (5.16) can be written as follows:

$$f(x;\boldsymbol{z}|\mathbf{M}) = \int_{\lambda_X=0}^{+\infty}\int_{\mu_X=-\infty}^{+\infty} \mathcal{N}(x|\mu_{\boldsymbol{z}}'', \lambda_{\boldsymbol{z}}'')\,\mathcal{N}(\mu_X|\mu_n, \kappa_n\lambda_X)\,\mathcal{G}(\lambda_X|\alpha_n, \beta_n)\,\mathrm{d}\mu_X\mathrm{d}\lambda_X. \tag{5.19}$$

Solution of the integral in Equation (5.19) results in the following marginal posterior predictive PDF:

$$f(x;\boldsymbol{z}|\mathbf{M}) = f_t(x|\mu_{\boldsymbol{z},t}, \lambda_{\boldsymbol{z},t}, \nu_t) = \frac{\Gamma\left(\frac{\nu_t}{2}+\frac{1}{2}\right)}{\Gamma\left(\frac{\nu_t}{2}\right)}\left(\frac{\lambda_{\boldsymbol{z},t}}{\pi\nu_t}\right)^{\frac{1}{2}}\left(1+\frac{\lambda_{\boldsymbol{z},t}\,(x-\mu_{\boldsymbol{z},t})^2}{\nu_t}\right)^{-\frac{\nu_t}{2}-\frac{1}{2}}, \tag{5.20}$$

where $f_t(x|\mu_t, \lambda_t, \nu_t)$ denotes the PDF of the Student's t-distribution with location parameter μ_t, scale parameter λ_t and degrees of freedom ν_t [6].

The spatial functions for the parameters of the posterior predictive Student's t-distribution are given in closed form by the following expressions:

$$\mu_{\boldsymbol{z},t} = \mu_n + \boldsymbol{R}_{\boldsymbol{z},m}\mathbf{R}_m^{-1}(\boldsymbol{x}_m - \mu_n\mathbf{1}_n)^{\mathsf{T}}, \tag{5.21}$$

$$\lambda_{\boldsymbol{z},t} = \frac{\alpha_n}{\beta_n\left(1-\boldsymbol{R}_{\boldsymbol{z},m}\mathbf{R}_m^{-1}\boldsymbol{R}_{\boldsymbol{z},m}^{\mathsf{T}} + \left(1-\boldsymbol{R}_{\boldsymbol{z},m}\mathbf{R}_m^{-1}\mathbf{1}_n^{\mathsf{T}}\right)^2\kappa_n^{-1}\right)}, \tag{5.22}$$

$$\nu_t = 2\alpha_n. \tag{5.23}$$

The parameters μ_n, κ_n, α_n and β_n are obtained following the updating rules in Equations (5.11) to (5.14). A detailed derivation of the parameter update can be found in Appendix 5.B.

5.2.6 Posterior predictive random field

The approach presented in Section 5.2.5 enables predicting the marginal distribution of quantity X at any location $\boldsymbol{z} \in \Omega$ given spatial data $\mathbf{M}$. This is useful in cases where the correlation among values of X at different locations needs not be accounted for in further predictions [41]. However, in many cases the spatial dependence of X is required for predictions. In such cases, the joint distribution of X at k different locations is given by the k-th order posterior predictive PDF of $X(\boldsymbol{z})$:

$$f(\boldsymbol{x};\mathbf{Z}|\mathbf{M}) = \int_{\boldsymbol{\Theta}} f(\boldsymbol{x};\mathbf{Z}|\boldsymbol{\theta},\mathbf{M})\,f(\boldsymbol{\theta}|\mathbf{M})\,\mathrm{d}\boldsymbol{\theta}. \tag{5.24}$$

The posterior distribution for the parameter vector $\boldsymbol{\theta}$ is the same as the one appearing in Equation (5.16). The prior distribution of the RF $X(\boldsymbol{z})$ given $\boldsymbol{\theta}$ is Gaussian and, hence, $f(\boldsymbol{x};\mathbf{Z}|\boldsymbol{\theta})$ is k-variate Gaussian. Since the updating rules for a conditional Gaussian distribution of Equations (5.17) and (5.18) can be extended to the multivariate case, $f(\boldsymbol{x};\mathbf{Z}|\boldsymbol{\theta},\mathbf{M})$ is also k-variate Gaussian with mean vector $\boldsymbol{\mu}_{\mathbf{Z}}''$ and precision matrix $\boldsymbol{\Lambda}_{\mathbf{Z}}''$, which can be calculated by the following equations [6]:

$$\boldsymbol{\mu}_{\mathbf{Z}}'' = \mu_X\mathbf{1}_k^{\mathsf{T}} + \mathbf{R}_{\mathbf{Z},m}\mathbf{R}_m^{-1}(\boldsymbol{x}_m - \mu_X\mathbf{1}_n)^{\mathsf{T}}, \tag{5.25}$$

$$\boldsymbol{\Lambda}_{\mathbf{Z}}'' = \lambda_X\left(\mathbf{R}_{\mathbf{Z}} - \mathbf{R}_{\mathbf{Z},m}\mathbf{R}_m^{-1}\mathbf{R}_{\mathbf{Z},m}^{\mathsf{T}}\right)^{-1}, \tag{5.26}$$

where $\mathbf{R}_{\mathbf{Z},m} : \mathbb{R}^{k\times d} \to \mathbb{R}^{k\times n}$ is a matrix function with element i,j defined as $\rho\left(\boldsymbol{z}_i, \boldsymbol{z}_{m,j}\right)$. $\mathbf{R}_{\mathbf{Z}} : \mathbb{R}^{k\times d} \to \mathbb{R}^{k\times k}$ is a matrix function with element i,j defined as $\rho\left(\boldsymbol{z}_i, \boldsymbol{z}_j\right)$. $\mathbf{R}_m$ is the matrix containing the correlation of the measurement locations and a potential measurement error, as introduced in Section 5.2.3. $\mathbf{1}_k$ is a $1 \times k$ vector of ones.

Equation (5.24) takes the following form:

$$f\left(\boldsymbol{x}; \mathbf{Z}|\mathbf{M}\right) = \int_{\lambda_X=0}^{+\infty} \int_{\mu_X=-\infty}^{+\infty} \mathcal{N}\left(\boldsymbol{x}_z|\boldsymbol{\mu}_{\mathbf{Z}}'', \boldsymbol{\Lambda}_{\mathbf{Z}}''\right) \mathcal{N}\left(\mu_X|\mu_n, \kappa_n\lambda_X\right) \mathcal{G}\left(\lambda_X|\alpha_n, \beta_n\right) \mathrm{d}\mu_X \mathrm{d}\lambda_X. \quad (5.27)$$

The integral in Equation (5.27) results in the following k-th order posterior predictive PDF

$$f\left(\boldsymbol{x}; \mathbf{Z}|\mathbf{M}\right) = f_t\left(\boldsymbol{x}|\boldsymbol{\mu}_{\mathbf{Z},t}, \boldsymbol{\Lambda}_{\mathbf{Z},t}, \nu_t\right) = \frac{\Gamma\left(\frac{\nu_t}{2} + \frac{k}{2}\right)}{\Gamma\left(\frac{\nu_t}{2}\right)} \frac{\left(\det\left(\boldsymbol{\Lambda}_{\mathbf{Z},t}\right)\right)^{\frac{1}{2}}}{\left(\pi\nu_t\right)^{\frac{k}{2}}} \left(1 + \frac{\left(\boldsymbol{x} - \boldsymbol{\mu}_{\mathbf{Z},t}\right) \boldsymbol{\Lambda}_{\mathbf{Z},t} \left(\boldsymbol{x} - \boldsymbol{\mu}_{\mathbf{Z},t}\right)^{\mathsf{T}}}{\nu_t}\right)^{-\frac{\nu_t}{2} - \frac{k}{2}}. \quad (5.28)$$

where $f_t\left(\boldsymbol{x}|\boldsymbol{\mu}_{\mathbf{Z},t}, \boldsymbol{\Lambda}_{\mathbf{Z},t}, \nu_t\right)$ is the k-variate Student's t-distribution [29, 6]. As in the univariate case, ν_t is a scalar parameter denoting the degrees of freedom. ν_t is given by Equation (5.23) and the parameters $\boldsymbol{\mu}_{\mathbf{Z},t}$ and $\boldsymbol{\Lambda}_{\mathbf{Z},t}$ are given in closed form:

$$\boldsymbol{\mu}_{\mathbf{Z},t} = \mu_n \mathbf{1}_k^{\mathsf{T}} + \mathbf{R}_{\mathbf{Z},m} \mathbf{R}_m^{-1} \left(\boldsymbol{x}_m - \mu_n \mathbf{1}_n\right)^{\mathsf{T}}, \quad (5.29)$$

$$\boldsymbol{\Lambda}_{\mathbf{Z},t} = \frac{\alpha_n}{\beta_n} \left(\mathbf{R}_{\mathbf{Z}} - \mathbf{R}_{\mathbf{Z},m} \mathbf{R}_m^{-1} \mathbf{R}_{\mathbf{Z},m}^{\mathsf{T}} + \left(\mathbf{1}_k^{\mathsf{T}} - \mathbf{R}_{\mathbf{Z},m} \mathbf{R}_m^{-1} \mathbf{1}_n^{\mathsf{T}}\right) \kappa_n^{-1} \left(\mathbf{1}_k^{\mathsf{T}} - \mathbf{R}_{\mathbf{Z},m} \mathbf{R}_m^{-1} \mathbf{1}_n^{\mathsf{T}}\right)^{\mathsf{T}}\right)^{-1}, \quad (5.30)$$

$\mathbf{R}_{\mathbf{Z}}$, $\mathbf{R}_{\mathbf{Z},m}$ and $\mathbf{R}_m$ follow the definitions for Equations (5.25) and (5.26) and the parameters μ_n, κ_n, α_n and β_n are obtained following the updating rules in Equations (5.11) to (5.14). The analytical expressions for the parameters of the multivariate posterior predictive Student's t-distribution are derived in detail in Appendix 5.C.

The multivariate Student's t-distribution as predictive distribution for the multivariate Gaussian distribution also appears in Bayesian regression for the normal linear model [7, 21, 2]. In fact, the presented model forms a special case of weighted linear Bayesian regression with a single explanatory variable.

Equation (5.28) can be used for multivariate predictions of X accounting for the information in $\mathbf{M}$. It is noted that for $k = 1$, Equation (5.28) reduces to the expression for the marginal posterior predictive Student's t-distribution given in Equation (5.20), accordingly Equations (5.29) and (5.30) reduce to Equations (5.21) and (5.22). Equations (5.29) and (5.30) can be directly transformed to the spatial parameter functions of the posterior predictive RF, i.e., the mean function $\mu_t(\boldsymbol{z})$ and the precision function $\lambda_t\left(\boldsymbol{z}_1, \boldsymbol{z}_2\right)$:

$$\mu_t(\boldsymbol{z}) = \mu_n + \boldsymbol{R}_{\boldsymbol{z},m} \mathbf{R}_m^{-1} \left(\boldsymbol{x}_m - \mu_n \mathbf{1}_n\right)^{\mathsf{T}}, \quad (5.31)$$

$$\lambda_t\left(\boldsymbol{z}_1, \boldsymbol{z}_2\right) = \frac{\alpha_n}{\beta_n} \left(\rho\left(\boldsymbol{z}_1, \boldsymbol{z}_2\right) - \boldsymbol{R}_{\boldsymbol{z}_1,m} \mathbf{R}_m^{-1} \boldsymbol{R}_{\boldsymbol{z}_2,m}^{\mathsf{T}} + \left(1 - \boldsymbol{R}_{\boldsymbol{z}_1,m} \mathbf{R}_m^{-1} \mathbf{1}_n^{\mathsf{T}}\right) \kappa_n^{-1} \left(1 - \boldsymbol{R}_{\boldsymbol{z}_2,m} \mathbf{R}_m^{-1} \mathbf{1}_n^{\mathsf{T}}\right)\right)^{-1}, \quad (5.32)$$

where $\rho\left(\boldsymbol{z}_1, \boldsymbol{z}_2\right)$ is the prior correlation of $\boldsymbol{z}_1$ and $\boldsymbol{z}_2$. $\boldsymbol{R}_{\boldsymbol{z},m}$ and $\mathbf{R}_m$ are utilized as in Equations (5.17) and (5.18). The posterior predictive RF is fully defined by the parameters specified by Equations (5.23), (5.31) and (5.32).

5.2.7 Choice of correlation parameters

The choice of the prior autocorrelation function $\rho(\boldsymbol{z}_1, \boldsymbol{z}_2)$ has significant influence on the predictive distribution of the proposed RF model; it controls the spatial variability of the prior RF and the correlation of the measurement locations in $\mathbf{R}_m$. Hence, the autocorrelation function and its parameters need to be chosen carefully. Although literature is available on different parametric correlation models, their advantages and disadvantages [e.g., 1, 33, 23], the specific parameter choice for a problem at hand remains challenging if little information about the modeled quantity is available. This problem can be addressed by treating the vector $\boldsymbol{\tau}$ of correlation parameters as a random vector with associated prior distribution $f(\boldsymbol{\tau})$. The dependency between $\boldsymbol{\tau}$ and the multivariate posterior predictive distribution can be expressed explicitly by extending Equation (5.24) as follows:

$$f(\boldsymbol{x}; \mathbf{Z}|\mathbf{M}, \boldsymbol{\tau}) = \int_{\boldsymbol{\Theta}} f(\boldsymbol{x}; \mathbf{Z}|\boldsymbol{\theta}, \mathbf{M}, \boldsymbol{\tau})\, f(\boldsymbol{\theta}|\mathbf{M}, \boldsymbol{\tau})\, \mathrm{d}\boldsymbol{\theta}. \tag{5.33}$$

$f(\boldsymbol{x}; \mathbf{Z}|\mathbf{M})$ can then be determined by marginalization of $f(\boldsymbol{x}; \mathbf{Z}, \boldsymbol{\tau}|\mathbf{M})$:

$$f(\boldsymbol{x}; \mathbf{Z}|\mathbf{M}) = \int_{\mathbf{T}} f(\boldsymbol{x}; \mathbf{Z}, \boldsymbol{\tau}|\mathbf{M})\, \mathrm{d}\boldsymbol{\tau} = \int_{\mathbf{T}} f(\boldsymbol{x}; \mathbf{Z}|\mathbf{M}, \boldsymbol{\tau})\, f(\boldsymbol{\tau}|\mathbf{M})\, \mathrm{d}\boldsymbol{\tau}, \tag{5.34}$$

with $\mathbf{T}$ denoting the domain of definition of $\boldsymbol{\tau}$. Figure 5.2 illustrates the adapted hierarchical Bayesian model where $\boldsymbol{\tau}$ is considered as additional uncertain parameter, in contrast to the deterministic choice illustrated in Figure 5.1. The closed-form updating procedure for the posterior predictive expressions can only be used to find $f(\boldsymbol{x}; \mathbf{Z}|\mathbf{M}, \boldsymbol{\tau})$. Direct evaluation of Equation (5.34) can be cumbersome or even impossible, as it requires evaluation of $f(\boldsymbol{\tau}|\mathbf{M})$, which depends on the choice of the correlation model and most likely cannot be evaluated in closed form.

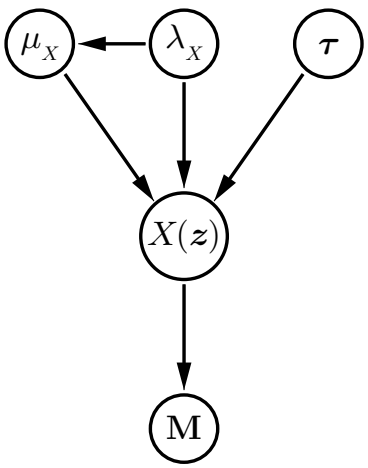

Figure 5.2: Adapted hierarchical Bayesian model to consider $\boldsymbol{\tau}$ as uncertain parameter. The dependence of the resulting RF model on $\boldsymbol{\tau}$ can be integrated out when $\boldsymbol{\tau}$ is modeled as random vector.

Through application of Bayes' theorem, $f(\boldsymbol{\tau}|\mathbf{M})$ is given by the following expression:

$$f(\boldsymbol{\tau}|\mathbf{M}) \propto f(\boldsymbol{\tau}) \cdot f(\mathbf{M}|\boldsymbol{\tau})\,. \tag{5.35}$$

Including the dependency on $\boldsymbol{\tau}$ in the definition of the likelihood function of Equation (5.2) gives

$$\mathrm{L}\left(\boldsymbol{\theta}|\mathbf{M},\boldsymbol{\tau}\right) = \frac{\lambda_X^{\frac{n}{2}}}{(2\pi)^{\frac{n}{2}}\det\left(\mathbf{R}_m\left(\boldsymbol{\tau}\right)\right)}\exp\left(-\frac{\lambda_X}{2}\left(\boldsymbol{x}_m-\mu_X\mathbf{1}_n\right)\left(\mathbf{R}_m\left(\boldsymbol{\tau}\right)\right)^{-1}\left(\boldsymbol{x}_m-\mu_X\mathbf{1}_n\right)^{\mathsf{T}}\right). \tag{5.36}$$

$f\left(\mathbf{M}|\boldsymbol{\tau}\right)$ is the proportionality constant in $f\left(\boldsymbol{\theta}|\mathbf{M},\boldsymbol{\tau}\right) \propto f\left(\boldsymbol{\theta}\right)\cdot \mathrm{L}\left(\boldsymbol{\theta}|\mathbf{M},\boldsymbol{\tau}\right)$, hence

$$f\left(\mathbf{M}|\boldsymbol{\tau}\right) = \frac{f\left(\boldsymbol{\theta}\right)\cdot \mathrm{L}\left(\boldsymbol{\theta}|\mathbf{M},\boldsymbol{\tau}\right)}{f\left(\boldsymbol{\theta}|\mathbf{M},\boldsymbol{\tau}\right)}. \tag{5.37}$$

Note that $\boldsymbol{\theta}$ and $\boldsymbol{\tau}$ are independent and thus, $f\left(\boldsymbol{\theta}|\boldsymbol{\tau}\right) = f\left(\boldsymbol{\theta}\right)$. $f\left(\boldsymbol{\theta}|\mathbf{M},\boldsymbol{\tau}\right)$ is the posterior PDF of $\boldsymbol{\theta}$ for a given $\boldsymbol{\tau}$, which is a $\mathcal{NG}$ PDF with parameters given in Section 5.2.4. Splitting the densities and their respective normalizing constants in Equation (5.37) gives

$$f\left(\mathbf{M}|\boldsymbol{\tau}\right) = \frac{\mathcal{C}_0}{\mathcal{C}_n\left(\boldsymbol{\tau}\right)}\cdot(2\pi)^{-\frac{n}{2}}\det\left(\mathbf{R}_m\left(\boldsymbol{\tau}\right)\right)^{-\frac{1}{2}}\frac{\hat{f}\left(\boldsymbol{\theta}\right)\cdot\hat{\mathrm{L}}\left(\boldsymbol{\theta}|\mathbf{M},\boldsymbol{\tau}\right)}{\hat{f}\left(\boldsymbol{\theta}|\mathbf{M},\boldsymbol{\tau}\right)}, \tag{5.38}$$

where $\mathcal{C}_0$ and $\mathcal{C}_n$ are defined in Equations (5.4) and (5.10). $\hat{f}\left(\boldsymbol{\theta}\right)$ and $\hat{f}\left(\boldsymbol{\theta}|\mathbf{M},\boldsymbol{\tau}\right)$ are the unnormalized prior and posterior $\mathcal{NG}$ distributions. $\hat{\mathrm{L}}\left(\boldsymbol{\theta}|\mathbf{M},\boldsymbol{\tau}\right)$ is the exponential term of the likelihood function and is equal to the ratio of $\hat{f}\left(\boldsymbol{\theta}|\mathbf{M},\boldsymbol{\tau}\right)$ and $\hat{f}\left(\boldsymbol{\theta}\right)$ (cf. Appendix 5.A). Thus, the fraction disappears in Equation (5.38). Inserting the expressions for $\mathcal{C}_0$ and $\mathcal{C}_n$ into Equation (5.38) yields

$$f\left(\mathbf{M}|\boldsymbol{\tau}\right) = \left(\frac{\kappa_0}{\kappa_n\left(\boldsymbol{\tau}\right)}\right)^{\frac{1}{2}}\frac{\Gamma\left(\alpha_n\right)\beta_0^{\alpha_0}}{\Gamma\left(\alpha_0\right)\left(\beta_n\left(\boldsymbol{\tau}\right)\right)^{\alpha_n}}(2\pi)^{-\frac{n}{2}}\det\left(\mathbf{R}_m\left(\boldsymbol{\tau}\right)\right)^{-\frac{1}{2}}. \tag{5.39}$$

Using Equation (5.39), sampling from $f\left(\boldsymbol{\tau}|\mathbf{M}\right)$ can be achieved, e.g. by using Markov chain Monte Carlo methods [8]. These samples $\boldsymbol{\tau}_i,\ i=1,\ldots,N_{MCMC}$ can then be used to approximate $f\left(\boldsymbol{x};\mathbf{Z}|\mathbf{M}\right)$:

$$f\left(\boldsymbol{x};\mathbf{Z}|\mathbf{M}\right) \approx \frac{1}{N_{MCMC}}\sum_{i=1}^{N_{MCMC}} f\left(\boldsymbol{x};\mathbf{Z}|\mathbf{M},\boldsymbol{\tau}_i\right). \tag{5.40}$$

Alternatively, the posterior distribution of $\boldsymbol{\tau}$ can be approximated by its maximum a-posteriori (MAP) estimate [36]. That is, Equation (5.34) is approximated by

$$f\left(\boldsymbol{x};\mathbf{Z}|\mathbf{M}\right) \approx f\left(\boldsymbol{x};\mathbf{Z}|\mathbf{M},\boldsymbol{\tau}^*\right), \tag{5.41}$$

where $\boldsymbol{\tau}^*$ is the MAP estimate of $\boldsymbol{\tau}$. It is found by maximizing Equation (5.35) with respect to $\boldsymbol{\tau}$. Using Equation (5.39), this is equivalent to solving the following optimization problem:

$$\arg\max_{\boldsymbol{\tau}\in\mathbf{T}} f\left(\boldsymbol{\tau}|\mathbf{M}\right) = \arg\min_{\boldsymbol{\tau}\in\mathbf{T}} \ln\left(\kappa_n\left(\boldsymbol{\tau}\right)\right) + 2\alpha_n\ln\left(\beta_n\left(\boldsymbol{\tau}\right)\right) + \ln\left(\det\left(\mathbf{R}_m\left(\boldsymbol{\tau}\right)\right)\right) - 2\ln\left(f(\boldsymbol{\tau})\right), \tag{5.42}$$

where κ_n, α_n and β_n follow the definitions in Section 5.2.4 conditional on $\boldsymbol{\tau}$.

The parametric form of the correlation model can be chosen among a set of models by means of Bayesian model selection. To this end, the marginal likelihood, i.e., the normalizing constant of Eq. (5.35), must be evaluated for the different parametric model choices and multiplied with the prior beliefs in the models [46].

5.2.8 Extension to non-Gaussian prior random fields

The presented Bayesian approach is applicable to Gaussian prior RFs and data assigned with additive Gaussian measurement error. Its applicability can be extended to the class of so-called translation RFs, defined as [24, 30]

$$Y(\boldsymbol{z}) = T(U(\boldsymbol{z})), \tag{5.43}$$

where $U(\boldsymbol{z})$ is a zero-mean and unit-variance Gaussian RF. If the marginal cumulative distribution function (CDF) of the non-Gaussian RF $F_{Y;\boldsymbol{z}}(y(\boldsymbol{z}))$ is given and it is strictly increasing, one can define the transformation of Equation (5.43) as $T(\cdot) = F^{-1}_{Y;\boldsymbol{z}}(\Phi(\cdot))$, with $F^{-1}_{Y;\boldsymbol{z}}(\cdot)$ denoting the inverse of $F_{Y;\boldsymbol{z}}(\cdot)$ and $\Phi(\cdot)$ the standard normal CDF [31]. $U(\boldsymbol{z})$ is obtained from $Y(\boldsymbol{z})$ by inversion of Equation (5.43):

$$U(\boldsymbol{z}) = T^{-1}(Y(\boldsymbol{z})). \tag{5.44}$$

To apply the proposed hierarchical Bayesian approach to the non-Gaussian RF $Y(\boldsymbol{z})$, each measurement outcome $y_{m,i}$ transformed to the Gaussian space through Equation (5.44) should be associated with an additive Gaussian error. This can be equivalently stated as follows:

$$y_{m,i} = T(u(\boldsymbol{z}_{m,i}) + \varepsilon_i), \tag{5.45}$$

where ε_i is a zero-mean Gaussian measurement error. A special case is a lognormal RF $Y(\boldsymbol{z})$ with parameters $\mu_{\ln Y}$ and $\lambda_{\ln Y}$ and a multiplicative lognormal measurement error, i.e., $y_{m,i} = y(\boldsymbol{z}_{m,i}) \cdot \varepsilon_{y,i}$. In such case, Equations (5.43) and (5.45) can be rewritten as functions of a Gaussian RF $X(\boldsymbol{z})$:

$$Y(\boldsymbol{z}) = \exp(X(\boldsymbol{z})), \tag{5.46}$$

$$y_{m,i} = \exp(x(\boldsymbol{z}_{m,i}) + \varepsilon_i) = \exp(x(\boldsymbol{z}_{m,i})) \cdot \exp(\varepsilon_i) = \exp(x(\boldsymbol{z}_{m,i})) \cdot \varepsilon_{y,i}. \tag{5.47}$$

$\mu_{\ln Y}$ and $\lambda_{\ln Y}$ are the mean value and precision respectively of the underlying Gaussian RF $X(\boldsymbol{z})$ including the precision of the measurement error, i.e., $\mu_X = \mu_{\ln Y}$ and $\lambda_X = \lambda_{\ln Y}$. As defined in Section 5.2.3, λ_X is given as the overall precision of $X(\boldsymbol{z}) + \varepsilon$. The error term $\varepsilon_{y,i}$ follows a lognormal distribution with median 1. Its parameters are $\mu_{\ln\varepsilon} = 0$ and $\lambda_{\ln\varepsilon} = \frac{\lambda_X}{\gamma_\varepsilon}$, which are mean value and precision respectively of the underlying Gaussian measurement error. γ_ε has to be chosen accordingly to reflect the contribution of ε to the overall variance of the underlying Gaussian random field. That is, the hierarchical Bayesian approach is directly applicable by a simple logarithmic transformation of the data and the measurement error. After the updating procedure, the posterior predictive RF can be transformed back to the original space by applying Equation (5.46). The transformed marginal distribution of the posterior predictive RF has the form of a log-Student's t-distribution. This distribution model is used in finance for the pricing of options [11, 10] and belongs to the family of log-symmetric distributions [50]. The marginal PDF of the posterior predictive RF is defined as follows:

$$f(y;\boldsymbol{z}|\mathbf{M}) = f_{t,\ln}(y|\mu_{z,t},\lambda_{z,t},\nu_t) = y^{-1}\frac{\Gamma\left(\frac{\nu_t}{2}+\frac{1}{2}\right)}{\Gamma\left(\frac{\nu_t}{2}\right)}\left(\frac{\lambda_{z,t}}{\pi\nu_t}\right)^{\frac{1}{2}}\left(1+\frac{\lambda_{z,t}\left(\ln(y)-\mu_{z,t}\right)^2}{\nu_t}\right)^{-\frac{\nu_t}{2}-\frac{1}{2}} \tag{5.48}$$

The finite-dimensional PDF can be derived in a similar manner. It is noted that the log-Student's t-distribution has divergent integer moments of any order. A short proof of this can

be found in Appendix 5.D. The parametrization of $Y(\boldsymbol{z})$ conditional on $\mathbf{M}$ is done by means of $\mu_{\boldsymbol{z},t}$, $\lambda_{\boldsymbol{z},t}$ and ν_t, i.e., in terms of the parameters of the underlying Student's t-RF $X(\boldsymbol{z})$. For $\nu_t \to \infty$, $f_{t,\ln}(y_{\boldsymbol{z}}|\mathbf{M})$ converges to a lognormal distribution with location parameter $\mu_{\boldsymbol{z},t}$ and scale parameter $\lambda_{\boldsymbol{z},t}^{-\frac{1}{2}}$.

5.2.9 Sampling the posterior predictive random field

The finite-dimensional distribution of the posterior predictive RF is the multivariate Student's t-distribution with parameters $\boldsymbol{\mu}_{\mathbf{Z},t}, \boldsymbol{\Lambda}_{\mathbf{Z},t}$ and ν_t. The posterior predictive random vector $\boldsymbol{X}(\mathbf{Z})$ corresponding to locations $\mathbf{Z}$ can be expressed as follows [29]:

$$\boldsymbol{X}(\mathbf{Z}) = \frac{\boldsymbol{U}(\mathbf{Z})}{\sqrt{\frac{V}{\nu_t}}} + \boldsymbol{\mu}_{\mathbf{Z},t}, \tag{5.49}$$

where $\boldsymbol{U}(\mathbf{Z})$ is a zero-mean Gaussian random vector with precision matrix $\boldsymbol{\Lambda}_{\mathbf{Z},t}$. V is a random variable that follows the chi-square distribution with ν_t degrees of freedom and is independent of $\boldsymbol{U}(\mathbf{Z})$. Replacing $\boldsymbol{U}(\mathbf{Z})$ in Equation (5.49) by $U(\boldsymbol{z})$, a zero-mean Gaussian RF with spatial precision function $\lambda_t(\boldsymbol{z}_1, \boldsymbol{z}_2)$ as given by Equation (5.32), and furthermore replacing $\boldsymbol{\mu}_{\mathbf{Z},t}$ by $\mu_t(\boldsymbol{z})$, the spatial function for the mean value defined in Equation (5.31), yields the corresponding expression for the posterior predictive Student's t-RF. Hence, the Student's t-RF $X(\boldsymbol{z})$ can be expressed as a function of a Gaussian RF and one additional independent chi-square random variable. In case of sampling from a translation RF $Y(\boldsymbol{z})$, the transformation of Equation (5.43) has to be adapted accordingly. Samples from $U(\boldsymbol{z})$ can be generated by a variety of existing methods [e.g., 32].

5.2.10 Connection to the Bayesian approach of EN 1990

Annex D.7 of EN 1990 (Eurocode 0) on the basis of structural design offers a method to determine design values for material properties when samples are available [20]. The samples are used to estimate a quantile value of the underlying probability distribution, the so-called characteristic value. This approach distinguishes between the cases where (a) mean and variance of the material property are unknown and (b) only its variance is unknown. In case (a), the characteristic value can be estimated based on the sample mean, sample standard deviation and the number of samples n. The underlying theory is a Bayesian approach and the calculated value is the 5% quantile value of the posterior predictive distribution [41, 22]. We show in the following that the hierarchical approach presented in this paper is a generalization of case (a) in Annex D.7 of EN 1990.

We consider a material property X that follows a normal distribution with unknown parameters $\boldsymbol{\theta}$ and that a set of samples $\boldsymbol{x}_m = [x_{m,1},\ x_{m,2}, \ldots,\ x_{m,n}]^\mathsf{T}$ are available. If no prior information about $f(\boldsymbol{\theta})$ is available, a non-informative choice can be made by choosing a $\mathcal{NG}$ distribution with the following parameters [17]:

$$[\mu_0, \kappa_0, \alpha_0, \beta_0] = \left[/, 0, -\frac{1}{2}, 0\right], \tag{5.50}$$

resulting in $f(\boldsymbol{\theta}) = \lambda_X^{-1}$.

Furthermore, we assume independence of the random variables corresponding to the measurement locations and neglect the measurement error, i.e., $\mathbf{R}_m = \mathbf{I}$. This leads to a simplification

of Equations (5.11) to (5.14):

$$\mu_n = \frac{\mathbf{1}_n \boldsymbol{x}_m^\mathsf{T}}{n} = \frac{1}{n}\sum_{i=1}^{n} x_{m,i}, \tag{5.51}$$

$$\kappa_n = n, \tag{5.52}$$

$$\alpha_n = \frac{n-1}{2}, \tag{5.53}$$

$$\beta_n = \frac{1}{2}\left(\boldsymbol{x}_m \boldsymbol{x}_m^\mathsf{T} - \frac{\left(\mathbf{1}_n \boldsymbol{x}_m^\mathsf{T}\right)^2}{n}\right) = \frac{1}{2}\sum_{i=1}^{n}\left(x_{m,i} - \mu_n\right)^2. \tag{5.54}$$

If one neglects the dependence between the measurements and the RF at the predictive locations, the posterior predictive distribution $f\left(x|\boldsymbol{x}_m\right)$ is obtained following Equation (5.15) and is space-invariant. It is a Student's t-distribution with the following parameters:

$$\mu_t = \mu_n = \frac{1}{n}\sum_{i=1}^{n} x_{m,i}, \tag{5.55}$$

$$\lambda_t = \frac{\alpha_n}{\beta_n\left(1+\kappa_n^{-1}\right)} = \frac{n(n-1)}{(n+1)\sum_{i=1}^{n}\left(x_{m,i}-\mu_n\right)^2}, \tag{5.56}$$

$$\nu_t = 2\alpha_n = n-1. \tag{5.57}$$

The characteristic values in the method in EN 1990 are defined as 5% quantile values of a Student's t-distribution with parameters given by Equations (5.55) to (5.57). An additional transformation step is added for ease of use, in which the Student's t-distributed random variable X is normalized:

$$U_t = \left(X - \mu_t\right)\lambda^{\frac{1}{2}}, \tag{5.58}$$

where U_t follows the standard Student's t-distribution with ν_t degrees of freedom, i.e., $\mu_t = 0$ and $\lambda_t = 1$. This normalization allows the use of standardized coefficients (k_n values), which only depend on n:

$$k_n = -F_{U_t}^{-1}(p)\sqrt{\frac{n+1}{n}}, \tag{5.59}$$

where $F_{U_t}^{-1}(\cdot)$ is the inverse CDF of U_t and $p = 0.05$, since the characteristic value x_k is defined as the 5% quantile value. Using the k_n value, x_k is obtained as follows:

$$x_k = \bar{\mu}_X\left(1 - k_n\bar{\delta}_X\right), \tag{5.60}$$

where $\bar{\mu}_X = \frac{1}{n}\sum_{i=1}^{n} x_{m,i}$ is the sample mean and $\bar{\delta}_X = \frac{\bar{\sigma}_X}{\bar{\mu}_X}$ is the sample coefficient of variation with $\bar{\sigma}_X^2 = \frac{1}{n-1}\sum_{i=1}^{n}\left(x_{m,i}-\bar{\mu}_X\right)^2$. EN 1990 provides tabulated values of k_n for varying n.

The method in EN 1990 also covers the case when the material property Y follows a lognormal distribution and $\boldsymbol{y}_m = [y_{m,1},\ y_{m,2},\ldots,\ y_{m,n}]^\mathsf{T}$ are the available samples. In this case, the Bayesian analysis underlying the method is conducted as described above for the Gaussian random variable $X = \ln(Y)$ with the logarithmic samples $x_{m,i} = \ln(y_{m,i}),\ i = 1,\ldots,n$. The

posterior predictive distribution $f\left(y|\boldsymbol{y}_m\right)$ is a log-Student's t-distribution parameterized in terms of the parameters of the underlying Student's t-distribution given by Equations (5.55) to (5.57). The characteristic value y_k is the 5% quantile value of $f\left(y|\boldsymbol{y}_m\right)$, which is equivalent to the exponential of the 5% quantile value of the underlying Student's t-distribution. Thus, y_k can be calculated as

$$y_k = \exp\left(\bar{\mu}_X\left(1 - k_n\bar{\delta}_X\right)\right), \tag{5.61}$$

where $\bar{\mu}_X$ and $\bar{\delta}_X$ are the sample mean and sample coefficient of variation of the logarithmic samples and k_n is given by Equation (5.59).

In a nutshell, the method in Annex D.7 of EN 1990 to determine characteristic values for the design of structures is a special case of the presented RF analysis, which assumes a non-informative prior distribution, independent measurements without measurement error and independence between measurement locations and the material parameter at the predictive locations.

5.3 Numerical examples

In this section, the proposed approach is applied to two numerical examples. The first one involves a one-dimensional RF of a geotechnical material, while the second one models the concrete compressive strength of a ship lock wall with a two-dimensional anisotropic RF.

5.3.1 Tip resistance of cohesive soil

Soil parameters are often determined based on measurements from cone penetration testing (CPT). In CPT, the tip resistance q_T measures the force required to push the cone through the soil and can be used to infer further soil parameters. In this example, data from a CPT is used, where the tip resistance of a cohesive soil layer was measured in depths from $z = 3.900\,\mathrm{m}$ to $z = 10.275\,\mathrm{m}$ resulting in 256 equidistant measurements of the tip resistance. The data is taken from [34] and was also used by Wang and Zhao to illustrate the performance of Bayesian compressive sampling when sparse data is available [53]. The tip resistance is modeled by the one-dimensional RF $q_T(z)$ in vertical direction with lognormal prior marginal distribution. Hence, the transformation of Equation (5.46) is applied:

$$q_T\left(z\right) = \exp\left(X\left(\boldsymbol{z}\right)\right). \tag{5.62}$$

The underlying prior RF $X\left(\boldsymbol{z}\right)$ is a homogeneous Gaussian RF with unknown mean value μ_X and unknown precision λ_X. The prior autocorrelation function is modeled by the exponential model with unknown correlation length l_c:

$$\rho\left(z_i, z_j\right) = \exp\left(-\frac{|z_j - z_i|}{l_c}\right) \tag{5.63}$$

Furthermore, no prior information on μ_X or λ_X are available and thus a non-informative prior $\mathcal{NG}$ distribution is chosen with the parameters from Equation (5.50).

It is assumed that knowledge of the full data set is not available but only a subset of 13 measurement values taken at equidistant locations, as illustrated by the blue dots in panel a) of Figure (5.3). It is assumed that the measurements are associated with a multiplicative lognormal measurement error, where the portion of the total variance attributed to the transformed Gaussian measurement error is given as $\gamma_\varepsilon = 0.01$. In a first step, the MAP estimate for l_c

is obtained by solving the minimization problem of Equation (5.42), where the vector $\boldsymbol{\tau}$ only consists of l_c. A uniform prior on the positive numbers is employed for l_c and hence the term $\ln(f(\boldsymbol{\tau}))$ in the optimization problem can be dropped and the MAP estimate reduces to a maximum likelihood estimate [44]. The resulting estimate for l_c is obtained as $l_c^* = 0.74\,\text{m}$.

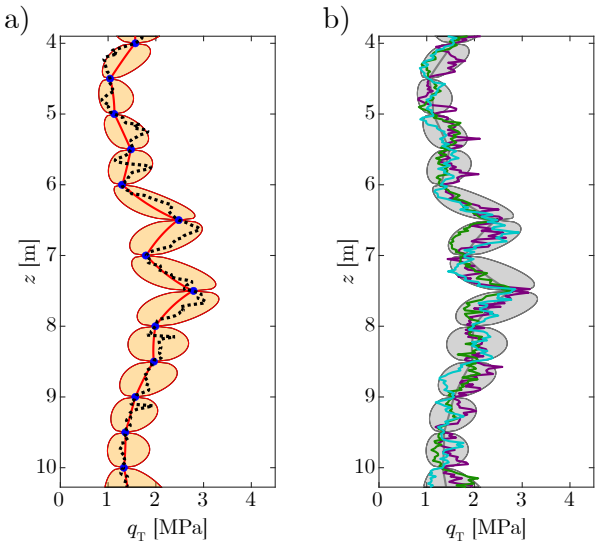

Figure 5.3: Posterior predictive RF of the tip resistance q_T. Panel a) shows the median (red line) and the two-sided 90% credible interval, i.e., the area between the 5% and 95% quantile value (orange area) of the marginal log-Student's t-distributions. The 13 blue dots mark the used measurement locations and values while the full data set is illustrated by the dotted black line. Panel b) shows three independent realizations of the posterior predictive RF in comparison to the two-sided 90% credible interval in gray.

Consequently, the posterior parameters of the $\mathcal{NG}$ distribution are obtained by application of Equations (5.11) to (5.14) in combination with Equation (5.47) to account for the log-transformation of the measurements. The spatial parameter functions of the posterior predictive Student's t-RF are calculated by means of Equations (5.31) and (5.32). From Equation (5.23) the degrees of freedom are calculated as $\nu_t = 12$. These are the parameters of the RF $q_T(z)$ given $\mathbf{M}$, which has log-Student's t-marginal distribution with PDF given by Equation (5.48). As the moments are not defined, the illustration in panel a) of Figure (5.3) shows the median of the posterior predictive tip resistance and the corresponding 5% and 95% quantile values along the depth of the soil layer. The increasing width of the orange area shows that the uncertainty is very small close to the measurement locations and increases away from the measurements. The full data set of 256 measurements is indicated by a black dotted line. Panel b) of Figure 5.3 shows three independent realizations of the posterior predictive RF. Comparison of the random realizations with the full data set shows good accordance regarding the number and amplitude of strong local deviations from the posterior predictive median. Hence, the proposed approach can sufficiently approximate both the overall trend of the RF and the associated uncertainty. To illustrate the influence of the number of measurements on the posterior prediction, the above calculations are repeated for $n = 6$ and $n = 64$ equidistant measurements. Figure 5.4 illustrates the measurement values and locations by blue dots in panel a) and panel c), respectively. For $n = 6$, the MAP optimization results in $l_{c,6}^* = 3.89\,\text{m}$ and for $n = 64$ it gives $l_{c,64}^* = 1.17\,\text{m}$. This large difference in the MAP estimates is due to the assumed uninformative prior distribution for the correlation length, in which case, the MAP estimate only depends on the data. Large differences in the data can lead to significant variation in the estimated correlation length. The median and corresponding 5% and 95% quantile values of $q_T(z)$ are illustrated in panel

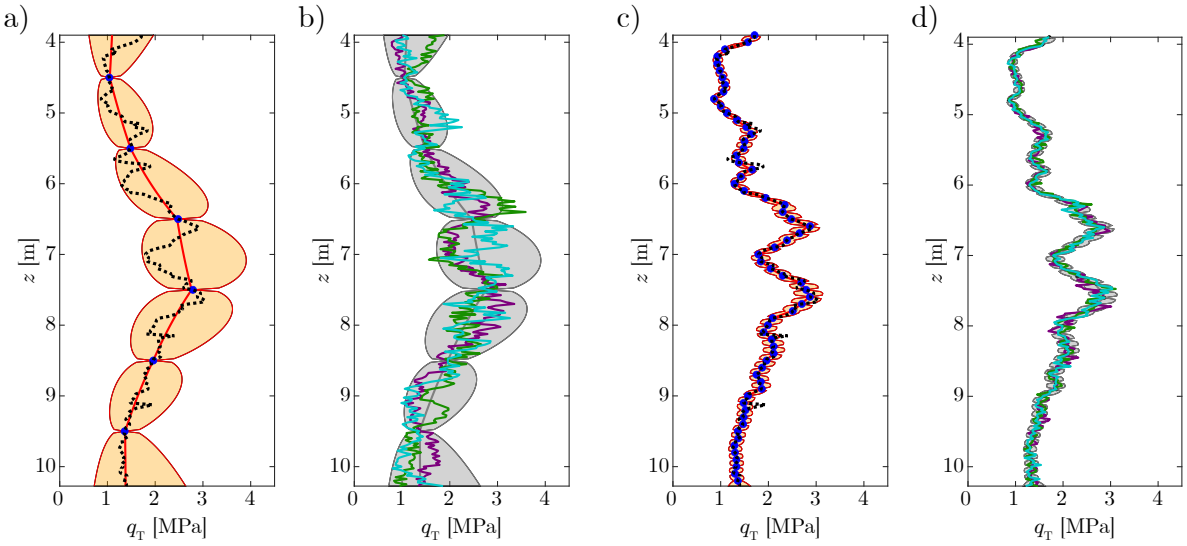

Figure 5.4: Posterior predictive RF of the tip resistance q_T for $n = 6$ (panel a) and b)) and $n = 64$ (panel c) and d)). Panel a) and c) show the median (red line) and the two-sided 90% credible intervals of the marginal log-Student's t-distributions. The blue dots mark the used measurement locations and values while the full data set is illustrated by the dotted black line. Panel b) and c) each show three independent realizations of the posterior predictive RF in comparison to the two-sided 90% credible intervals in gray.

a) and c), respectively of Figure 5.4. Comparison to Figure 5.3 shows that with increasing amount of data, the uncertainty, i.e., the variability of $q_T(z)$ is reduced. However, even with a small amount of data ($n = 6$), the global trend of the tip resistance can be predicted and the location-specific information can be used efficiently to set up an RF model. The large variability in the areas between the measurements is illustrated by three independent realizations in panel b) of Figure 5.4. When the amount of data is relatively large ($n = 64$), the remaining uncertainty in the tip resistance becomes comparatively small and random realizations of the RF do not differ significantly from the full data set, as can be seen in panel d) of Figure 5.4.

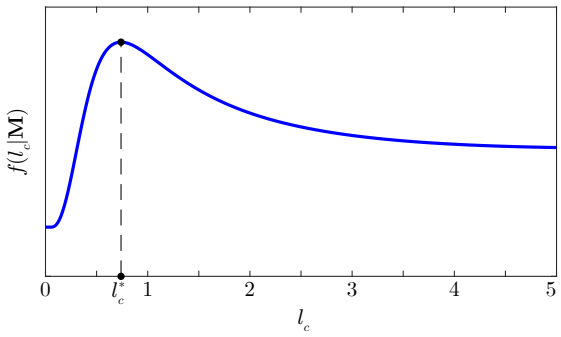

Figure 5.5: Posterior distribution of the correlation length $f(l_c|\mathbf{M})$ as function of the correlation length l_c and the corresponding MAP estimate l_c^*.

Figure 5.5 plots $f(l_c|\mathbf{M})$ with the MAP estimate $l_c^* = 0.74\,\text{m}$ located at the mode of $f(l_c|\mathbf{M})$. It appears that, although the posterior distribution has a distinct mode, it covers a broad range by remaining relatively flat for increasing values of l_c. This is caused by the uniform prior distribution for l_c and shows that such a uniform prior can lead to an improper posterior distribution of the correlation length. While this is not a problem when using MAP, it is an issue when the full posterior distribution of l_c is to be used. In such cases, a different prior distribution should be chosen.

5.3.2 Concrete compressive strength of a ship lock wall

In this example, we investigate the concrete compressive strength f_c of a ship lock wall made of tamped concrete in the 1920s. The length of the wall is 105 m and the height of the tamped concrete layer is 8 m, the third dimension is not taken into account for this study. 24 measurements of f_c are available from three vertical core samples taken at the quarter points of the wall [22]. The situation is illustrated in Figure 5.6 and the measurement data and corresponding locations are shown in Table 5.1. We assume that the measurements are associated with a multiplicative lognormal measurement error with coefficient of variation $\mathrm{CV}_\varepsilon = 0.025$.

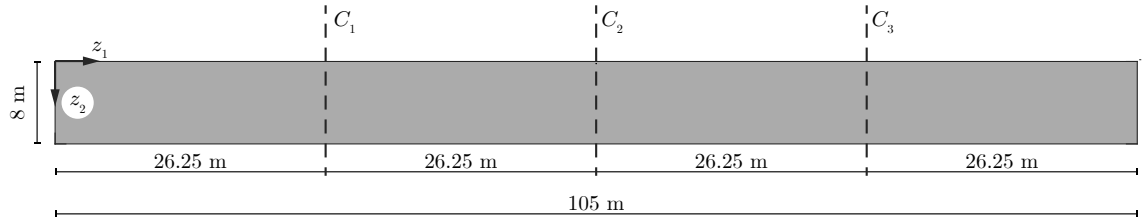

Figure 5.6: Ship lock wall with a total length of 105 m and a total height of 8 m made of tamped concrete from the 1920s. Three vertical core samples (C_1, C_2 and C_3) were taken at the quarter points of the wall indicated by the three dashed lines.

Table 5.1: Measurements of the concrete compressive strength f_c and the corresponding measurement locations of 24 specimens from 3 vertical core samples (C_1, C_2 and C_3) in the quarter points of the ship lock wall.

Core sample C_1			Core sample C_2			Core sample C_3		
z_1 [m]	z_2 [m]	$f_{c,m}$ [MPa]	z_1 [m]	z_2 [m]	$f_{c,m}$ [MPa]	z_1 [m]	z_2 [m]	$f_{c,m}$ [MPa]
26.25	0.40	29.2	52.5	0.21	21.2	78.75	0.34	18.5
	1.24	15.5		1.25	16.0		1.34	10.3
	2.25	8.7		2.05	32.0		2.17	13.2
	3.15	12.3		3.33	20.7		3.24	14.5
	4.12	16.2		4.15	13.8		4.27	25.4
	5.33	11.6		5.25	12.1		5.12	14.5
	6.15	13.4		6.40	8.6		6.23	13.2
	7.05	13.9		7.45	14.8		7.08	33.0

Applying the transformation of Equation (5.46), the logarithm of f_c is modeled with a two-dimensional Gaussian RF with non-informative prior $\mathcal{NG}$ distribution (cf. Equation (5.50)).

Typically, massive concrete structures made of tamped concrete from that time have been built in layers [57]. Hence, we employ a transverse anisotropic exponential correlation function, where the correlation length $l_{c,1}$ in direction z_1 differs from the correlation length $l_{c,2}$ in direction z_2 [59]:

$$\rho\left(\boldsymbol{z}_i, \boldsymbol{z}_j\right) = \exp\left(-\sqrt{\frac{\left(\Delta_1\left(\boldsymbol{z}_i, \boldsymbol{z}_j\right)\right)^2}{l_{c,1}^2} + \frac{\left(\Delta_2\left(\boldsymbol{z}_i, \boldsymbol{z}_j\right)\right)^2}{l_{c,2}^2}}\right), \tag{5.64}$$

where $\Delta_1\left(\boldsymbol{z}_i, \boldsymbol{z}_j\right)$ and $\Delta_2\left(\boldsymbol{z}_i, \boldsymbol{z}_j\right)$ denote the canonical distances of $\boldsymbol{z}_i$ and $\boldsymbol{z}_j$ in directions z_1 and z_2 respectively. Assuming a uniform prior on $l_{c,1}$ and $l_{c,2}$ results in the following MAP estimate

for the two correlation lengths:

$$\boldsymbol{l}_c^* = \left[l_{c,1}^*,\ l_{c,2}^*\right] = [1.54\,\text{m}, 0.58\,\text{m}] \tag{5.65}$$

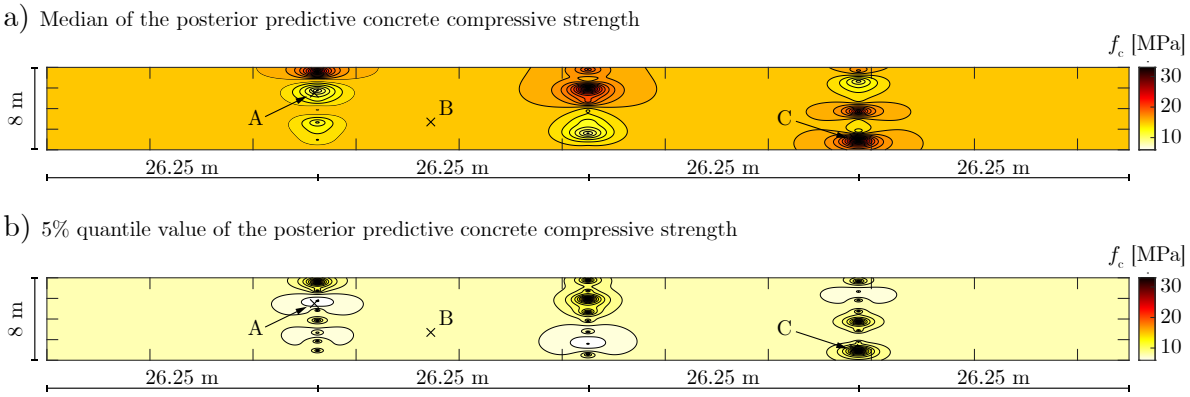

Figure 5.7: Posterior predictive median (panel a)) and 5% quantile value (panel b)) of the concrete compressive strength f_c of a ship lock wall obtained with data from three vertical core samples ($n = 24$ measurements of the concrete compressive strength). The median and 5% quantile value at points A, B and C are listed in Table 5.2.

These values are used in the Bayesian updating to obtain the posterior predictive RF for f_c. As the marginal posterior predictive PDF is a log-Student's t-distribution, the moments cannot be evaluated and thus, Figure 5.7 illustrates the median (panel a)) and the corresponding 5% quantile value (panel b)) of $f_c(\boldsymbol{z})$ given $\mathbf{M}$ across the ship lock wall. The measured values and the information about their location are clearly reflected, as regions close to low measurement values show low median and 5% quantile values, and regions close to high measurement values show higher median and 5% quantile values. This is illustrated by the example of three points (A, B and C) at different locations of the ship lock wall, where the median and 5% quantile values have been extracted and listed in Table 5.2. Point A, located close to a low measurement

Table 5.2: Median (50% quantile value, $f_{c,0.5}$) and 5% quantile value ($f_{c,0.05}$) of the marginal posterior predictive concrete compressive strength at three different locations (A, B and C) of the ship lock wall.

	z_1 [m]	z_2 [m]	$f_{c,0.5}$ [MPa]	$f_{c,0.05}$ [MPa]
Point A	25.95	2.5	10.7	6.6
Point B	37.25	5.3	15.9	8.2
Point C	78.3	6.85	23.1	14.1

value, features a posterior median of 10.7 MPa and a 5% quantile value of 6.6 MPa, both of which are significantly lower than those at point C with a median of 23.1 MPa and a 5% quantile value of 14.1 MPa. Contrary to point A, point C is located close to a high measurement value (cf. Table 5.1). The median of 15.9 MPa and 5% quantile of 8.2 MPa at point B are representative values for all locations far away from the measurements, i.e., all points with negligible spatial correlation to any measurement location.

Section 5.2.10 demonstrates the connection of the proposed RF approach and the established Bayesian approach in EN 1990. Next, we compare this approach to the results of the proposed hierarchical RF model using the data of Table 5.1. The mean and standard deviation of the log-transformed measurement values are $\bar{\mu}_X = 2.75$ and $\bar{\sigma}_X = 0.37$ with a corresponding k_n value of $k_n(n_m = 24) = 1.75$. Applying Equation (5.61) gives a characteristic value (5% quantile

value) of $f_{c,k} = 8.2\,\text{MPa}$. This value matches the 5% quantile value at locations without spatial correlation to the measurement points (cf. point C in Table 5.2). We note that this congruence depends on the chosen prior parameters of the RF and, thus, is the exception, not the rule.

The correlation length is an important parameter in any RF model. To illustrate this, the Bayesian analysis has been carried out for $\boldsymbol{l}_c = 0.5\boldsymbol{l}_c^*$ and $\boldsymbol{l}_c = 2\boldsymbol{l}_c^*$. The resulting marginal median of $f_c(\boldsymbol{z})$ in the area around the core sample C_2 is illustrated in Figure 5.8. Obviously, the larger the correlation length, the bigger the area that is influenced by the spatial correlation to the measurements. For $\boldsymbol{l}_c = 0.5\boldsymbol{l}_c^*$ the spatial effect of the measurements on the median is restricted to a domain of length $\approx 2\,\text{m}$, wheres for $\boldsymbol{l}_c = 2\boldsymbol{l}_c^*$ this effect spans over a length of $\approx 10\,\text{m}$. It is mentioned that this is the effect of the final step of the Bayesian approach, where the posterior predictive distribution is obtained. The whole RF is influenced by the data and the chosen correlation length by the global posterior parameters of the $\mathcal{NG}$ distribution, as can be seen by the different median values of $f_c(\boldsymbol{z})$ at locations D_a, D_b and D_c indicated in Figure 5.8. These locations are chosen exemplarily for all points with negligible spatial correlation to any measurement location. For $\boldsymbol{l}_c = 0.5\boldsymbol{l}_c^*$ the median is 15.7 MPa and for $\boldsymbol{l}_c = 2\boldsymbol{l}_c^*$ it is 16.3 MPa, compared to 15.9 MPa when $\boldsymbol{l}_c = \boldsymbol{l}_c^*$.

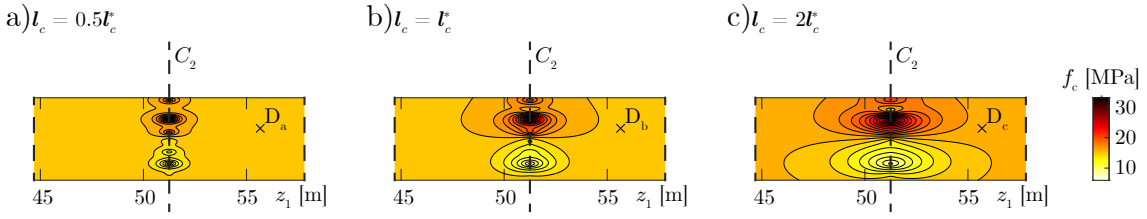

Figure 5.8: Posterior predictive median of the concrete compressive strength of a ship lock wall in the area around core sample C_2 obtained with varying correlation lengths.

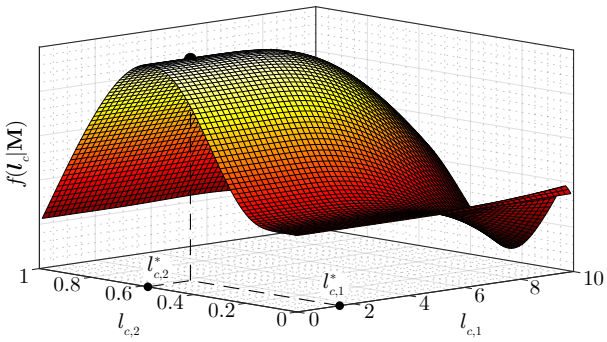

Figure 5.9: Two-dimensional posterior distribution of the correlation lengths in z_1 (horizontal) and z_2 (vertical) direction, $f(\boldsymbol{l}_c|\mathbf{M})$. The maximum of $f(\boldsymbol{l}_c|\mathbf{M})$ is located at $l_{c,1} = 1.54\,\text{m}$ and $l_{c,2} = 0.58\,\text{m}$, which is equivalent to the MAP estimate $\boldsymbol{l}_c^*$.

When employing the MAP procedure to approximate $f(\boldsymbol{\tau}|\mathbf{M})$, it is important to be aware of the sensitivity of the estimate and the amount of information provided by the data. In this example, the vertical distance of the measurement locations is relatively small while the horizontal distance is either 0 or very large. Hence, the MAP estimate for $l_{c,1}$ is subject to larger uncertainty than the MAP estimate for $l_{c,2}$, which is illustrated in Figure 5.9. While $f(\boldsymbol{\tau}|\mathbf{M})$ has a distinct maximum in direction $l_{c,2}$ at $l_{c,2} = 0.58\,\text{m}$, it is relatively flat in direction $l_{c,1}$. In fact, any $l_{c,1}$ smaller than 5 m is approximately equally likely given the data at hand. Only for $l_{c,1} > 5\,\text{m}$ the measurements of different core samples are noticeably correlated. This behavior is of special interest when no prior information on the correlation length is assumed, since in such

case the MAP estimate is only controlled by the data. In general, learning the correlation length from limited amount of data is not a trivial task, especially if no prior information on the RF parameters is available. In a study on the correlation length of soil parameters, a minimum of 5 measurement values within one correlation length are recommended for learning the correlation length of the exponential correlation model [37].

5.4 Conclusion

This paper presents a comprehensive hierarchical Bayesian approach to model random material properties with spatially distributed data. It is based on modeling a Gaussian random field assuming a normal-gamma prior distribution on its parameters. Closed-form expressions for the posterior normal-gamma distribution of the parameters of the random field are derived by making use of the conjugacy of the normal-gamma distribution and a multivariate Gaussian likelihood function. Subsequently, closed-form expressions for the spatial parameter function of the posterior predictive random field are derived, resulting in a non-homogeneous Student's t-random field. That is, the marginal distribution of the posterior predictive random field is a Student's t-distribution with location-specific parameters.

Sampling from such a random field can be achieved by expressing the Student's t-random field in terms of a Gaussian random field and one additional chi-squared random variable. For estimating the correlation parameters, a maximum a-posteriori estimation approach is proposed that accounts for the available data and potential prior information. In addition, an extension of the approach to non-Gaussian translation prior random fields is discussed and closed-form expressions for the case of a lognormal marginal prior distribution are derived.

The applicability of the presented approach to different engineering fields is illustrated by two examples, one from the field of geotechnical engineering and one from structural engineering. The derived posterior random field models reflect the location-specific information from the measurements, whereas their uncertainty increases with increasing distance from the measurement locations. Furthermore, it is demonstrated that the uncertainty can be reduced by increasing the amount of data. The spatial fluctuation of the posterior random field is sensitive to the choice of the correlation length parameter. When no information is available on the prior autocorrelation function, the maximum a-posteriori estimate for the correlation length is sensitive to the measurement data and should be handled with care, especially in the case where limited data is available.

A measurement error can be included to account for uncertainty in the measurements, in which case the variance contribution of the error to the total random field variance needs to be specified. This contribution can be learned from the data in a similar way as the parameters of the correlation model, which remains a topic of future investigations.

The presented modeling approach can be extended to account for a trend function in the prior random field parameters. A trend in the prior mean can be included by employing a linear basis function model, similar to the work of [14]. A parametric dependence can also be included in the prior precision parameter, which leads to a model known as weighted Bayesian linear regression [21]. Investigation of these models in the context of material modeling is left to future studies.

Declaration of competing interest

The authors declare that they have no known competing financial interests or personal relationships that could have appeared to influence the work reported in this paper.

Acknowledgments

This work has been financially supported by the *Bundesanstalt für Wasserbau* (Federal Waterways Engineering and Research Institute, Germany). The corresponding author would like to thank Claus Kunz from the *Bundesanstalt für Wasserbau* who motivated the idea to develop the presented approach and Prof. Lori Graham-Brady from Johns Hopkins University for many discussions that have considerably enhanced the quality of the paper.

5.A The posterior normal-gamma distribution

The posterior parameters of the normal-gamma distribution for the parameter vector $\boldsymbol{\theta} = [\mu_X, \lambda_X]^\mathsf{T}$, as specified in Equations (5.11) to (5.14) are derived in the following.

According to Bayes' theorem, the posterior distribution $f(\boldsymbol{\theta}|\mathbf{M})$ is proportional to the product of prior distribution $f(\boldsymbol{\theta})$ and likelihood $\mathrm{L}(\boldsymbol{\theta}|\mathbf{M})$, which are defined in Equations (5.3) and (5.5). Using the normal-gamma prior distribution and the multivariate Gaussian likelihood gives the following expression:

$$f(\boldsymbol{\theta}|\mathbf{M}) \propto \lambda_X^{\alpha_0+\frac{n}{2}-\frac{1}{2}} \cdot \exp\left(-\frac{\kappa_0\lambda_X}{2}(\mu_X-\mu_0)^2\right) \cdot \exp\left(-\lambda_X\beta_0\right) \cdot \\ \cdot \exp\left(-\frac{\lambda_X}{2}(\boldsymbol{x}_m-\mu_X\mathbf{1}_n)\,\mathbf{R}_m^{-1}\,(\boldsymbol{x}_m-\mu_X\mathbf{1}_n)^\mathsf{T}\right). \tag{5.66}$$

With the definition of $\mathbf{A} = \kappa_0(\mu_X-\mu_0)^2 - 2\mu_X\mathbf{1}_n\mathbf{R}_m^{-1}\boldsymbol{x}_m^\mathsf{T} + \mu_X^2\mathbf{1}_n\mathbf{R}_m^{-1}\mathbf{1}_n^\mathsf{T}$, Equation (5.66) can be rearranged as

$$f(\boldsymbol{\theta}|\mathbf{M}) \propto \lambda_X^{\alpha_0+\frac{n}{2}-\frac{1}{2}} \cdot \exp\left(-\lambda_X\left(\beta_0 + \frac{1}{2}\boldsymbol{x}_m\mathbf{R}_m^{-1}\boldsymbol{x}_m^\mathsf{T} + \frac{1}{2}\mathbf{A}\right)\right). \tag{5.67}$$

Initially, the focus lies on $\mathbf{A}$ which is expanded and modified as follows:

$$\mathbf{A} = \left(\kappa_0 + \mathbf{1}_n\mathbf{R}_m^{-1}\mathbf{1}_n^\mathsf{T}\right)\left(\mu_X^2 - 2\mu_X\frac{\kappa_0\mu_0 + \mathbf{1}_n\mathbf{R}_m^{-1}\boldsymbol{x}_m^\mathsf{T}}{\kappa_0 + \mathbf{1}_n\mathbf{R}_m^{-1}\mathbf{1}_n^\mathsf{T}}\right) + \kappa_0\mu_0^2. \tag{5.68}$$

Next, the square of the expression inside the second parenthesis is completed:

$$\mathbf{A} = \underbrace{\left(\kappa_0 + \mathbf{1}_n\mathbf{R}_m^{-1}\mathbf{1}_n^\mathsf{T}\right)\left(\mu_X - \frac{\kappa_0\mu_0 + \mathbf{1}_n\mathbf{R}_m^{-1}\boldsymbol{x}_m^\mathsf{T}}{\kappa_0 + \mathbf{1}_n\mathbf{R}_m^{-1}\mathbf{1}_n^\mathsf{T}}\right)^2}_{\mathbf{B}} + \underbrace{\kappa_0\mu_0^2 - \frac{\left(\kappa_0\mu_0 + \mathbf{1}_n\mathbf{R}_m^{-1}\boldsymbol{x}_m^\mathsf{T}\right)^2}{\kappa_0 + \mathbf{1}_n\mathbf{R}_m^{-1}\mathbf{1}_n^\mathsf{T}}}_{\mathbf{C}}. \tag{5.69}$$

The terms of $\mathbf{C}$ in Equation (5.69) are expanded and converted to a common denominator:

$$\mathbf{C} = \left(\kappa_0\mu_0^2\mathbf{1}_n\mathbf{R}_m^{-1}\mathbf{1}_n^\mathsf{T} - 2\kappa_0\mu_0\mathbf{1}_n\mathbf{R}_m^{-1}\boldsymbol{x}_m^\mathsf{T} - \left(\mathbf{1}_n\mathbf{R}_m^{-1}\boldsymbol{x}_m^\mathsf{T}\right)^2\right)\left(\kappa_0 + \mathbf{1}_n\mathbf{R}_m^{-1}\mathbf{1}_n^\mathsf{T}\right)^{-1}. \tag{5.70}$$

Inserting the expression for $\mathbf{B}$ and $\mathbf{C}$ into Equation (5.67) gives:

$$f(\boldsymbol{\theta}|\mathbf{M}) \propto \lambda_X^{\alpha_0+\frac{n}{2}-\frac{1}{2}} \cdot \exp\left(-\lambda_X\left(\beta_0 + \frac{1}{2}\boldsymbol{x}_m\mathbf{R}_m^{-1}\boldsymbol{x}_m^\mathsf{T} + \frac{1}{2}\mathbf{C}\right)\right) \cdot \exp\left(-\frac{\lambda_X}{2}\mathbf{B}\right). \tag{5.71}$$

The parametric form of the posterior normal-gamma distribution as defined in Section 5.2.4 is

as follows:

$$\mathcal{NG}\left(\mu_X, \lambda_X | \mu_n, \kappa_n, \alpha_n, \beta_n\right) = \mathcal{C}_n \lambda_X^{\alpha_n - \frac{1}{2}} \cdot \exp\left(-\frac{\kappa_n \lambda_X}{2}\left(\mu_X - \mu_n\right)^2\right) \cdot \exp\left(-\lambda_X \beta_n\right). \tag{5.72}$$

Writing out all the terms in Equation (5.71) and comparing it to (5.72) one can see that up to the normalizing constant $\mathcal{C}_n$, the resulting expression of Equation (5.71) is a normal-gamma distribution with parameters as follows:

$$\mu_n = \frac{\kappa_0 \mu_0 + \mathbf{1}_n \mathbf{R}_m^{-1} \boldsymbol{x}_m^\mathsf{T}}{\kappa_0 + \mathbf{1}_n \mathbf{R}_m^{-1} \mathbf{1}_n^\mathsf{T}}, \tag{5.73}$$

$$\kappa_n = \kappa_0 + \mathbf{1}_n \mathbf{R}_m^{-1} \mathbf{1}_n^\mathsf{T}, \tag{5.74}$$

$$\alpha_n = \alpha_0 + \frac{n}{2}, \tag{5.75}$$

$$\beta_n = \beta_0 + \frac{1}{2}\left(\boldsymbol{x}_m \mathbf{R}_m^{-1} \boldsymbol{x}_m^\mathsf{T} + \frac{\kappa_0 \mu_0^2 \mathbf{1}_n \mathbf{R}_m^{-1} \mathbf{1}_n^\mathsf{T} - 2\kappa_0 \mu_0 \mathbf{1}_n \mathbf{R}_m^{-1} \boldsymbol{x}_m^\mathsf{T} - \left(\mathbf{1}_n \mathbf{R}_m^{-1} \boldsymbol{x}_m^\mathsf{T}\right)^2}{\kappa_0 + \mathbf{1}_n \mathbf{R}_m^{-1} \mathbf{1}_n^\mathsf{T}}\right). \tag{5.76}$$

The normalizing constant is

$$\mathcal{C}_n = \frac{\beta_n^{\alpha_n} \kappa_n^{\frac{1}{2}}}{\Gamma\left(\alpha_n\right)\left(2\pi\right)^{\frac{1}{2}}}. \tag{5.77}$$

5.B The marginal posterior predictive Student's t-distribution

In Section 5.2.5, the Student's t-distribution is introduced as the marginal posterior predictive distribution of the RF $X(\boldsymbol{z})$ for the normal-gamma conjugate prior distribution of the RF parameters. This appendix derives the analytical expressions for the parameters of the marginal posterior predictive distribution as given in Equations (5.21) to (5.23).

The marginal posterior predictive PDF at any point $\boldsymbol{z} \in \Omega$ is defined by

$$f\left(x; \boldsymbol{z} | \mathbf{M}\right) = \int_{\boldsymbol{\Theta}} f\left(x; \boldsymbol{z} | \boldsymbol{\theta}, \mathbf{M}\right) f\left(\boldsymbol{\theta} | \mathbf{M}\right) \mathrm{d}\boldsymbol{\theta}. \tag{5.78}$$

$f\left(\boldsymbol{\theta}|\mathbf{M}\right)$ is the posterior normal-gamma distribution as defined in Equation (5.9) and $f\left(x; \boldsymbol{z}|\boldsymbol{\theta}, \mathbf{M}\right)$ is a location-specific normal distribution with parameters $\mu_{\boldsymbol{z}}''$ and $\lambda_{\boldsymbol{z}}''$ given by Equations (5.17) and (5.18). Hence, Equation (5.78) can be expanded as follows:

$$f\left(x; \boldsymbol{z} | \mathbf{M}\right) = \int_{\lambda_X=0}^{+\infty} \int_{\mu_X=-\infty}^{+\infty} \mathcal{N}\left(x | \mu_{\boldsymbol{z}}'', \lambda_{\boldsymbol{z}}''\right) \mathcal{N}\left(\mu_X | \mu_n, \kappa_n \lambda_X\right) \mathrm{d}\mu_X \mathcal{G}\left(\lambda_X | \alpha_n, \beta_n\right) \mathrm{d}\lambda_X. \tag{5.79}$$

The inner integral involves the convolution of two normal densities:

$$\int_{\mu_X=-\infty}^{+\infty} \mathcal{N}\left(x | \mu_{\boldsymbol{z}}'', \lambda_{\boldsymbol{z}}''\right) \mathcal{N}\left(\mu_X | \mu_n, \kappa_n \lambda_X\right) \mathrm{d}\mu_X = f\left(x; \boldsymbol{z} | \lambda_X, \mathbf{M}\right). \tag{5.80}$$

For the solution of the integral, the expression for $\mu_{\boldsymbol{z}}''$, given in Equation (5.17) is rewritten as

follows:

$$\mu_{\boldsymbol{z}}'' = \mu_X + \boldsymbol{R}_{\boldsymbol{z},m}\mathbf{R}_m^{-1}\left(\boldsymbol{x}_m - \mu_X\mathbf{1}_n\right)^{\mathsf{T}} = \mu_X \underbrace{\left(1 - \boldsymbol{R}_{\boldsymbol{z},m}\mathbf{R}_m^{-1}\mathbf{1}_n^{\mathsf{T}}\right)}_{\psi} + \underbrace{\boldsymbol{R}_{\boldsymbol{z},m}\mathbf{R}_m^{-1}\boldsymbol{x}_m^{\mathsf{T}}}_{\xi}. \tag{5.81}$$

For this special case and noting that $\lambda_{\boldsymbol{z}}''$ does not depend on μ_X, the marginalization in Equation (5.80) can be solved analytically and results in a normal density $f\left(x;\boldsymbol{z}|\lambda_X,\mathbf{M}\right) = \mathcal{N}\left(x|\tilde{\mu}_{\boldsymbol{z}},\tilde{\lambda}_{\boldsymbol{z}}\right)$, where $\tilde{\mu}_{\boldsymbol{z}}$ and $\tilde{\lambda}_{\boldsymbol{z}}$ are given by the following equations [6]:

$$\tilde{\mu}_{\boldsymbol{z}} = \psi\mu_n + \xi, \tag{5.82}$$

$$\tilde{\lambda}_{\boldsymbol{z}} = \left(\left(\lambda_{\boldsymbol{z}}''\right)^{-1} + \psi^2\lambda_X^{-1}\kappa_n^{-1}\right)^{-1} = \lambda_X \underbrace{\left(1 - \boldsymbol{R}_{\boldsymbol{z},m}\mathbf{R}_m^{-1}\boldsymbol{R}_{\boldsymbol{z},m}^{\mathsf{T}} + \left(1 - \boldsymbol{R}_{\boldsymbol{z},m}\mathbf{R}_m^{-1}\mathbf{1}_n^{\mathsf{T}}\right)^2\kappa_n^{-1}\right)^{-1}}_{\tilde{\kappa}_{\boldsymbol{z}}}. \tag{5.83}$$

Inserting in Equation (5.79) results in

$$f\left(x;\boldsymbol{z}|\mathbf{M}\right) = \frac{\beta_n^{\alpha_n}\left(\tilde{\kappa}_{\boldsymbol{z}}\right)^{\frac{1}{2}}}{\Gamma\left(\alpha_n\right)\left(2\pi\right)^{\frac{1}{2}}}\int_{\lambda_X=0}^{+\infty}\lambda_X^{\alpha_n-\frac{1}{2}}\exp\left(-\lambda_X\left(\beta_n + \frac{\tilde{\kappa}_{\boldsymbol{z}}}{2}\left(x_{\boldsymbol{z}} - \tilde{\mu}_{\boldsymbol{z}}\right)^2\right)\right)\mathrm{d}\lambda_X. \tag{5.84}$$

A solution of the integral in Equation (5.84) is readily available and the resulting expression is as follows [6]:

$$f\left(x;\boldsymbol{z}|\mathbf{M}\right) = \frac{\beta_n^{\alpha_n}\left(\tilde{\kappa}_{\boldsymbol{z}}\right)^{\frac{1}{2}}}{\Gamma\left(\alpha_n\right)\left(2\pi\right)^{\frac{1}{2}}}\left(\beta_n + \frac{\tilde{\kappa}_{\boldsymbol{z}}}{2}\left(x_{\boldsymbol{z}} - \tilde{\mu}_{\boldsymbol{z}}\right)^2\right)^{-\frac{1}{2}-\alpha_n}\Gamma\left(\alpha_n + \frac{1}{2}\right). \tag{5.85}$$

To bring $f\left(x;\boldsymbol{z}|\mathbf{M}\right)$ into a standardized format, we define $\mu_{\boldsymbol{z},t} = \tilde{\mu}_{\boldsymbol{z}}$, $\lambda_{\boldsymbol{z},t} = \frac{\tilde{\kappa}_{\boldsymbol{z}}\alpha_n}{\beta_n}$ and $\nu_t = 2\alpha_n$ [6]. This gives

$$f\left(x;\boldsymbol{z}|\mathbf{M}\right) = \frac{\Gamma\left(\frac{\nu_t+1}{2}\right)}{\Gamma\left(\frac{\nu_t}{2}\right)}\left(\frac{\lambda_{\boldsymbol{z},t}}{\pi\nu_t}\right)^{\frac{1}{2}}\left(1 + \frac{\lambda_{\boldsymbol{z},t}}{\nu_t}\left(x_{\boldsymbol{z}} - \mu_{\boldsymbol{z},t}\right)^2\right)^{-\frac{\nu_t}{2}-\frac{1}{2}}. \tag{5.86}$$

Equation (5.86) describes the marginal posterior predictive distribution of the RF $X(\boldsymbol{z})$ given measurement data $\mathbf{M}$, which is a Student's t-distribution with location parameter $\mu_{\boldsymbol{z},t}$, scale parameter $\lambda_{\boldsymbol{z},t}$ and degrees of freedom ν_t defined as follows:

$$\mu_{\boldsymbol{z},t} = \mu_n + \boldsymbol{R}_{\boldsymbol{z},m}\mathbf{R}_m^{-1}\left(\boldsymbol{x}_m - \mu_n\mathbf{1}_n\right)^{\mathsf{T}}, \tag{5.87}$$

$$\lambda_{\boldsymbol{z},t} = \frac{\alpha_n}{\beta_n\left(1 - \boldsymbol{R}_{\boldsymbol{z},m}\mathbf{R}_m^{-1}\boldsymbol{R}_{\boldsymbol{z},m}^{\mathsf{T}} + \left(1 - \boldsymbol{R}_{\boldsymbol{z},m}\mathbf{R}_m^{-1}\mathbf{1}_n^{\mathsf{T}}\right)^2\kappa_n^{-1}\right)}, \tag{5.88}$$

$$\nu_t = 2\alpha_n, \tag{5.89}$$

where μ_n, κ_n, α_n and β_n are the posterior parameters of the normal-gamma distribution given by Equations (5.11) to (5.14).

5.C The multivariate posterior predictive Student's t-distribution

This section extends the derivation of Appendix 5.B to the multivariate case to derive the parameters for the k-th order posterior predictive Student's t-distribution as given by Equations (5.23), (5.29) and (5.30) in Section 5.2.6.

The PDF of the posterior predictive distribution of the RF $X(\boldsymbol{z})$ is

$$f\left(\boldsymbol{x};\mathbf{Z}|\mathbf{M}\right)=\int_{\boldsymbol{\Theta}}f\left(\boldsymbol{x};\mathbf{Z}|\boldsymbol{\theta},\mathbf{M}\right)f\left(\boldsymbol{\theta}|\mathbf{M}\right)\mathrm{d}\boldsymbol{\theta}, \tag{5.90}$$

with $\boldsymbol{x}\in\mathbb{R}^k$ and $\mathbf{Z}=[\boldsymbol{z}_1,\ldots,\boldsymbol{z}_k]\in\mathbb{R}^{k\times d}$ denoting any set of spatial points in Ω. $f\left(\boldsymbol{x};\mathbf{Z}|\boldsymbol{\theta},\mathbf{M}\right)$ is a k-variate normal density with mean vector $\boldsymbol{\mu}_{\mathbf{Z}}''$ and precision matrix $\boldsymbol{\Lambda}_{\mathbf{Z}}''$ given by Equations (5.25) and (5.26). $f\left(\boldsymbol{\theta}|\mathbf{M}\right)$ is a normal-gamma distribution as defined in Equation (5.9) and is independent of the locations $\mathbf{Z}$. Equation (5.90) is expanded as follows:

$$f\left(\boldsymbol{x};\mathbf{Z}|\mathbf{M}\right)=\int_{\lambda_X=0}^{+\infty}\int_{\mu_X=-\infty}^{+\infty}\mathcal{N}\left(\boldsymbol{x}|\boldsymbol{\mu}_{\mathbf{Z}}'',\boldsymbol{\Lambda}_{\mathbf{Z}}''\right)\cdot\mathcal{N}\left(\mu_X|\mu_n,\lambda_X\kappa_n\right)\mathrm{d}\mu_X\cdot\mathcal{G}\left(\lambda_X|\alpha_n,\beta_n\right)\mathrm{d}\lambda_X. \tag{5.91}$$

The inner integral can be solved by rewriting Equation (5.25) as follows:

$$\boldsymbol{\mu}_{\mathbf{Z}}''=\mu_X\mathbf{1}_k+\mathbf{R}_{\mathbf{Z},m}\mathbf{R}_m^{-1}\left(\boldsymbol{x}_m-\mu_X\mathbf{1}_n\right)^{\mathsf{T}}=\mu_X\underbrace{\left(\mathbf{1}_k-\mathbf{R}_{\mathbf{Z},m}\mathbf{R}_m^{-1}\mathbf{1}_n^{\mathsf{T}}\right)}_{\boldsymbol{\psi}}+\underbrace{\mathbf{R}_{\mathbf{Z},m}\mathbf{R}_m^{-1}\boldsymbol{x}_m^{\mathsf{T}}}_{\boldsymbol{\xi}}. \tag{5.92}$$

Using this expression, the integration over μ_X can be performed analytically and results in the density of a multivariate normal distribution $\mathcal{N}\left(\boldsymbol{x}|\tilde{\boldsymbol{\mu}}_{\mathbf{Z}},\tilde{\boldsymbol{\Lambda}}_{\mathbf{Z}}\right)$ with parameters given as [6]

$$\tilde{\boldsymbol{\mu}}_{\mathbf{Z}}=\mu_n\boldsymbol{\psi}+\boldsymbol{\xi}, \tag{5.93}$$

$$\tilde{\boldsymbol{\Lambda}}_{\mathbf{Z}}=\left(\left(\boldsymbol{\Lambda}_{\mathbf{Z}}''\right)^{-1}+\boldsymbol{\psi}^{\mathsf{T}}\left(\lambda_X\kappa_n\right)^{-1}\boldsymbol{\psi}\right)^{-1}. \tag{5.94}$$

Substituting Equations (5.26) and (5.92) into Equation (5.94), $\tilde{\boldsymbol{\Lambda}}_{\mathbf{Z}}$ can be expresssed as the following linear function of λ_X:

$$\tilde{\boldsymbol{\Lambda}}_{\mathbf{Z}}=\lambda_X\underbrace{\left(\mathbf{R}_{\mathbf{Z}}-\mathbf{R}_{\mathbf{Z},m}\mathbf{R}_m^{-1}\mathbf{R}_{\mathbf{Z},m}^{\mathsf{T}}+\left(\mathbf{1}_k-\mathbf{R}_{\mathbf{Z},m}\mathbf{R}_m^{-1}\mathbf{1}_n^{\mathsf{T}}\right)^{\mathsf{T}}\kappa_n^{-1}\left(\mathbf{1}_k-\mathbf{R}_{\mathbf{Z},m}\mathbf{R}_m^{-1}\mathbf{1}_n^{\mathsf{T}}\right)\right)^{-1}}_{\tilde{\mathbf{K}}_{\mathbf{Z}}}. \tag{5.95}$$

Inserting $\mathcal{N}\left(\boldsymbol{x}|\tilde{\boldsymbol{\mu}}_{\mathbf{Z}},\tilde{\boldsymbol{\Lambda}}_{\mathbf{Z}}\right)$ into Equation (5.91) gives

$$f\left(\boldsymbol{x};\mathbf{Z}|\mathbf{M}\right)=\int_{\lambda_X=0}^{+\infty}\mathcal{N}\left(\boldsymbol{x}|\tilde{\boldsymbol{\mu}}_{\mathbf{Z}},\tilde{\mathbf{K}}_{\mathbf{Z}}\lambda_X\right)\mathcal{G}\left(\lambda_X|\alpha_n,\beta_n\right)\mathrm{d}\lambda_X. \tag{5.96}$$

Next, an alternative parametrization is introduced, defining $\nu_t=2\alpha_n$ and $\eta=\frac{\lambda_X\beta_n}{\alpha_n}$. Inserted into Equation (5.96), this gives the following [6]:

$$f\left(\boldsymbol{x};\mathbf{Z}|\mathbf{M}\right)=\int_{\eta=0}^{+\infty}\mathcal{N}\left(\boldsymbol{x}\,\middle|\,\tilde{\boldsymbol{\mu}}_{\mathbf{Z}},\tilde{\mathbf{K}}_{\mathbf{Z}}\frac{\eta\alpha_n}{\beta_n}\right)\mathcal{G}\left(\eta\,\middle|\,\frac{\nu_t}{2},\frac{\nu_t}{2}\right)\mathrm{d}\eta, \tag{5.97}$$

for which a solution is available [6]. The resulting expression is

$$f\left(\boldsymbol{x};\mathbf{Z}|\mathbf{M}\right)=\frac{\Gamma\left(\frac{k+\nu_t}{2}\right)}{\Gamma\left(\frac{\nu_t}{2}\right)}\left|\tilde{\mathbf{K}}_{\mathbf{Z}}\right|^{\frac{1}{2}}\left(\frac{\alpha_n}{\beta_n\pi\nu_t}\right)^{\frac{k}{2}}\left(1+\frac{\alpha_n\left(\boldsymbol{x}-\tilde{\boldsymbol{\mu}}_{\mathbf{Z}}\right)\tilde{\mathbf{K}}_{\mathbf{Z}}\left(\boldsymbol{x}-\tilde{\boldsymbol{\mu}}_{\mathbf{Z}}\right)^{\mathsf{T}}}{\beta_n\nu_t}\right)^{-\frac{k+\nu_t}{2}}, \tag{5.98}$$

which is a k-variate Student's t-distribution with parameters $\tilde{\boldsymbol{\mu}}_{\mathbf{Z}}$, $\frac{\alpha_n}{\beta_n}\tilde{\mathbf{K}}_{\mathbf{Z}}$ and ν_t. Defining $\boldsymbol{\mu}_{\mathbf{Z},t}=\tilde{\boldsymbol{\mu}}_{\mathbf{Z}}$ and $\boldsymbol{\Lambda}_{\mathbf{Z},t}=\frac{\alpha_n}{\beta_n}\tilde{\mathbf{K}}_{\mathbf{Z}}$ yields the expression of Equation (5.28) for the k-th order posterior predictive distribution of $X(\boldsymbol{z})$ given measurement data $\mathbf{M}$. That is, $f\left(\boldsymbol{x};\mathbf{Z}|\mathbf{M}\right)=f_t\left(\boldsymbol{x}|\boldsymbol{\mu}_{\mathbf{Z},t},\boldsymbol{\Lambda}_{\mathbf{Z},t},\nu_t\right)$ with parameters given as

$$\boldsymbol{\mu}_{\mathbf{Z},t}=\mu_n\mathbf{1}_k+\mathbf{R}_{\mathbf{Z},m}\mathbf{R}_m^{-1}\left(\boldsymbol{x}_m-\mu_n\mathbf{1}_n\right)^{\mathsf{T}}, \tag{5.99}$$

$$\boldsymbol{\Lambda}_{\mathbf{Z},t}=\frac{\alpha_n}{\beta_n}\left(\mathbf{R}_{\mathbf{Z}}-\mathbf{R}_{\mathbf{Z},m}\mathbf{R}_m^{-1}\mathbf{R}_{\mathbf{Z},m}^{\mathsf{T}}+\left(\mathbf{1}_k-\mathbf{R}_{\mathbf{Z},m}\mathbf{R}_m^{-1}\mathbf{1}_n^{\mathsf{T}}\right)\kappa_n^{-1}\left(\mathbf{1}_k-\mathbf{R}_{\mathbf{Z},m}\mathbf{R}_m^{-1}\mathbf{1}_n^{\mathsf{T}}\right)^{\mathsf{T}}\right)^{-1}, \tag{5.100}$$

$$\nu_t=2\alpha_n, \tag{5.101}$$

where μ_n, κ_n, α_n and β_n are the posterior parameters of the normal-gamma distribution given by Equations (5.11) to (5.14).

5.D The log-Student's t-distribution

In Section 5.2.8, the log-Student's t-distribution is introduced as resulting marginal distribution of the posterior predictive RF when the prior RF has lognormal marginal distribution. In this appendix, the log-Student's t-distribution and some of its properties are described.

When X follows a Student's t-distribution, $Y=\exp\left(X\right)$ follows the log-Student's t-distribution [11, 50]. The PDF can be derived as follows:

$$f_{t,\ln}\left(y\right)=\left|\frac{\mathrm{d}\ln\left(y\right)}{\mathrm{d}y}\right|f_t\left(\ln\left(y\right)\right)=\frac{1}{y}f_t\left(\ln\left(y\right)\right), \tag{5.102}$$

where $f_t\left(\cdot\right)$ is the PDF of the Student's t-distribution, which gives

$$f_{t,\ln}\left(y|\mu_t,\lambda_t,\nu_t\right)=y^{-1}\frac{\Gamma\left(\frac{\nu_t}{2}+\frac{1}{2}\right)}{\Gamma\left(\frac{\nu_t}{2}\right)}\left(\frac{\lambda_t}{\pi\nu_t}\right)^{\frac{1}{2}}\left(1+\frac{\lambda_t\left(\ln\left(y\right)-\mu_t\right)^2}{\nu_t}\right)^{-\frac{\nu_t}{2}-\frac{1}{2}}, \tag{5.103}$$

where μ_t, λ_t and ν_t are the parameters of the underlying Student's t-distribution. The CDF of Y is given by the CDF of the underlying Student's t-distribution with argument $\ln\left(y\right)$:

$$F_{t,\ln}\left(y|\mu_t,\lambda_t,\nu_t\right)=F_t\left(\ln\left(y\right)|\mu_t,\lambda_t,\nu_t\right). \tag{5.104}$$

The log-Student's t-distribution does not have finite moments of any order. A simple proof is given in the following. The expected value of Y is defined as:

$$\mathrm{E}\left[Y\right]=\mathrm{E}\left[\exp\left(X\right)\right], \tag{5.105}$$

where X follows the Student's t-distribution. The exponential function can be written in terms

of the following power series [e.g., 45]:

$$\exp(x) = \sum_{k=0}^{\infty} \frac{x^k}{k!}, \tag{5.106}$$

which can be substituted into Equation (5.105) to give:

$$\mathrm{E}[Y] = \mathrm{E}\left[\sum_{k=0}^{\infty} \frac{X^k}{k!}\right] = \sum_{k=0}^{\infty} \frac{\mathrm{E}\left[X^k\right]}{k!}. \tag{5.107}$$

$\mathrm{E}\left[X^k\right]$ is the k-th raw moment of the Student's t-distributed random variable X. However, the moments of the Student's t-distribution are only finite for orders $k < \nu_t$ [9] and thus, the following holds for $\mathrm{E}[Y]$ due to the sum in Equation (5.107):

$$\mathrm{E}[Y] \to \infty \text{ for } \nu_t < \infty. \tag{5.108}$$

Since the first-order moment of Y is infinite, all higher-order integer moments of Y, as well as joint moments for the multivariate case, will also be infinite. In the limiting case, when $\nu_t \to \infty$, the log-Student's t-distribution converges to the lognormal distribution, which has finite moments of any order.

References

[1] P. Abrahamsen. *A review of Gaussian random fields and correlation functions*. 2nd ed. Norwegian Computing Center, 1997.

[2] S. Banerjee. "Modeling massive spatial datasets using a conjugate Bayesian linear modeling framework". In: *Spatial Statistics* 37 (2020), p. 100417.

[3] S. Banerjee, B. P. Carlin, and A. E. Gelfand. *Hierarchical modeling and analysis for spatial data*. 2nd ed. Chapman & Hall/CRC monographs on statistics & applied probability. Boca Raton, FL: CRC, 2014.

[4] J. Benjamin and C. Cornell. *Probability, statistics, and decision for civil engineers*. New York City, NY: McGraw-Hill, 1970.

[5] W. Betz, I. Papaioannou, J. L. Beck, and D. Straub. "Bayesian inference with subset simulation: strategies and improvements". In: *Computer Methods in Applied Mechanics and Engineering* 331 (2018), pp. 72–93.

[6] C. M. Bishop. *Pattern recognition and machine learning*. Information science and statistics. New York City, NY: Springer, 2006.

[7] G. Box and G. Tiao. *Bayesian inference in statistical analysis*. revised new. Wiley Classics Library. Hoboken, NJ: John Wiley & Sons, 2011.

[8] S. Brooks, A. Gelman, G. Jones, and X.-L. Meng. *Handbook of Markov chain Monte Carlo*. Chapman & Hall/CRC handbooks of modern statistical methods. Boca Raton, FL: CRC, 2011.

[9] G. Casella and R. Berger. *Statistical inference*. 2nd ed. Duxbury advanced series in statistics and decision sciences. Pacific Grove, CA: Thomson Learning, 2002.

[10] D. T. Cassidy, M. J. Hamp, and R. Ouyed. "Log Student's t-distribution-based option sensitivities: Greeks for the Gosset formulae". In: *Quantitative Finance* 13.8 (2013), pp. 1289–1302.

[11] D. T. Cassidy, M. J. Hamp, and R. Ouyed. "Pricing European options with a log Student's t-distribution: a Gosset formula". In: *Physica A: Statistical Mechanics and its Applications* 389.24 (2010), pp. 5736–5748.

[12] J. Ching and Y.-C. Chen. "Transitional Markov chain Monte Carlo method for Bayesian model updating, model class selection, and model averaging". In: *Journal of Engineering Mechanics* 133.7 (2007), pp. 816–832.

[13] J. Ching, W.-H. Huang, and K.-K. Phoon. "3D probabilistic site characterization by sparse Bayesian learning". In: *Journal of Engineering Mechanics* 146.12 (2020), p. 04020134.

[14] J. Ching and K.-K. Phoon. "Characterizing uncertain site-specific trend function by sparse Bayesian learning". In: *Journal of Engineering Mechanics* 143.7 (2017), p. 04017028.

[15] J. Ching and J.-S. Wang. "Application of the transitional Markov chain Monte Carlo algorithm to probabilistic site characterization". In: *Engineering Geology* 203 (2016), pp. 151–167.

[16] J. Ching, Z. Yang, and K.-K. Phoon. "Dealing with nonlattice data in three-dimensional probabilistic site characterization". In: *Journal of Engineering Mechanics* 147.5 (2021), p. 06021003.

[17] M. DeGroot. *Optimal Statistical Decisions*. McGraw-Hill series in probability and statistics. New York City, NY: McGraw-Hill, 1969.

[18] P. Del Moral, A. Doucet, and A. Jasra. “Sequential Monte Carlo samplers”. In: *Journal of the Royal Statistical Society: Series B (Statistical Methodology)* 68.3 (2006), pp. 411–436.

[19] O. Ditlevsen, N. J. Tarp-Johansen, and H. Denver. “Bayesian soil assessments combining prior with posterior censored samples”. In: *Computers and Geotechnics* 26.3-4 (2000), pp. 187–198.

[20] *EN 1990:2002. Eurocode 0: basis of structural and geotechnical design*. European Standard, 2002.

[21] A. Gelman, J. Carlin, H. Stern, D. Dunson, A. Vehtari, and D. Rubin. *Bayesian data analysis*. 3rd. Chapman & Hall/CRC texts in statistical science. Boca Raton, FL: CRC, 2013.

[22] S. Geyer, I. Papaioannou, C. Kunz, and D. Straub. “Reliability assessment of large hydraulic structures with spatially distributed measurements”. In: *Structure and Infrastructure Engineering* 16 (4 2020), pp. 599–612.

[23] R. G. Ghanem and P. D. Spanos. *Stochastic finite elements. A spectral approach*. revised. Dover civil and mechanical engineering. Mineola, NY: Dover, 2012.

[24] M. Grigoriu. “Crossings of non-Gaussian translation processes”. In: *Journal of Engineering Mechanics* 110.4 (1984), pp. 610–620.

[25] M. S. Handcock and M. L. Stein. “A Bayesian analysis of kriging”. In: *Technometrics* 35.4 (1993), pp. 403–410.

[26] Y. Hu, T. Zhao, Y. Wang, C. Choi, and C. W. W. Ng. “Direct simulation of two-dimensional isotropic or anisotropic random field from sparse measurement using Bayesian compressive sampling”. In: *Stochastic Environmental Research and Risk Assessment* 33.8 (2019), pp. 1477–1496.

[27] F. V. Jensen and T. D. Nielsen. *Bayesian networks and decision graphs*. 2nd ed. Information science and statistics. New York City, NY: Springer, 2007.

[28] S.-H. Jiang, I. Papaioannou, and D. Straub. “Bayesian updating of slope reliability in spatially variable soils with in-situ measurements”. In: *Engineering Geology* 239 (2018), pp. 310–320.

[29] S. Kotz and S. Nadarajah. *Multivariate t-distributions and their applications*. Cambridge University, 2004.

[30] C.-C. Li and A. D. Kiureghian. “Optimal discretization of random fields”. In: *Journal of Engineering Mechanics* 119.6 (1993), pp. 1136–1154.

[31] P.-L. Liu and A. D. Kiureghian. “Multivariate distribution models with prescribed marginals and covariances”. In: *Probabilistic Engineering Mechanics* 1.2 (1986), pp. 105–112.

[32] Y. Liu, J. Li, S. Sun, and B. Yu. “Advances in Gaussian random field generation: a review”. In: *Computational Geosciences* 23.5 (2019), pp. 1011–1047.

[33] B. Matérn. *Spatial Variation*. Lecture notes in statistics. Springer, 1986.

[34] P. W. Mayne. *Seismic CPT Soundings at ANSS stations. Oct-Nov 2002, June-September 2003*. geosystems.ce.gatech.edu/Faculty/Mayne/Research/sound2003/anssall/index.htm (accessed Mar 09, 2020). 2003.

[35] S. Montoya-Noguera, T. Zhao, Y. Hu, Y. Wang, and K.-K. Phoon. “Simulation of non-stationary non-Gaussian random fields from sparse measurements using Bayesian compressive sampling and Karhunen–Loève expansion”. In: *Structural Safety* 79 (2019), pp. 66–79.

[36] K. P. Murphy. *Machine learning: a probabilistic perspective*. Adaptive computation and machine learning. Cambridge, MA: MIT, 2013.

[37] X. Nie, J. Zhang, H. Huang, Z. Liu, and S. Lacasse. "Scale of Fluctuation for Geotechnical Probabilistic Analysis". In: *Geotechnical Safety and Risk V*. IOS, 2015, pp. 834–840.

[38] I. Papaioannou and D. Straub. "Learning soil parameters and updating geotechnical reliability estimates under spatial variability - theory and application to shallow foundations". In: *Georisk: Assessment and Management of Risk for Engineered Systems and Geohazards* 11.1 (2017), pp. 116–128.

[39] K.-K. Phoon and F. H. Kulhawy. "Characterization of geotechnical variability". In: *Canadian Geotechnical Journal* 36.4 (1999), pp. 612–624.

[40] K.-K. Phoon, S.-T. Quek, and P. An. "Identification of Statistically Homogeneous Soil Layers Using Modified Bartlett Statistics". In: *Journal of Geotechnical and Geoenvironmental Engineering* 129.7 (2003), pp. 649–659.

[41] R. Rackwitz. "Predictive distribution of strength under control". In: *Matériaux et Constructions* 16 (1983), pp. 259–267.

[42] H. Raiffa and R. Schlaifer. *Applied statistical decision theory*. Studies in managerial economics. Cambridge, MA: Division of research, graduate school of business administration, Harvard University, 1961.

[43] C. E. Rasmussen and C. K. I. Williams. *Gaussian processes for machine learning*. Adaptive computation and machine learning. Cambridge, MA: MIT, 2006.

[44] C. P. Robert. *The Bayesian choice: from decision-theoretic foundations to computational implementation*. 2nd ed. New York City, NY: Springer Science+Business Media, 2007.

[45] W. Rudin. *Real and complex analysis*. 3rd ed. Higher mathematics. New York City, NY: McGraw-Hill, 1987.

[46] D. Savvas, I. Papaioannou, and G. Stefanou. "Bayesian identification and model comparison for random property fields derived from material microstructure". In: *Computer Methods in Applied Mechanics and Engineering* 365 (2020), p. 113026.

[47] M. Stein. *Interpolation of spatial data: some theory for kriging*. Springer series in statistics. New York City, NY: Springer, 1999.

[48] D. Straub and I. Papaioannou. "Bayesian updating with structural reliability methods". In: *Journal of Engineering Mechanics* 141.3 (2015), p. 04014134.

[49] F. Uribe, I. Papaioannou, W. Betz, and D. Straub. "Bayesian inference of random fields represented with the Karhunen-Loève expansion". In: *Computer Methods in Applied Mechanics and Engineering* 358 (2020), p. 112632.

[50] L. H. Vanegas and G. A. Paula. "Log-symmetric distributions: statistical properties and parameter estimation". In: *Brazilian Journal of Probability and Statistics* 30.2 (2016), pp. 196–220.

[51] E. Vanmarcke. *Random fields: analysis and synthesis*. Revised and expanded new edition. World Scientific, 2010.

[52] E. H. Vanmarcke. "Probabilistic Modeling of Soil Profiles". In: *Journal of the Geotechnical Engineering Division* 103.11 (1977), pp. 1227–1246.

[53] Y. Wang and T. Zhao. "Statistical interpretation of soil property profiles from sparse data using Bayesian compressive sampling". In: *Géotechnique* 67.6 (2017), pp. 523–536.

[54] Y. Wang, Z. Cao, and D. Li. "Bayesian perspective on geotechnical variability and site characterization". In: *Engineering Geology* 203 (2016), pp. 117–125.

[55] Y. Wang, T. Zhao, Y. Hu, and K.-K. Phoon. "Simulation of random fields with trend from sparse measurements without detrending". In: *Journal of Engineering Mechanics* 145.2 (2019), p. 04018130.

[56] Y. Wang, T. Zhao, and K.-K. Phoon. "Direct simulation of random field samples from sparsely measured geotechnical data with consideration of uncertainty in interpretation". In: *Canadian Geotechnical Journal* 55.6 (2018), pp. 862–880.

[57] A. Westendarp, H. Becker, J. Bödefeld, H. Fleischer, C. Kunz, M. Maisner, H. Müller, A. Rahimi, T. Reschke, and F. Spörel. "Erhaltung und Instandsetzung von massiven Verkehrswasserbauwerken [Maintenance and repair of massive hydraulic structures]". In: *Beton-Kalender 2015*. Hoboken, NJ: John Wiley & Sons, 2014, pp. 185–246.

[58] T. Zhao and Y. Wang. "Simulation of cross-correlated random field samples from sparse measurements using Bayesian compressive sensing". In: *Mechanical Systems and Signal Processing* 112 (2018), pp. 384–400.

[59] H. Zhu and L. Zhang. "Characterizing geotechnical anisotropic spatial variations using random field theory". In: *Canadian Geotechnical Journal* 50.7 (2013), pp. 723–734.

Chapter 6

Spatial modeling of concrete strength based on data

Original publication

S. Geyer, I. Papaioannou, and D. Straub. "Spatial modeling of concrete strength based on data". In: *Structural Safety* 103 (2023), p. 102345. DOI: 10.1016/j.strusafe.2023.102345.

Author's contribution

Sebastian Geyer, Iason Papaioannou, and Daniel Straub developed the concept of spatial modeling of concrete strength with data. The mathematical derivations were carried out by Sebastian Geyer, Iason Papaioannou, and Daniel Straub. Sebastian Geyer wrote the code underlying the numerical studies and carried out all numerical experiments. Sebastian Geyer wrote the original draft of the manuscript, which was then edited and finalized by himself, Iason Papaioannou, and Daniel Straub.

Abstract

Structural verification of concrete structures relies on an underlying probabilistic model of the concrete strength. This concrete strength exhibits a spatial variability, which is of particular relevance in existing concrete structures, for which the strength is assessed based on samples. To accurately account for the spatial variability of the concrete material, a random field modeling approach can be adopted, which includes a spatial correlation function. Unfortunately, the available literature on spatial variability of concrete strength is not sufficient to make an educated choice of this correlation function. In this paper, we propose a hierarchical Bayesian random field model, that enables learning the parameters of a selected correlation function with in-situ spatially distributed measurements of the concrete strength. We propose a correlation function that accounts for the composite nature of the material through distinguishing micro-scale and meso-scale variability. The predictive spatial distribution of the proposed random field model given the spatial data is then obtained through an analytical random field update, resulting in a non-homogeneous random field model with log-Student's t-marginal distribution. The proposed approach provides an effective means to employ in-situ measurements for updating verification predictions of concrete structures. We apply our approach to two case studies on chamber walls of ship locks, where measurements of the concrete strength are available from core samples.

6.1 Introduction

Structural analysis and verification requires the specification of material strength parameters. These parameters are subject to uncertainty, which needs to be accounted for in the analysis. In many instances, a conservative characteristic value of the strength parameter is employed to account for this uncertainty [40, 43, 19]. For the design of new structures, such values are given through the material classification, such as steel grade or concrete strength class [20, 21]. In contrast, the assessment of existing concrete structures typically relies on samples taken from the structure to estimate the characteristic value of the concrete strength [16, 18]. This is done via standardized procedures, which are based on assumptions on the underlying probability distribution model for the concrete strength [18, 19, 6]. These approaches do not account for a potential correlation of the measurements as they assume the samples to be drawn independently from a certain population (the structure of interest) [51, 23]. Neglecting such a correlation leads to approximate results. The extent of the approximation error is case-specific; it is larger in older concretes with higher variability in the concrete strength.

We focus on the assessment of existing structures where concrete strength exhibits higher variability and is commonly assessed based on samples from the actual structure. The corresponding measurement values and their locations provide the basis for a spatial analysis [33]. For these applications, we suggest to model concrete strength as a random field, whereby a random variable is assigned to each position in the structure. The dependence among the random variables at all locations is described by a spatial correlation function [60].

Learning the spatial distribution of material parameters from data has been addressed in other engineering fields, e.g., in particular in geotechnical engineering, due to the comparatively large spatial variability of soil parameters [e.g., 49]. Bayesian methods, such as Bayesian compressive sampling [62, 61, 44] or sparse Bayesian learning [9, 8, 10] have been applied to learn and simulate non-homogeneous random fields from sparse measurements of soil parameters.

An approach to model the concrete strength as a random field has been proposed in the context of the JCSS probabilistic model code [34]. However, this model is not appropriately reflecting the interplay between inter- and intra-site variability. Generally, the existing literature on random field models for concrete strength is rather sparse and has mostly found application in initial studies on structural reliability or response analysis [27, 7] or in investigations of its microstructure [e.g., 30, 54]. An extensive study has been carried out in [41] to investigate the variability of concrete strength within a structure in the context of seismic design of existing structures. Several studies have investigated spatial variability of concrete in the context of deterioration, especially chloride-induced corrosion [55, 48, 36, 38]. Measurements of non-destructive and destructive tests have been used to study the spatial variability of concrete parameters and for inferring the correlation of spatial measurements [47, 64].

Recently, an approach to model concrete strength on multiple hierarchical levels with focus on the hierarchy originating from the construction process has been proposed, where it is suggested to model the variability within a structural component with a random field [57]. In [29], the authors apply a hierarchical random field model to obtain location-specific characteristic values of the concrete strength. Therein, an assumption on the prior correlation function of the concrete strength is made relying on the limited available literature.

The modeling approach in this paper uses Bayesian methods to learn the distribution of the concrete strength through combining measurements with available prior information [25]. It employs the hierarchical modeling approach also used in [29], where not only the spatial variability but also the uncertainty of the distribution parameters is explicitly modeled and learned from the data [28, 51]. Hence, our model accounts for both the intra- and inter-site variability, the latter reflected by the uncertain distribution parameters. To take into account

the nature of concrete as a composite material, a novel spatial correlation model is developed, whose parameters can also be included in the Bayesian learning, hence, circumventing the need for an ad-hoc choice of the spatial correlation function. The resulting predictive random field has log-Student's t-marginal distribution and can be expressed as function of a Gaussian random field through a simple transformation [28]. The derived distribution model can be used in further uncertainty propagation and reliability analyses as well as to compute the spatial distribution of the characteristic value of the concrete strength to be used in structural verification.

The remainder of the paper is structured as follows: Section 6.2 briefly reviews the definition of the concrete compressive strength and its characteristic value, before introducing a hierarchical spatial model and describing the Bayesian learning of its parameters. Section 6.3 applies the methodology to two ship lock data sets, followed by a discussion and interpretation of the obtained results. The analysis of these data sets provides empirical evidence on concrete strength correlation in practice, but also highlights the challenges associated with the use of the spatial model in practice. Section 6.4 gives a brief summary of the results and conclusions. Some additional information on the log-Student's t-distribution are collected in Appendix 6.A.

6.2 Statistical modeling of concrete compressive strength

The strength of concrete depends on different factors, e.g., the water-cement ratio, the size and shape of the included aggregate, used admixtures or the quality of workmanship in the production process [e.g., 24, 34, 3]. The dominating strength parameter of concrete is its compressive strength f_c, which is the focus of this paper. The parameter f_c is used to classify concrete into different concrete classes (grades). In the following, we propose a spatial probabilistic model for f_c, and in Section 6.2.4 we show how the distribution can be learned with measurement data.

6.2.1 Compressive strength of concrete

Concrete is a composite material made of water, cement, aggregate and potential admixtures. After the hardening process, concrete can be divided into two phases, cement matrix and aggregate. Due to the two-phase nature of the concrete material, defining f_c as a point-in-space continuous property is not meaningful. Instead, f_c is defined as the compressive strength of a volume of finite size [22]. f_c depends not only on the compressive strengths of cement matrix and aggregate alone, but also on the quality of the connection between the two phases, which is determined by factors such as the surface of the aggregate and the type of cement [46]. Furthermore, f_c depends on other factors that are not directly related to the material itself, such as the direction of stress or the strain constraint due to size effects [2, 46, 40].

Due to the reasons above, the compressive strength of concrete is assessed in terms of the breaking load on reference specimens that have the shape of a cylinder ($f_{c,\mathrm{cyl}}$) or a cube ($f_{c,\mathrm{cube}}$) [22, 20, 34, 51]. Nowadays, typical cylinder specimen have a height-diameter ratio of 2 (e.g., a height of 300 mm and a diameter of 150 mm) and cube specimen have an edge length of 150 mm [22]. Cubical specimen are mostly used for verifications during the construction process as part of the quality control process. In contrast, cylindrical specimen are typically used in verifications of existing structures based on core samples taken from the structure. Classification of concrete into different strength classes is done with respect to requirements for $f_{c,\mathrm{cyl}}$ and $f_{c,\mathrm{cube}}$ [20]. The structural verification format of the Eurocode series is based on $f_{c,\mathrm{cyl}}$ as the critical parameter for all verifications regarding compression [20]. This paper focuses on modeling the concrete strength of existing structures and thus we employ $f_{c,\mathrm{cyl}}$ to denote the in-situ concrete strength.

Depending on the application at hand, the structural resistance R can differ from $f_{c,\mathrm{cyl}}$, e.g., when accounting for size effects [e.g., 2, 40] or when $f_{c,\mathrm{cyl}}$ is used to infer other concrete

parameters. In these cases, R is a function of $f_{c,\mathrm{cyl}}$, which will introduce additional uncertainty into the model. However, the focus of this paper lies on the probabilistic model of $f_{c,\mathrm{cyl}}$ and such uncertainty is not further investigated.

To improve readability, f_c denotes the compressive strength of a cylindrical core sample for the remainder of this paper.

6.2.2 Characteristic values of the concrete strength

Standardized verification formats rely on characteristic values $f_{c,\mathrm{k}}$ of the concrete strength. Characteristic values are generally defined as $p-$quantile values of an underlying probabilistic model, where p depends on the property and the type of analysis. The $5\%-$quantile value is typically chosen as characteristic value for the concrete compressive strength [19]:

$$f_{c,\mathrm{k}} = F_{f_c}^{-1}(p) = F_{f_c}^{-1}(0.05), \tag{6.1}$$

where $F_{f_c}^{-1}(\cdot)$ is the inverse cumulative distribution function (CDF) of the concrete compressive strength.

When strength data from in-situ concrete samples are available, they can be used to estimate the characteristic value $f_{c,\mathrm{k}}$. Different approaches have been developed and established in the engineering community to estimate $f_{c,\mathrm{k}}$ from data of in-situ concrete samples. The most common ones are based on sample moment estimates, i.e., the mean and variance of the samples, which are further used to obtain the characteristic value based on tabulated values [19, 18, 6]. While the approach in [6] is based on a frequentist perspective [23], the method in [19] and [18] relies on the Bayesian approach [51, 27, 28].

These approaches only require the number of measurements n_m and the measurement values and do not account for the spatial locations of the measurements. Moreover, they do not differentiate between the concrete strength of a standardized cylinder and the in-situ structural resistance. However, some prerequisites have to be fulfilled for their application: the measurements must be statistically independent, they have to be taken randomly in space and the sample size needs to be representative for the quantity of interest [51, 23]. While the last condition is assumed to be fulfilled by requiring a minimum number of samples for a given structure (depending on the size of the structure) [18], little attention is paid to the other two conditions in practice and these conditions are commonly violated. For example, in many instances multiple samples are taken from the same drilling core and sample locations are selected based on the perceived criticality or importance of the material or location. Local clustering of data in limited areas of the structure can lead to erroneous estimates of the variability of the quantity of interest and, hence, an erroneous estimate of its characteristic value. In order to obtain an accurate estimate, it is important to explicitly account for the locations of the samples. To explicitly consider these locations, the spatial variability of the concrete material should be modeled by a random field model.

6.2.3 Hierarchical random field model

Material parameters that vary randomly in space, such as the strength of concrete f_c, can be modeled by random fields. A random field (RF) represents a random variable at every point $\boldsymbol{z}$ in the spatial domain Ω [60]. In practice, the probabilistic description of the RF is parameterized in a way that enables its definition through a finite set of parameters $\boldsymbol{\Theta}$, the parameters of the marginal RF distribution, and a spatial correlation function $\rho(\boldsymbol{z}, \boldsymbol{z}')$. In hierarchical random field models, the parameters in $\boldsymbol{\Theta}$ are modeled by random variables described by a probability density function (PDF) $f(\boldsymbol{\theta})$. Such a modeling approach enables distinguishing two different types

of uncertainty: (i) the uncertainty associated with the parameters of the spatial distribution of the material property, and (ii) the spatial variability of the property for fixed parameters. Uncertainty (i) is related to the inter-structure variability, i.e., the variability of the material property when comparing different structures, whereas uncertainty (ii) represents the intra-structure variability, i.e., the variability of the property when comparing different locations within a specific structure. Examples of hierarchical random field models in the context of probabilistic material modeling can be found in [34, 51, 35]. In the following, we describe the two types of uncertainty in detail and set up a hierarchical RF model for f_c.

6.2.3.1 Intra-structure variability

The intra-structure spatial variability is modeled by a random field, which is a collection of random variables indexed by a continuous spatial coordinate $\boldsymbol{z} \in \Omega$ [60]. To completely define the RF $f_c(\boldsymbol{z})$, one needs to specify the joint distribution of the random variables corresponding to any selection of points in Ω. If this joint distribution is the multivariate Gaussian distribution for any collection of points, the corresponding RF is a Gaussian RF [1]. The use of a Gaussian RF is beneficial in practice due to its simple definition and the numerous computational advantages of the Gaussian distribution, which facilitate the numerical treatment of RFs, i.e., their representation in terms of a finite number of RVs [56, 39]. An RF is said to be homogeneous, if the marginal distribution is space-invariant and the joint distribution is invariant to a shift in $\boldsymbol{z}$.

If the quantity of interest is non-Gaussian, it is a common practice to define the corresponding RF as function of a zero-mean and unit-variance Gaussian RF $U(\boldsymbol{z})$ to simplify its application in practice. This type of non-Gaussian RF is termed translation RF and can be defined through the following marginal transformation [31, 37]:

$$X(\boldsymbol{z}) = F^{-1}_{X(\boldsymbol{z})|\boldsymbol{\theta}}(\Phi(U(\boldsymbol{z}))), \tag{6.2}$$

where $F^{-1}_{X(\boldsymbol{z})|\boldsymbol{\theta}}(\cdot)$ is the inverse CDF of $X(\boldsymbol{z})$ conditional on the realization $\boldsymbol{\theta}$ of $\boldsymbol{\Theta}$ and $\Phi(\cdot)$ is the CDF of the standard normal distribution.

The assumption that f_c follows a normal or lognormal distribution has been accepted and applied for many years [e.g., 53, 58, 43]. The lognormal distribution is more appropriate in cases of low concrete strengths or/and large variability of the concrete strength, since it is only defined for non-negative values and, thus, cannot result in a negative characteristic value. We limit ourselves to the lognormal model, for which the transformation of Equation (6.2) in the case of a homogeneous RF is

$$f_c(\boldsymbol{z}) = \exp\left(\mu_{f_{c,\ln}} + \lambda_{f_{c,\ln}}^{-\frac{1}{2}} U(\boldsymbol{z})\right). \tag{6.3}$$

The parameters $\boldsymbol{\Theta} = [\mu_{f_{c,\ln}}, \lambda_{f_{c,\ln}}]$ are the mean value $\mu_{f_{c,\ln}}$ and precision $\lambda_{f_{c,\ln}}$ of $\ln(f_c)$, where $\lambda_{f_{c,\ln}}$ is the inverse of the variance. Using Equation (6.3), the spatial variability of $f_c(\boldsymbol{z})$ is implicitly modeled through the spatial variability of the underlying RF $U(\boldsymbol{z})$ and, thus, $f_c(\boldsymbol{z})$ is fully defined by the parameters of its marginal distribution and $U(\boldsymbol{z})$.

To model the spatial variability, one needs to account for spatial correlation of different locations in a structure. The correlation between f_c at two locations $\boldsymbol{z}$ and $\boldsymbol{z}'$ is defined by the spatial correlation function $\rho(\boldsymbol{z}, \boldsymbol{z}')$.

When modeling spatial variability of concrete, one can distinguish between two types of spatial variability, related to two different spatial scales. The first type represents the spatial variability at the meso-scale, where the two phases of the concrete are not explicitly considered.

Reasons for this type of variability are different concrete batches, local clustering of aggregate or admixtures, decomposition through the vibration procedure, voids and factors related to the construction process. The second type is the micro-scale variability of concrete, which is caused by the composite nature of concrete. The effect of this type of spatial variability is restricted to a small area and wears off relatively fast. Figure 6.1 illustrates the two types of spatial variability through a potential realization of f_c in a one-dimensional concrete element of 10 m length (e.g., a core sample). On the one hand, $f_c(z)$ shows fluctuations over short distances due to the micro-scale variability. On the other hand, regions of rather large values of f_c (e.g., on the left side of the plot) and rather small values of f_c (in the center of the plot) can be detected due to the meso-scale variability.

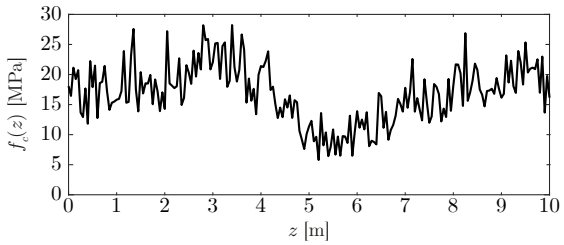

Figure 6.1: Illustration of the spatial behavior of f_c, combining the effects from micro-scale and meso-scale spatial variability.

As the spatial variability of f_c is affected by micro-scale and meso-scale variability, the correlation function $\rho(\boldsymbol{z}, \boldsymbol{z}')$ needs to consider both effects. This can be done by defining $\rho(\boldsymbol{z}, \boldsymbol{z}')$ as combination of two correlation functions:

$$\rho(\boldsymbol{z}, \boldsymbol{z}') = \gamma_{\text{micro}} \cdot \rho_{\text{micro}}(\boldsymbol{z}, \boldsymbol{z}') + (1 - \gamma_{\text{micro}}) \cdot \rho_{\text{meso}}(\boldsymbol{z}, \boldsymbol{z}'), \tag{6.4}$$

where $\gamma_{\text{micro}} \in [0, 1]$ is the share of correlation associated with the micro-scale variability, $\rho_{\text{micro}}(\boldsymbol{z}, \boldsymbol{z}')$ and $\rho_{\text{meso}}(\boldsymbol{z}, \boldsymbol{z}')$ are the spatial correlation functions for the micro- and meso-scale variability, respectively. An example of such a correlation model is given in Figure 6.2. The rapid decrease of $\rho(\boldsymbol{z}, \boldsymbol{z}')$ from 1 to values close to $1 - \gamma_{\text{micro}}$ for small distances $\Delta(\boldsymbol{z}, \boldsymbol{z}')$ between $\boldsymbol{z}$ and $\boldsymbol{z}'$ shows the immediate effect of the micro-scale variability on the spatial correlation. The effect of the meso-scale variability becomes apparent with increasing $\Delta(\boldsymbol{z}, \boldsymbol{z}')$.

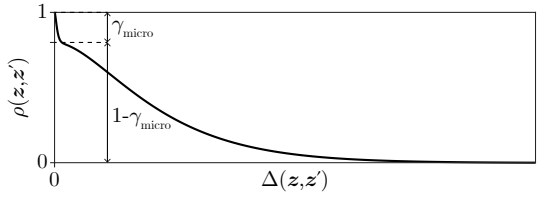

Figure 6.2: Spatial correlation function $\rho(\boldsymbol{z}, \boldsymbol{z}')$ combining the effect of micro-scale variability and meso-scale variability as function of the spatial distance $\Delta(\boldsymbol{z}, \boldsymbol{z}')$.

Different parametric models exist for the correlation function. We restrict the range of possible correlation models for the meso-scale variability to the Matérn correlation model $\rho_\nu(\boldsymbol{z}, \boldsymbol{z}')$, which is chosen due to its flexibility. It is defined as follows [42, 1]:

$$\rho_\nu(\boldsymbol{z}, \boldsymbol{z}') = \frac{2^{1-\nu}}{\Gamma(\nu)} \left(\sqrt{2\nu}\ \Delta_{\text{w}}(\boldsymbol{z}, \boldsymbol{z}')\right)^\nu K_\nu \left(\sqrt{2\nu}\ \Delta_{\text{w}}(\boldsymbol{z}, \boldsymbol{z}')\right), \tag{6.5}$$

where $\Gamma(\cdot)$ is the gamma function, $K_\nu(\cdot)$ is the modified Bessel function of the second kind and order ν, and $\Delta_{\text{w}}(\boldsymbol{z}, \boldsymbol{z}')$ is the weighted distance of $\boldsymbol{z}$ and $\boldsymbol{z}'$. In case of an isotropic spatial

correlation structure, i.e., all directions are weighted equally, $\Delta_{\mathrm{w}}(\boldsymbol{z},\boldsymbol{z}') = \frac{\Delta(\boldsymbol{z},\boldsymbol{z}')}{L_c}$, where $\Delta(\boldsymbol{z},\boldsymbol{z}')$ is the Euclidean distance $||\boldsymbol{z}-\boldsymbol{z}'||_2$. L_c is the correlation length determining the decrease of the correlation function. Large values of L_c correspond to a slow decay of $\rho_\nu(\boldsymbol{z},\boldsymbol{z}')$ with increasing $\Delta(\boldsymbol{z},\boldsymbol{z}')$, whereas small values of L_c indicate a fast decay of $\rho_\nu(\boldsymbol{z},\boldsymbol{z}')$ with increasing $\Delta(\boldsymbol{z},\boldsymbol{z}')$. The smoothness of $\rho_\nu(\boldsymbol{z},\boldsymbol{z}')$ is determined by the smoothness parameter ν. For half-integer values of ν, $\rho_\nu(\boldsymbol{z},\boldsymbol{z}')$ reduces to the product of an exponential term and a polynomial term [42]. It is noted that for $\nu = \frac{1}{2}$, Equation (6.5) reduces to the exponential correlation model, whereas for $\nu \to \infty$, it converges to the square-exponential correlation model:

$$\rho_{\frac{1}{2}}(\boldsymbol{z},\boldsymbol{z}') = \exp\left(-\Delta_{\mathrm{w}}(\boldsymbol{z},\boldsymbol{z}')\right), \tag{6.6}$$

$$\rho_{\infty}(\boldsymbol{z},\boldsymbol{z}') = \exp\left(-\frac{1}{2}\Delta_{\mathrm{w}}(\boldsymbol{z},\boldsymbol{z}')^2\right). \tag{6.7}$$

Concrete structures, especially massive structures, are typically built in blocks or layers. Hence, a transverse anisotropic correlation function is employed to distinguish between spatial directions [65]. This results in different correlation lengths $L_{c,i},\ i = 1,\dots d$, where d is the number of spatial dimensions (i.e., 1, 2 or 3). The vector $\boldsymbol{L_c}$ collects all correlation lengths. In this case, $\Delta_{\mathrm{w}}(\boldsymbol{z},\boldsymbol{z}')$ in Equation (6.5) is calculated as follows:

$$\Delta_{\mathrm{w}}(\boldsymbol{z},\boldsymbol{z}') = \sqrt{\sum_{i=1}^{d}\left(\frac{\Delta_i(\boldsymbol{z},\boldsymbol{z}')}{L_{c,i}}\right)^2}, \tag{6.8}$$

where $\Delta_i(\boldsymbol{z},\boldsymbol{z}')$ denotes the spatial distance of $\boldsymbol{z}$ and $\boldsymbol{z}'$ in spatial direction i.

The spatial correlation function $\rho(\boldsymbol{z},\boldsymbol{z}')$ defines the correlation of any two points $\{\boldsymbol{z},\ \boldsymbol{z}'\} \in \Omega$ and considers the effect of both the spatial variability on the meso-scale and on the micro-scale. In Section 6.2.4, we discuss how to employ data in learning the parameters of $\rho(\boldsymbol{z},\boldsymbol{z}')$. Due

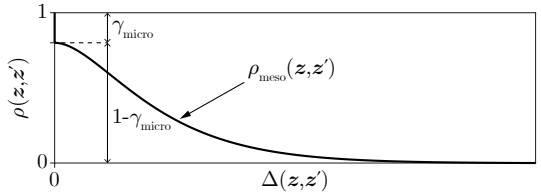

Figure 6.3: Approximation of spatial correlation function, where the effect of micro-scale variability is approximated by a Dirac function.

to the spatial dimension of the cylindrical specimen, it is impossible to learn the parameters of the micro-scale correlation function $\rho_{\mathrm{micro}}(\boldsymbol{z},\boldsymbol{z}')$ in practice. However, its exact shape is also not important for predicting the resulting strength of a structure. We therefore propose to approximate the micro-scale correlation by a Dirac delta function and Equation (6.4) thus reduces to

$$\rho(\boldsymbol{z},\boldsymbol{z}') = \gamma_{\mathrm{micro}} \cdot \delta_{\boldsymbol{z},\boldsymbol{z}'} + (1-\gamma_{\mathrm{micro}}) \cdot \rho_{\mathrm{meso}}(\boldsymbol{z},\boldsymbol{z}'), \tag{6.9}$$

where $\delta_{\boldsymbol{z},\boldsymbol{z}'}$ is the Dirac delta function returning 1 if $\boldsymbol{z} = \boldsymbol{z}'$ and 0 else. Figure 6.3 illustrates the approximated correlation function with a jump of $\rho(\boldsymbol{z},\boldsymbol{z}')$ from 1 to $1-\gamma_{\mathrm{micro}}$ when $\Delta_{\boldsymbol{z},\boldsymbol{z}'} > 0$ to account for the effect of the micro-scale variability on the spatial correlation. Approximating the micro-scale correlation by a Dirac function reduces the number of unknown model parameters and only affects the micro-scale variability. The effect of this assumption on the resulting estimate of the concrete strength is negligible.

When using Equation (6.9) to model an RF, the RF can be expressed as superposition of two random fields, one of which with correlation function $\rho_{\text{meso}}(\boldsymbol{z}, \boldsymbol{z}')$ and an additional noise RF without spatial correlation. Note that this leads to a discontinuous sample path when drawing random realizations of the RF.

6.2.3.2 Inter-structure variability

Inter-structure variability leads to uncertainty of the overall material property at a specific structure or site. This uncertainty is at the top level of the hierarchical RF model of the concrete strength f_c [34]. It is modeled by the marginal random field parameters $\boldsymbol{\Theta}$ with joint PDF $f(\boldsymbol{\theta})$. $\boldsymbol{\Theta}$ are the mean and the precision of f_c in a specific structure.

Figure 6.4 illustrates the hierarchical RF model for the concrete compressive strength $f_c(\boldsymbol{z})$ including the macro-scale variability and the chosen spatial correlation function $\rho(\boldsymbol{z}, \boldsymbol{z}')$. Four random realizations of $f_c(\boldsymbol{z})$ are plotted at the bottom of the figure. The corresponding realizations of $\boldsymbol{\Theta}$ and choices of $\rho(\boldsymbol{z}, \boldsymbol{z}')$ are indicated in the respective colors.

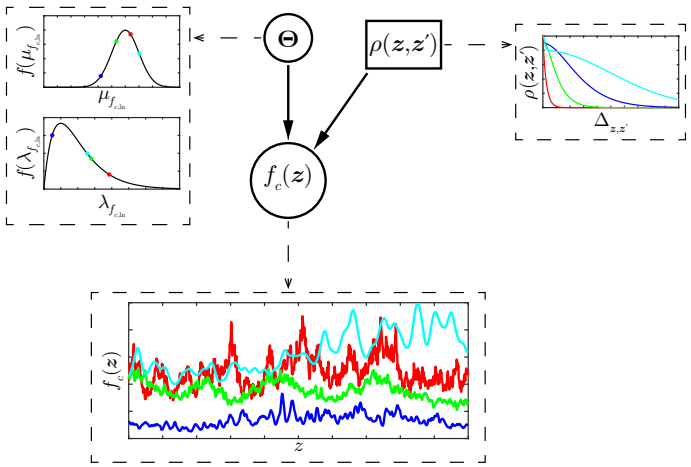

Figure 6.4: Hierarchical model of the in-situ concrete compressive strength modeled as random field $f_c(\boldsymbol{z})$ with spatial correlation function $\rho(\boldsymbol{z}, \boldsymbol{z}')$. The four colors correspond to four random realizations of $f_c(\boldsymbol{z})$ and $f_c(\boldsymbol{z})$ and choices of $\rho(\boldsymbol{z}, \boldsymbol{z}')$.

6.2.4 Learning the random field model from data

Measurements of the in-situ concrete strength form an important part of structural verification of existing structures. Although non-destructive test techniques can be used to get indirect measurements of the concrete strength (e.g., testing with a rebound hammer [15] or measurements of the ultrasonic pulse velocity [17]), the most accurate results are obtained by taking core samples from the structure and directly testing the concrete strength of standardized cylindrical specimen [16, 18]. Especially for the verification of existing massive concrete structures, taking core samples is essential for getting detailed information on the concrete properties [63]. The number of core samples as well as their orientation depends on the investigated structure and the aim of the investigation [6, 18]. Standardized specimen are visually selected from the available drilling cores before being extracted, prepared and tested to determine their concrete compressive strength.

6.2.4.1 Data uncertainty

In-situ data is subject to uncertainty associated with the measured value (measurement uncertainty) and - if the measurements are not properly documented - the location of the measurement (position uncertainty).

There are different sources of measurement uncertainty; some are related to the measurement procedure (e.g., the laboratory operator or the measurement device [33]), others stem from an underlying transformation (e.g., when inferring the splitting tensile strength via the indirect tensile strength test [14] or from the conversion of cylindrical core samples with small diameters [18]). Contrary to the field of geotechnical engineering, where probabilistic models have been developed to account for this measurement uncertainty [e.g., 49], only little attention is paid to it in structural engineering applications. The measurement outcomes of concrete samples from drilling cores are typically set equal to the in-situ concrete parameters, as long as the test specimen fulfills certain requirements [18]. The only exception to this rule is the case of outliers, which are eliminated using outlier tests [e.g., 32, 13].

The main reason for position uncertainty is the lack of documentation, since information about the exact measurement location is not required in standard methods for estimating characteristic values [19, 18, 6]. Position uncertainty can hinder the applicability of a spatial analysis.

6.2.4.2 Bayesian random field update

The hierarchical RF model of Section 6.2.3 forms the basis for explicitly including the spatial locations of the data in learning the distribution parameters and the predictive spatial distribution of f_c. In the following, we summarize a Bayesian approach to learn the RF and its parameters based on [28]. The approach reduces to the Bayesian approach for calculating characteristic values in [19] for specific parameter choices [28].

It is assumed that measurement data $\mathbf{M}$ is available from cylindrical specimen extracted from core samples of an existing concrete structure. $\mathbf{M} = [\boldsymbol{x}_m, \mathbf{Z}_m]$, where $\boldsymbol{x}_m = [x_{m,1}, x_{m,2}, \dots, x_{m,n}]^\mathsf{T}$ are the n_m measurement outcomes and $\mathbf{Z}_m = [\boldsymbol{z}_{m,1}, \boldsymbol{z}_{m,2}, \dots, \boldsymbol{z}_{m,n}]^\mathsf{T}$ the corresponding locations. Figure 6.5 extends the hierarchical RF model of Figure 6.4 by including the data $\mathbf{M}$ associated with measurement uncertainty ε.

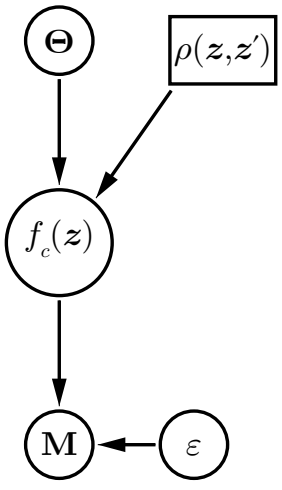

Figure 6.5: Hierarchical random field model for learning the in-situ concrete compressive strength $f_c(\boldsymbol{z})$ from data $\mathbf{M}$ of standardized cylindrical samples taken from the structure. The measurements in $\mathbf{M}$ are associated with measurement uncertainty ε.

Due to the hierarchical modeling approach, the updating needs to be done in two steps. The data $\mathbf{M}$ is included in a first step to update the distribution of $\boldsymbol{\Theta}$, by application of Bayes' rule [25]:

$$f(\boldsymbol{\theta}|\mathbf{M}) \propto f(\boldsymbol{\theta}) \cdot \mathrm{L}(\boldsymbol{\theta}|\mathbf{M}), \tag{6.10}$$

where $f(\boldsymbol{\theta})$ is the prior distribution of $\boldsymbol{\Theta}$ and $f(\boldsymbol{\theta}|\mathbf{M})$ is the posterior distribution of $\boldsymbol{\Theta}$ given the data $\mathbf{M}$, which enters the model via the likelihood function $\mathrm{L}(\boldsymbol{\theta}|\mathbf{M})$. $f(\boldsymbol{\theta}|\mathbf{M})$ can then be used in a second updating step to find the spatial posterior predictive distribution of $f_c(\boldsymbol{z})$. In the general case, the posterior distribution in Equation (6.10) needs to be approximated numerically, e.g., through Markov chain Monte Carlo (MCMC) methods [e.g., 5]. For certain cases, however, closed-form expressions can be found for updating the hierarchical RF model. The following modeling choices are made in order to enable such a closed-form update [12, 51, 28]:

i) The marginal distribution of $f_c(\boldsymbol{z})$ is a lognormal distribution, which is the standard choice for concrete strength in the literature [e.g., 43]. Then, $f_{c,\ln}(\boldsymbol{z}) = \ln\left(f_c(\boldsymbol{z})\right)$ follows a normal distribution with mean function $\mu_{f_{c,\ln}}(\boldsymbol{z})$ and precision function $\lambda_{f_{c,\ln}}(\boldsymbol{z})$. The hierarchical modeling and updating process is done for the corresponding RF $f_{c,\ln}(\boldsymbol{z})$, a Gaussian RF completely defined by its spatial functions for the mean $\mu_{f_{c,\ln}}(\boldsymbol{z})$, the precision $\lambda_{f_{c,\ln}}(\boldsymbol{z})$ and the autocorrelation function $\rho(\boldsymbol{z}, \boldsymbol{z}')$ (cf. Section 6.2.3.1).

ii) Before including site-specific information, $f_{c,\ln}(\boldsymbol{z})$ is assumed to be homogeneous, i.e., the spatial moments are space-invariant and the spatial correlation is a function of the difference in location. That is, $\mu_{f_{c,\ln}}(\boldsymbol{z}) = \mu_{f_{c,\ln}} \; \forall \; \boldsymbol{z} \in \Omega$ and $\lambda_{f_{c,\ln}}(\boldsymbol{z}) = \lambda_{f_{c,\ln}} \; \forall \; \boldsymbol{z} \in \Omega$. $\rho(\boldsymbol{z}, \boldsymbol{z}')$ is defined according to Equation (6.9) with $\rho_{\mathrm{meso}}(\boldsymbol{z}, \boldsymbol{z}')$ given by the Matérn model of Equation (6.5).

iii) The prior distribution of $\boldsymbol{\Theta} = [\mu_{f_{c,\ln}}, \lambda_{f_{c,\ln}}]^{\mathsf{T}}$, $f(\boldsymbol{\theta})$ is modeled with a normal-gamma ($\mathcal{NG}$) distribution, where $\lambda_{f_{c,\ln}}$ follows a gamma distribution and $\mu_{f_{c,\ln}}$ follows a normal distribution conditional on $\lambda_{f_{c,\ln}}$[51]. It covers a broad range of possible prior distributions, including a non-informative prior distribution when no prior information is available [12].

iv) The measurement uncertainty is defined through a multiplicative error, i.e., the measurement outcome $f_{c,m,i}$ at location $\boldsymbol{z}_{m,i}$ is given as

$$f_{c,m,i} = f_c(\boldsymbol{z}_{m,i}) \cdot \varepsilon_i. \tag{6.11}$$

The ε_i are modeled as independent lognormal random variables with median 1. To retain the analytical form of the update, it is necessary to account for the measurement error in the correlation function. This results in a modified correlation function that takes an identical form as Equation (6.9), i.e,

$$\rho_{\mathrm{mod}}(\boldsymbol{z}, \boldsymbol{z}') = \gamma \cdot \delta_{\boldsymbol{z},\boldsymbol{z}'} + (1 - \gamma) \cdot \rho_{\mathrm{meso}}(\boldsymbol{z}, \boldsymbol{z}'), \tag{6.12}$$

where $\gamma \in [0, 1]$ lumps the contribution of both micro-scale variability and measurement error into a single factor [28]. $\gamma = \gamma_{\mathrm{micro}} + \gamma_\varepsilon - \gamma_{\mathrm{micro}}\gamma_\varepsilon$, where $\gamma_\varepsilon \in [0, 1]$ is the contribution of the measurement error. We work with the lumped factor γ because a distinction of the contribution of the individual effects is not possible based on spatial data.

Note that assumptions i) and iii) are in line with the theory underlying the standardized approach to estimate characteristic values from data in the Eurocode [19]. Assumption ii) is not strictly required for the method but it is reasonable to assume homogeneity of the prior random field and the assumption reduces the number of unknown model parameters.

Using the assumptions above, the posterior predictive RF for $f_c(\boldsymbol{z})$ has log-Student's t-marginal distribution [59]. A log-Student's t-RF is parameterized in terms of the spatial functions for the parameters of the underlying Student's t-RF given by the following equations [28]:

$$\mu_t(\boldsymbol{z}) = \mu_n + \boldsymbol{R}_{\boldsymbol{z},m}\mathbf{R}_m^{-1}(\boldsymbol{x}_m - \mu_n\mathbf{1}_n)^\mathsf{T}, \tag{6.13}$$

$$\lambda_t(\boldsymbol{z}_1,\boldsymbol{z}_2) = \frac{\alpha_n}{\beta_n}\left(\rho(\boldsymbol{z}_1,\boldsymbol{z}_2) - \boldsymbol{R}_{\boldsymbol{z}_1,m}\mathbf{R}_m^{-1}\boldsymbol{R}_{\boldsymbol{z}_2,m}^\mathsf{T} + (1-\boldsymbol{R}_{\boldsymbol{z}_1,m}\mathbf{R}_m^{-1}\mathbf{1}_n^\mathsf{T})\kappa_n^{-1}(1-\boldsymbol{R}_{\boldsymbol{z}_2,m}\mathbf{R}_m^{-1}\mathbf{1}_n^\mathsf{T})\right)^{-1}, \tag{6.14}$$

$$\nu_t = 2\alpha_n. \tag{6.15}$$

$\boldsymbol{R}_{\boldsymbol{z},m} : \mathbb{R}^d \to \mathbb{R}^{1\times n_m}$ is a row vector function with element i defined as $\rho_{\text{mod}}(\boldsymbol{z},\boldsymbol{z}_{m,i})$ and the parameters μ_n, κ_n, α_n and β_n are given as [28]

$$\mu_n = \frac{\kappa_0\mu_0 + \mathbf{1}_n\mathbf{R}_m^{-1}\boldsymbol{x}_m^\mathsf{T}}{\kappa_0 + \mathbf{1}_n\mathbf{R}_m^{-1}\mathbf{1}_n^\mathsf{T}}, \tag{6.16}$$

$$\kappa_n = \kappa_0 + \mathbf{1}_n\mathbf{R}_m^{-1}\mathbf{1}_n^\mathsf{T}, \tag{6.17}$$

$$\alpha_n = \alpha_0 + \frac{n_m}{2}, \tag{6.18}$$

$$\beta_n = \beta_0 + \frac{1}{2}\left(\boldsymbol{x}_m\mathbf{R}_m^{-1}\boldsymbol{x}_m^\mathsf{T} + \frac{\kappa_0\mu_0^2\mathbf{1}_n\mathbf{R}_m^{-1}\mathbf{1}_n^\mathsf{T} - 2\kappa_0\mu_0\mathbf{1}_n\mathbf{R}_m^{-1}\boldsymbol{x}_m^\mathsf{T} - (\mathbf{1}_n\mathbf{R}_m^{-1}\boldsymbol{x}_m^\mathsf{T})^2}{\kappa_0 + \mathbf{1}_n\mathbf{R}_m^{-1}\mathbf{1}_n^\mathsf{T}}\right). \tag{6.19}$$

$\mathbf{1}_n$ denotes a $1\times n_m$-vector of ones and $\mathbf{R}_m$ is the $n_m \times n_m$ correlation matrix of the measurement locations, where element (i,j) is defined as $\rho_{\text{mod}}(\boldsymbol{z}_{m,i},\boldsymbol{z}_{m,j})$. μ_0, κ_0, α_0 and β_0 are the parameters of the prior $\mathcal{NG}$ distribution $f(\boldsymbol{\theta})$. Appendix 6.A gives the PDF and CDF of the log-Student's t-distribution. Random realizations of the posterior predictive RF with log-Student's t-marginal distribution can be obtained by expressing the RF as function of a Gaussian RF and one additional random variable which follows the chi-square distribution [28]. A variety of methods are available for sampling from the resulting Gaussian RF [e.g., 39].

6.2.4.3 Learning the correlation model

The closed-form update in Section 6.2.4.2 is valid for a fixed correlation function $\rho_{\text{mod}}(\boldsymbol{z},\boldsymbol{z}')$. However, $\rho_{\text{mod}}(\boldsymbol{z},\boldsymbol{z}')$ is typically not known in practical applications and, hence, is treated as uncertain model input with parameter vector $\mathbf{T}$. $\mathbf{T} = [\gamma,\nu,\boldsymbol{L_c}]$ includes the meso-scale (with the transverse anisotropic Matérn model) and micro-scale variability (approximated by a Dirac function) for the hierarchical RF model (cf. Section 6.2.3.1) as well as the measurement uncertainty ε, which is included in $\rho_{\text{mod}}(\boldsymbol{z},\boldsymbol{z}')$ through γ. Figure 6.6 illustrates the extended hierarchical RF model when the parameters of $\rho_{\text{mod}}(\boldsymbol{z},\boldsymbol{z}')$ are treated as random vector.

Bayes' theorem can be used to learn the posterior distribution of the correlation parameters from the data:

$$f(\boldsymbol{\tau}|\mathbf{M}) \propto f(\boldsymbol{\tau})\cdot f(\mathbf{M}|\boldsymbol{\tau}). \tag{6.20}$$

The specific model choices of Section 6.2.4.2 lead to the following expression for $f(\mathbf{M}|\boldsymbol{\tau})$ [28]:

$$f(\mathbf{M}|\boldsymbol{\tau}) = \left(\frac{\kappa_0}{\kappa_n(\boldsymbol{\tau})}\right)^{\frac{1}{2}} \frac{\Gamma(\alpha_n)\beta_0^{\alpha_0}}{\Gamma(\alpha_0)(\beta_n(\boldsymbol{\tau}))^{\alpha_n}}(2\pi)^{-\frac{n}{2}}\det(\mathbf{R}_m(\boldsymbol{\tau}))^{-\frac{1}{2}}, \tag{6.21}$$

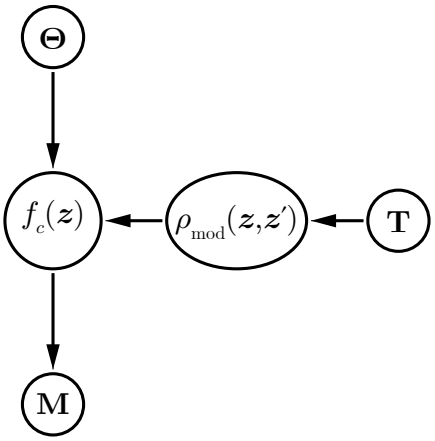

Figure 6.6: Hierarchical random field model for learning the in-situ concrete compressive strength $f_c(\boldsymbol{z})$ from data $\mathbf{M}$ with uncertain correlation model $\rho_{\text{mod}}(\boldsymbol{z},\boldsymbol{z}')$ with model parameters $\mathbf{T}$.

where $\kappa_n(\boldsymbol{\tau})$, α_n, $\beta_n(\boldsymbol{\tau})$ and $\mathbf{R}_m(\boldsymbol{\tau})$ follow the definitions in Section 6.2.4.2 conditional on the chosen correlation model parameters.

The maximum a-posteriori (MAP) estimate can be employed to learn a point estimate of the correlation parameters from the data $\mathbf{M}$ [45]. That is, instead of inferring the full posterior distribution $f(\boldsymbol{\tau}|\mathbf{M})$, it is approximated by its mode, $\boldsymbol{\tau}^*$. This is done by solving the following optimization problem [28]:

$$\boldsymbol{\tau}^* = \arg\min_{\boldsymbol{\tau}\in\mathbf{T}} \ln(\kappa_n(\boldsymbol{\tau})) + 2\alpha_n \ln(\beta_n(\boldsymbol{\tau})) + \ln(\det(\mathbf{R}_m(\boldsymbol{\tau}))) - 2\ln(f(\boldsymbol{\tau})), \tag{6.22}$$

where $f(\boldsymbol{\tau})$ is the prior distribution of $\mathbf{T}$. $\boldsymbol{\tau}^*$ is equivalent to the maximum likelihood estimate of $\mathbf{T}$ in the case of a uniform prior distribution $f(\boldsymbol{\tau})$ [52]. After selecting the correlation model, the RF model can be learned from $\mathbf{M}$ as described in Section 6.2.4.2.

Alternatively, the posterior mean $\boldsymbol{\mu}_{\mathbf{T}|\mathbf{M}}$ can be used as an approximation for $\mathbf{T}$ given $\mathbf{M}$. Unlike the MAP estimate, the posterior mean is not dominated by local extrema of the posterior distribution. Given $n_{\mathbf{T}}$ unknown correlation parameters in the vector $\mathbf{T}$, the marginal posterior mean of T_i, $i = 1,\dots,n_{\mathbf{T}}$ is given as

$$\mu_{T_i|\mathbf{M}} = \mathrm{E}\left[T_i|\mathbf{M}\right] = \frac{1}{\mathcal{C}_{\mathbf{T}}} \int_{\mathbf{T}} \tau_i f(\boldsymbol{\tau}) f(\mathbf{M}|\boldsymbol{\tau}) \mathrm{d}\boldsymbol{\tau}, \tag{6.23}$$

where $\mathcal{C}_{\mathbf{T}}$ is the following normalization constant:

$$\mathcal{C}_{\mathbf{T}} = \int_{\mathbf{T}} f(\boldsymbol{\tau}) f(\mathbf{M}|\boldsymbol{\tau}) \mathrm{d}\boldsymbol{\tau}. \tag{6.24}$$

If a point-estimate of $\mathbf{T}$ is not sufficient, the analytical update to learn the posterior predictive model for the concrete strength is not sufficient. However, it can be approximated numerically, e.g., by means of MCMC algorithms [5]. The analytical update is employed in generating samples from $f(\boldsymbol{\tau}|\mathbf{M})$, which are then used to approximate the posterior predictive distribution. The point-wise marginal posterior predictive PDF $f(f_{c,\boldsymbol{z}}|\mathbf{M})$, $\boldsymbol{z}\in\Omega$ can be approximated as follows:

$$f(f_{c,\boldsymbol{z}}|\mathbf{M}) \approx \frac{1}{N_{MCMC}} \sum_{i=1}^{N_{MCMC}} f(f_{c,\boldsymbol{z}}|\mathbf{M},\boldsymbol{\tau}_i), \tag{6.25}$$

where N_{MCMC} is the sample size in the MCMC algorithm and $\boldsymbol{\tau}_i$, $i = 1,\dots,N_{MCMC}$ are

samples from $f(\boldsymbol{\tau}|\mathbf{M})$. The posterior predictive CDF can be approximated accordingly:

$$F(f_{c,\boldsymbol{z}}|\mathbf{M}) \approx \frac{1}{N_{MCMC}} \sum_{i=1}^{N_{MCMC}} F(f_{c,\boldsymbol{z}}|\mathbf{M}, \boldsymbol{\tau}_i). \tag{6.26}$$

The evaluation of $F(f_{c,\boldsymbol{z}}|\mathbf{M})$ requires the analytical Bayesian update for each of the N_{MCMC} samples. Using the model assumptions of Section 6.2.4.2, $F(f_{c,\boldsymbol{z}}|\mathbf{M}, \boldsymbol{\tau}_i)$ is the CDF of the log-Student's t-distribution (cf. Appendix 6.A).

6.2.4.4 Choosing the prior normal-gamma distribution parameters from data

The parameters of the prior distribution should be chosen based on expertise and literature, or selected as a non-informative prior. Alternatively, the prior parameters can be determined from available data from similar structures, which are not part of the analysis at hand. We suggest to employ maximum likelihood estimation (MLE) to estimate these prior parameters, specifically the parameters μ_0, κ_0, α_0 and β_0 of the prior $\mathcal{NG}$ distribution $f(\boldsymbol{\theta})$. Here we consider data sets from n_{MLE} structures, each set consisting of n_i measurements of f_c at the specific structure i. The following sample estimators are calculated for each data set:

$$\bar{\mu}_i = \frac{1}{n_i} \sum_{j=1}^{n_i} \ln\left(f_{c,m,j}\right), \tag{6.27}$$

$$\bar{\lambda}_i = \left(\frac{1}{n_i - 1} \sum_{j=1}^{n_i} \left(\ln\left(f_{c,m,j}\right) - \bar{\mu}_i\right)^2 \right)^{-1}. \tag{6.28}$$

They are used to define the following:

$$\bar{\boldsymbol{\mu}} = \left[\bar{\mu}_1, \ldots, \bar{\mu}_{n_{\text{MLE}}}\right], \tag{6.29}$$

$$\bar{\boldsymbol{\lambda}} = \left[\bar{\lambda}_1, \ldots, \bar{\lambda}_{n_{\text{MLE}}}\right], \tag{6.30}$$

$$\bar{\boldsymbol{\Lambda}} = \operatorname{diag}\left(\bar{\boldsymbol{\lambda}}\right). \tag{6.31}$$

$\bar{\boldsymbol{\Lambda}}$ is a diagonal matrix with the entries of $\bar{\boldsymbol{\lambda}}$ on the main diagonal and zeros elsewhere.

The MLE estimators for the prior $\mathcal{NG}$ distribution are then given as [50, 51]:

$$\hat{\mu}_0 = \frac{\mathbf{1}\bar{\boldsymbol{\Lambda}}\bar{\boldsymbol{\mu}}^{\mathsf{T}}}{\mathbf{1}\bar{\boldsymbol{\Lambda}}\mathbf{1}^{\mathsf{T}}}, \tag{6.32}$$

$$\hat{\kappa}_0 = \frac{n_{\text{MLE}}}{(\bar{\boldsymbol{\mu}} - \hat{\mu}_0\mathbf{1})\bar{\boldsymbol{\Lambda}}(\bar{\boldsymbol{\mu}} - \hat{\mu}_0\mathbf{1})^{\mathsf{T}}}, \tag{6.33}$$

$$\hat{\alpha}_0 = \Psi^{-1}\left(\ln\left(\hat{\beta}_0\right) + \frac{1}{n_{\text{MLE}}} \sum_{i}^{n_{MLE}} \ln\left(\bar{\lambda}_i\right)\right), \tag{6.34}$$

$$\hat{\beta}_0 = \frac{n_{\text{MLE}} \cdot \hat{\alpha}_0}{\mathbf{1}\bar{\boldsymbol{\Lambda}}\mathbf{1}^{\mathsf{T}}}. \tag{6.35}$$

$\mathbf{1}$ denotes a $1 \times n_{\text{MLE}}$-vector of ones and $\Psi^{-1}(\cdot)$ is the inverse digamma function. $\hat{\alpha}_0$ and $\hat{\beta}_0$ have to be found iteratively, since both parameters appear in Equation (6.34) and in Equation (6.35).

The MLE estimators in Equations (6.32) to (6.35) are only valid under the assumption that f_c conditional on $\boldsymbol{\Theta}$ follows a lognormal distribution. They do not account for potential correlation among the measurements in the available data sets and can only be applied if $n_{\mathrm{MLE}} > 1$. The spatial update of Section 6.2.4.2 is directly applicable after replacing the prior $\mathcal{NG}$ distribution parameters by the respective MLE estimates.

Sometimes, site-specific data (e.g., from previous investigations on the structure) is available but the measurement locations are not documented, as this information is not needed in the standard methods to learn the characteristic values of the concrete strength [19, 18, 6]. Such data can be included in the above MLE procedure for learning the prior $\mathcal{NG}$ distribution parameters.

6.2.4.5 Bayesian learning of random field parameters without site-specific data

If no site-specific data is available, but data from similar structures (and site-specific data without measurement locations) can be used, one can still set up an RF model. Based on the MLE estimators in Equations (6.32) to (6.35), the predictive RF has log-Student's t-marginal distribution and is parameterized in terms of the parameters of the underlying Student's t-RF. Unlike the case where the spatial location of the measurements is available, the predictive RF is a homogeneous RF with parameters given by

$$\mu_t = \hat{\mu}_0, \tag{6.36}$$

$$\lambda_t(\boldsymbol{z}_1, \boldsymbol{z}_2) = \frac{\hat{\alpha}_0}{\hat{\beta}_0} \left(\rho_{\mathrm{mod}}(\boldsymbol{z}_1, \boldsymbol{z}_2) + \hat{\kappa}_0^{-1} \right)^{-1}, \tag{6.37}$$

$$\nu_t = 2\hat{\alpha}_0. \tag{6.38}$$

The parameters obtained in this way define the prior predictive RF, since the model is learned without site-specific information, and can be used for predictions about the spatially variable quantity [25].

6.3 Data analysis

This section applies the proposed methodology to learn a spatial model for the compressive strength of two ship lock chamber walls. The data analysis serves to investigate and demonstrate the proposed model, shows possible correlation models for specific structures and highlights challenges with the proposed approach encountered in practice.

The considered walls were built in layers of tamped concrete and, thus, show significant anisotropic behavior [63, 28]. A transverse anisotropic correlation function, distinguishing between horizontal (z_1, z_2) and vertical (z_3) distances is employed to account for this behavior. The resulting $\Delta_{\mathrm{w}}(\boldsymbol{z}, \boldsymbol{z}')$ is given by

$$\Delta_{\mathrm{w}}(\boldsymbol{z}, \boldsymbol{z}') = \sqrt{\left(\frac{\Delta_h(\boldsymbol{z}, \boldsymbol{z}')}{L_{c,h}} \right)^2 + \left(\frac{\Delta_v(\boldsymbol{z}, \boldsymbol{z}')}{L_{c,v}} \right)^2}, \tag{6.39}$$

where $\Delta_h(\boldsymbol{z}, \boldsymbol{z}')$ and $\Delta_v(\boldsymbol{z}, \boldsymbol{z}')$ denote the horizontal and vertical distance respectively between $\boldsymbol{z}$ and $\boldsymbol{z}'$. $L_{c,h}$ and $L_{c,v}$ denote the horizontal and vertical correlation lengths.

The vector $\mathbf{T}$ of correlation parameters is treated as random vector and learned from the data. However, the prior information on the elements in $\mathbf{T}$ is vague, which makes the choice of a prior distribution a challenging task. Hence, the multivariate uniform distribution on the

domain of definition is chosen as prior distribution. The measurement uncertainty is accounted for in the correlation function through the factor γ.

6.3.1 Ship lock Oldenburg

This case study investigates the ship lock at the river Hunte in Oldenburg, Germany. It was built in the 1920s from unreinforced tamped concrete. The chamber has a length of 128 m and a usable width of 12 m between the chamber walls. During an extensive repair in 1983, the upper 2 m of the chamber walls were replaced by reinforced concrete. The focus of this study is the original concrete of one of the chamber walls, for which strength measurements are available at three vertical core samples from an investigation in 2014. Figure 6.7 shows a front view and the cross section of the chamber wall with the two concrete layers of different age and the position of the core samples. Table 6.1 lists the 24 measurements of the concrete compressive strength and their corresponding measurement location in z_1 and z_3 ($z_2 = -1.0$ m for all 24 measurements).

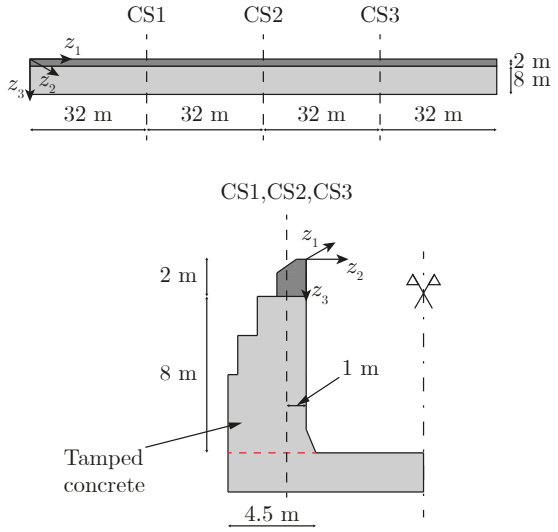

Figure 6.7: Front view (top) and cross section (bottom) of the ship lock wall in Oldenburg including the locations of three vertical core samples (CS1, CS2 and CS3), from which 24 measurements of the concrete compressive strength have been taken. Tamped concrete is indicated in light gray, reinforced concrete is shown in dark gray.

The prior parameters for the $\mathcal{NG}$ distribution $f(\boldsymbol{\theta})$ are chosen as follows:

$$[\mu_0, \kappa_0, \alpha_0, \beta_0] = \left[/, 0, -\frac{1}{2}, 0\right], \tag{6.40}$$

which gives the non-informative prior distribution $f(\boldsymbol{\theta}) = \lambda_X^{-1}$ [12, 28].

6.3.1.1 Learning the correlation model

The correlation model contains four unknown parameters, namely the two correlation lengths, the parameter for the micro-scale variability and the smoothness parameter of the Matérn corrrelation model. The 24 measurements are not sufficient to learn all parameters without the support from an informative prior distribution. It has been reported in previous studies that learning the smoothness parameter and the correlation length at the same time is a difficult task in general [11]. Thus, the Matérn smoothness parameter is set to $\nu = 0.5$, corresponding to the exponential correlation model. In addition, the parameter for the micro-scale variability γ is not learned from the data either. Instead, the analysis is carried out for different values of γ.

Table 6.1: Measurements of the concrete compressive strength obtained from three core samples in the north wall of the ship lock Oldenburg. The locations of the core samples are indicated in Figure 6.7.

CS1 ($z_1 = 32.00\,\text{m}$)		CS2 ($z_1 = 64.00\,\text{m}$)		CS3 ($z_1 = 96.00\,\text{m}$)	
z_3 [m]	$f_{c,m}$ [N mm^{-2}]	z_3 [m]	$f_{c,m}$ [N mm^{-2}]	z_3 [m]	$f_{c,m}$ [N mm^{-2}]
2.40	29.2	2.21	21.2	2.34	18.5
3.24	15.5	3.25	16.0	3.34	10.3
4.25	8.7	4.05	32.0	4.17	13.2
5.15	12.3	5.33	20.7	5.24	14.5
6.12	16.2	6.15	13.8	6.27	25.4
7.33	11.6	7.25	12.1	7.12	14.5
8.15	13.4	8.40	8.6	8.23	13.2
9.05	13.9	9.45	14.8	9.08	33.0

The correlation length estimates are obtained via a solution of the optimization problem of Equation (6.22) resulting in the following MAP estimates for $L_{c,h}$ and $L_{c,v}$:

$$\gamma = 0.1: \quad \left[L^*_{c,h},\ L^*_{c,v}\right] = [2.08\,\text{m},\ 0.62\,\text{m}]\,, \tag{6.41}$$

$$\gamma = 0.3: \quad \left[L^*_{c,h},\ L^*_{c,v}\right] = [2.70\,\text{m},\ 0.71\,\text{m}]\,, \tag{6.42}$$

$$\gamma = 0.5: \quad \left[L^*_{c,h},\ L^*_{c,v}\right] = [3.75\,\text{m},\ 0.87\,\text{m}]\,. \tag{6.43}$$

From these values, it appears that an increase in the micro-scale variability leads to an increase in the MAP estimates of the correlation lengths. Large correlation lengths correspond to RFs with smooth spatial variability, while small correlation lengths indicate a highly fluctuating RF. When γ is large, a large portion of the variability observed in the data is attributed to the micro-scale variability (and the measurement uncertainty). In this case, a smaller part of the data variability is attributed to spatial variability and the associated correlation length is larger. To illustrate this, the posterior distribution of the two correlation lengths is plotted in Figure 6.8 for varying γ. The respective MAP estimates of $\boldsymbol{L_c}$ are indicated by blue dots. In panel a, the micro-scale variability only plays a minor role for the overall variability ($\gamma = 0.1$), leading to a clear mode of the posterior distribution $f(\boldsymbol{L_c}|\mathbf{M}, \gamma)$. Increasing the influence of the micro-scale variability flattens the posterior distribution and shifts the mode towards larger values for the correlation lengths, as can be seen in panels b ($\gamma = 0.3$) and c ($\gamma = 0.5$). All three panels show an additional local maximum of $f(\boldsymbol{L_c}|\mathbf{M}, \gamma)$ in the bottom right corner, i.e., in regions of large $L_{c,h}$ and small $L_{c,v}$. This behavior is caused by the local horizontal clustering of the measurements in three vertical core samples, whereas they are approximately evenly distributed in vertical direction. Such an arrangement reduces the learning effect for $L_{c,h}$ and makes $f(\boldsymbol{L_c}|\mathbf{M}, \gamma)$ more sensitive to changes in $L_{c,v}$.

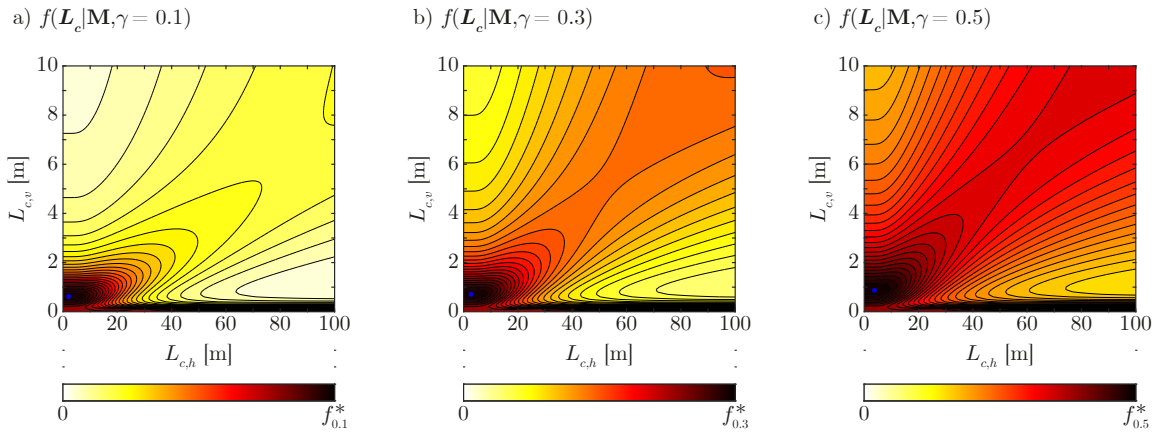

Figure 6.8: Posterior distribution of the correlation lengths in horizontal ($L_{c,h}$) and vertical ($L_{c,v}$) direction for $\nu = 0.5$ and varying values of γ. The blue dots indicate the MAP estimates at the respective modes of the posterior distribution. $f^*_{0.1}$, $f^*_{0.3}$ and $f^*_{0.5}$ are the values of $f(\boldsymbol{L_c}|\mathbf{M},\gamma)$ at the respective distribution modes.

6.3.1.2 Spatial posterior predictive concrete compressive strength

The Bayesian RF update is used to learn the posterior predictive random field of the concrete compressive strength. The following posterior $\mathcal{NG}$ distribution parameters are calculated from Equations (6.16) to (6.19):

$$\gamma = 0.1: \quad [\mu_n, \kappa_n, \alpha_n, \beta_n] = [2.76,\ 17.27,\ 11.5,\ 1.61]\,, \tag{6.44}$$

$$\gamma = 0.3: \quad [\mu_n, \kappa_n, \alpha_n, \beta_n] = [2.76,\ 17.30,\ 11.5,\ 1.59]\,, \tag{6.45}$$

$$\gamma = 0.5: \quad [\mu_n, \kappa_n, \alpha_n, \beta_n] = [2.76,\ 17.33,\ 11.5,\ 1.59]\,. \tag{6.46}$$

Since α_n only depends on the number of measurements, it is constant for any choice of γ. Although the other three $\mathcal{NG}$ distribution parameters depend on the spatial correlation of the measurements, they differ only slightly for different choices of γ. This is due to the fact that an increase in γ automatically decreases the spatial correlation of two locations in the random field (cf. Equation (6.4)) and, thus, compensates the increased spatial correlation of the measurement locations that comes with larger correlation lengths.

The random field parameters can be determined by application of Equations (6.13) to (6.15). With these parameters, the spatial characteristic value $f_{c,\mathrm{k}}(\boldsymbol{z})$ can be determined as the 5%−quantile value of the log-Student's t-RF. It is illustrated in Figure 6.9 for the $z_1 - z_3$ plane in which the core samples have been taken. While $f_{c,\mathrm{k}}(\boldsymbol{z})$ is strongly influenced by the measurement values in regions close to the measurement locations, one can see convergence to a global value in regions away from the measurements. It is noted that the extreme values of $f_{c,\mathrm{k}}(\boldsymbol{z})$ are located in the illustrated $z_1 - z_3$ plane, the point-wise values tend towards the global value for a shift in z_2. The effect of a variation in γ on the global characteristic value is negligible, as it is 8.2 MPa for all three cases. The global characteristic value appears in regions without spatial correlation to the measurement locations and, thus, is determined by the posterior parameters of the $\mathcal{NG}$ distribution. Those parameters are almost constant for all three choices of γ, leading to a similar global characteristic value. Using the standardized Bayesian approach of EN 1990 with the 24 measurements from Table 6.1 leads to a space-invariant characteristic value of $f_{c,\mathrm{k,EN}} = 8.4\,\mathrm{MPa}$, i.e., it is slightly higher than the global characteristic value obtained with the spatial model.

The effect of the different values of $\boldsymbol{L_c}$ can be seen in Figure 6.9 by comparing the regions

of the wall where $f_{c,\mathrm{k}}(\boldsymbol{z})$ differs from the global value. In panel a, the spatial effect of the measurement locations is restricted to regions close to the core sample locations, while these regions become larger in panels b and c, where $\boldsymbol{L_c}$ takes larger values.

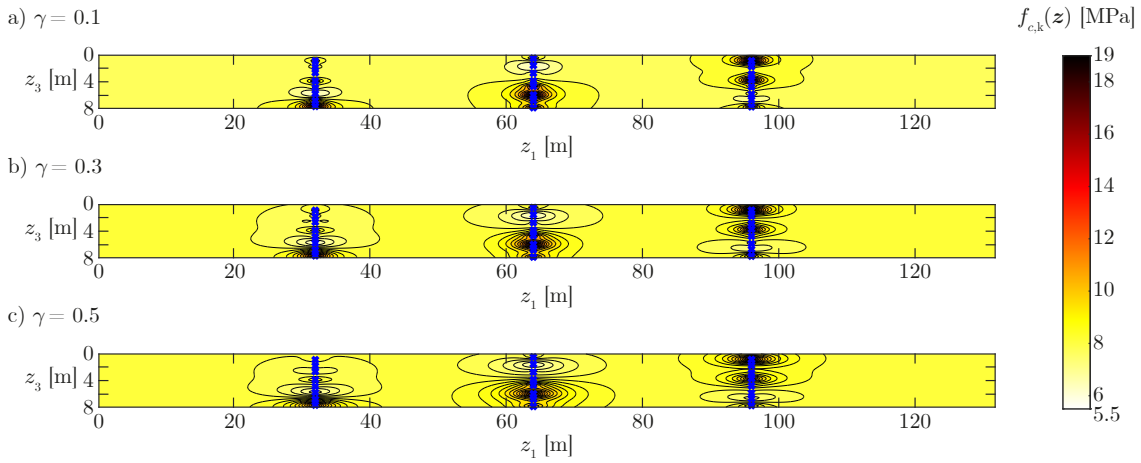

Figure 6.9: Spatial characteristic value $f_{c,\mathrm{k}}(\boldsymbol{z})$ of the posterior predictive random field for different choices of γ.

The correlation function of $f_c(\boldsymbol{z})$ contains the effect of micro- and of meso-scale variability through the parameter γ. For each of the above choices of γ, Figure 6.10 illustrates two random realizations of the corresponding posterior predictive RF at location $z_1 = 64\,\mathrm{m}$, i.e., at the location of core sample CS2. For $\gamma = 0.1$ (panel a of Figure 6.10), the realizations are dominated by the meso-scale variability with a clear trend defined by the measurement values (indicated by blue dots). With increasing distance to the measurement values, the uncertainty, and accordingly the variability increases. This changes in panels b and especially panel c of Figure 6.10, where the effect of the micro-scale correlation is stronger. This leads to sudden changes in the RF realizations and larger uncertainty, even close to or directly at the measurement locations. This is due to the fact that $f_c(\boldsymbol{z})$ can be seen as superposition of an RF with spatial correlation and a noise RF (cf. Section 6.2.3.1), where the latter one dominates the overall variability of $f_c(\boldsymbol{z})$ for large values of γ.

One of the key attributes of the proposed model is its flexibility regarding the amount of available information. To illustrate this, the analysis is repeated for $\gamma = 0.1$ with the correlation length taken as $L_{c,h} = L_{c,v} = 5\,\mathrm{m}$ as suggested in the JCSS probabilistic model code [34]. The resulting posterior parameters of the $\mathcal{NG}$ distribution are

$$[\mu_n, \kappa_n, \alpha_n, \beta_n] = [2.78,\ 8.01,\ 11.50,\ 2.09]. \tag{6.47}$$

Comparison of the parameters with the ones in Equation (6.44) shows that fixing the correlation lengths to 5 m mainly affects the parameter κ_n and β_n in this case. Figure 6.11 illustrates the spatial characteristic value $f_{c,\mathrm{k}}(\boldsymbol{z})$ of the resulting posterior predictive RF. The comparison with panel a of Figure 6.9 shows that a correlation length of 5 m leads to more conservative estimates of the characteristic concrete compressive strength in regions far away from the measurements. The reason for that is the increased spatial correlation of measurements caused by the larger vertical correlation length of 5 m compared to 0.62 m when estimating the correlation length from the data. Consequently, the posterior predictive random field is forced to be highly variable in order to explain the data variability, which leads to a more conservative estimate of the global characteristic value. This application shows that the suggested approach can be adjusted to the degree of available prior information. However, problems can arise when information from

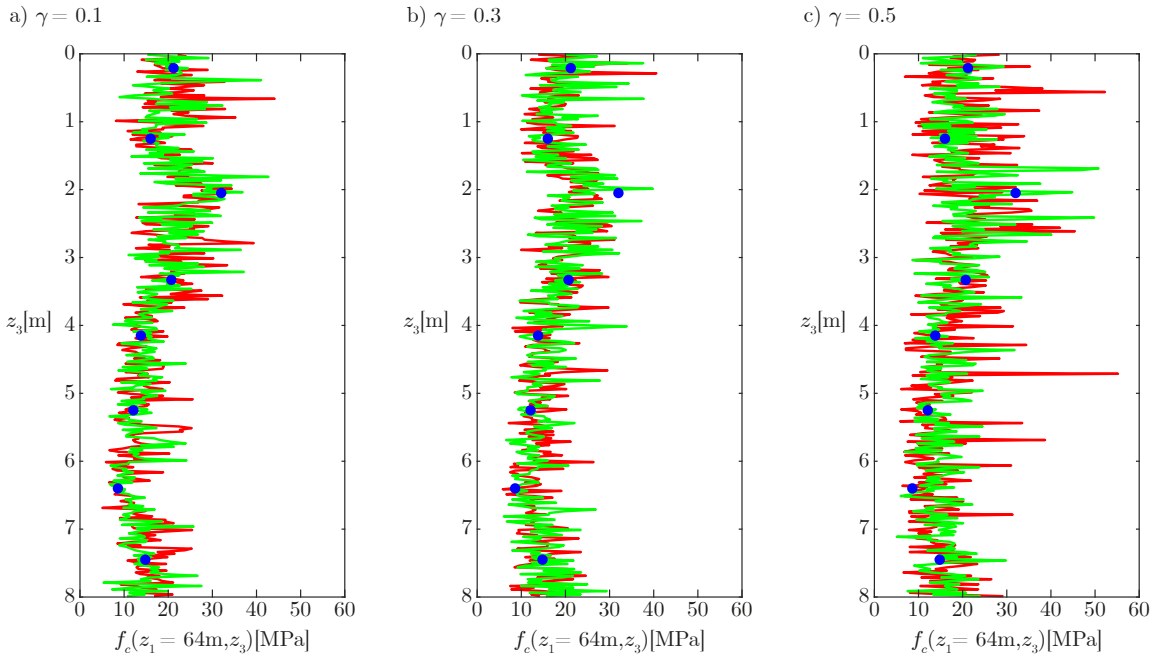

Figure 6.10: Random realizations of the posterior predictive RF at $z_1 = 64\,\text{m}$ for different choices of γ.

inconsistent sources are used, due to the interdependence of the model parameters (e.g., γ and $L_{c,h}$). In addition, the approach can be used to verify recommendations from the literature and compare them with results from an analysis based only on site-specific data.

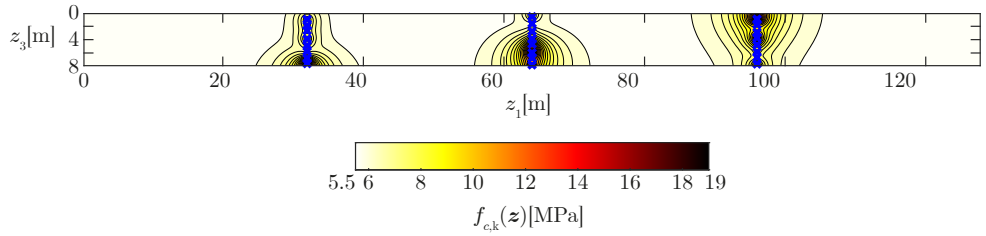

Figure 6.11: Spatial characteristic value $f_{c,\text{k}}(\boldsymbol{z})$ of the posterior predictive random field with fixed correlation lengths $L_{c,h} = L_{c,v} = 5\,\text{m}$ and $\gamma = 0.1$.

6.3.1.3 Effect of an informative prior distribution

In addition to the 24 measurements of Table 6.1, three data sets are available, one from previous investigations on the same ship lock and two from similar ship locks (one of which is analyzed in Section 6.3.2). The following sample moments are used to obtain the MLE estimates of the prior $\mathcal{NG}$ parameters (cf. Equations (6.27) to (6.30)):

$$\bar{\boldsymbol{\mu}} = [2.83,\ 2.12,\ 2.03], \tag{6.48}$$

$$\bar{\boldsymbol{\lambda}} = [3.50,\ 3.78,\ 2.53]. \tag{6.49}$$

From these, the prior $\mathcal{NG}$ parameters are estimated:

$$[\hat{\mu}_0,\ \hat{\kappa}_0,\ \hat{\alpha}_0,\ \hat{\beta}_0] = [2.35,\ 2.37,\ 34.52,\ 10.56]. \tag{6.50}$$

Using an informative prior distribution reduces the uncertainty in the RF parameters and therefore also affects the posterior estimates of the spatial correlation structure. Setting $\gamma = 0.1$, the following MAP estimates for $L_{c,h}$ and $L_{c,v}$ are obtained:

$$\left[L^*_{c,h},\ L^*_{c,v}\right] = [33.33\,\text{m},\ 2.49\,\text{m}]. \tag{6.51}$$

Both correlation lengths are several times larger than in the case of an uninformative prior distribution. Figure 6.12 shows the posterior distribution of $\boldsymbol{L_c}$ and the corresponding MAP estimate at its mode. Although the uncertainty in $\boldsymbol{L_c}$ remains large, the informative prior distribution has a strong effect on possible regions of $\boldsymbol{L_c}$, as not much of the probability mass of $f(\boldsymbol{L_c}|\mathbf{M}, \gamma)$ remains in regions of extremely small or large correlation lengths (unlike panel a of Figure 6.8). The local maxima in the bottom right corner remains unaffected by the informative prior distribution.

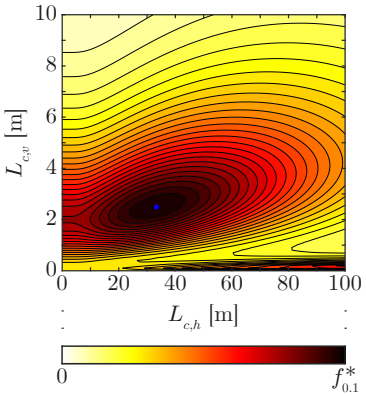

Figure 6.12: Posterior distribution of the correlation lengths in horizontal ($L_{c,h}$) and vertical ($L_{c,v}$) direction for $\nu = 0.5$ and $\gamma = 0.1$ with informative prior $\mathcal{NG}$ distribution parameters. The blue dot indicates the MAP estimate at the mode of the posterior distribution. $f^*_{0.1}$ is the value of $f(\boldsymbol{L_c}|\mathbf{M}, \gamma)$ at the distribution mode.

The posterior $\mathcal{NG}$ parameters corresponding to the MAP estimate are calculated as

$$[\mu_n, \kappa_n, \alpha_n, \beta_n] = [2.67,\ 6.59,\ 46.52,\ 13.67]. \tag{6.52}$$

While μ_n is close to the value obtained with the non-informative prior distribution, the other parameters differ. The global characteristic value of the posterior predictive RF $f_c(\boldsymbol{z})$ is 5.5 MPa, i.e., it is significantly smaller than when using the non-informative prior distribution (8.2 MPa). Figure 6.13 shows the spatial characteristic value $f_{c,\mathrm{k}}(\boldsymbol{z})$ for the $z_1 - z_3$ plane in which the core samples have been taken. The larger correlation lengths lead to an increased area that is affected by the measurement values, in this case spanning almost all over the chamber wall.

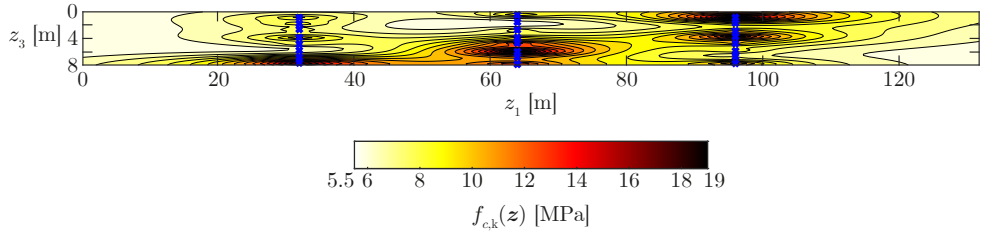

Figure 6.13: Spatial characteristic value $f_{c,\mathrm{k}}(\boldsymbol{z})$ of the posterior predictive random field with informative prior and $\gamma = 0.1$.

6.3.2 Ship lock Feudenheim

This ship lock is located at the river Neckar in Feudenheim, a district of Mannheim, Germany, and was built in the 1920s. It consists of two chambers and three chamber walls, which are made of unreinforced tamped concrete. The chamber walls have a length of 108 m, a height of 14.5 m and are separated into six construction blocks of equal length. The amount of data in this study is significantly larger than in the previous study, with a total of 369 measurement values of the concrete compressive strength from 18 vertical core samples (6 core samples per chamber wall, where one core sample has been extracted from each construction block). The three walls are analyzed independently, since there is no knowledge about the construction process available.

As in Section 6.3.1, a smoothness parameter of $\nu = 0.5$ is employed for the Matérn correlation model. It is assumed that the concrete strength in different construction blocks is not spatially correlated. Hence, the horizontal correlation length cannot be learned because only one vertical core sample is available for each construction block.

As before, a non-informative $\mathcal{NG}$ prior distribution is chosen with parameters given in Equation (6.40).

6.3.2.1 Learning the correlation model

To learn the free correlation parameters, namely γ and $L_{c,v}$, the optimization problem of Equation (6.22) is solved for each wall, resulting in the following MAP estimates:

$$\text{left chamber wall}: \quad \left[L_{c,v}^*,\ \gamma^*\right] = [0.64\,\text{m},\ 0.70], \tag{6.53}$$

$$\text{middle chamber wall}: \quad \left[L_{c,v}^*,\ \gamma^*\right] = [2.72\,\text{m},\ 0.86], \tag{6.54}$$

$$\text{right chamber wall}: \quad \left[L_{c,v}^*,\ \gamma^*\right] = [2.32\,\text{m},\ 0.75]. \tag{6.55}$$

According to the MAP estimates, the RF variability is dominated by the micro-scale variability and the meso-scale variability only plays a minor role. The joint posterior distributions of γ and $L_{c,v}$ are illustrated in Figure 6.14. In the left chamber wall (panel a), most of the probability mass of $f(L_{c,v}, \gamma|\mathbf{M})$ concentrates in a region of small vertical correlation length, while it distributes over a broad range of γ. The situation is different for the middle and right chamber wall, where the probability mass is concentrated in a region of $\gamma \approx 0.6 - 0.8$, while a broad range of $L_{c,v}$ is covered. It is noted, that the case $\gamma = 1$ is equivalent to a correlation length of 0 m, resulting in a white noise random field without any spatial correlation. This equivalence is the reason for the tail of $f(L_{c,v}, \gamma|\mathbf{M})$ towards small values of $L_{c,v}$ for small values of γ in Figure 6.14, i.e., the model accounts for the micro-scale variability through $L_{c,v}$ instead of γ in these regions.

To investigate the importance of the parameter γ, we compare the correlation model of Equation (6.12) with a model where we set $\gamma = 0$ using the data from the three chamber walls through Bayesian model comparison [25]. That is, we evaluate and compare the model evidence (or marginal likelihood), i.e., the normalizing constant of the posterior distribution of Equation (6.20), for the two cases. The results given in Table 6.2 demonstrate that neglecting the micro-scale variability, i.e., setting $\gamma = 0$, leads to a model evidence that is orders of magnitude smaller than including γ as a free parameter. This shows that the parameter γ has significant influence on the obtained predictions and neglecting it could lead to an overestimation of the spatial variability of concrete strength.

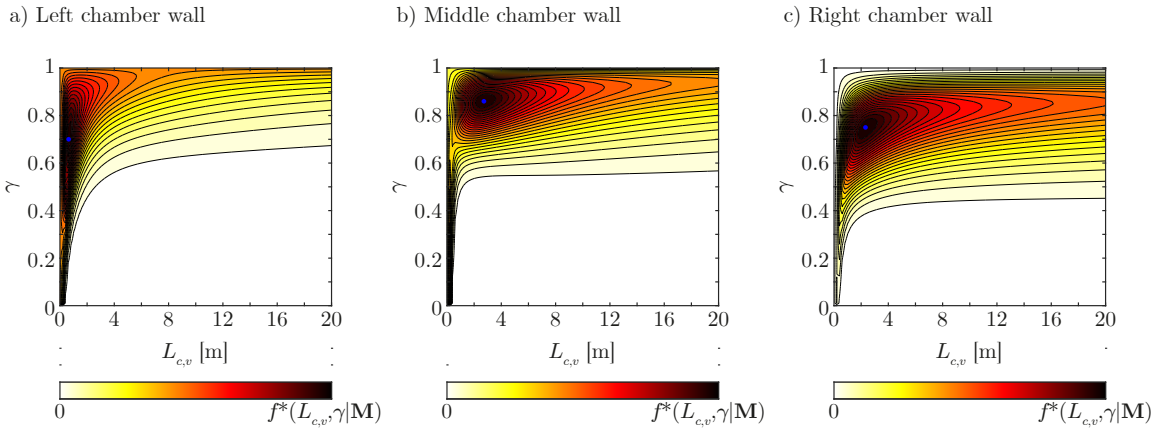

Figure 6.14: Posterior distribution of the vertical correlation length $L_{c,v}$ and the parameter γ for the left, middle and right chamber wall of the Feudenheim ship lock. The blue dots indicate the MAP estimates at the respective modes of the posterior distribution. $f^*(L_{c,v}, \gamma|\mathbf{M})$ indicates the value of $f(L_{c,v}, \gamma|\mathbf{M})$ at the respective distribution modes.

Table 6.2: Model evidence of the posterior of Equation (6.20) for the three chamber walls of the ship lock Feudenheim. We note that the evidence is evaluated up to a normalizing constant due to the uninformative prior employed.

left wall		middle wall		right wall	
$\gamma = 0$	γ uncertain	$\gamma = 0$	γ uncertain	$\gamma = 0$	γ uncertain
3.6×10^{-52}	3.1×10^{-46}	1.8×10^{-90}	2.1×10^{-84}	4.1×10^{-81}	4.5×10^{-74}

6.3.2.2 Spatial posterior predictive concrete compressive strength

A horizontal correlation length needs to be chosen for the Bayesian RF update, since it cannot be learned from the data. The previous results show that the correlation length is a sensitive choice with a strong influence on the posterior predictive RF. For illustration purposes, we choose $L_{c,h} = 5\,\text{m}$, as recommended in [34]. The following posterior parameters for the $\mathcal{NG}$ distribution are calculated:

$$\text{left chamber wall}: \quad [\mu_n, \kappa_n, \alpha_n, \beta_n] = [1.94,\ 72.51,\ 46.5,\ 11.79], \tag{6.56}$$

$$\text{middle chamber wall}: \quad [\mu_n, \kappa_n, \alpha_n, \beta_n] = [2.17,\ 70.47,\ 73.5,\ 16.06], \tag{6.57}$$

$$\text{right chamber wall}: \quad [\mu_n, \kappa_n, \alpha_n, \beta_n] = [2.21,\ 48.82,\ 62,\ 19.28]. \tag{6.58}$$

Each chamber wall is split into 6 spatially independent RFs corresponding to the construction blocks. These are only correlated through the inter-structure variability, i.e., they have the same posterior $\mathcal{NG}$ distribution parameters. The posterior predictive RFs are determined and the resulting 5%−quantile values in the $z_1 - z_3$ plane of the measurement locations are illustrated in Figure 6.15. The left chamber wall (panel a) shows the largest variability in the spatial characteristic value, since it has the smallest vertical correlation lengths. Regions of high (low) characteristic values can be clearly identified and are located close to high (low) measurement values. In the middle chamber wall (panel b), the spatial variability of the characteristic value is small compared to panel a. This is due to the dominance of the micro-scale variability, which reduces the impact of the spatial variability. In addition, the vertical correlation length is significantly larger than in panel a, which leads to a smoother spatial behavior of the RF. The

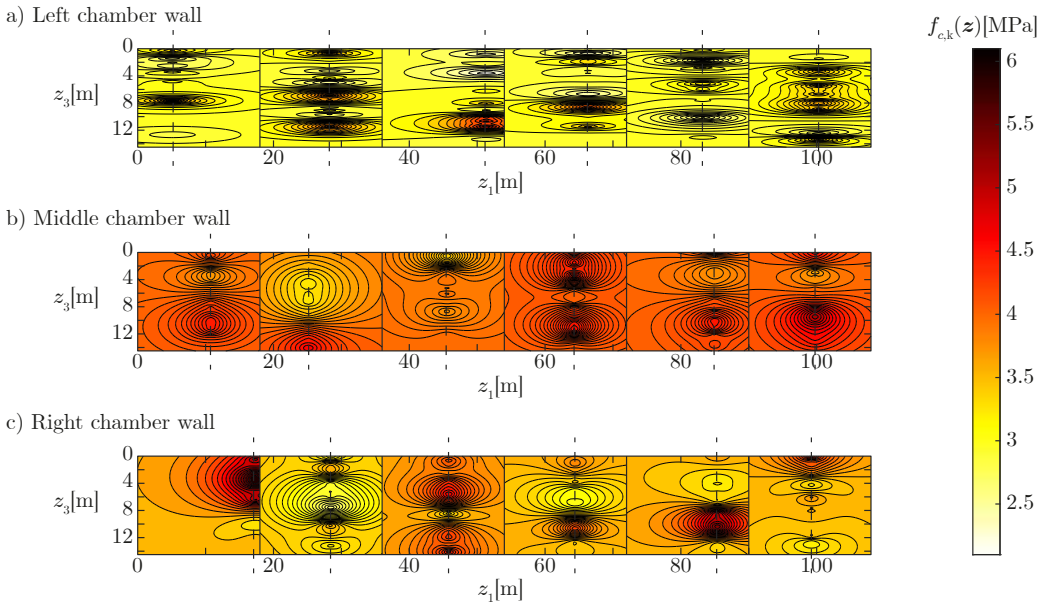

Figure 6.15: Spatial characteristic value $f_{c,\mathrm{k}}(\boldsymbol{z})$ of the posterior predictive random fields for the three chamber walls of the ship lock Feudenheim. Each wall is split into six blocks. The locations of the core samples are indicated by the dashed lines.

correlation length of the right chamber wall (panel c) is in the same range as the one in panel b, whereas the micro-scale variability is closer to the value of panel a. This leads to larger regions of high (low) characteristic values (in vertical direction) than in panel a and a smooth spatial variability. In general, γ is large in all three chamber walls, which leads to a relatively small range of $f_{c,\mathrm{k}}(\boldsymbol{z})$.

6.3.2.3 Influence of the smoothness parameter

So far, the smoothness parameter of the Matérn correlation model has been set to $\nu = 0.5$. A study on ν is carried out to investigate the effect of that choice. To this end, two additional choices of ν are analyzed, namely $\nu = 2.5$ and $\nu \to \infty$. The following MAP estimates are obtained for the parameters of the correlation model of the left chamber wall:

$$\nu = 2.5: \quad \left[L_{c,v}^{*},\ \gamma^{*}\right] = [0.66\,\mathrm{m},\ 0.75], \tag{6.59}$$

$$\nu \to \infty: \quad \left[L_{c,v}^{*},\ \gamma^{*}\right] = [0.62\,\mathrm{m},\ 0.75], \tag{6.60}$$

which are relatively close to the MAP estimates for $\nu = 0.5$ ($[L_{c,v}^{*},\ \gamma^{*}] = [0.64\,\mathrm{m},\ 0.70]$). The same holds for the posterior $\mathcal{NG}$ distribution parameters, which result in

$$\nu = 2.5: \quad [\mu_n, \kappa_n, \alpha_n, \beta_n] = [1.94,\ 71.84,\ 46.5,\ 11.79], \tag{6.61}$$

$$\nu \to \infty: \quad [\mu_n, \kappa_n, \alpha_n, \beta_n] = [1.94,\ 72.31,\ 46.5,\ 11.78], \tag{6.62}$$

compared to $[\mu_n, \kappa_n, \alpha_n, \beta_n] = [1.94,\ 72.51,\ 46.5,\ 11.79]$ for $\nu = 0.5$. We select a single construction block of the left chamber wall ($z_1 \in [36\,\mathrm{m},\ 54\,\mathrm{m}]$) to perform the spatial update. The resulting 5%−quantile values in the $z_1 - z_3$ plane of the measurement locations are illustrated in Figure 6.16. The smoother correlation model leads to a smoother spatial characteristic value, especially in regions with several measurements close to each other, as can be seen by the

increasing smoothness of the contour lines in panel b and c compared to panel a. However, the overall contribution of ν to $f_{c,\mathrm{k}}(\boldsymbol{z})$ is minor in this case.

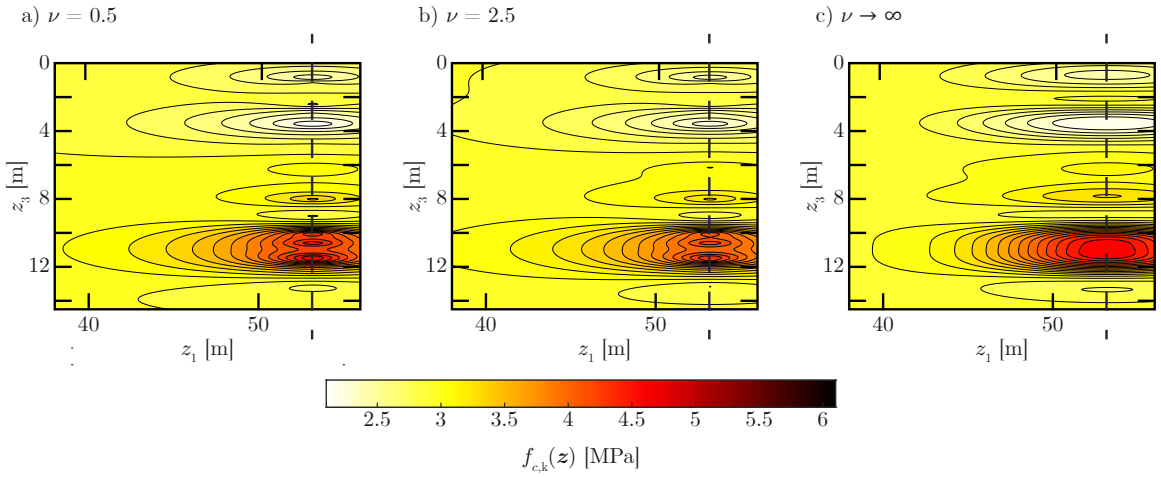

Figure 6.16: Spatial characteristic value $f_{c,\mathrm{k}}(\boldsymbol{z})$ of the posterior predictive random field in a single block of the left chamber wall ($z_1 \in [36\,\mathrm{m},\ 54\,\mathrm{m}]$) for different choices of the smoothness parameter ν. The dashed line indicates the location of the core sample.

6.3.3 Interpretation of results

The two examples in Sections 6.3.1 and 6.3.2 demonstrate the ability of the proposed model to learn the spatial distribution of the concrete strength. The two structures differ in the construction process and the availability of data. The results show that the identification of the parameters of the correlation model is a critical factor of the presented model that significantly impacts the resulting predictions, e.g., the spatial distribution of the characteristic value. Learning the parameters of the proposed correlation model from the data is a challenging task, especially because only limited data is typically available. This is illustrated by the obtained posterior distributions of the correlation parameters, which are rather flat. A prior reduction of the uncertainty in the correlation parameters proves difficult, as the relevant literature is scarce. The anisotropy of the concrete compressive strength RF, confirmed by the data in the first example, results in an additional parameter of the spatial correlation function, adding further to the problem. Significant differences are observed in the estimated correlation parameters, not only for different structures but also for different structural elements, indicating the difficulty in identifying an appropriate correlation function with limited data. However, the results also indicate that the suggested correlation model is capable of representing the spatial variability of concrete strength. Given an extensive set of spatial measurements that includes sufficiently dense measurements, the parameter γ can be learned, which simplifies learning the remaining parameters. In addition, the findings of such studies can be used to calibrate the parameters for an informative prior distribution of the unknown model parameters in future studies.

The spatial behavior of the posterior predictive characteristic value, defined as the pointwise 5%−quantile value of the resulting log-Student's t-distribution, strongly depends on the micro-scale component of the correlation function. A strong micro-scale variability reduces the spatial correlation and the spatial influence of the measurements. In the latter case, the characteristic value is dominated by the marginal distribution away from the measurements, which is determined by the parameters of the marginal distribution of the RF. If the variability is dominated by a strong micro-scale variability, the choice of the smoothness parameter for the correlation function only plays a minor role.

The unidentifiability of the correlation parameters with limited amount of data can partially be attributed to the equivalence of limiting cases of the parameter values. If the variability is completely defined by the micro-scale variability, the spatial correlation function and its parameters are irrelevant, the resulting RF will have no spatial correlation, i.e., it is given by a white noise field. The same result is obtained when the correlation lengths are zero, in which case the meso-scale correlation function reduces to the Dirac function.

6.4 Concluding remarks

We propose a new spatial probabilistic model for the concrete strength, which is hierarchical and distinguishes micro-scale and meso-scale variability. Our modeling approach enables the use of spatially distributed measurements of the concrete strength to learn the parameters of its spatial correlation function. The predictive distribution of the proposed random field given the spatial measurements can be obtained in closed form and can be further used in structural verification predictions. The proposed model enables a detailed probabilistic description of the spatial distribution of the concrete strength in existing structures. This allows identification of critical regions within the structure, which can be used for further investigation of the structural condition.

The ability of the proposed model to quantify the uncertainty on the concrete strength in regions far away from the measurements can be used to potentially avoid the use of destructive testing techniques. One does not want to weaken the structure in the regions with the highest mechanical demand on the material, but these are typically the regions where knowledge of the concrete strength is of most interest. In addition, the regions of interest may not be accessible for testing purposes in some cases. Using the suggested model allows estimating the concrete strength in such regions including the remaining uncertainty.

The results show that additional empirical studies are required for effective learning of the correlation function and prior parameters of the concrete compressive strength (prior parameters of the $\mathcal{NG}$ distribution). Particularly, a reliable identification of the anisotropic behavior of the concrete strength in the investigated structures requires additional studies based on horizontal and vertical core samples. The proposed model can be used to study the influence of the measurement spacing on the identifiability of the vertical and horizontal correlation lengths. However, this goes beyond the scope of the present paper.

Although learning a random field model without spatial information is possible, much of the potential information is lost when the measurement values are not assigned a location. Hence, for effective application of the spatial modeling approach, detailed documentation of the measurement location is inevitable, which is not always the case in practical applications. Using additional studies with well-documented data, the model can be calibrated for practical application.

The resulting predictive random field model offers opportunities for application in advanced modeling approaches, e.g., in reliability analyses with finite element models accounting for the spatial variability of the concrete material, which is not possible with the standard approaches for learning concrete strength from data. When integrating the random field model in standard structural analysis, spatial averaging of the random field over the areas associated with the relevant failure modes ensures a consistent treatment of the spatial variability [26].

The proposed model can be used also to identify regions within the structure, where additional measurements should be taken, e.g., in the context of inspection planning and maintenance schemes. It can also help to validate potential outliers in the data set by comparing them to measurements close-by and to avoid a selection bias originating from the fact that several measurements are taken from a single core sample.

Acknowledgments

This work has been financially supported by the *Bundesanstalt für Wasserbau* (Federal Waterways Engineering and Research Institute, Germany). The authors thank Claus Kunz from the *Bundesanstalt für Wasserbau* for many discussions and providing data, and Maximilian Stupp and Nick Pfeiffer for preparing the data and performing initial studies.

6.A The log-Student's t-distribution

The marginal distribution of the predictive RF for the concrete compressive strength f_c is the log-Student's t-distribution. Thus, $f_{c,\ln} = \ln(f_c)$ follows the Student's t-distribution with following PDF [4]:

$$f_t(f_{c,\ln}) = \frac{\Gamma\left(\frac{\nu_t}{2} + \frac{1}{2}\right)}{\Gamma\left(\frac{\nu_t}{2}\right)} \left(\frac{\lambda_t}{\pi\nu_t}\right)^{\frac{1}{2}} \left(1 + \frac{\lambda_t \left(f_{c,\ln} - \mu_t\right)^2}{\nu_t}\right)^{-\frac{\nu_t}{2}-\frac{1}{2}}. \tag{6.63}$$

Therein, $\Gamma(\cdot)$ is the gamma function, and μ_t, λ_t and ν_t are the location parameter, scale parameter and degrees of freedom of the Student's t-distribution. The PDF of f_c can then be derived as [59, 28]

$$f_{t,\ln}(f_c) = \frac{1}{f_c} f_t\left(\ln\left(f_c\right)\right). \tag{6.64}$$

The CDF of f_c is defined in terms of the CDF of $f_{c,\ln}$:

$$F_{t,\ln}(f_c) = F_t\left(\ln\left(f_c\right)\right). \tag{6.65}$$

$F_t(\ln(f_c))$ can be written in closed form in terms of the regularized incomplete beta function. Alternatively, it can easily be evaluated numerically. We note that the log-Student's t-distribution has infinite moments of any order [28].

References

[1] P. Abrahamsen. *A review of Gaussian random fields and correlation functions*. 2nd ed. Norwegian Computing Center, 1997.

[2] Z. P. Bažant. "Size effect on structural strength: a review". In: *Archive of Applied Mechanics* 69.9 (1999), pp. 703–725.

[3] J. Benjamin and C. Cornell. *Probability, statistics, and decision for civil engineers*. New York City, NY: McGraw-Hill, 1970.

[4] C. M. Bishop. *Pattern recognition and machine learning*. Information science and statistics. New York City, NY: Springer, 2006.

[5] S. Brooks, A. Gelman, G. Jones, and X.-L. Meng. *Handbook of Markov chain Monte Carlo*. Chapman & Hall/CRC handbooks of modern statistical methods. Boca Raton, FL: CRC, 2011.

[6] Bundesanstalt für Wasserbau. *Bewertung der Tragfähigkeit bestehender, massiver Wasserbauwerke [Assessment of the bearing capacity of existing, massive hydraulic structures]*. BAW guideline, 2016.

[7] J. Chen, J. He, X. Ren, and J. Li. "Stochastic harmonic function representation of random fields for material properties of structures". In: *Journal of Engineering Mechanics* 144.7 (2018), p. 04018049.

[8] J. Ching, W.-H. Huang, and K.-K. Phoon. "3D probabilistic site characterization by sparse Bayesian learning". In: *Journal of Engineering Mechanics* 146.12 (2020), p. 04020134.

[9] J. Ching and K.-K. Phoon. "Characterizing uncertain site-specific trend function by sparse Bayesian learning". In: *Journal of Engineering Mechanics* 143.7 (2017), p. 04017028.

[10] J. Ching, Z. Yang, and K.-K. Phoon. "Dealing with nonlattice data in three-dimensional probabilistic site characterization". In: *Journal of Engineering Mechanics* 147.5 (2021), p. 06021003.

[11] V. De Oliveira. "Bayesian prediction of clipped Gaussian random fields". In: *Computational Statistics & Data Analysis* 34.3 (2000), pp. 299–314.

[12] M. DeGroot. *Optimal Statistical Decisions*. McGraw-Hill series in probability and statistics. New York City, NY: McGraw-Hill, 1969.

[13] W. J. Dixon. "Analysis of extreme values". In: *The Annals of Mathematical Statistics* 21.4 (1950), pp. 488–506.

[14] *EN 12390-6:2009. Testing hardened concrete - Part 6: Tensile splitting strength of test specimens*. European Standard, 2009.

[15] *EN 12504-2:2019. Testing concrete in structures - Part 2: Non-destructive testing - Determination of rebound number*. European Standard, 2019.

[16] *EN 12504-2:2021. Testing concrete in structures - Part 1: Cored specimens - taking, examining and testing in compression*. European Standard, 2021.

[17] *EN 12504-4:2019. Testing concrete in structures - Part 4: Determination of ultrasonic pulse velocity*. European Standard, 2019.

[18] *EN 131791:2019. Assessment of in-situ compressive strength in structures and precast concrete components*. European Standard, 2019.

[19] *EN 1990:2002. Eurocode 0: basis of structural and geotechnical design*. European Standard, 2002.

[20] *EN 1992-1-1:2004. Eurocode 2: design of concrete structures - part 1-1: general rules and rules for buildings.* European Standard, 2004.

[21] *EN 1993-1-1:2005. Eurocode 3: design of steel structures - part 1-1: general rules and rules for buildings.* European Standard, 2020.

[22] *EN 206-1:2000. Concrete - Part 1: Specification, performance, production and conformity.* European Standard, 2000.

[23] L. Fischer. "Bestimmung der 5%-Quantile im Zuge der Bauwerksprüfung [Determination of 5% quantile values in the course of inspection of structures]". In: *Bautechnik* 72.11 (1995), pp. 712–722.

[24] A. M. Freudenthal. "Safety and the probability of structural failure". In: *Transactions of the American Society of Civil Engineers* 121.1 (1956), pp. 1337–1375.

[25] A. Gelman, J. Carlin, H. Stern, D. Dunson, A. Vehtari, and D. Rubin. *Bayesian data analysis.* 3rd. Chapman & Hall/CRC texts in statistical science. Boca Raton, FL: CRC, 2013.

[26] S. Geyer, I. Papaioannou, L. Graham-Brady, and D. Straub. "The spatial averaging method for non-homogeneous random fields with application to reliability analysis". In: *Engineering Structures* 253 (2022), p. 113761.

[27] S. Geyer, I. Papaioannou, C. Kunz, and D. Straub. "Reliability assessment of large hydraulic structures with spatially distributed measurements". In: *Structure and Infrastructure Engineering* 16 (4 2020), pp. 599–612.

[28] S. Geyer, I. Papaioannou, and D. Straub. "Bayesian analysis of hierarchical random fields for material modeling". In: *Probabilistic Engineering Mechanics* 66 (2021), p. 103167.

[29] S. Geyer, I. Papaioannou, and D. Straub. "Characteristic values of spatially varying material properties in existing structures". In: *Proceedings of the seventh international symposium on life-cycle civil engineering.* Ed. by A. Chen, X. Ruan, and D. M. Frangopol. CRC Press/Balkema, 2020, pp. 479–486.

[30] M. Grigoriu, E. Garboczi, and C. Kafali. "Spherical harmonic-based random fields for aggregates used in concrete". In: *Powder Technology* 166.3 (2006), pp. 123–138.

[31] M. Grigoriu. "Crossings of non-Gaussian translation processes". In: *Journal of Engineering Mechanics* 110.4 (1984), pp. 610–620.

[32] F. E. Grubbs. "Sample criteria for testing outlying observations". In: *The Annals of Mathematical Statistics* 21.1 (1950), pp. 27–58.

[33] *ISO 5725-1:1994. Accuracy (trueness and precision) of measurement methods and results - Part 1: General principles and definitions.* International Standard, 1994.

[34] *JCSS probabilistic model code. Part 3 - resistance models.* Joint Committee on Structural Safety, 2001.

[35] M. Kersken-Bradley and R. Rackwitz. *Stochastic Modeling of Material Properties and Quality Control.* JCSS working document. International Association for Bridge and Structural Engineering, 1991.

[36] S. Keßler, J. Fischer, D. Straub, and C. Gehlen. "Updating of service-life prediction of reinforced concrete structures with potential mapping". In: *Cement and Concrete Composites* 47 (2014). Special issue: Durability of concrete, pp. 47–52.

[37] C.-C. Li and A. D. Kiureghian. "Optimal discretization of random fields". In: *Journal of Engineering Mechanics* 119.6 (1993), pp. 1136–1154.

[38] Y. Li, T. Vrouwenvelder, G. H. Wijnants, and J. Walraven. "Spatial variability of concrete deterioration and repair strategies". In: *Structural Concrete* 5.3 (2004), pp. 121–129.

[39] Y. Liu, J. Li, S. Sun, and B. Yu. "Advances in Gaussian random field generation: a review". In: *Computational Geosciences* 23.5 (2019), pp. 1011–1047.

[40] H. O. Madsen, S. Krenk, and N. C. Lind. *Method of Structural Safety*. Mineola, NY: Dover, 2006.

[41] A. Masi, A. Digrisolo, and G. Santarsiero. "Analysis of a large database of concrete core tests with emphasis on within-structure variability". In: *Materials* 12.12 (2019), p. 1985.

[42] B. Matérn. *Spatial Variation*. Lecture notes in statistics. Springer, 1986.

[43] R. Melchers and A. Beck. *Structural reliability analysis and prediction*. 3rd ed. Hoboken, NJ: John Wiley & Sons, 2018.

[44] S. Montoya-Noguera, T. Zhao, Y. Hu, Y. Wang, and K.-K. Phoon. "Simulation of non-stationary non-Gaussian random fields from sparse measurements using Bayesian compressive sampling and Karhunen–Loève expansion". In: *Structural Safety* 79 (2019), pp. 66–79.

[45] K. P. Murphy. *Machine learning: a probabilistic perspective*. Adaptive computation and machine learning. Cambridge, MA: MIT, 2013.

[46] A. Neville. *Properties of Concrete*. 5th ed. Pearson, 2011.

[47] N. T. Nguyen, Z.-M. Sbartaï, J.-F. Lataste, D. Breysse, and F. Bos. "Assessing the spatial variability of concrete structures using NDT techniques – Laboratory tests and case study". In: *Construction and Building Materials* 49 (2013), pp. 240–250.

[48] F. Pedrosa and C. Andrade. "Spatial variability of concrete electrical resistivity and corrosion rate in laboratory conditions". In: *Construction and Building Materials* 306 (2021), p. 124777.

[49] K.-K. Phoon and F. H. Kulhawy. "Characterization of geotechnical variability". In: *Canadian Geotechnical Journal* 36.4 (1999), pp. 612–624.

[50] S. Pöhlmann and R. Rackwitz. *Zwei Schätzprobleme bei Gauß'schen Folgen [Two estimation problems with Gaussian sequences]*. Berichte zur Zuverlässigkeitstheorie der Bauwerke, Sonderforschungsbereich 96, Heft 53. Technische Universität München, 1981.

[51] R. Rackwitz. "Predictive distribution of strength under control". In: *Matériaux et Constructions* 16 (1983), pp. 259–267.

[52] C. P. Robert. *The Bayesian choice: from decision-theoretic foundations to computational implementation*. 2nd ed. New York City, NY: Springer Science+Business Media, 2007.

[53] H. Rüsch, R. Sell, and R. Rackwitz. *Statistische Analyse der Betonfestigkeit [Statistical analysis of concrete strength]*. Deutscher Ausschuss für Stahlbeton 206, 1969.

[54] G. Stefanou, D. Savvas, and P. Metsis. "Random material property fields of 3D concrete microstructures based on CT image reconstruction". In: *Materials* 14.6 (2021), p. 1423.

[55] M. G. Stewart and Q. Suo. "Extent of spatially variable corrosion damage as an indicator of strength and time-dependent reliability of RC beams". In: *Engineering Structures* 31.1 (2009), pp. 198–207.

[56] B. Sudret and A. Der Kiureghian. *Stochastic finite element methods and reliability: a state-of-the-art report*. Report on research No. UCB/SEMM-2000/08. University of California, Berkeley, 2000.

[57] J. Tao and J. Chen. “A hierarchy model for the uncertainty quantification of spatial variability in the constitutive parameters of concrete in structures”. In: *Structural Safety* 95 (2022), p. 102181.

[58] R. J. Torrent. “The log-normal distribution: a better fitness for the results of mechanical testing of materials”. In: *Matériaux et Construction* 11.4 (1978), pp. 235–245.

[59] L. H. Vanegas and G. A. Paula. “Log-symmetric distributions: statistical properties and parameter estimation”. In: *Brazilian Journal of Probability and Statistics* 30.2 (2016), pp. 196–220.

[60] E. Vanmarcke. *Random fields: analysis and synthesis*. Revised and expanded new edition. World Scientific, 2010.

[61] Y. Wang and T. Zhao. “Statistical interpretation of soil property profiles from sparse data using Bayesian compressive sampling”. In: *Géotechnique* 67.6 (2017), pp. 523–536.

[62] Z. Wang and J. Song. “Cross-entropy-based adaptive importance sampling using von Mises-Fisher mixture for high dimensional reliability analysis”. In: *Structural Safety* 59 (2016), pp. 42–52.

[63] A. Westendarp, H. Becker, J. Bödefeld, H. Fleischer, C. Kunz, M. Maisner, H. Müller, A. Rahimi, T. Reschke, and F. Spörel. “Erhaltung und Instandsetzung von massiven Verkehrswasserbauwerken [Maintenance and repair of massive hydraulic structures]”. In: *Beton-Kalender 2015*. Hoboken, NJ: John Wiley & Sons, 2014, pp. 185–246.

[64] T. Xu and J. Li. “Assessing the spatial variability of the concrete by the rebound hammer test and compression test of drilled cores”. In: *Construction and Building Materials* 188 (2018), pp. 820–832.

[65] H. Zhu and L. Zhang. “Characterizing geotechnical anisotropic spatial variations using random field theory”. In: *Canadian Geotechnical Journal* 50.7 (2013), pp. 723–734.

Chapter 7

The spatial averaging method for non-homogeneous random fields with application to reliability analysis

Original publication

S. Geyer, I. Papaioannou, L. Graham-Brady, and D. Straub. "The spatial averaging method for non-homogeneous random fields with application to reliability analysis". In: *Engineering Structures* 235 (2022), p. 113761. DOI: 10.1016/j.engstruct.2021.113761.

Author's contribution

Sebastian Geyer, Iason Papaioannou, Lori Graham-Brady, and Daniel Straub developed the concept for applying the spatial averaging method to non-homogeneous random fields. The mathematical derivations were carried out by Sebastian Geyer, Iason Papaioannou, and Daniel Straub. Sebastian Geyer wrote the code underlying the numerical studies and carried out all numerical experiments. Sebastian Geyer wrote the original draft of the manuscript, which was then edited and finalized by himself, Iason Papaioannou, Lori Graham-Brady, and Daniel Straub.

Abstract

In probabilistic assessments, inputs with significant spatial variability should be modeled with random fields. Random fields can be non-homogeneous with location-specific marginal distributions, for example, due to site-specific information incorporated through Bayesian analysis or due to spatial trends in the mean or variance of the uncertain quantity. This paper investigates the spatial averaging method for the discretization of non-homogeneous random fields. In this approach, the random field is reduced to a set of random variables representing its local averages over a corresponding set of elemental domains. This is of particular benefit when coupling the random field model with finite elements for structural analysis. We extend the application of the method to non-homogeneous Gaussian and non-Gaussian translation random fields with lognormal, Student's t- and log-Student's t-marginal distribution. The latter two distributions are particularly relevant if spatial data is used in a hierarchical Bayesian random field modeling. Two numerical investigations assess the ability of the method to efficiently represent the response variability and probability of failure of structural systems with spatially variable inputs. The investigations include the effect of different element sizes for the spatial averaging on the system

response and applicability of the spatial averaging method to assessing local and global failure modes.

7.1 Introduction

Many engineering applications require the consideration of physical quantities that vary randomly in space. Common examples include material properties in large structures [15], soil properties in geotechnical sites [30] and the apparent properties of composite materials [33]. Spatially variable properties can be modeled by random fields (RF) [41]. By definition an RF consists of an infinite number of random variables. Hence, numerical treatment of RFs requires their approximation in terms of a finite number of random variables, a task known as RF discretization. An overview of existing discretization methods can be found in [36] (with focus on the dimensionality reduction aspect) and, more recently, in [26] (with focus on the simulation cost).

The spatial averaging (SA) method expresses the RF through a set of random variables representing local averages of the field over a set of elements. The method was originally proposed by Vanmarcke and Grigoriu [42] and is extensively described in [41]. SA has been applied to homogeneous RFs in various applications and is commonly employed in the context of geotechnical analyses to approximate spatially variable soil properties [31, 9, 11, 6, 37]. Such problems have the advantage that geotechnical failure modes are typically dominated by average behavior and not by local extrema of the soil properties. Thus, an RF can often be sufficiently approximated by a small set of random variables or even a single random variable representing the averaging behavior of the RF over a spatial domain (e.g., a failure surface). SA has also been applied to problems in structural analysis to explicitly account for the spatial variability of loads and material properties [42, 40, 7, 18, 43].

The theory of SA supports the application of the method to non-homogeneous RFs, although it has been reported that it leads to increased numerical effort [44]. SA for non-homogeneous RFs has recently been applied in the context of reliability analysis in [14] and [28]. Non-homogeneous RFs occur, for example, when the spatial moment functions (mean and variance) follow a trend [e.g., 10, 5], or when a homogeneous RF is updated with measurement data through a Bayesian analysis [e.g., 13, 29, 15, 38, 35]. While in the first case it may be possible to express the RF as function of a homogeneous RF by means of a transformation or standardization [41], this does not hold for the latter case. This paper focuses on the second case, i.e., when the non-homogeneous behavior of the RF results from a Bayesian updating of the RF parameters. Such non-homogeneous RFs are characterized by local changes in the spatial mean function, local reductions of the spatial standard deviation function and a complex location-specific autocorrelation structure.

One of the advantages of SA over other RF discretization methods applicable to non-homogeneous RFs is the compact form of the resulting set of averaging random variables. If the RF is Gaussian, the averaging random variables are Gaussian random variables fully defined by a mean vector and a covariance matrix evaluated through spatial integration of the RF moment functions. Hence, it does not require the spectral decomposition of the covariance operator as is the case, e.g., for the Karhunen-Loève expansion [34, 17]. Moreover, each of the random variables directly represents the RF in a specific domain. That is, coupling of the method with a finite element model is straightforward, which makes it ideally suited for use in engineering applications [42, 40, 7]. In addition, the method can account for the fact that the response of structural systems is often determined by regions of high or low values and not by local extrema of random quantities. Last but not least, the illustrative character of the SA random variables can significantly enhance understanding and acceptance of spatial variability and thus increase the motivation in the engineering community for explicit modeling of RFs in engineering

assessments. A closely related method, termed local average subdivision tackles the problem by using a hierarchical approach from global to local averaging integrals of RFs to account for spatial variability and the effect of averaging behavior of properties [12]. It was originally developed for homogeneous RFs but can be extended to the general non-homogeneous case.

This paper presents the SA method for non-homogeneous Gaussian RFs following the theory in [41]. In the homogeneous case, the mean is not affected by the averaging operation and, thus, the mean of the spatially averaging random variables equals the mean of the random field. The covariance of the spatially averaging random variables is obtained by integration over the spatial autocorrelation function multiplied by the constant point-variance of the random field [41]. This is not possible for non-homogeneous random fields, where the parameters of the averaging random variables need to be calculated from the spatial mean function and the spatial covariance function. We provide the required expressions for the non-homogeneous case of one- and two-dimensional Gaussian random fields. Furthermore, we extend SA to a special class of non-Gaussian RFs, so-called translation RFs [19], and present application for RF models with lognormal, Student's t- and log-Student's t-marginal distribution. Student's t- and log-Student's t-RFs appear as predictive RFs when learning is performed with spatial data [16]. RFs with lognormal or log-Student's t-marginal distribution are advantageous for modeling non-negative quantities, such as strength parameter of materials, as the support of these distributions is limited to the positive axis.

The focus of the paper is the applicability of the SA method to forward uncertainty propagation and reliability analysis. We investigate the SA method by means of an application to a one-dimensional elastic beam structure with spatially variable beam flexibility. Thereby, we assess the effects of different mesh choices for the RF discretization with SA on the system response and the structural reliability. In a second numerical investigation, the SA method is applied for the reliability analysis of a ship lock chamber wall with spatial data on the concrete friction coefficient. The effect of varying dimension in the SA approximation on the accuracy in representing different failure mechanisms is investigated. On this basis, we conclude with recommendations on the implementation of the SA method for structural reliability analysis.

The remainder of this paper is structured as follows. In Section 7.2, the spatial averaging method is introduced and explained in detail for the case of one- and two-dimensional Gaussian random fields. An extension to a special class of non-Gaussian random fields can be found in Section 7.2.3. The presented methodology is illustrated with two numerical examples in Section 7.3 followed by short conclusions in Section 7.4.

7.2 Random field discretization with the spatial averaging method

An RF $X(\boldsymbol{z})$ is defined as a collection of random variables indexed by a continuous spatial coordinate $\boldsymbol{z} \in \boldsymbol{Z}$, where $\boldsymbol{Z} \subset \mathbb{R}^d$ is the spatial domain of definition of the RF, i.e., $d = 1,\ 2$ or 3. An RF is said to be Gaussian if the n-th order joint distribution of the random variables corresponding to any collection of points $\mathbf{z} = [\boldsymbol{z}_1, \ldots, \boldsymbol{z}_n] \in \boldsymbol{Z}$ is a multivariate Gaussian distribution. Gaussian RFs are completely defined by their spatial mean value $\mu_X(\boldsymbol{z})$, their spatial standard deviation $\sigma_X(\boldsymbol{z})$ and their autocorrelation function $\rho(\boldsymbol{z}_i, \boldsymbol{z}_j)$, defining the correlation at two locations $\boldsymbol{z}_i$ and $\boldsymbol{z}_j$ [1]. Any linear mapping of a Gaussian RF is also Gaussian since the Gaussian distribution remains closed under linear transformations [24].

An RF is called homogeneous if its n-th order joint PDF is invariant for a shift in $\boldsymbol{z}$, which implies that the marginal PDF $f_X(\boldsymbol{z})$ of the RF and its moments are space-invariant [21]. For Gaussian RFs, homogeneity is implied by homogeneity of the first two moment-functions, i.e., it

suffices to know that $\mu_X(\boldsymbol{z})$ and $\sigma_X(\boldsymbol{z})$ are constant in space, i.e., $\mu_X(\boldsymbol{z}) = \mu_X \ \forall \ \boldsymbol{z} \in \boldsymbol{Z}$ and $\sigma_X(\boldsymbol{z}) = \sigma_X \ \forall \ \boldsymbol{z} \in \boldsymbol{Z}$ and that the autocorrelation function $\rho(\boldsymbol{z}_i, \boldsymbol{z}_j)$ can be expressed as $\rho(\boldsymbol{d}_{i,j})$, where $\boldsymbol{d}_{i,j} = \boldsymbol{z}_i - \boldsymbol{z}_j$ is the difference in location of $\boldsymbol{z}_i$ and $\boldsymbol{z}_i$.

The spatial averaging method approximates the RF $X(\boldsymbol{z})$ by a set of random variables $\hat{X}_i, \ i = 1, \ldots, n_{SA}$, where each random variable represents the local average of $X(\boldsymbol{z})$ over the domain $\boldsymbol{Z}_i$ defined by the following integral [41]:

$$\hat{X}_i = \frac{I_i}{\Omega_i} = \frac{1}{\Omega_i} \int_{\boldsymbol{Z}_i} X(\boldsymbol{\zeta}) \mathrm{d}\boldsymbol{\zeta}, \tag{7.1}$$

where Ω_i is the volume of the spatial domain $\boldsymbol{Z}_i$. I_i is the local integral of $X(\boldsymbol{z})$ over the domain $\boldsymbol{Z}_i$. All derivations in this study restrict to one- and two-dimensional RFs but the theoretical approach can be extended to three-dimensional RFs and the general d-dimensional case [41].

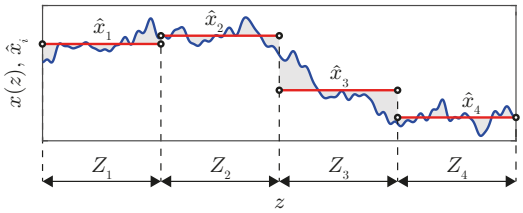

Figure 7.1: Random realization of a one-dimensional RF $x(z)$ (blue line) and its approximation with four averaging elements of equal length (red lines, $\hat{x}_i, \ i = 1, \ldots, 4$).

Figure 7.1 shows a random realization of a one-dimensional RF $x(z)$ in blue and its corresponding realization with an SA discretization of four averaging elements of equal length in red ($\hat{x}_i, \ i = 1, \ldots, 4$). Each $\hat{x}_i, \ i = 1, \ldots, 4$ represents the average of the RF realization $x(z)$ over the corresponding interval Z_i. Figure 7.2 shows a realization of a two-dimensional RF (panel a) and its corresponding realization with an SA discretization of 16 square averaging elements of equal size. Both figures show that local fluctuations of the RF average out and thus disappear in the SA realization while on a larger scale the spatial variability of the RF is identified and represented. An increasing number of averaging elements results in a more accurate representation of the RF and thus in better representation of local fluctuations.

If $X(\boldsymbol{z})$ is a Gaussian RF, the random variables $\hat{X}_i, \ i = 1, \ldots, _{SA}$, for the discretization with SA are also Gaussian because of the linearity of the integral operation in Equation (7.1). It is possible to use SA for non-Gaussian RFs if the RF can be expressed as function of an underlying Gaussian RF by an isoprobabilistic marginal transformation [19]. Examples of such translation random fields where the transformation is available in closed form are presented in Section 7.2.3.

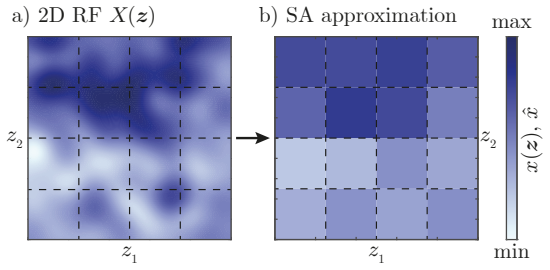

Figure 7.2: Random realization of a two-dimensional RF $X(z)$ (panel a) and its SA approximation with 16 square averaging elements of equal size (panel b).

The mean of the random variable $\hat{X}_i$ can be found by integration of the spatial function for

the mean $\mu_X(\boldsymbol{z})$ over the averaging domain $\boldsymbol{Z}_i$ [41]:

$$\mu_{\hat{X}_i} = \frac{1}{\Omega_i} \int_{\boldsymbol{Z}_i} \mu_X(\boldsymbol{\zeta}) \, \mathrm{d}\boldsymbol{\zeta}. \tag{7.2}$$

By integration over the spatial autocovariance function $C_X(\boldsymbol{z}_1, \boldsymbol{z}_2)$ the variance of $\hat{X}_i$ can be found [41, 14]:

$$\mathrm{Var}\left(\hat{X}_i\right) = \frac{1}{\Omega_i^2} \int_{\boldsymbol{Z}_i} \int_{\boldsymbol{Z}_i} C_X(\boldsymbol{\zeta}_1, \boldsymbol{\zeta}_2) \, \mathrm{d}\boldsymbol{\zeta}_1 \mathrm{d}\boldsymbol{\zeta}_2. \tag{7.3}$$

The integration in Equation (7.2) is d-dimensional, where d is the spatial dimension of $X(\boldsymbol{z})$. Accordingly, the total dimension of the integration in Equation (7.3) is $2d$. The covariance of two random variables $\hat{X}_i$ and $\hat{X}_j$ cannot be obtained directly from the autocovariance function. Its derivation is presented for the one- and two-dimensional case in the respective subsections.

If $X(\boldsymbol{z})$ is a homogeneous RF, the mean and variance are constant over $\boldsymbol{Z}$. In this case, the mean is not affected by the averaging integration, i.e., $\mu_{\hat{X}_i} = \mu_X, \ i = 1, \dots, n_{SA}$ and the variance is given as linear function of the RF variance: $\mathrm{Var}\left(\hat{X}_i\right) = \gamma_i \mathrm{Var}(X), \ i = 1, \dots, n_{SA}$, where γ_i is the variance function representing the average of the autocorrelation function of the field [40, 41]. γ_i expresses the reduction in the variance caused by the averaging operation and, hence, decreases with increasing size of the averaging element. It holds that $\gamma_i = 1$ if $\Omega_i = 0$ and $\gamma_i \to 0$ for $\Omega_i \to \infty$ [22, 41]. In the homogeneous case, SA underestimates the true variance of the RF in each SA element for $\Omega_i > 0$ [7, 27]. This property cannot be directly transferred to the non-homogeneous case on the element level due to a potentially strong fluctuation of the spatial variance function, but remains true in a global view of the RF variability.

For homogeneous RFs, the SA method is extensively described in [41]. This paper focuses on non-homogeneous RFs that have a complex autocorrelation structure and, hence, cannot be transformed into homogeneous RFs.

7.2.1 Spatial averaging for one-dimensional Gaussian random fields

For the discretization of a one-dimensional RF $X(z)$ with n_{SA} spatially averaging domains, Equations (7.2) and (7.3) can be rewritten for element $i, \ i = 1, \dots, n_{SA}$ as follows [41, 14]:

$$\mu_{\hat{X}_i} = \frac{1}{L_i} \int_{z_{i_0}}^{z_{i_1}} \mu_X(z) \, \mathrm{d}z, \tag{7.4}$$

$$\mathrm{Var}\left(\hat{X}_i\right) = \frac{1}{L_i^2} \int_{z_{i_0}}^{z_{i_1}} \int_{z_{i_0}}^{z_{i_1}} C_X(z, z') \, \mathrm{d}z \mathrm{d}z', \tag{7.5}$$

where z_{i_0} and z_{i_1} denote beginning and end of the averaging domain Z_i and L_i is the length of this domain, i.e., $L_i = z_{i_1} - z_{i_0}$.

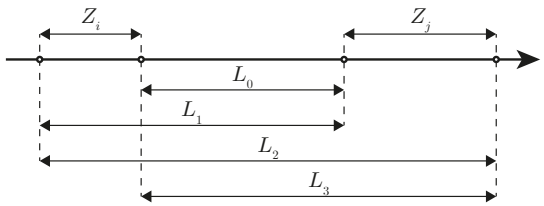

Figure 7.3: Lengths $L_k, \ k = 0, \dots 3$ of the auxiliary intervals for the calculation of the covariance of the random variables $\hat{X}_i$ and $\hat{X}_j$ representing the average behavior of the RF $X(z)$ in the local intervals Z_i and Z_j.

The calculation of the covariance of two averaging random variables $\hat{X}_i$ and $\hat{X}_j$ requires four auxiliary lengths $L_k,\ k = 0, \dots 3$, which are illustrated in Figure 7.3 together with the averaging domains Z_i and Z_j. The following algebraic identity can be defined using the local integrals $I_k = \int_{L_k} X(\boldsymbol{\zeta}) \mathrm{d}\boldsymbol{\zeta}$, (cf. Equation (7.1)) over the illustrated domains [41]:

$$2 I_i I_j = I_0^2 - I_1^2 + I_2^2 - I_3^2. \tag{7.6}$$

Applying the expectation operator on both sides of Equation (7.6) gives

$$2 \mathrm{E}\left[I_i I_j\right] = \mathrm{E}\left[I_0^2\right] - \mathrm{E}\left[I_1^2\right] + \mathrm{E}\left[I_2^2\right] - \mathrm{E}\left[I_3^2\right]. \tag{7.7}$$

Taking the expectation of the individual terms in Equation (7.6) results in [41]

$$2 \mathrm{E}\left[I_i\right] \mathrm{E}\left[I_j\right] = \mathrm{E}^2\left[I_0\right] - \mathrm{E}^2\left[I_1\right] + \mathrm{E}^2\left[I_2\right] - \mathrm{E}^2\left[I_3\right]. \tag{7.8}$$

Subtracting Equation (7.8) from Equation (7.7) gives the following expression for the covariance of I_i and I_j:

$$C\left(I_i, I_j\right) = \frac{1}{2}\Big(\mathrm{Var}\left(I_0\right) - \mathrm{Var}\left(I_1\right) + \mathrm{Var}\left(I_2\right) - \mathrm{Var}\left(I_3\right)\Big). \tag{7.9}$$

The covariance of $\hat{X}_i$ and $\hat{X}_j$ can be calculated making use of their proportionality to I_i and I_j defined in Equation (7.1):

$$C\left(\hat{X}_i, \hat{X}_j\right) = \frac{C\left(I_i, I_j\right)}{L_i L_j}. \tag{7.10}$$

Using Equation (7.9), one gets [41, 14]:

$$C\left(\hat{X}_i, \hat{X}_j\right) = \frac{1}{2 L_i L_j} \sum_{k=0}^{3} (-1)^k \Delta\left(Z_k\right), \tag{7.11}$$

where $\Delta\left(Z_k\right)$ is given by

$$\Delta\left(Z_k\right) = L_k^2 \mathrm{Var}\left(\hat{X}_k\right). \tag{7.12}$$

When $Z_j = Z_i$, Equation (7.11) simplifies to $L_0 = L_2 = L_i$ and $L_1 = L_3 = 0$ (cf. Figure 7.3). Accordingly, $\Delta\left(Z_0\right) = \Delta\left(Z_2\right) = L_i^2 \mathrm{Var}\left(\hat{X}_i\right)$ and $\Delta\left(Z_1\right) = \Delta\left(Z_3\right) = 0$ and hence Equation (7.11) reduces to Equation (7.5). The random variables $\hat{X}_i,\ i = 1, \dots n_{SA}$ are Gaussian random variables and thus the discretization of $X(z)$ is fully defined by the mean vector $\boldsymbol{\mu}_{\hat{X}}$ containing the individual mean values $\mu_{\hat{X}_i}, i = 1, \dots n$ and the covariance matrix $\mathbf{C}_{\hat{X}}$, where $C_{\hat{X}}\left(i, j\right), i = 1, \dots n_{SA},\ j = 1, \dots n_{SA}$ is given by the covariance of $\hat{X}_i$ and $\hat{X}_j$.

7.2.2 Spatial averaging for two-dimensional Gaussian random fields

Let $X(\boldsymbol{z})$ be a two-dimensional Gaussian RF, where $\boldsymbol{z} \in \boldsymbol{Z}$ describes a position in the two-dimensional domain $\boldsymbol{Z}$. SA proceeds by dividing $\boldsymbol{Z}$ into n_{SA} rectangular elements with edges parallel to the coordinate axes z_1 and z_2. Expressions for the mean and variance of the random variables $\hat{X}_i,\ i = 1, \dots n_{SA}$ representing the average of $X(\boldsymbol{z})$ in the i-th element can be found from Equations (7.2) and (7.3) [41]:

$$\mu_{\hat{X}_i} = \frac{1}{A_i} \int_{z_{2,i_0}}^{z_{2,i_1}} \int_{z_{1,i_0}}^{z_{1,i_1}} \mu_X(z_1, z_2)\ \mathrm{d}z_1 \mathrm{d}z_2, \tag{7.13}$$

$$\mathrm{Var}\left(\hat{X}_i\right) = \frac{1}{A_i^2}\int_{z_{2,i_0}}^{z_{2,i_1}}\int_{z_{2,i_0}}^{z_{2,i_1}}\int_{z_{1,i_0}}^{z_{1,i_1}}\int_{z_{1,i_0}}^{z_{1,i_1}} C_X(z_1, z_2; z_1', z_2')\,\mathrm{d}z_1\mathrm{d}z_1'\mathrm{d}z_2\mathrm{d}z_2', \tag{7.14}$$

where $A_i = Z_{1,i}Z_{2,i}$ denotes the area of the averaging domain. $Z_{1,i}$ and $Z_{2,i}$ are the lengths of the edges in z_1, z_2 respectively, i.e., $Z_{1,i} = z_{1,i_1} - z_{1,i_0}$ and $Z_{2,i} = z_{2,i_1} - z_{2,i_0}$.

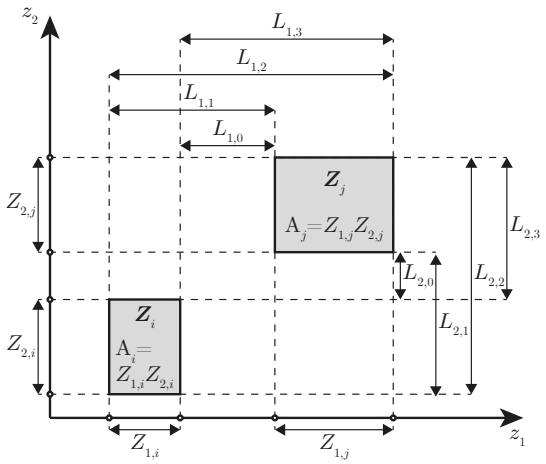

Figure 7.4: Edges $L_{1,k}$ and $L_{2,l}$ of the auxiliary domains $\boldsymbol{Z}_{kl}$, $k = 0, \ldots 3$, $l = 0, \ldots 3$ for calculating the covariance of the random variables $\hat{X}_i$ and $\hat{X}_j$ representing the average behavior of the RF $X(\boldsymbol{z})$ in the rectangular domains $\boldsymbol{Z}_i$ and $\boldsymbol{Z}_j$.

Equations (7.6) to (7.11) can be extended to the two-dimensional case (cf. Figure 7.4) to obtain the following expression for the covariance of two averaging random variables $\hat{X}_i$ and $\hat{X}_j$ [41]:

$$C\left(\hat{X}_i, \hat{X}_j\right) = \frac{1}{4A_iA_j}\sum_{k=0}^{3}\sum_{l=0}^{3}(-1)^k(-1)^l\,\Delta\left(Z_{1,k}, Z_{2,l}\right), \tag{7.15}$$

where A_i and A_j denote the areas of $\boldsymbol{Z}_i$ and $\boldsymbol{Z}_j$, which are the averaging domains for $\hat{X}_i$ and $\hat{X}_j$. $\Delta\left(Z_{1,k}, Z_{2,l}\right)$ is defined as

$$\Delta\left(Z_{1,k}, Z_{2,l}\right) = A_{kl}^2\,\mathrm{Var}\left(\hat{X}_{kl}\right). \tag{7.16}$$

$A_{kl} = L_{1,k}L_{2,l}$ is the area of the rectangular auxiliary domain $\boldsymbol{Z}_{kl}$, $k = 0, \ldots, 3$, $l = 0, \ldots, 3$. Figure 7.4 shows the averaging domains $\boldsymbol{Z}_i$ and $\boldsymbol{Z}_j$ and the edges of the auxiliary domains. The random variables $\hat{X}_i$, $i = 1, \ldots n_{SA}$ are Gaussian random variables. Hence, similar to the one-dimensional case, the mean vector $\boldsymbol{\mu}_{\hat{X}}$ and covariance matrix $\mathbf{C}_{\hat{X}}$ of the random variables $\hat{X}_i$, $i = 1, \ldots n_{SA}$, are sufficient to discretize $X(\boldsymbol{z})$.

Equations (7.13) to (7.15) are only applicable for rectangular averaging elements. If the domain $\boldsymbol{Z}$ cannot be divided into rectangular averaging domains, it needs to be approximated by such a domain [41]. An example is shown in Figure 7.5, where $\boldsymbol{Z}$ is approximated by the enveloping domain $\tilde{\boldsymbol{Z}}$. A prescribed degree of accuracy for the approximation can be achieved by adjusting the size of the rectangular elements and, if necessary, introducing a rotation of the coordinate system. The studies in this paper are restricted to the case where $\boldsymbol{Z}$ can be divided into rectangular averaging elements.

7.2.3 Spatial averaging for non-Gaussian translation random fields

Although, in theory, the SA method is applicable to non-Gaussian RFs, in practice, the derived equations for the parameters of the averaging random variables are only sufficient in the Gaussian

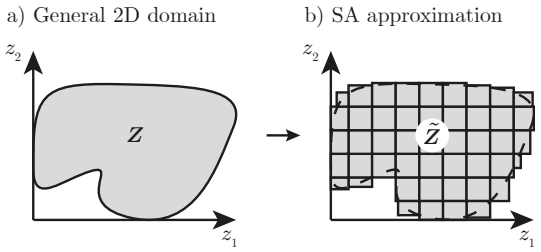

Figure 7.5: Approximation of a non-rectangular two-dimensional domain $\boldsymbol{Z}$ by an enveloping domain $\tilde{\boldsymbol{Z}}$ consisting of rectangular elements of variable size.

case. For most other cases it is difficult or even impossible to find all required expressions for obtaining a complete probabilistic description of the resulting RVs $\hat{X}_i$ [7]. However, it is possible to extend the applicability of the method to the class of so-called translation RFs, given by the following marginal transformation [20, 24]:

$$X(\boldsymbol{z}) = T\left(U(\boldsymbol{z})\right). \tag{7.17}$$

$U(\boldsymbol{z})$ is a zero-mean and unit-variance Gaussian RF with autocorrelation coefficient function $\rho_U(\boldsymbol{z}, \boldsymbol{z}')$. The mapping of Equation (7.17) is designed to preserve a given marginal cumulative distribution function (CDF) $F_X(x)$ of the RF $X(\boldsymbol{z})$. Given that $F_X(x)$ is strictly increasing, $T(\cdot)$ can be defined as $T(\cdot) = F_X^{-1}\left(\Phi(\cdot)\right)$, where $F_X^{-1}(\cdot)$ denotes the inverse CDF of $X(\boldsymbol{z})$ and $\Phi(\cdot)$ is the standard normal CDF [25]. $U(\boldsymbol{z})$ can be obtained from $X(\boldsymbol{z})$ by inversion of Equation (7.17), i.e., $U(\boldsymbol{z}) = T^{-1}\left(X(\boldsymbol{z})\right)$. Note that, in order to approximate the RF with a set of Gaussian random variables, the spatial correlation needs to be modeled for the underlying Gaussian RF. Three special cases of translation RFs, for which $T(\cdot)$ is given by an analytic expression, are presented in the following. The equations are given for a single averaging element over the entire domain of definition but can be generalized by dividing $\boldsymbol{Z}$ into subdomains and applying the Equations for mean and covariance derived for the Gaussian case.

7.2.3.1 Lognormal random field

In contrast to a Gaussian RF, a lognormal RF can be used to model non-negative quantities, which makes it preferable, e.g., for modeling mechanical properties. Consider an RF $Y(\boldsymbol{z})$ on the domain $\boldsymbol{Z}$ defined by the following function of a zero-mean and unit-variance Gaussian RF $U(\boldsymbol{z})$:

$$Y(\boldsymbol{z}) = \exp\Big(U(\boldsymbol{z}) \cdot \sigma_X(\boldsymbol{z}) + \mu_X(\boldsymbol{z})\Big) = \exp\Big(X\left(\boldsymbol{z}\right)\Big). \tag{7.18}$$

$X(\boldsymbol{z})$ is a Gaussian RF with mean function $\mu_X(\boldsymbol{z})$ and standard deviation function $\sigma_X(\boldsymbol{z})$. F_Y at any $\boldsymbol{z} \in \boldsymbol{Z}$ is a lognormal distribution, with parameters $\mu_{\ln Y}(\boldsymbol{z}) = \mu_X(\boldsymbol{z})$ and $\sigma_{\ln Y}(\boldsymbol{z}) = \sigma_X(\boldsymbol{z})$:

$$Y(\boldsymbol{z}) \sim \log\mathcal{N}\left(\mu_{\ln Y}(\boldsymbol{z}), \sigma_{\ln Y}(\boldsymbol{z})\right). \tag{7.19}$$

Spatial averaging is then performed for $X(\boldsymbol{z})$ resulting in a Gaussian random variable $\hat{X}_{\boldsymbol{Z}}$ with parameters $\mu_{\hat{X}}$ and $\sigma_{\hat{X}} = \sqrt{\mathrm{Var}\left(\hat{X}_{\boldsymbol{Z}}\right)}$ given by Equations (7.2) and (7.3). Applying the transformation of Equation (7.18) gives

$$\hat{Y}_{\boldsymbol{Z}} = \exp\left(\frac{1}{\Omega_{\boldsymbol{Z}}} \int_{\boldsymbol{Z}} X(\boldsymbol{\zeta}) \mathrm{d}\boldsymbol{\zeta}\right) = \exp\left(\hat{X}_{\boldsymbol{Z}}\right), \tag{7.20}$$

where $\hat{Y}_{\boldsymbol{Z}}$ is a lognormal distributed random variable with parameters $\mu_{\ln\hat{Y}} = \mu_{\hat{X}}$ and $\sigma_{\ln\hat{Y}} = \sigma_{\hat{X}}$. Due to the non-linear transformation, $\hat{Y}_{\boldsymbol{Z}}$ does not represent the arithmetic average but the geometric average of $Y(\boldsymbol{z})$ over $\boldsymbol{z}$. It is noted that the geometric average is always smaller than or equal to the arithmetic average. Hence, using the geometric average for the SA discretization of a lognormal RF provides a lower bound on the spatial average of the RF. While this is reasonable and conservative for some modeling cases (e.g., for low-strength dominated soil properties [e.g., 9, 11]), it may provide a non-appropriate approximation of the true RF when the RF represents a load/demand on the structure [e.g., 6].

7.2.3.2 Student's t-random field

The Student's t-distribution can be used to model a Gaussian quantity accounting for the uncertainty in the parameters of the Gaussian distribution [e.g., 3]. Consider a Student's t-RF $Y(\boldsymbol{z})$, in which F_Y at any $\boldsymbol{z} \in \boldsymbol{Z}$ is a Student's t-distribution, with location parameter $\mu_Y(\boldsymbol{z})$, scale parameter $\sigma_Y(\boldsymbol{z})$ and degrees of freedom ν_Y [3, 23, 16]:

$$Y(\boldsymbol{z}) \sim \mathcal{T}\left(\mu_Y(\boldsymbol{z}), \sigma_Y(\boldsymbol{z}), \nu_Y\right). \tag{7.21}$$

Note that ν_Y is space-invariant. The transformation of Equation (7.17) is given as [23]:

$$Y(\boldsymbol{z}) = \sqrt{\frac{\nu_Y}{\chi}}\Big(U(\boldsymbol{z}) \cdot \sigma_Y(\boldsymbol{z})\Big) + \mu_Y(\boldsymbol{z}) = \sqrt{\frac{\nu_Y}{\chi}} X(\boldsymbol{z}) + \mu_Y(\boldsymbol{z}), \tag{7.22}$$

where $X(\boldsymbol{z})$ is a zero-mean Gaussian RF with standard deviation $\sigma_X(\boldsymbol{z}) = \sigma_Y(\boldsymbol{z})$ and χ is a random variable that follows the χ^2 distribution with ν_Y degrees of freedom. As only $X(\boldsymbol{z})$ and the function for the mean value $\mu_Y(\boldsymbol{z})$ are subject to spatial variability, the spatial average $\hat{Y}_{\boldsymbol{Z}}$ over the domain $\boldsymbol{Z}$ can be expressed by the following averaging integral:

$$\begin{aligned}
\hat{Y}_{\boldsymbol{Z}} &= \frac{1}{\Omega_{\boldsymbol{Z}}} \int_{\boldsymbol{Z}} Y(\boldsymbol{\zeta}) \mathrm{d}\boldsymbol{\zeta} = \frac{1}{\Omega_{\boldsymbol{Z}}} \int_{\boldsymbol{Z}} \sqrt{\frac{\nu_Y}{\chi}} X(\boldsymbol{\zeta}) + \mu_Y(\boldsymbol{\zeta}) \mathrm{d}\boldsymbol{\zeta} = \\
&= \frac{\sqrt{\frac{\nu_Y}{\chi}}}{\Omega_{\boldsymbol{Z}}} \int_{\boldsymbol{Z}} X(\boldsymbol{\zeta}) \mathrm{d}\boldsymbol{\zeta} + \frac{1}{\Omega_{\boldsymbol{Z}}} \int_{\boldsymbol{Z}} \mu_Y(\boldsymbol{\zeta}) \mathrm{d}\boldsymbol{\zeta} = \\
&= \sqrt{\frac{\nu_Y}{\chi}} \hat{X}_{\boldsymbol{Z}} + \mu_{\hat{Y}},
\end{aligned} \tag{7.23}$$

where $\hat{X}_{\boldsymbol{Z}}$ is a zero-mean Gaussian random variable with variance calculated according to Equation (7.3) and $\mu_{\hat{Y}}$ is the mean of the spatial average of $Y(\boldsymbol{z})$ over $\boldsymbol{Z}$ as defined in Equation (7.2).

7.2.3.3 Log-Student's t-random field

The log-Student's t-distribution combines the lognormal and the Student's t-distribution and thus, can be used to model non-negative quantities accounting for parameter uncertainty [16]. Consider a log-Student's t-RF $V(\boldsymbol{z})$, i.e., F_V at any $\boldsymbol{z} \in \boldsymbol{Z}$ is a log-Student's t-distribution [16, 39]:

$$V(\boldsymbol{z}) \sim \ln\mathcal{T}\left(\mu_{\ln V}(\boldsymbol{z}), \sigma_{\ln V}(\boldsymbol{z}), \nu_V\right). \tag{7.24}$$

The parametrization of F_V is done by means of the parameters of the underlying Student's t-distribution. At any $\boldsymbol{z} \in \boldsymbol{Z}$ it holds that $Y(\boldsymbol{z}) = \ln(V(\boldsymbol{z}))$ follows a Student's t-distribution with location parameter $\mu_Y(\boldsymbol{z}) = \mu_{\ln V}(\boldsymbol{z})$, scale parameter $\sigma_Y(\boldsymbol{z}) = \sigma_{\ln V}(\boldsymbol{z})$ and degrees of freedom $\nu_Y = \nu_V$ [16]. By combining Equation (7.18) and (7.22), the transformation of Equation (7.17)

is given as follows:

$$V(\boldsymbol{z}) = \exp\left(\sqrt{\frac{\nu_V}{\chi}} \cdot (U(\boldsymbol{z}) \cdot \sigma_{\ln V}(\boldsymbol{z})) + \mu_{\ln V}(\boldsymbol{z})\right) = \exp\left(\sqrt{\frac{\nu_V}{\chi}} X(\boldsymbol{z}) + \mu_{\ln V}(\boldsymbol{z})\right). \tag{7.25}$$

$X(\boldsymbol{z})$ is a zero-mean Gaussian RF with standard deviation $\sigma_X(\boldsymbol{z}) = \sigma_{\ln V}(\boldsymbol{z})$ and χ is a random variable that follows the χ^2 distribution with ν_V degrees of freedom. The spatial average $\hat{V}_{\boldsymbol{Z}}$ over the domain $\boldsymbol{Z}$ can be calculated as follows:

$$\hat{V}_{\boldsymbol{Z}} = \exp\left(\frac{1}{\Omega_{\boldsymbol{Z}}} \int_{\boldsymbol{Z}} Y(\boldsymbol{\zeta}) \mathrm{d}\boldsymbol{\zeta}\right) = \exp\left(\frac{\sqrt{\frac{\nu_V}{\chi}}}{\Omega_{\boldsymbol{Z}}} \int_{\boldsymbol{Z}} X(\boldsymbol{\zeta}) \mathrm{d}\boldsymbol{\zeta} + \frac{1}{\Omega_{\boldsymbol{Z}}} \int_{\boldsymbol{Z}} \mu_{\ln V}(\boldsymbol{\zeta}) \mathrm{d}\boldsymbol{\zeta}\right) =$$

$$= \exp\left(\sqrt{\frac{\nu_V}{\chi}} \hat{X}_{\boldsymbol{Z}} + \mu_{\ln \hat{V}}\right). \tag{7.26}$$

$\hat{X}_{\boldsymbol{Z}}$ is a zero-mean Gaussian random variable with variance calculated according to Equation (7.3) and $\mu_{\ln \hat{V}}$ is the mean of the spatial average of $\ln(V(\boldsymbol{z})) = Y(\boldsymbol{z})$ over $\boldsymbol{Z}$. Similar to the lognormal RF in Section 7.2.3.1, $\hat{V}_{\boldsymbol{Z}}$ represents the geometric average of $V(\boldsymbol{z})$ over $\boldsymbol{Z}$ instead of the arithmetic average.

7.3 Numerical investigations

In this Section, the accuracy of the SA method for approximating non-homogeneous RFs is investigated by means of two numerical investigations. The non-homogeneity of the RFs in both cases stems from the combination of a homogeneous prior RF with measurement data. The first investigation is a one-dimensional beam under uniform load with spatially variable beam flexibility analyzed in a statically determinate setting with analytical solution and a statically indeterminate setting where the system response is evaluated using a finite element model. Different SA settings regarding element size and number are investigated for different output quantities of the structural system. The second investigation is a sliding failure mechanism in a ship lock chamber wall where the friction coefficient in a construction joint is modeled as a two-dimensional RF. Two different failure mechanisms are considered and the effect of the chosen SA discretization on the reliability estimates is analyzed.

7.3.1 Measures for the accuracy of the random field discretization

Discretizing an RF $X(\boldsymbol{z})$ with a finite number of random variables $\hat{X}_i,\ i = 1, \dots n$, yields an approximation error. If the $\hat{X}_i,\ i = 1, \dots n$, are used for uncertainty propagation through a numerical model, this error typically propagates through the model and is reflected in the model response. However, depending on the type of the quantity of interest, the error in the model response may be larger or smaller than the error in the RF approximation [38]. The point-wise approximation error is defined as the difference of the quantity of interest Q and its approximation $\hat{Q}$ at spatial location $\boldsymbol{z}$, i.e., $\varepsilon(\boldsymbol{z}) = Q(\boldsymbol{z}) - \hat{Q}(\boldsymbol{z})$. Based on $\varepsilon(\boldsymbol{z})$, numerous local and global error measures can be defined to assess the accuracy of a RF discretization. e.g., the bias, error variance or mean-square error [e.g., 24, 36, 2]. The latter two, include the covariance of $Q(\boldsymbol{z})$ and $\hat{Q}(\boldsymbol{z})$, which can require the numerical solution of a complex integral equation. In addition, their interpretation is not always straightforward and hence they are not further discussed here. Instead, we use the normalized bias $\varepsilon_\mu(\boldsymbol{z})$ and the normalized variance

error $\varepsilon_{\mathrm{V}}(\boldsymbol{z})$ as point-wise error measures in this study. They are defined as [38]

$$\varepsilon_{\mu}(\boldsymbol{z}) = \frac{\mathrm{E}\left[Q(\boldsymbol{z})\right] - \mathrm{E}\left[\hat{Q}(\boldsymbol{z})\right]}{\mathrm{E}\left[Q(\boldsymbol{z})\right]}, \tag{7.27}$$

$$\varepsilon_{\mathrm{V}}(\boldsymbol{z}) = \frac{\mathrm{Var}\left(Q(\boldsymbol{z})\right) - \mathrm{Var}\left(\hat{Q}(\boldsymbol{z})\right)}{\mathrm{Var}\left(Q(\boldsymbol{z})\right)}. \tag{7.28}$$

Taking the weighted integral of Equations (7.27) and (7.28) over the domain $\boldsymbol{Z}$ yields the corresponding global error measures [2]:

$$\bar{\varepsilon}_{\mu} = \frac{1}{\Omega}\int_{\boldsymbol{Z}} |\varepsilon_{\mu}(\boldsymbol{z})| \ \mathrm{d}\boldsymbol{z}, \tag{7.29}$$

$$\bar{\varepsilon}_{\mathrm{V}} = \frac{1}{\Omega}\int_{\boldsymbol{Z}} |\varepsilon_{\mathrm{V}}(\boldsymbol{z})| \ \mathrm{d}\boldsymbol{z}. \tag{7.30}$$

In addition, the influence of the RF discretization on the system response is assessed in terms of the system reliability, or equivalently its probability of failure. The failure event F is expressed in terms of a limit state function $g(X(\boldsymbol{z}))$, such that failure occurs if $g(X(\boldsymbol{z})) \leq 0$. That is, the probability of failure is $P_F = \Pr\Big(g(X(\boldsymbol{z})) \leq 0\Big)$. We will be comparing P_F with $\hat{P}_F = \Pr\Big(g(\hat{X}(\boldsymbol{z})) \leq 0\Big)$. Typically, $g(X(\boldsymbol{z}))$ is a function of an output quantity of interest $Q(\boldsymbol{z})$ and F occurs with a small probability. Hence, through assessing the influence of the RF discretization on the probability of failure, we evaluate the ability of the discretization to accurately represent the tails of the distribution of $Q(\boldsymbol{z})$.

7.3.2 Analysis of a one-dimensional beam

A one-dimensional beam subject to uniformly distributed vertical load is investigated, whose flexibility $F(z)$ is modeled by a Gaussian RF that is updated with measurement data. The beam has length $L = 2\,\mathrm{m}$ and the applied load is $q = 1.4\,\mathrm{kNm}^{-1}$. $\hat{F}(z)$ is the piece-wise constant SA approximation of $F(z)$ by using n_{SA} averaging elements. Euler-Bernoulli beam theory is used to evaluate the response of the structural system. We consider two different settings for the boundary conditions of the beam; a statically determinate case and a statically indeterminate case.

7.3.2.1 Random field model of the beam flexibility

The prior model of $F(z)$ is a homogeneous RF with a mean of $\mu'_F = 0.5\,\mathrm{MN}^{-1}\mathrm{m}^{-2}$ and a standard deviation of $\sigma'_F = 0.1\,\mathrm{MN}^{-1}\mathrm{m}^{-2}$. The prior autocorrelation function is modeled by the exponential correlation function [1]:

$$\rho'(z_i, z_j) = \exp\left(-\frac{2\,|z_j - z_i|}{\vartheta}\right), \tag{7.31}$$

where ϑ is the scale of fluctuation, which is set to $1\,\mathrm{m}$.

We assume that measurement data $\mathbf{M}$ is available in the form of n_m direct measurements of the beam flexibility $\boldsymbol{x}_m = [x_{m,1}, \ldots, x_{m,n_m}]$ and the corresponding measurement locations $\boldsymbol{z}_m = [z_{m,1}, \ldots, z_{m,n_m}]$. These measurements are associated with an additive zero-mean Gaussian measurement error ε with standard deviation $\sigma^2_{\varepsilon} = 0.05\mu'_F$. In this case, updating of $F(z)$ can be done in closed form by making use of the self-conjugacy of the Gaussian distribution, resulting

in the following posterior mean and covariance functions [41, 29, 15]:

$$\mu''_F(z) = \mu'_F + \boldsymbol{R}_{\boldsymbol{z}_m}(z) \cdot \mathbf{R}^{-1}_{\boldsymbol{z}_m,\varepsilon} \cdot \left(\boldsymbol{x}_m - \mu'_F\right)^{\mathsf{T}}, \tag{7.32}$$

$$C''_F(z_i, z_j) = \left(\sigma'_F\right)^2 \cdot \left(\rho(z_i, z_j) - \boldsymbol{R}_{\boldsymbol{z}_m}(z_i) \cdot \mathbf{R}^{-1}_{\boldsymbol{z}_m,\varepsilon} \cdot \boldsymbol{R}^{\mathsf{T}}_{\boldsymbol{z}_m}(z_j)\right). \tag{7.33}$$

$\boldsymbol{R}_{\boldsymbol{z}_m}(z)$ is a $1 \times n_m$ row vector function with element i equal to $\rho'(z, z_{m,i})$. $\mathbf{R}_{\boldsymbol{z}_m,\varepsilon} = \mathbf{R}_{\boldsymbol{z}_m,\boldsymbol{z}_m} + \mathbf{R}_\varepsilon$, where $\mathbf{R}_{\boldsymbol{z}_m,\boldsymbol{z}_m}$ is an $n_m \times n_m$ matrix with element (i,j) equal to $\rho'(z_{m,i}, z_{m,j})$ and $\mathbf{R}_\varepsilon = \left(\frac{\sigma_\varepsilon}{\sigma'_F}\right)^2 \cdot \mathrm{I}$, where I is the $n_m \times n_m$ identity matrix.

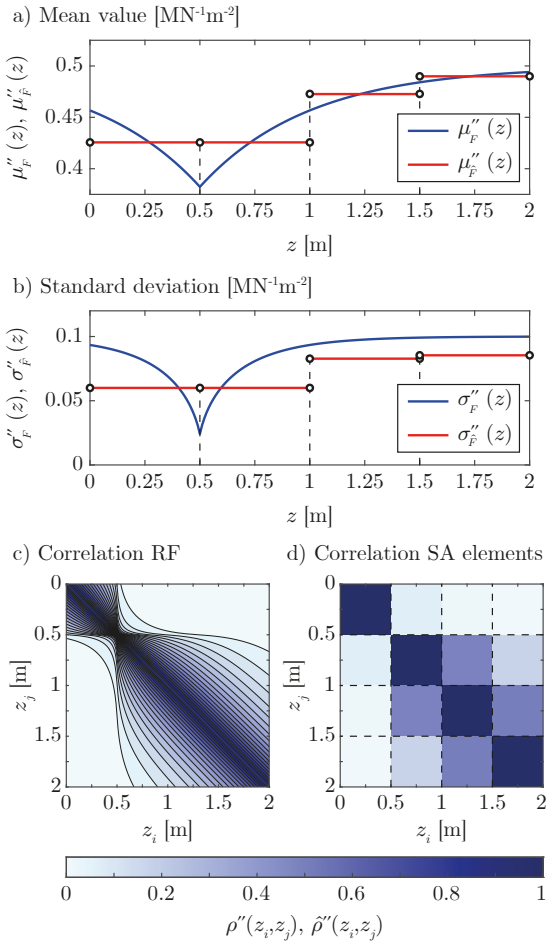

Figure 7.6: Posterior spatial mean value (panel a) and standard deviation (panel b) of the RF for the beam flexibility $F''(z)$ (blue) and its approximation with four averaging elements $\hat{F}''(z)$ (red); posterior spatial autocorrelation of the RF $F''(z)$ (panel c) and correlation of the four averaging random variables for the approximation of $F''(z)$ with SA (panel d).

A single measurement $f_m = 0.75 \cdot \mu'_F = 0.375\,\mathrm{MN}^{-1}\mathrm{m}^{-2}$ at measurement location $z_m = 0.25L = 0.5\,\mathrm{m}$ is considered in the RF update. The resulting posterior RF parameters of the beam flexibility are obtained by application of Equations (7.32) and (7.33). We first set the number of SA elements to $n_{SA} = 4$. Figure 7.6 illustrates the posterior RF parameters together with the parameters of the corresponding four spatial averaging random variables calculated by means of Equations (7.4), (7.5) and (7.11). The measurement leads to a reduction in the mean value at the measurement location and in the region around the measurement compared to the prior mean (blue line in panel a). In addition, the uncertainty and hence the standard deviation at the measurement location and in its vicinity is reduced (blue line in panel b). These

effects decrease with increasing distance from the measurement location and thus the posterior parameters converge to the prior parameters. A similar effect can be observed in the posterior correlation structure (panel c). The parameters of the spatial averaging random variables reflect the non-homogeneity, however the local extrema in the spatial mean and standard deviation average out when applying the averaging operations for the discretization with SA (red lines in panel a and b). The spatial autocorrelation function of the RF is approximated by a 4×4 correlation matrix (panel d). Again, the SA discretization accounts for the non-homogeneity of the RF but local effects average out.

7.3.2.2 Statically determinate cantilever beam

The statically determinate cantilever beam is illustrated in Figure 7.7. The internal forces are independent of the flexibility and hence the bending moment $M(z)$ can be directly calculated as $M(z) = -\frac{q}{2}(L-z)^2$. Using the Euler-Bernoulli beam theory, the rotation $\varphi(z)$ and vertical displacement $w(z)$ as illustrated in Figure 7.7 are obtained as follows:

$$\varphi(z) = -\frac{q}{2}\int_0^z (L-t)^2 F(t)\,\mathrm{d}t, \tag{7.34}$$

$$w(z) = -\frac{q}{2}\int_0^z \int_0^s (L-t)^2 F(t)\,\mathrm{d}t\mathrm{d}s. \tag{7.35}$$

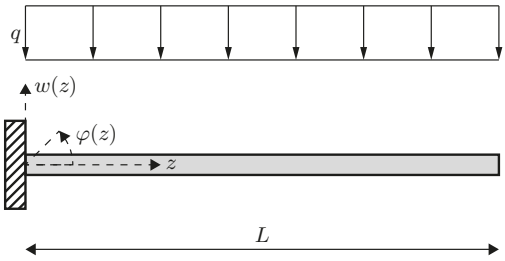

Figure 7.7: Statically determinate cantilever beam under uniform vertical load q.

Since $F(z)$ is modeled with a Gaussian RF and $\varphi(z)$ and $w(z)$ are linear functions of $F(z)$, they are also Gaussian RFs. Based on Equations (7.34) and (7.35), spatial functions for the mean and autocovariance of the system response RFs can be derived:

$$\mu_\varphi(z) = -\frac{q}{2}\int_0^z (L-t)^2 \mu_F(t)\,\mathrm{d}t, \tag{7.36}$$

$$C_\varphi(z_i, z_j) = \frac{q^2}{4}\int_0^{z_j}\int_0^{z_i} (L-t_i)^2 (L-t_j)^2 C_F(t_i, t_j)\,\mathrm{d}t_i\mathrm{d}t_j, \tag{7.37}$$

$$\mu_w(z) = -\frac{q}{2}\int_0^z \int_0^s (L-t)^2 \mu_F(t)\,\mathrm{d}t\mathrm{d}s, \tag{7.38}$$

$$C_w(z_i, z_j) = \frac{q^2}{4}\int_0^{z_j}\int_0^{z_i}\int_0^{s_j}\int_0^{s_i} (L-t_i)^2 (L-t_j)^2 C_F(t_i, t_j)\,\mathrm{d}t_i\mathrm{d}t_j\mathrm{d}s_i\mathrm{d}s_j. \tag{7.39}$$

Replacing $\mu_F(t)$ and $C_F(t_i, t_j)$ in Equations (7.36) to (7.39) with the element-wise constant approximations obtained by means of Equations (7.4) and (7.11) results in $\mu_{\hat{\varphi}}(z)$, $C_{\hat{\varphi}}(z_i, z_j)$, $\mu_{\hat{w}}(z)$ and $C_{\hat{w}}(z_i, z_j)$, i.e., the spatial functions for the system response when $F(z)$ is approximated

Table 7.1: Average normalized bias $\bar{\varepsilon}_\mu$ and variance error $\bar{\varepsilon}_V$ of the beam rotation φ'' and vertical displacement w'' for varying number of spatial averaging elements n_{SA} to discretize the posterior beam flexibility RF.

	$\bar{\varepsilon}_\mu$		$\bar{\varepsilon}_V$	
n_{SA}	φ''	w''	φ''	w''
2	0.009	0.019	0.301	0.458
4	0.010	0.020	0.144	0.240
8	0.003	0.005	0.044	0.063

by $\hat{F}(z)$ with n_{SA} spatial averaging elements. Due to the linearity of the averaging operations, $\hat{\varphi}(z)$ and $\hat{w}(z)$ are also Gaussian RFs. The system response RFs and their SA discretization

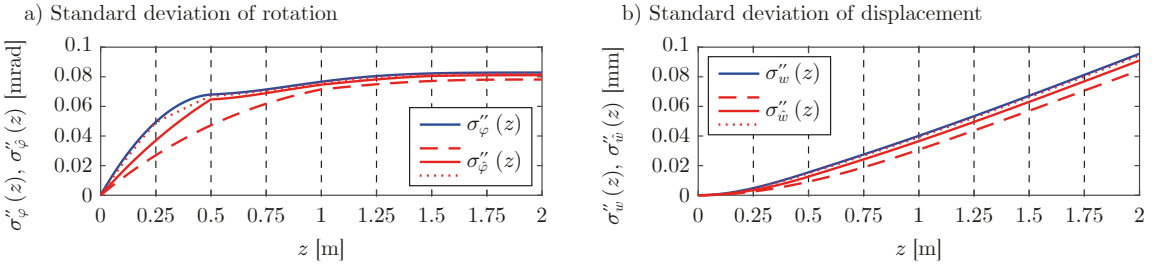

Figure 7.8: Posterior spatial standard deviation of the system response (rotation: panel a; displacement: panel b) for the cantilever beam. The blue lines mark the analytical RF solution and the red lines mark the SA approximation with $n_{SA} = 2$ (dashed line), 4 (solid line) and 8 (dotted line).

with $n_{SA} = 2$, 4 and 8 are evaluated using Equations (7.36) to (7.39). The spatial mean value is approximated well with any chosen SA discretization. For $n_{SA} = 2$, the maximum of the point-wise error $\varepsilon_\mu(z)$ is in the order of 5% (close to the fixed end of the beam) and <1% for most spatial locations z. $\varepsilon_\mu(z)$ decreases further for $n_{SA} = 4$ and $n_{SA} = 8$. In general, $\varepsilon_\mu(z)$ decreases with increasing distance to the fixed end. Figure 7.8 shows the spatial standard deviation of the beam rotation (panel a) and vertical displacement (panel b). The spatial standard deviation of the system response RFs is underestimated throughout the length of the beam, with decreasing approximation error for increasing n_{SA}. The local effect of the measurement appears in the shape of $\sigma''_\varphi(z)$ and $\sigma''_{\hat{\varphi}}(z)$ but not in $\sigma''_w(z)$ and $\sigma''_{\hat{w}}(z)$ due to the smoothing caused by the additional integration when calculating the vertical displacement.

The average error measures for the system response according to Equations (7.29) and (7.30) are listed in Table 7.1 for $n_{SA} = 2$, 4 and 8. The average bias is small for all configurations and the variance error decreases with increasing n_{SA}. In general, the average error is larger for the displacement than it is for the rotation.

To investigate the effect of the SA discretization on the failure probability of the system, a maximum allowable vertical displacement of $w_{\text{lim}} = -1.5\,\text{mm}$ is defined. Since the vertical displacement of a cantilever beam reaches its maximum at the free end, the following limit state function can be formulated:

$$g(F(z)) = w''(z = 2\,\text{m}) - w_{\text{lim}}, \tag{7.40}$$

Replacing $w''(z = 2\,\text{m})$ by $\hat{w}''(z = 2\,\text{m})$ in Equation (7.40) yields the SA approximation of the failure event. Both $w''(z = 2\,\text{m})$ and $\hat{w}''(z = 2\,\text{m})$ are Gaussian random variables with mean value and standard deviation directly computable by means of Equations (7.38) and (7.39).

Thus, P_F is given as

$$P_F = \Phi\left(\frac{w_{\text{lim}} - \mu''_w(z = 2\,\text{m})}{\sigma''_w(z = 2\,\text{m})}\right), \tag{7.41}$$

where $\Phi(\cdot)$ is the cumulative distribution function of the standard normal distribution. The reference solution is $P_F = 9.9 \times 10^{-4}$. The SA approximation of P_F is obtained by replacing $\mu''_w(z = 2\,\text{m})$ and $\sigma''_w(z = 2\,\text{m})$ by the respective SA approximations.

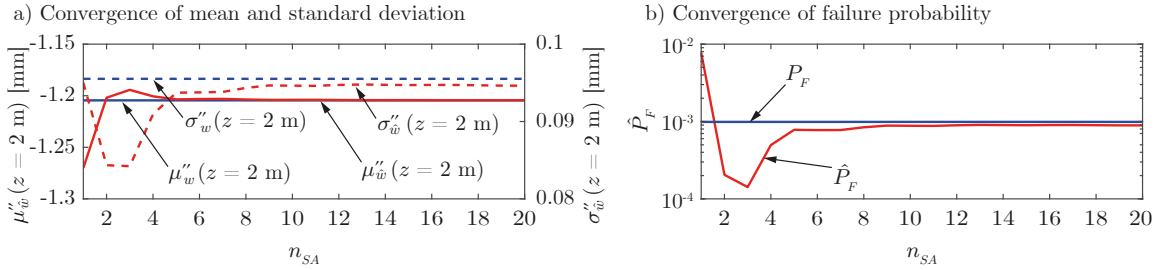

Figure 7.9: Panel a shows the SA approximation of the mean (solid red line, left ordinate) and standard deviation (dashed red line, right ordinate) for the tip displacement of the cantilever beam as function of the number of equisized averaging elements n_{SA}. The blue lines show the analytical mean value $\mu''_w(z = 2\,\text{m})$ (solid blue line) and standard deviation $\sigma''_w(z = 2\,\text{m})$ (dashed blue line). Panel b shows the corresponding SA approximation of the failure probability $\hat{P}_F$ (red line) as function of the number of equisized averaging elements n_{SA}. The blue line shows the analytical failure probability P_F.

Figure 7.9 illustrates the approximated mean and standard deviation of the displacement at the free end and the corresponding failure probability estimate as function of n_{SA} and compares them to the respective analytical solutions. It appears that a single averaging element results in a strong overestimation of the failure probability as $\hat{P}_F$ is approximately eight times larger than P_F. When increasing n_{SA}, $\hat{P}_F$ becomes negatively biased and converges to the analytical solution P_F with increasing n_{SA}. The relative error in the probability of failure falls below 30% for $n_{SA} \geq 5$. The overestimation for $n_{SA} = 1$ results from the fact that the RF $F''(z)$ is discretized with a single random variable that averages over the whole length of the beam, which reduces the local effect of the measurement at $z_m = 0.5\,\text{m}$ and leads to an overestimation of the flexibility in that region. This error propagates through the model evaluation and, on the one hand, leads to a strong bias of the vertical displacement. On the other hand, it leads to an almost perfect approximation of $\sigma''_w(z = 2\,\text{m})$ with a single averaging element, since it counteracts the underestimation of the variance that is typically observed when using a small number of averaging elements.

So far, the SA elements have been equisized, i.e., $L_i = \frac{L}{n_{SA}}, i = 1, \ldots, n_{SA}$ independent of the location within the structural system. In the following, the SA mesh is chosen such that it is finer in regions that may be critical for the system response, in this case the fixed end of the beam $z = 0\,\text{m}$ and the measurement location $z_m = 0.5\,\text{m}$. Figure 7.10 shows the parameters of the

Table 7.2: Average normalized bias $\bar{\varepsilon}_\mu$ and variance error $\bar{\varepsilon}_V$ of the vertical displacement w'' and estimated probability of failure $\hat{P}_F$ with eight SA elements of uniform size, a refined mesh at the fixed end and a refined mesh at the measurement location.

	$\bar{\varepsilon}_\mu$	$\bar{\varepsilon}_V$	$\hat{P}_F$
Uniform mesh	0.005	0.063	8.4×10^{-4}
Fine mesh at fixed end	0.001	0.025	9.6×10^{-4}
Fine mesh at z_m	0.004	0.044	9.0×10^{-4}

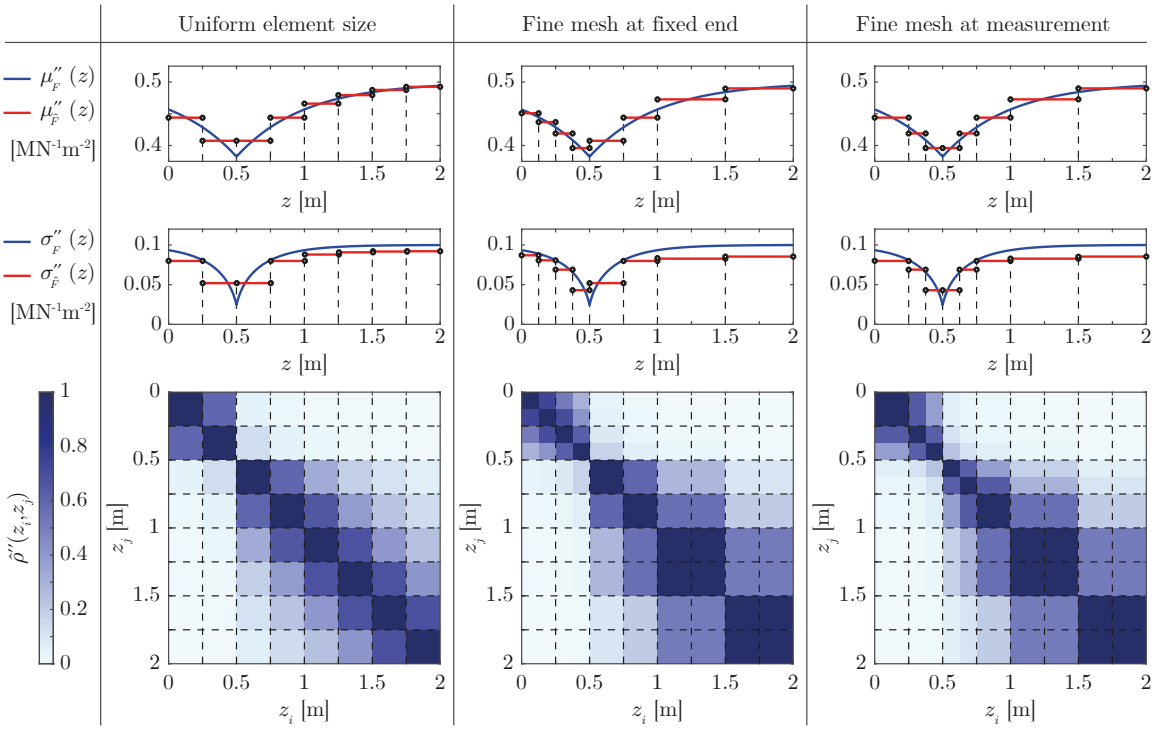

Figure 7.10: Posterior mean value (top row), standard deviation (middle row) and correlation (bottom row) of the SA approximation of the posterior flexibility RF with eight equisized averaging elements (left column), refined mesh at the fixed end (middle column) and refined mesh at the measurement location z_m (right column).

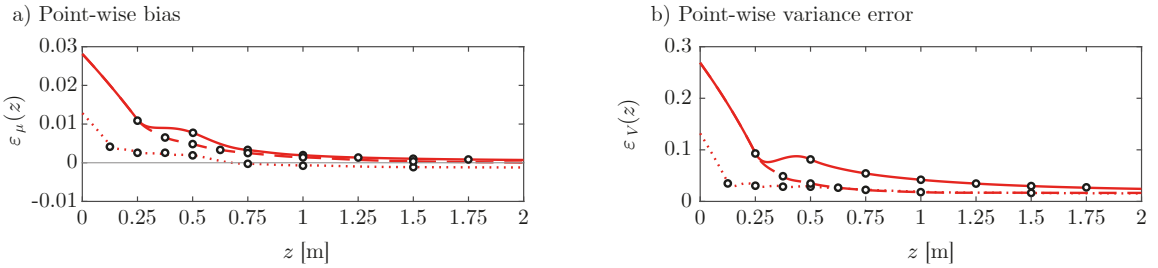

Figure 7.11: Effect of adaptive SA element size in an 8-element mesh (solid line: equisized elements, dotted line: refined mesh at the fixed end, dashed line: refined mesh around the measurement location) on the point-wise normalized bias (panel a) and variance error (panel b) of the vertical displacement.

random variables and their correlation for $n_{SA} = 8$ with equisized elements (left column), refined mesh at the fixed end (middle column) and refined mesh around the measurement location $z_m = 0.5\,\mathrm{m}$ (right column). As $n_{SA} = 8$ for all three settings, a refinement of the SA mesh in one region of the beam necessarily leads to a coarser mesh in other parts of the domain, in this case towards the free end of the beam. Figure 7.11 illustrates the effect on the point-wise error in approximating the vertical displacement.

Refining the mesh leads to smaller bias and variance error in that region compared to the error with equisized elements. The coarser mesh towards the free end of the beam leads to slightly larger bias and variance error for the two adaptive mesh choices. The average error measures are listed in Table 7.2 showing the minor effect on the average variance error of the vertical displacement. The investigated adaptive mesh choices lead to a failure probability estimate of $\hat{P}_F = 9.6 \times 10^{-4}$ (mesh refinement at fixed end) and $\hat{P}_F = 9.0 \times 10^{-4}$ (mesh refinement at measurement location), respectively compared to $\hat{P}_F = 8.4 \times 10^{-4}$ with $n_{SA} = 8$ equisized averaging elements. It is reminded that the reference solution is $P_F = 9.9 \times 10^{-4}$. However, although the results with the adaptive mesh choices are more accurate, they are also more sensitive to the analysis at hand and thus should be handled with caution. This sensitivity is illustrated by using another adaptive SA mesh with $n_{SA} = 8$, where the refinement is towards the free end of the beam, i.e., the region of interest with respect to the limit state function of Equation (7.40). The SA mesh is a left-to-right reversion of the adaptive SA mesh with the refinement at the fixed end (cf. middle column of Figure 7.10). The resulting failure probability estimate is $\hat{P}_F = 5.0 \times 10^{-4}$, which underestimates P_F significantly. In the general case, it might be difficult to find a suitable adaptive SA mesh, especially in cases where the relation between the RF discretization and the output quantity of interest is hidden by a black box model evaluation, as is the case for complex finite element models.

7.3.2.3 Propped cantilever beam

The structural system is modified by adding an additional vertical support at the free end of the beam as illustrated in Figure 7.12. The resulting propped cantilever beam is statically indeterminate and thus, Equations (7.34) and (7.35) cannot be used to evaluate the beam rotation and displacement.

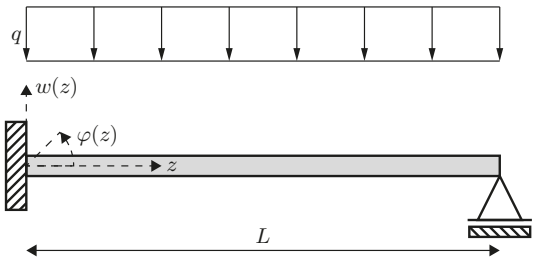

Figure 7.12: Statically indeterminate propped cantilever beam under uniform vertical load q.

Due to the spatial variability of the beam flexibility, the inner forces of the beam depend on the flexibility. Therefore, the system response is evaluated with the linear finite element method based on the Euler-Bernoulli beam theory with a finite element size of $l_{FE} = 0.01\,\mathrm{m}$. Since the system response RFs and their moments cannot be calculated analytically, a numerical reference solution is employed. To this end, the posterior flexibility RF is discretized with the Karhunen-Loève (KL) expansion with a large number of terms ($m_{KL} = 500$) [17]. The KL expansion is based on a spectral decomposition of the autocovariance operator of the RF and can be used for homogeneous and non-homogeneous RFs [2, 38, 15]. Using the KL expansion,

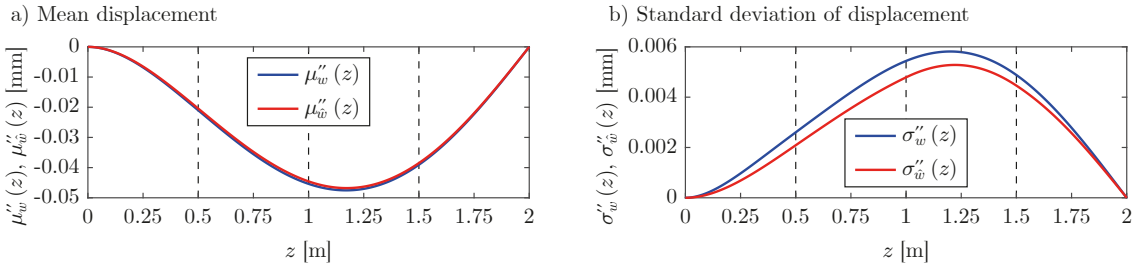

Figure 7.13: Posterior spatial mean value (panel a) and standard deviation (panel b) of the vertical displacement for the propped cantilever beam. The KL expansion in the reference solution (blue) discretizes the RF $F''(z)$ with $m_{KL} = 500$ terms, the SA approximation (red) with four averaging elements of equal size.

Table 7.3: Average normalized bias $\bar{\varepsilon}_\mu$ and variance error $\bar{\varepsilon}_V$ of the propped cantilever vertical displacement w'' for varying number of spatial averaging elements n_{SA} to discretize the posterior beam flexibility RF.

n_{SA}	$\bar{\varepsilon}_\mu$	$\bar{\varepsilon}_V$
2	0.016	0.322
4	0.023	0.278
8	0.007	0.070

the mean value of an RF is represented exactly, while there is an approximation error in the covariance operator. The average variance error of the beam flexibility with the chosen number of terms for the reference solution is smaller than 1%. The parameters of the posterior flexibility RF $F''(z)$ are the same as in the previous investigation and its SA discretization is done with four equisized averaging elements (cf. Figure 7.6). The reference solution as well as the SA solution for the moments of the vertical displacement are obtained by running a Monte Carlo simulation with $N_{MCS} = 1 \times 10^4$ independent samples and is illustrated in Figure 7.13.

Panel a shows that the mean displacement is approximated well with four SA elements, concerning both shape and magnitude of the curve. The standard deviation of the displacement is underestimated throughout the beam and the magnitude increases with increasing distance to one of the supports.

Table 7.3 lists the average bias and variance error of the vertical displacement for $n_{SA} = 2$, 4 and 8. Increasing n_{SA} to eight elements leads to large error reductions while the difference between $n_{SA} = 2$ and $n_{SA} = 4$ is comparatively small. Comparison of Table 7.3 with Table 7.1 for the statically determinate cantilever beam indicates that the average error is larger for the propped cantilever beam than for the statically determinate cantilever beam.

Due to the non-uniform flexibility of the propped cantilever beam, the inner forces (i.e., bending moment and shear) are functions of the applied load and the support reactions, which need to be evaluated numerically, e.g., by means of the finite element method. The bending moment in a propped cantilever beam is calculated as follows:

$$M(z) = M(z=0) \cdot \frac{L-z}{L} + q \cdot \left(L \cdot \frac{z}{2} - \frac{z^2}{2} \right), \tag{7.42}$$

where $M(z=0)$ is the bending moment at the fixed end of the beam. For constant beam flexibility, the support reactions can be determined analytically and $M(z=0) = -q \cdot \frac{L^2}{8}$. As $F(z)$ is modeled by an RF, the evaluated bending moment at the fixed end depends on the chosen discretization. To illustrate this, a reliability analysis with the following limit state

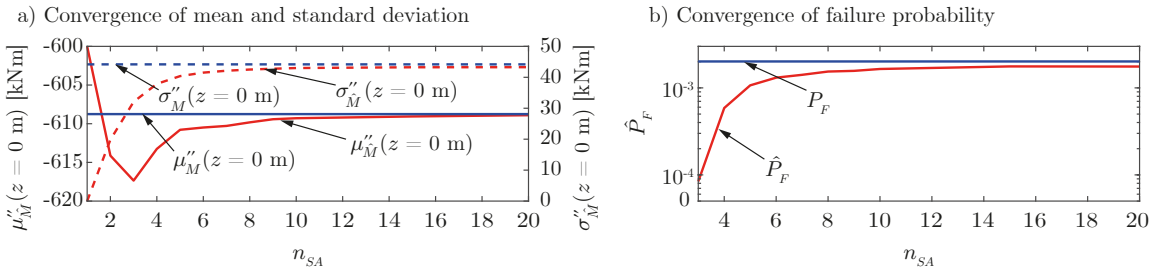

Figure 7.14: Panel a shows the SA approximation of the mean (solid red line, left ordinate) and standard deviation (dashed red line, right ordinate) for the bending moment at the fixed end of the propped cantilever beam as function of the number of equisized averaging elements n_{SA}. The blue lines show the analytical mean value $\mu''_M(z=0\,\mathrm{m})$ (solid blue line) and standard deviation $\sigma''_M(z=0\,\mathrm{m})$ (dashed blue line). Panel b shows the corresponding SA approximation of the failure probability $\hat{P}_F$ (red line) as function of the number of equisized averaging elements n_{SA}. The blue line shows the analytical failure probability P_F.

function is performed:

$$g(F(z)) = M(z=0\,\mathrm{m}) - M_{\mathrm{lim}}, \tag{7.43}$$

where M_{lim} is chosen as $-1.25 \cdot q \cdot \frac{L^2}{8} = -750\,\mathrm{kNm}$. It is noted that $M(z=0\,\mathrm{m})$ is not a Gaussian random variable and thus, evaluation of the probability of failure in terms of the normal integral is not possible. Instead, a Monte Carlo simulation with $N_{MCS} = 1 \times 10^6$ samples is employed to estimate P_F, where the full finite element model of the propped cantilever beam is evaluated for each realization of the beam flexibility. A reference solution is obtained based on the KL expansion with $m_{KL} = 500$ terms to discretize the beam flexibility in a Monte Carlo simulation with $N_{MCS} = 1 \times 10^7$ resulting in $P_F = 2.01 \times 10^{-3}$. The results for varying number of averaging elements in the SA discretization are illustrated in Figure 7.14. The SA approximations for mean (red line) and standard deviation (dashed red line) are plotted as function of n_{SA} in panel a and compared to the respective reference solution (blue line and dashed blue line). If $n_{SA} = 1$, the beam flexibility is uniform throughout the domain, leading to a deterministic bending moment at the fixed end ($\hat{\mu}''_M(z=0) = -q \cdot \frac{L^2}{8} = -600\,\mathrm{kNm}$ and $\hat{\sigma}''_M(z=0) = 0\,\mathrm{kNm}$). The SA method underestimates both mean $\hat{\mu}''_M(z=0)$ and standard deviation $\hat{\sigma}''_M(z=0)$ before converging to the reference solution with increase of n_{SA}. Panel b shows the convergence of the estimated failure probability $\hat{P}_F$ (red line) towards the reference solution (blue line). Failure cannot occur for $n_{SA} = 1$ because the uniform flexibility results in a deterministic bending moment that does not lead to a failed state of the system. No failure sample was observed for $n_{SA} = 2$ in the Monte Carlo simulation with the chosen sample size, indicating that $\hat{P}_F$ strongly underestimates P_F. Choosing $n_{SA} \geq 3$ leads to negatively biased estimates of the failure probability converging towards the reference solution with increasing n_{SA}. $\hat{P}_F$ is of the correct order of magnitude for $n_{SA} \geq 5$.

7.3.2.4 Summary and interpretation of results

The one-dimensional beam example shows that SA can be used to approximate non-homogeneous RFs in reliability analyses of simple beam structures. Due to the smoothing effect of the forward operator, local fluctuations in the beam flexibility average out and thus, the system response can be approximated well with spatially averaging elements. Not surprisingly, a larger number of averaging elements and thus, a larger number of random variables to approximate the RF leads to a better global accuracy of the system response approximation. However, due to the changing interval bounds when changing the number of SA elements, this does not necessarily hold for all error measures when the RF is non-homogeneous. The distribution tails of the

system response are especially important when performing reliability analysis. Our results show that the distribution tails can be sufficiently well approximated with a reasonable number of random variables for the RF discretization, although the required number is larger than for estimating the mean response. The choice of an adaptive size of the averaging elements can lead to a better accuracy of the results, but at the same time increases the sensitivity of the SA discretization to the behavior of the numerical model. Hence, it cannot be recommended for general use; in general problems, the underlying numerical model may be more complex, in which case the choice of an appropriate adaptive mesh is not straightforward. The influence of the spatial variability of the beam flexibility on the system response depends on the quantity of interest and the problem setting. Local failure mechanisms (in our investigation the bending moment) require a larger number of averaging elements than failure mechanisms dominated by global behavior of the flexibility (in our investigation the maximum displacement). Other than in statically determinate settings, the inner forces in a statically indeterminate setting are influenced by spatially variable beam flexibility and thus are spatially variable functions. This leads to larger approximation error in the spatial system response when using SA for the RF discretization.

7.3.3 Sliding failure in the construction joint of a ship lock

The chamber of a fictitious ship lock is investigated. It has a length of $L = 109\,\text{m}$, a usable width between the chamber walls of 12 m and is made of unreinforced tamped concrete. Several failure mechanisms can occur in a ship lock, one of them being sliding of the construction joint between the chamber wall and the base slab. The cross section of the wall including the joint with a width of $W = 4.5\,\text{m}$ and the surrounding soil are illustrated in Figure 7.15. In

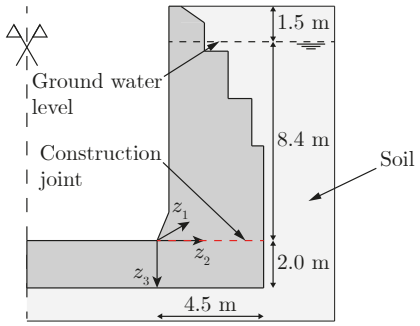

Figure 7.15: Half cross section of a ship lock chamber with construction joint between base slab and chamber wall.

structural verifications, sliding of this joint due to shear is one of the failure mechanisms that are investigated by checking the following condition [8, 4]:

$$V_{Ed} \leq S_{Rd}, \tag{7.44}$$

where V_{Ed} denotes the applied design shear force at the interface and S_{Rd} is the design sliding resistance of the joint. In practice, both V_{Ed} and S_{Rd} depend on a number of factors and additional variables to cover different effects on the sliding failure. For simplicity, a slimmed-down version is used here. V_{Ed} consists of all forces acting horizontally on the structure, i.e., the horizontal earth and water pressure. S_{Rd} is the product of the vertical forces N_{Ed} and the friction coefficient τ of the construction joint. Further contributions to S_{Rd} (e.g., the concrete tensile strength) are neglected at this point. N_{Ed} is given by the self weight of the chamber wall plus the vertical earth and water pressure, wall friction, and crack and pore water pressure.

In this example, two failure events are considered. The first one is a local exceedance of the sliding resistance along z_2, defined by the following limit state function:

$$g_1(z_1, \tau(\boldsymbol{z})) = \gamma_R \cdot S_R(z_1) - V_E(z_1), \tag{7.45}$$

where $\gamma_R = 1.3$ is a deterministic coefficient to account for the spatial load bearing behavior of the chamber wall in a simplified manner. A detailed mechanical model for the spatial load bearing would go beyond the scope of the investigation at this point. $S_R(z_1)$ is defined as the average sliding resistance along the construction joint in z_2:

$$S_R(z_1) = \frac{N_E(z_1)}{4.5\,\mathrm{m}} \int_{0\,\mathrm{m}}^{4.5\,\mathrm{m}} \tau(\boldsymbol{z})\, \mathrm{d}z_2. \tag{7.46}$$

$V_E(z_1)$ and $N_E(z_1)$ are the loads acting on the structure in horizontal and vertical direction. The second limit state function is defined as exceedance of the average sliding resistance of a substantial part of the chamber wall:

$$g_2(\zeta_1, \tau(\boldsymbol{z})) = \int_{\zeta_1 - \frac{\bar{z}_1}{2}}^{\zeta_1 + \frac{\bar{z}_1}{2}} S_R(z_1)\, \mathrm{d}z_1 - \int_{\zeta_1 - \frac{\bar{z}_1}{2}}^{\zeta_1 + \frac{\bar{z}_1}{2}} V_E(z_1)\, \mathrm{d}z_1, \tag{7.47}$$

where $\bar{z}_1 = \frac{L}{5}$ is the length in z_1 that is assumed critical for the sliding failure mechanism of a substantial part of the wall and $\zeta_1 \in (\frac{\bar{z}_1}{2}, L - \frac{\bar{z}_1}{2})$ is the location of the potential failure point along the wall.

Failure of the chamber wall occurs if any of the two described limit state functions gives a value smaller than zero at any point in z_1 direction. Thus, the limit state function for system failure is given as a function of the two individual failure probabilities:

$$g_{\mathrm{sys}}(\tau(\boldsymbol{z})) = \min \left\{ \begin{array}{l} \min_{z_1} \left\{ g_1(z_1, \tau(\boldsymbol{z})) \right\}, \; z_1 \in (0\,\mathrm{m}, L) \\ \min_{\zeta_1} \left\{ g_2(\zeta_1, \tau(\boldsymbol{z})) \right\}, \; \zeta_1 \in (\frac{\bar{z}_1}{2}, L - \frac{\bar{z}_1}{2}) \end{array} \right\}. \tag{7.48}$$

7.3.3.1 Two-dimensional random field for the friction coefficient

The friction coefficient τ in the construction joint is modeled by a two-dimensional RF $\tau(\boldsymbol{z})$ in z_1 and z_2. The prior RF $\tau'(\boldsymbol{z})$ is homogeneous with lognormal marginal distribution F'_τ. The corresponding parameters are $\mu'_{\ln\tau}$ and $\sigma'_{\ln\tau}$, which are the mean value and standard deviation of the Gaussian distribution $F'_{\ln\tau}$ of the underlying homogeneous Gaussian RF $\tau_{\ln}(\boldsymbol{z})$. The spatial correlation of $\tau'_{\ln}(\boldsymbol{z})$ is modeled with the Matérn correlation model with a smoothness parameter of $\nu = 1.5$ [1, 32]:

$$\rho'(\boldsymbol{z}_i, \boldsymbol{z}_j) = \left(1 + \frac{\sqrt{3}\delta_z}{l_c}\right) \cdot \exp\left(-\frac{\sqrt{3}\delta_z}{l_c}\right). \tag{7.49}$$

The correlation length is chosen as $l_c = 4\,\mathrm{m}$.

A typical assumption for the friction coefficient in indented construction joints of concrete structures is $\tau = 0.9$ [8], while in-situ measurements often show significantly higher friction coefficients. Hence, the prior RF distribution parameters are chosen such that $\tau = 0.9$ approximately equals the 5%-quantile value of the lognormal distribution. This is achieved by choosing $\mu'_{\ln\tau} = 0.25$ and $\sigma'_{\ln\tau} = 0.2$. The corresponding mean value and standard deviation are $\mu'_\tau = 1.31$ and $\sigma'_\tau = 0.26$. Note that this prior distribution is based on relatively strong assumptions and may not hold in practice.

It is assumed that data from concrete core samples of the chamber wall is available including $n_m = 8$ spatial measurements of the friction coefficient τ in the construction joint (i.e., $z_3 = 0\,\mathrm{m}$).

Table 7.4: Measurement values τ_m of the friction coefficient and corresponding locations in the construction joint of the ship lock chamber wall.

	1	2	3	4	5	6	7	8
z_1 [m]	17.80	22.30	46.55	52.05	54.70	54.70	76.25	81.40
z_2 [m]	0.75	0.50	1.25	1.45	0.85	1.75	0.35	1.00
τ_m	2.6	2.1	1.2	1.7	3.1	2.1	2.9	5.0

Table 7.4 lists the measurements $\boldsymbol{\tau}_m = [\tau_{m,1}, \ldots, \tau_{m,8}]$ and corresponding locations. It is further assumed that the data are associated with a lognormal multiplicative measurement error with median 1 and coefficient of variation $\mathrm{CV}_\varepsilon = 0.1$, which is equivalent to an additive zero-mean Gaussian measurement error for the logarithmic transformation of the measurements $\ln(\boldsymbol{\tau}_m)$. Equations (7.32) and (7.33) can be adapted for the two-dimensional update of the mean and covariance function of the Gaussian RF $\tau_{\ln}(\boldsymbol{z})$:

$$\mu''_{\ln\tau}(\boldsymbol{z}) = \mu'_{\ln\tau} + \boldsymbol{R}_{\boldsymbol{z}_m}(\boldsymbol{z}) \cdot \mathbf{R}^{-1}_{\boldsymbol{z}_m,\varepsilon} \cdot \left(\ln(\boldsymbol{\tau}_m) - \mu'_{\ln\tau}\right)^{\mathsf{T}}, \tag{7.50}$$

$$C''_{\ln\tau}(\boldsymbol{z}_i, \boldsymbol{z}_j) = \left(\sigma'_{\ln\tau}\right)^2 \cdot \left(\rho(\boldsymbol{z}_i, \boldsymbol{z}_j) - \boldsymbol{R}_{\boldsymbol{z}_m}(\boldsymbol{z}_i) \cdot \mathbf{R}^{-1}_{\boldsymbol{z}_m,\varepsilon} \cdot \boldsymbol{R}^{\mathsf{T}}_{\boldsymbol{z}_m}(\boldsymbol{z}_j)\right). \tag{7.51}$$

$\boldsymbol{R}_{\boldsymbol{z}_m}(z)$ is a $1 \times n_m$ row vector function with element i equal to $\rho'(\boldsymbol{z}, \boldsymbol{z}_{m,i})$. $\mathbf{R}_{\boldsymbol{z}_m,\varepsilon} = \mathbf{R}_{\boldsymbol{z}_m,\boldsymbol{z}_m} + \mathbf{R}_\varepsilon$, where $\mathbf{R}_{\boldsymbol{z}_m,\boldsymbol{z}_m}$ is an $n_m \times n_m$ matrix with element (i,j) equal to $\rho'(\boldsymbol{z}_{m,i}, \boldsymbol{z}_{m,j})$ and $\mathbf{R}_\varepsilon = \sigma^2_{\ln\varepsilon} \cdot \mathrm{I}$, where I is the $n_m \times n_m$ identity matrix. The resulting posterior mean value and standard deviation of the marginal lognormal distributions of $\tau''(\boldsymbol{z})$ are plotted in Figure 7.16.

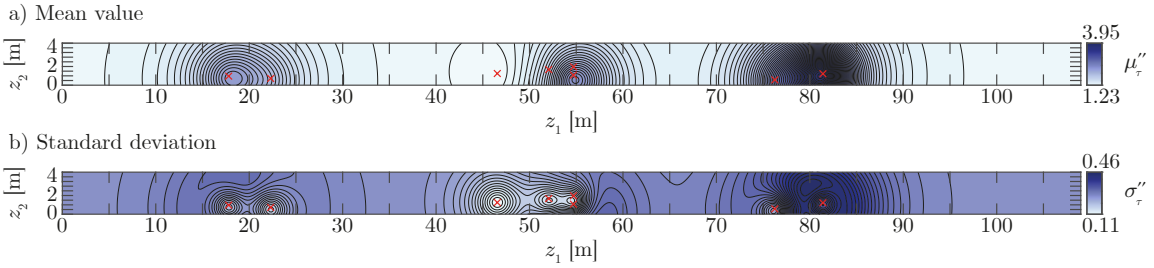

Figure 7.16: Posterior spatial mean value (panel a) and standard deviation (panel b) of the two-dimensional RF for the friction coefficient in the construction joint of a ship lock chamber wall. The red crosses indicate the locations of the $n_m = 8$ measurements of the friction coefficient.

To approximate $\tau''(\boldsymbol{z})$ with SA, the domain of the construction joint is divided into rectangular averaging domains. Their length is $\frac{L}{n_{SA,1}}$ in z_1 and $\frac{W}{n_{SA,2}}$ in z_2, resulting in $n_{SA} = n_{SA,1} \cdot n_{SA,2}$ rectangular elements of equal size. The corresponding parameters of the lognormal averaging random variables and their correlation are found by application of Equations (7.13) to (7.15) in combination with the transformation in Equation (7.20). The mean values and standard deviations for $n_{SA,1} = 20$ and $n_{SA,2} = 1$ are illustrated in Figure 7.17. It can be seen that local extrema of the RF parameters resulting from high or low measurement values are not fully reflected in the SA parameters but regions of high or low values are visible.

7.3.3.2 Loads acting on the structure

The vertical forces from self weight, vertical earth and water pressure, wall friction and crack and pore water pressure are modeled space-invariant and deterministically. They sum up to $N_E(z_1) = 580\,\mathrm{kNm}^{-1}$ per running length. The horizontal water pressure is assumed deterministic

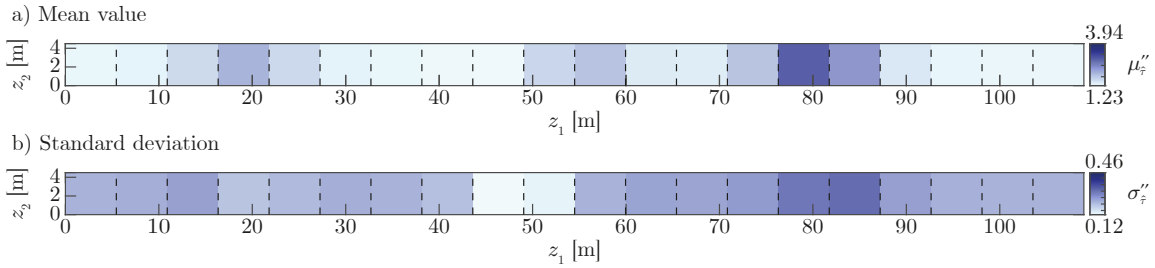

Figure 7.17: Posterior spatial mean value (panel a) and standard deviation (panel b) of the SA discretization of the two-dimensional RF for the friction coefficient in the construction joint of a ship lock chamber wall. The number of elements is $n_{SA} = 20$ with $n_{SA,1} = 20$ and $n_{SA,2} = 1$.

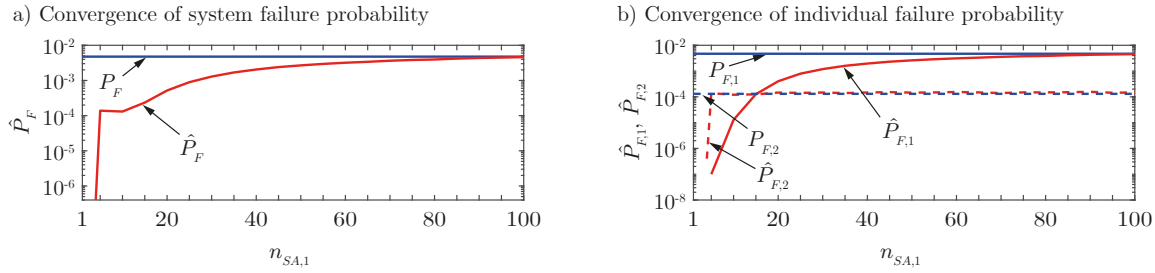

Figure 7.18: Failure probability estimates for the sliding failure of the ship lock chamber wall as function of the number of equisized averaging elements in z_1 direction $n_{SA,1}$. Panel a shows the estimate of the system failure probability $\hat{P}_F$ (red line) and panel b shows the estimates of the individual failure probabilities $\hat{P}_{F,1}$ (solid red line) and $\hat{P}_{F,2}$ (dashed red line). The blue lines mark the corresponding reference failure probabilities P_F, $P_{F,1}$ and $P_{F,2}$ (dashed blue line).

based on the given ground water level (cf. Figure 7.15), resulting in a value of $V_{E,w} = 353\,\mathrm{kNm}^{-1}$ per running length. The horizontal earth pressure consists of a basic value of $V_{E,e} = 159\,\mathrm{kNm}^{-1}$ and is multiplied with a location-specific random term. This term is modeled with a one-dimensional KL representation using a fixed number of terms ($m_{KL} = 10$). It has mean value $\mu_p = 1$, standard deviation $\sigma_p = 0.05$ and exponential spatial correlation (cf. Equation (7.31)) with a scale of fluctuation of $\vartheta = 40\,\mathrm{m}$.

7.3.3.3 Reliability analysis

The reliability analysis is carried out with MCS using 10^7 independent samples. A reference solution is obtained by discretizing the two-dimensional RF $\tau''(\boldsymbol{z})$ with the KL expansion with $m_{KL} = 500$ terms. Figure 7.18 illustrates the resulting failure probability estimates as function of the number of SA elements in z_1 direction $n_{SA,1}$. Panel a shows that $\hat{P}_F$ (red line) strongly underestimates P_F (blue line) for small $n_{SA,1}$ but converges to the reference solution with increasing $n_{SA,1}$. $\hat{P}_F = 0$ when $n_{SA,1} < 4$, confirming the trend to underestimate P_F for small $n_{SA,1}$. The system failure probability can be split up into the two individual failure probabilities $P_{F,1}$ and $P_{F,2}$ for failure as defined by Equation (7.45) and (7.47), respectively. Panel b of Figure 7.18 shows the convergence of the individual probability estimates $\hat{P}_{F,1}$ (solid red line) and $\hat{P}_{F,2}$ (dashed red line) to the reference solution (respective blue lines) with increasing $n_{SA,1}$. For $n_{SA,1} < 5$ (4), the estimated individual failure probability for failure mechanism 1 (2) is 0. The required number of averaging elements for obtaining a good approximation of $P_{F,1}$ is significantly larger than for $P_{F,2}$. This is related to the nature of the two considered failure mechanisms. $g_1(z_1, \tau(\boldsymbol{z}))$ describes a failure mechanism that is located at a single point in direction z_1, i.e., it is sensitive to local spatial variability. $g_2(\zeta_1, \tau(\boldsymbol{z}))$ on the other hand

Table 7.5: Effect of the number of SA elements in z_2 direction $n_{SA,2}$ on the failure probability estimate $\hat{P}_F$ for sliding failure of the ship lock chamber, exemplarily for $n_{SA,1} = 25$, $n_{SA,1} = 50$ and $n_{SA,1} = 75$.

	$\hat{P}_F$		
$n_{SA,1}$	$n_{SA,2} = 1$	$n_{SA,2} = 2$	$n_{SA,2} = 3$
25	8.9×10^{-4}	8.4×10^{-4}	8.4×10^{-4}
50	2.7×10^{-3}	2.6×10^{-3}	2.6×10^{-3}
75	3.8×10^{-3}	3.7×10^{-3}	3.6×10^{-3}

describes the average resistance over the length $\bar{z}_1$, which is dominated by regions of high and low values of the friction coefficient. This type of failure mechanism is less sensitive to local variations of the RF approximation error, and thus, can be well approximated with a smaller number of averaging elements. Increasing the number of elements in z_2 direction has a minor effect on the estimated failure probability, as shown in Table 7.5 for $n_{SA,1} = 25$, $n_{SA,1} = 50$ and $n_{SA,1} = 75$. The reason is that both failure mechanisms include an integration of the sliding resistance over W in z_2 direction. The minor changes in $\hat{P}_F$ can be attributed to the fact that $\tau''(\boldsymbol{z})$ is approximated by the geometric average in each SA element. Increasing the number of elements leads to a smaller difference between the integration of geometric averages (with SA) and the integration of $\tau''(\boldsymbol{z})$ (in the reference solution).

This example shows that, for an efficient reliability analysis, the number of SA elements should be chosen depending on the problem at hand. Local failure mechanisms require a larger number of averaging elements than failure mechanisms dominated by averages over specific regions or even determined by global averages. By an intelligent choice of the SA mesh, the stochastic dimension, i.e., the number of random variables, can be significantly reduced without loss of accuracy. This is of special interest in multi-dimensional settings, where on the one hand the number of random variables increases exponentially when the SA mesh is refined and on the other hand, as illustrated above, the SA mesh might need to be fine in one direction but can be relatively coarse in the other direction(s).

7.4 Conclusion

This paper presents the spatial averaging method for discretizing non-homogeneous random fields with focus on application in reliability analysis with forward engineering models. Non-homogeneous random fields can be induced through a spatial Bayesian update of the random field with measurement data. Each random variable in the discretization with spatial averages represents the average behaviour of the random field in a chosen linear (in one dimension) or rectangular (in higher dimensions) spatial domain. Equations to calculate the mean vector and the covariance matrix of the set of averaging random variables are presented. These equations enable direct application of the method to Gaussian random fields. Additionally, we present application of the method to non-Gaussian translation fields and derive the required transformation for fields with lognormal, Student's t- and log-Student's t-marginal distribution.

The performance of the method is investigated through two numerical examples, a one-dimensional beam and a two-dimensional ship lock chamber wall. Thereby, the method is assessed in terms of its ability to accurately represent output quantities of interest and, particularly, the reliability of engineering structures. It is shown that the spatial averaging method is suitable to approximate non-homogeneous random fields with a relatively small set of random variables, especially when the numerical model of the system response involves integration of the spatially

variable quantity. In such cases, even a single random variable can be sufficient for obtaining a reasonable approximation of the output variability. The examples highlight that understanding of the mechanical model is essential for efficient application of the spatial averaging method in conjunction with structural models. It is shown that not only the number of averaging elements but also the size of the individual elements are critical parameters for the performance of the method. An adaptive element size can increase the accuracy of the discretization by increasing the quality of the random field discretization in regions of special importance. However, it cannot be recommended for general application as it requires detailed knowledge of the effect of spatial variability in the input on the output quantity of interest. Thus, a uniform mesh size is to be preferred since it is more robust in terms of the approximation error of the random field discretization. In the absence of an insight on the mechanical model, the number of elements can be chosen by defining a target average relative bias and variance error on the input random field.

The method is particularly suitable for coupling with black box models of engineering systems, such as finite element models, and, hence, enables consideration of spatial variability in practical reliability analyses. Additionally, the presented method can be used to account for spatial variability in the verification of structures, e.g., by determining a conservative estimate for the spatial average of material properties or by accounting for spatial load bearing behavior but still maintaining the simplifications of a plane structural model. It is left to future studies to investigate the suitability of the spatial averaging method for practical application in structural verification.

Acknowledgments

This work has been financially supported by the *Bundesanstalt für Wasserbau* (Federal Waterways Engineering and Research Institute, Germany). The corresponding author would like to thank Claus Kunz from the *Bundesanstalt für Wasserbau* for discussions that have considerably enhanced the quality of the paper.

References

[1] P. Abrahamsen. *A review of Gaussian random fields and correlation functions*. 2nd ed. Norwegian Computing Center, 1997.

[2] W. Betz, I. Papaioannou, and D. Straub. "Numerical methods for the discretization of random fields by means of the Karhunen-Loève expansion". In: *Computer Methods in Applied Mechanics and Engineering* 271 (2014), pp. 109–129.

[3] C. M. Bishop. *Pattern recognition and machine learning*. Information science and statistics. New York City, NY: Springer, 2006.

[4] Bundesanstalt für Wasserbau. *Bewertung der Tragfähigkeit bestehender, massiver Wasserbauwerke [Assessment of the bearing capacity of existing, massive hydraulic structures]*. BAW guideline, 2016.

[5] J. Ching and K.-K. Phoon. "Characterizing uncertain site-specific trend function by sparse Bayesian learning". In: *Journal of Engineering Mechanics* 143.7 (2017), p. 04017028.

[6] J. Ching, X.-W. Tong, and Y.-G. Hu. "Effective Young's modulus for a spatially variable soil mass subjected to a simple stress state". In: *Georisk: Assessment and Management of Risk for Engineered Systems and Geohazards* 10.1 (2016), pp. 11–26.

[7] A. Der Kiureghian and J.-B. Ke. "The stochastic finite element method in structural reliability". In: *Probabilistic Engineering Mechanics* 3.2 (1988), pp. 83–91.

[8] *EN 1992-1-1:2004. Eurocode 2: design of concrete structures - part 1-1: general rules and rules for buildings*. European Standard, 2004.

[9] G. A. Fenton and D. V. Griffiths. "Bearing-capacity prediction of spatially random $c - \phi$ soils". In: *Canadian Geotechnical Journal* 40.1 (2003), pp. 54–65.

[10] G. A. Fenton. "Random field modeling of CPT data". In: *Journal of geotechnical and geoenvironmental engineering* 125.6 (1999), pp. 486–498.

[11] G. A. Fenton and D. V. Griffiths. "Three-dimensional probabilistic foundation settlement". In: *Journal of Geotechnical and Geoenvironmental Engineering* 131.2 (2005), pp. 232–239.

[12] G. A. Fenton and E. H. Vanmarcke. "Simulation of random fields via local average subdivision". In: *Journal of Engineering Mechanics* 116.8 (1990), pp. 1733–1749.

[13] A. Gelman, J. Carlin, H. Stern, D. Dunson, A. Vehtari, and D. Rubin. *Bayesian data analysis*. 3rd. Chapman & Hall/CRC texts in statistical science. Boca Raton, FL: CRC, 2013.

[14] S. Geyer, I. Papaioannou, C. Kunz, and D. Straub. "Bayesian reliability assessment with spatially variable measurements: the spatial averaging approach". In: *Proceedings of the 13th international conference on application of statistics and probability in civil engineering*. Ed. by J. Song. Seoul: Seoul National University open repository, 2019, pp. 1–8.

[15] S. Geyer, I. Papaioannou, C. Kunz, and D. Straub. "Reliability assessment of large hydraulic structures with spatially distributed measurements". In: *Structure and Infrastructure Engineering* 16 (4 2020), pp. 599–612.

[16] S. Geyer, I. Papaioannou, and D. Straub. "Bayesian analysis of hierarchical random fields for material modeling". In: *Probabilistic Engineering Mechanics* 66 (2021), p. 103167.

[17] R. G. Ghanem and P. D. Spanos. *Stochastic finite elements. A spectral approach*. revised. Dover civil and mechanical engineering. Mineola, NY: Dover, 2012.

[18] L. Graham and G. Deodatis. “Variability response functions for stochastic plate bending problems”. In: *Structural Safety* 20.2 (1998), pp. 167–188.

[19] M. Grigoriu. “Existence and construction of translation models for stationary non-Gaussian processes”. In: *Probabilistic Engineering Mechanics* 24.4 (2009), pp. 545–551.

[20] M. Grigoriu. “Crossings of non-Gaussian translation processes”. In: *Journal of Engineering Mechanics* 110.4 (1984), pp. 610–620.

[21] M. Grigoriu. *Stochastic systems: uncertainty quantification and propagation*. Springer series in reliability engineering. Springer London, 2012. 532 pp.

[22] W. Knabe, J. Przewłócki, and G. Różyński. “Spatial averages for linear elements for two-parameter random field”. In: *Probabilistic Engineering Mechanics* 13.3 (1998), pp. 147–167.

[23] S. Kotz and S. Nadarajah. *Multivariate t-distributions and their applications*. Cambridge University, 2004.

[24] C.-C. Li and A. D. Kiureghian. “Optimal discretization of random fields”. In: *Journal of Engineering Mechanics* 119.6 (1993), pp. 1136–1154.

[25] P.-L. Liu and A. D. Kiureghian. “Multivariate distribution models with prescribed marginals and covariances”. In: *Probabilistic Engineering Mechanics* 1.2 (1986), pp. 105–112.

[26] Y. Liu, J. Li, S. Sun, and B. Yu. “Advances in Gaussian random field generation: a review”. In: *Computational Geosciences* 23.5 (2019), pp. 1011–1047.

[27] H. G. Matthies, C. E. Brenner, C. G. Bucher, and C. Guedes Soares. “Uncertainties in probabilistic numerical analysis of structures and solids - stochastic finite elements”. In: *Structural Safety* 19.3 (1997), pp. 283–336.

[28] I. Papaioannou, S. Geyer, and D. Straub. “Bayesian updating of foundation reliability with spatially variable measurements: a spatial averaging approach”. In: *Proceedings of the 7th International Symposium on Geotechnical Safety and Risk*. Ed. by J. Ching, D. Q. Li, and J. Zhang. Research publishing, 2019, pp. 619–624.

[29] I. Papaioannou and D. Straub. “Learning soil parameters and updating geotechnical reliability estimates under spatial variability - theory and application to shallow foundations”. In: *Georisk: Assessment and Management of Risk for Engineered Systems and Geohazards* 11.1 (2017), pp. 116–128.

[30] K.-K. Phoon and F. H. Kulhawy. “Characterization of geotechnical variability”. In: *Canadian Geotechnical Journal* 36.4 (1999), pp. 612–624.

[31] R. Rackwitz. “Reviewing probabilistic soils modelling”. In: *Computers and Geotechnics* 26.3 (2000), pp. 199–223.

[32] C. E. Rasmussen and C. K. I. Williams. *Gaussian processes for machine learning*. Adaptive computation and machine learning. Cambridge, MA: MIT, 2006.

[33] D. Savvas, I. Papaioannou, and G. Stefanou. “Bayesian identification and model comparison for random property fields derived from material microstructure”. In: *Computer Methods in Applied Mechanics and Engineering* 365 (2020), p. 113026.

[34] P. Spanos and R. Ghanem. “Stochastic finite element expansion for random media”. In: *Journal of Engineering Mechanics* 15.5 (1989), pp. 1035–1053.

[35] M. Stein. *Interpolation of spatial data: some theory for kriging*. Springer series in statistics. New York City, NY: Springer, 1999.

[36] B. Sudret and A. Der Kiureghian. *Stochastic finite element methods and reliability: a state-of-the-art report*. Report on research No. UCB/SEMM-2000/08. University of California, Berkeley, 2000.

[37] M. Tabarroki, J. Ching, K.-K. Phoon, and Y.-Z. Chen. "Mobilisation-based characteristic value of shear strength for ultimate limit states". In: *Georisk: Assessment and Management of Risk for Engineered Systems and Geohazards* 0.0 (2021), pp. 1–22.

[38] F. Uribe, I. Papaioannou, W. Betz, and D. Straub. "Bayesian inference of random fields represented with the Karhunen-Loève expansion". In: *Computer Methods in Applied Mechanics and Engineering* 358 (2020), p. 112632.

[39] L. H. Vanegas and G. A. Paula. "Log-symmetric distributions: statistical properties and parameter estimation". In: *Brazilian Journal of Probability and Statistics* 30.2 (2016), pp. 196–220.

[40] E. Vanmarcke, M. Shinozuka, S. Nakagiri, G. Schuëller, and M. Grigoriu. "Random fields and stochastic finite elements". In: *Structural Safety* 3.3 (1986), pp. 143–166.

[41] E. Vanmarcke. *Random fields: analysis and synthesis*. Revised and expanded new edition. World Scientific, 2010.

[42] E. Vanmarcke and M. Grigoriu. "Stochastic finite element analysis of simple beams". In: *Journal of Engineering Mechanics* 109.5 (1983), pp. 1203–1214.

[43] M. Vořechovský and J. Eliáš. "Fracture in random quasibrittle media: II. Analytical model based on extremes of the averaging process". In: *Engineering Fracture Mechanics* 235 (2020), p. 107155.

[44] W. Q. Zhu, Y. J. Ren, and W. Q. Wu. "Stochastic FEM based on local averages of random vector fields". In: *Journal of Engineering Mechanics* 118.3 (1992), pp. 496–511.